DEPARTMENT OF ELECTRONIC & ELECTRICAL ENGINEERING

University of Strathclyde Engineering

NON-THERMAL PLASMA TECHNOLOGY FOR NITRIC OXIDE REMOVAL

A thesis presented in fulfilment of the requirement for the degree of

Doctor of Philosophy

Linghe Zhou, B.Eng (Honours)

2017

Department of Electronic and Electrical Engineering

University of Strathclyde

Glasgow, UK

Declaration of Authenticity and Author's Rights

‘This thesis is the result of the author’s original research. It has been composed by the author and has not been previously submitted for examination which has led to the award of a degree.’

Signed:

Date:

ACKNOWLEDGEMENTS

I would firstly like to thank Dr. Tao Wang for his continuous supervision, guidance and encouragement throughout my PhD study. His passion and curiosity about the nature and research was always inspiring me to go forward. His rigorous research attitude and strong commitment to excellence in research also have provided a good example for me and motivated me to pursue the extraordinary in my future career.

I would also like to thank Dr. Qingchun Ren for his financial support and encouragement in my PhD study. I would also like to express my gratitude to Prof. Scott MacGregor for the opportunity and support. Many thanks to Dr. Igor Timoshkin, Dr. Mark Wilson, Dr. Michelle MacLean and Dr. Athanasios Mermigkas for their suggestions and help at group meetings. In particular, I would like to express my gratitude to Dr. Mark Wilson for his advice and corrections on my academic papers and thesis throughout the study.

Thanks to all the guys in the High-Voltage Mechanical Workshop: Sean Doak, Andy Carlin, Frank May, and David Griffin for all their help with designing and machining reactors and other experimental equipment during my PhD study. Thanks to Mrs. Maureen Cooper for all her assistance, particularly in ordering experimental equipment and organising conference trips.

Thanks to all my colleagues in the HVT Research Group and also to my friends for providing technical discussions of the study and bringing fun to my life over the years. In particular, I would like to thank Dr. Guangming Huang, Dr. Yiyi Zhao, Yingjia Zhou and Zhongshu Zhang for all their valuable discussion and help to me.

I would also like to thank my family for their deep love and continuous support in my life. Especially, thanks my wife Ms Jing Zhang for her endless support and understanding.

Abstract

Non-thermal plasma, as a potential nitric oxide (NO) removal technology, has been researched for more than one decade. The advantage of direct non-thermal plasma treatment is that it is able to generate reactive species from the existing components in the flue gas without additional catalyst, oxidant or reductant, so any NO removal system based upon this technology is simple and easy to operate. However, the energy efficiency of non-thermal plasma technology is lower than the most commonly used selective catalytic reduction system for NO removal. In order to understand the possible reasons, it is important to investigate the mechanism of NO removal by direct non-thermal plasma treatment. Two of the most commonly used non-thermal plasma sources, dielectric barrier discharge (DBD) and corona discharge, are investigated. The most important reactive species include oxygen atom (O), ozone (O_3) and hydroxyl radical (OH). Different reactive species lead to different chemical reaction pathways for NO removal. Under different NO concentration and discharge configurations, the dominant reactive species was found to change from one to another.

For dielectric barrier discharge, when the initial NO concentration was higher than 420 ppm under dry condition, it was found that O was the dominant reactive species for NO oxidation and NO oxidation was independent on O_2 concentration. When initial NO concentration was lower than 100 ppm under dry condition, it was found that O_3 was the dominant reactive species and NO oxidation was dependent on O_2 concentration. When NO concentration was in the range of 120 ppm to 190 ppm, there was a synergistic effect of O and O_3 on NO oxidation. NO removal depended on the initial NO concentration. However, no matter what the initial NO concentration was, the NO removal energy efficiency was lower than 25g/kWh.

When water vapour (H_2O) was introduced into the gas mixture, reactive species OH was generated and provided an alternative chemical reaction pathway for NO removal. When initial NO concentration was 1000 ppm, NO removal was in the range of 150 ppm to 200 ppm, but the energy efficiency was in the range of 7 to 12 g/kWh. With an increase of temperature in DBD reactor, the effect of OH on NO removal was promoted. To further investigate the OH effect, a novel pin to water corona discharge configuration was used. The effect of discharge modes from Trichel pulse, pulseless and arc discharge was investigated. Under arc discharge mode, 200 ppm NO was generated at 6W discharge power. Under

Trichel and pulseless discharge modes, NO removal increased with increasing discharge power. When initial NO concentration was 1000 ppm, the highest NO removal achieved was 715 ppm with 5.5 g/kWh energy efficiency. In addition, it was found that the energy efficiency did not reduce with increasing discharge power.

In order to increase the possibility of chemical reaction between NO and reactive species, higher initial NO concentration was used. To obtain higher NO concentration a process of NO absorption by activated carbon and thermal desorption was used. This increased the NO concentration from 1000 ppm up to 6%. It is found that at 6% level, NO could be partially oxidized by oxygen molecule (O_2) and higher O_2 concentration would obtain higher NO oxidation rate.

Direct non-thermal plasma treatment can be used for NO removal but the energy efficiency (less than 30g/kWh) is too low to compete with the mature technologies including selective catalytic reduction (SCR) and low temperature oxidation (LoTOx) whose energy efficiencies are higher than 60 g/kWh.

Although the energy efficiency is not improved in this research, the mechanism and chemical reaction pathways of NO removal are quantitatively analysed under different initial NO concentration levels by two different non-thermal plasma technologies (DBD and corona discharge). The dominant reactive species for NO removal can shift from O, O_3 to OH.

In addition, a novel technology which is a combination of non-thermal plasma, NO absorption and desorption processes is developed in this research. It offers a new mechanism for NO removal, because increasing the concentration of NO from ppm level to a few percentages creates a regime where NO removal can be effectively done by O_2 rather than strong oxidants like O and O_3. As the formation of O and O_3 is more expensive than that of O_2, this is a promising research direction for NO removal. However, based on the investigation in this research, some challenges are found. One is the poor selection between NO and H_2O for activated carbon and the other one is high energy consumption for the desorption process.

Contents

List of Abbreviations

AC	Alternative Current
BET	Brunauer-Emmett-Teller
DBD	Dielectric Barrier Discharge
DC	Direct Current
$DeNO_x$	De-Nitrification
EB	Electron Beam
FGR	Flue Gas Recirculation
FR	Flow Rate
ID	Inner Diameter
LoTOx	Low Temperature Oxidation
kΩ	kilo-Ohms
kV	kilo-Volt
ns	nanosecond
mA	milli-Amp
MΩ	Mega-Ohms
µA	micro-Amp
µs	microsecond
OD	Outer Diameter
ppm	Parts Per Million
PTFE	Polytetrafluoroethylene
PVC	Polyvinyl Chloride
RNS	Reactive Nitrogen Species
ROS	Reactive Oxygen Species
sccm	Standard Cubic Centimetre per Minute
SCR	Selective Catalytic Reduction
slpm	Standard Litre per Minute
SNCR	Selective Non-Catalytic Reduction
SS	Stainless Steel
VOC	Volatile Organic Compounds

List of Symbols

a	Reaction order with respect to reactant A
[A]	Concentration of Reactant A
α	Ionization coefficient
b	Reaction order with respect to reactant B
[B]	Concentration of Reactant B
C_{NO}	Concentration of Nitric Oxide
C_{NO2}	Concentration of Nitrogen Dioxide
C_{O3}	Concentration of Ozone
C_g	Gas Gap Capacitor
C_d	Dielectric Barrier Capacitor
C_{tot}	The DBD Reactor Total Capacitor
C_m	Measurement capacitor
d	Gap Distance
k	Reaction Rate Constant
E_a	Activation Energy for a Chemical Reaction
f	Energization frequency of AC power
F_{O3}	Ozone Formation Rate
H	Hydrogen Atom
HO_2	Hydroperoxyl Radical
H_2O	Water Molecule
HNO_2	Nitrous Acid
HNO_3	Nitric Acid
I	External Discharge Current
M_v	Molar Volume of Gases
M_m	Molar Mass of Gases
N	Nitrogen Atom
N_2	Nitrogen Molecule
NH_2	Amidogen Radical
NH_3	Ammonia
NO	Nitric Oxide
NO_2	Nitrogen Dioxide
NOx	Nitrogen Oxides

N_2O_3	Dinitrogen Trioxide
N_2O_4	Dinitrogen Tetroxide
N_2O_5	Dinitrogen Pentoxide
η_{NO}	Nitric Oxide Removal Energy Efficiency
O	Oxygen Atom
O_2	Oxygen Molecule
O_3	Ozone
OH	Hydroxyl Radical
P	non-thermal plasma discharge power in W
p	Absolute Gas Pressure in bar
ΔQ_{AB}	Charge transfer during time interval from A to B
R	Universal gas constant
R_{NO}	Nitric Oxide Removal
T	Absolute Temperature
V_a	Applied voltage across the DBD reactor
V_b	Discharge gap breakdown voltage
V_d	Voltage across the dielectric barrier
V_g	Voltage across the discharge gap
V_{cm}	Voltage across the measurement capacitor C_m
Z_o	Characteristic impedance of RG405 Coaxial Cable

Chapter 1 INTRODUCTION

1.1 Overview

Nitric oxide (NO) and nitrogen dioxide (NO_2), commonly named as the combined term nitrogen oxides (NOx), mainly come from the combustion of fossil fuels, especially coal and diesel. Because 95% of NOx is NO [1], De-nitrification (DeNOx) processes are focused on NO removal and it is the reason why this research is focused on NO removal. High combustion temperature and oxygen rich conditions play important roles in forming NOx [2].

There are three main sources for NOx formation during burning fossil fuel [1].

Thermal NOx – The nitrogen component of thermal NOx comes from the air. During high temperature combustion processes, oxygen molecules are dissociated into oxygen atoms which can react with nitrogen molecules to form nitric oxide and nitrogen atom. The resulting nitrogen atom is able to form nitric oxide by reacting with an oxygen molecule according to the Zeldovich's mechanism [3, 4], as shown in Equations (1-1) and (1-2).

$$O + N_2 \rightarrow NO + N \quad \textbf{(1-1)}$$

$$N + O_2 \rightarrow NO + O \quad \textbf{(1-2)}$$

Fuel NOx – The nitrogen component comes from fossil fuel rather than from nitrogen in the air. It is easier to form fuel NOx because of the presence of pre-ionised nitrogen species, such as -CN, -HCN and -NH in fossil fuel. More than 80% of NO comes from fuel NOx in coal combustion [5].

Prompt NOx – Nitrogen for prompt NOx comes from the air but relies on the species generated in fossil fuel reactions. Nitrogen oxidation occurs alongside the processes in Fuel NOx reactions, as some nitrogen reacts with hydrocarbon species from the fuel (like -C, -CH or $-CH_2$) to firstly form nitrogen species (-CN, -HCN and -NH) and then, following the reaction paths of the fuel NOx process to generate NOx.

In general, the concentration of NOx in the flue gas of a coal-fired power plant is in the range from 200 to 600 ppm depending on the source of coal, i.e. lignite, subbituminous or bituminous. The flue gas components from coal-fired power plant are shown in Table 1-1.

Table 1-1 Components of flue gas and corresponding volume in flue gas [6]

N_2	CO_2	O_2	H_2O	SO_2	NO_x
80.85%	9.5%	4.5%	5%	1100ppm	200-600ppm

where: 1%=10,000ppm.

Even though the main output from combustion is NO, NO_2 is more stable than NO under atmospheric or even lower temperature. Tropospheric NO_2 columns are used as an indicator of where most NOx emissions come from in the world, see Figure 1-1. The locations with high concentration NO_2 are predominantly in three areas, North America, Europe and Southeast Asia (mostly China and Japan)[7].

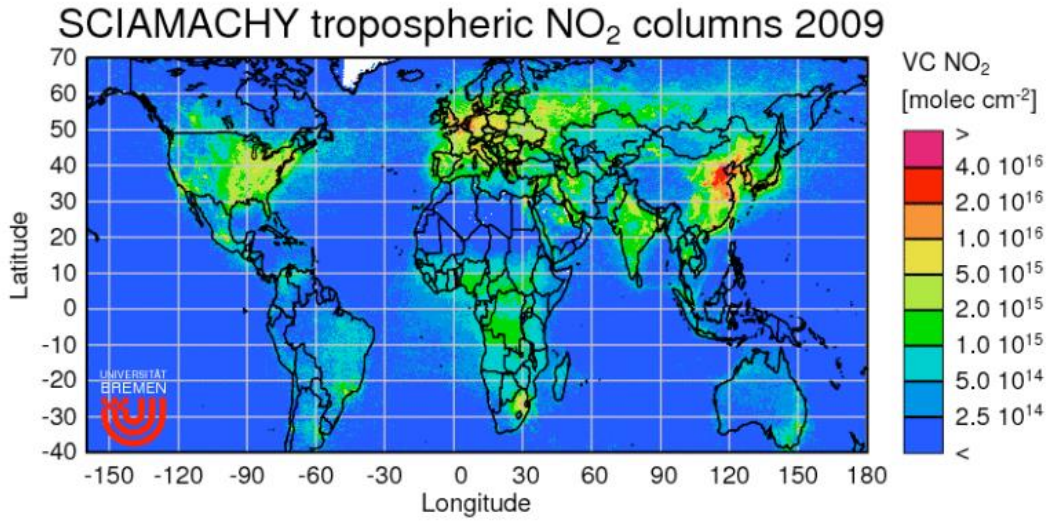

Figure 1-1 Satellite map of the global distribution of tropospheric NO_2 in 2009 [7]

NOx could bring many problems to people and the environment [8-10]. For example, high concentration of NOx in the environment can weaken lung function and cause some respiratory symptoms. In the United Kingdom (UK), legislation limits the concentration of NO_2 in the air to less than 40 $\mu g/m^3$ [11]. Chauhan et al [12] showed that with an increase of 50$\mu g/m^3$ (25 ppb) NO_2, there was a 2.6% increase in asthma hospital admissions and a 1.3% increase in daily mortality. In addition, nitric acid generated from NOx can hinder plant growth because of the change of pH in soil. Odiyi and Enida [13] showed a change of plant height by watering with different pH solution for fifteen weeks. The height of the control plants grew to 54.74cm by watering with distilled water of pH 7, but the height of other plants grew to only 10.01cm by watering with a solution of pH 2.

As a result of the effect of NOx on human health and the environment, NOx emission standards are enforced in most of countries. The data for the European Union (EU), the United State (US) and China are shown in

Table 1-2.

Table 1-2 NOx emission standards in EU, US and China, (unit: ppm)

Economical entities	Emission standard for new boiler	Emission standard for existing boiler
EU[14]	250[(a)]/100[(b)]	250[(a)]/100[(b)]
US[15]	60[(c)]	60[(c)]/80[(d)]
China[16]	50[(e)]	50[(e)]/100[(f)]

NOx emission standard for boiler built
(a) before 2016, (b) after 2016.
(c) after 2005; (d) between 1997 and2005;
(e) after 2004; (f) before 2004.

At present, the most widely used technologies for DeNOx is selective catalytic reduction (SCR) and low temperature oxidation (LoTOx). SCR uses ammonia as reductant to reduce NO to N_2 in the presence of a catalyst. The two most expensive components of SCR are the catalyst and reductant (ammonia), which are approximately 60% of the total cost [17]. Moreover, the lifetime of the catalyst is approximately 2 years and, because 17g of ammonia is needed to remove 30g of NO [17], large volumes of ammonia are used continuously. LoTOx follows an oxidation mechanism to remove NOx by ozone (O_3) and, therefore, an ozone generator and oxygen gas source are needed for the technology. For both technologies, an additional gas source with or without catalyst is needed so, to improve the process efficiency and reduce ongoing costs, it is necessary to explore new technologies for NO removal without use of catalyst and additional gas source. Non-thermal plasma has been investigated as a potential solution for NO removal by researchers, because it can be used to treat the flue gas directly without additional catalyst and gas source. Although early work indicates low efficiencies, it is worthwhile further investigating the potential of non-thermal plasma technology for NO removal.

1.2 Research objectives

The objectives of this research are listed below:

- To understand the effect of discharge characteristics of DBD and corona discharge on NO removal through experiments.
- To assess ways of improving NO removal energy efficiency by DBD and corona discharge.
- To understand the effect of concentration of nitric oxide, oxygen and water vapour on reactive species formation for NO removal under DBD and corona discharge, when NO is in ppm level.
- To understand the mechanism of NO removal in high concentration (a few percentage in volume).
- To quantitatively identify the dominant reactive species for NO removal under different circumstances.

1.3 Thesis outline

This research is focused on DBD and corona discharge for NO removal under different gas compositions and chemical reaction pathways. The thesis is divided into seven chapters and the contents of the subsequent chapters are presented as follows.

Chapter 2 gives a comprehensive introduction to present commercial and laboratory technologies for DeNOx. Their mechanisms, advantages and disadvantages are discussed and compared. Two of the most commonly used non-thermal plasma technologies, DBD and corona discharges, are introduced. The characteristics of DBD and corona, such as the electron density in DBD discharge filament and different discharge modes under corona discharge, are discussed. In addition, the relevant chemical kinetics are investigated in detail, including the dissociation and ionization energies of different gas species. The chemical reaction pathways for NO removal by different reactive species (including N, O, OH and O_3) are explained.

Chapter 3 introduces experimental setups and related methodologies. A pneumatic control system is used to control the flow rate of different gas species. Two types of power supply are utilised in this research, one is 50Hz AC power supply with maximum 7kV peak voltage and the second is a DC power supply with maximum 20kV. The electrical signal measurement system is introduced. In order to measure the signal as accurately as possible,

nano-second discharge current impulse signals are measured under matched impedance condition. In addition, in order to quantitatively investigate the discharge characteristics of DBD, studies of the discharge current amplitude distribution are conducted. The mechanisms of NOx and ozone measurement are given and calculation of NO removal and energy efficiency are presented.

Chapter 4 presents the investigation of NO removal under DBD. First, the design of the DBD reactor and experimental procedures are discussed in detail, including the size of the reactor, thickness of dielectric and gap and how to get different concentration of NO and O_2 in the gas mixture. The discharge characteristics of DBD are analysed, including use of the Lissajous figure, which provides the capacitances of dielectric, gas gap and total capacitors and the discharge power, and the discharge current amplitude distribution, which implies the change of the gas components. Under different gas mixtures, the discharge current amplitude shows a significant difference. Second, the effectiveness of NO removal is investigated under different initial NO and O_2 concentration. In order to analyse the effect of O_3 on NO removal, a reference gas mixture only including N_2 and O_2 is used to measure the O_3 formation. Comparing the O_3 formation in the reference gas with that of others, the dominant reactive species can be identified quantitatively. After the investigation of NO removal under dry gas conditions, 2.31% H_2O vapour is added to the gas mixture to evaluate the effect of OH reactive species. Study of the results from the coexistence of H_2O and O_2 allows the effect of OH and O for NO removal to be discussed. In addition, the effect of higher temperature on NO removal is investigated. Finally, conclusions are given including NO removal and energy efficiency, the contribution of this research for NO removal technology and its limitations and challenges.

Chapter 5 presents the investigation of the pin-water configuration corona discharge for NO removal. First, the pin-water reactor configuration and experimental procedures are introduced. Compared to a conventional pin-metal plane configuration, the pin-water configuration can bring more H_2O vapour into the gas mixture with the increase of discharge power, so more OH can be generated. Because of the characteristics of corona discharge, reactive species are mainly formed at the tip of the pin. The contact between NO and the reactive species in the gas plasma is important in removing NO. In order to quantitatively analyse this effect, two gas flow conditions are investigated. One is a controlled gas flow condition, where a nylon tube is used to guide the simulated flue gas through the volume around the pin's tip. The other is an open gas flow condition, where no nylon tube covers the tip and simulated flue gas can leave the containment vessel above the pin's tip. For negative

corona discharge, the effects of discharge modes (including Trichel pulse, pulseless and arc discharge), gap distance, O_2 concentration and the pin's radius of curvature are investigated. A comparison between the pin-water and the pin-metal plane configurations for NO removal is made. Finally, the NO removal and energy efficiency are given. The potential and challenges of this NO treatment technology for industry are discussed.

Chapter 6 introduces a novel technology which combines a NO absorption process by activated carbon, a thermal desorption process and reactions under a non-thermal plasma. The aim of this technology is to investigate the NO removal under higher concentration regime (up to 6%, 60,000ppm) rather than lower level (less than 1000ppm) as discussed in chapter 4 and 5. NO absorption, thermal desorption and non-thermal plasma treatments are investigated, respectively. For the NO absorption process, the effects of O_2 and H_2O concentrations, temperature, and flow rate are investigated. For the thermal desorption process, a DC power supply is directly connected to conductive activated carbon to heat the material and release the trapped species into the N_2 carrier gas. The effects of N_2 carrier gas flow rate and DC current, which controls the heating rate of activated carbon, are analysed to increase the thermal desorption energy efficiency. The DBD treatment of the desorbed NO by pure N_2 and a mixture of N_2 and O_2 in 10.5% and 50% O_2 conditions are analysed and are shown to result in different NO removal mechanisms. Finally, the advantages and limitations of this novel technology for NO removal are discussed.

Chapter 7 summarises the findings of this research, including the discharge characteristics of DBD and corona discharge, the corresponding chemical reaction pathways for NO removal by different reactive species, NO removal and energy efficiency for NO removal under three different methods. The contributions of this research to industrial NO removal technology are introduced. Some unsolved challenges are discussed, such as low energy efficiency for direct non-thermal plasma treatment and high thermal desorption energy requirement to desorb NO from activated carbon. Proposed future work is listed in the final part, including the combination of non-thermal plasma with catalyst, the use of nano-second pulse power to increase the energy efficiency, the investigation of an alternative absorbent which has higher selectivity on NO alone and the dynamic process analysis during the gas discharge by laser induced fluorescence spectroscopic method or building a chemical kinetics model by simulation.

Chapter 2 LITERATURE REVIEW

2.1 Introduction

In this chapter, some industrial technologies for NO removal are reviewed. There are two NO removal pathways, one is NO reduction to N_2 by selective catalytic reduction (SCR) and selective non-catalytic reduction (SNCR) technologies. The other one is NO oxidation to HNO_3 to NH_4NO_3 by Electron beam (EB) and low temperature O_3 oxidation (LoTOx) technologies. The advantages and disadvantages of each industrial technology for NO removal are discussed in this chapter. In terms of their disadvantages, what the non-thermal plasma technology can possibly do to overcome them is introduced. The mechanism of how non-thermal plasma can initiate gas molecule dissociation and ionization is explained. The chemical kinetics of NO removal are important as this provides theoretical support to the identification of the dominant reactive species for NO removal in Chapters 4, 5 and 6. There is more than one reactive species which can remove NO, e.g. N, O, OH and O_3, and they brings different reaction pathway for NO removal. However, some reactive species can introduce side reactions and some can catalytically react with others, which limits the NO removal performance. The details of how different reactive species interact with each other for NO removal are discussed. In addition, some investigations by other researchers, including work on DBD and corona discharge, are reviewed, as these can provide a good reference and justification of the experiments conducted in this research.

2.2 DeNOx technologies

2.2.1 Selective catalytic reduction (SCR)

SCR is the most widely used technology to treat NOx, which exists in the effluent gases from the coal-fired power plant, and other stationary sources. The catalyst applied in SCR is based on vanadium pentoxide and titanium dioxide. The basic process of SCR has been explained by Topsoe Nan-Yu [18, 19] and is shown in Figure 2-1.

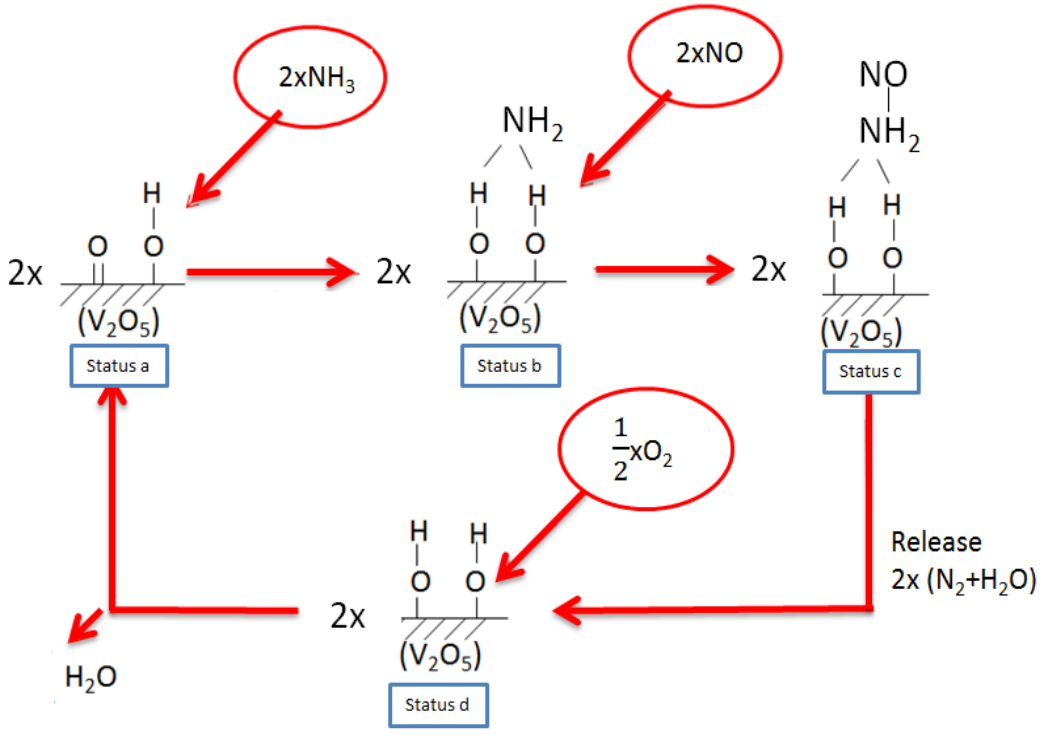

Figure 2-1 Process of vanadia-titania based catalyst for NOx removal [18]

On the surface of vanadium pentoxide (V_2O_5), there are some oxygen functional groups which are acidic. They can selectively extract ammonia (NH_3) (usually hundreds of ppm) from the gas phase to the surface of the catalyst. As a result, NH_3 is chemically absorbed and a new chemical bond is formed between the catalyst's oxygen atom and ammonia's nitrogen atom, as shown in the transition from status a to status b in Figure 2-1. A restrained amidogen ($-NH_2$) radical is exposed on the surface of the catalyst; this radical species will react with NO to remove the molecule from the gaseous atmosphere. The advantage of SCR is in providing a stable, longer lived site for amidogen to survive on. This dramatically increases the possibility of reaction between restrained NH_2 and NO. Finally, in order to

make the catalytic cycle work, additional hydrogen atoms have to be removed from the surface oxygen functional group. O_2 is used to remove hydrogen atoms to form water and convert the catalyst back to its original status as shown in Figure 2-1. The general reaction formula is given by equation 2-1:

$$2NH_3 + 2NO + \frac{1}{2}O_2 \rightarrow 2N_2 + 3H_2O \quad \textbf{(2-1)}$$

According to (2-1), the molar ratio between NH_3 and NO is one.

In terms of SCR technology for NO removal, another advantage of the catalyst is in reducing the activation energy for NH_2 formation. As shown in Table 2-1, the energy requirement is reduced by more than five times the original amount because of the presence of the catalyst.

Table 2-1 Activation energy of NH_2 formation with or without catalyst

	With catalyst	**Without catalyst**
Activation energy of NH_2 formation (eV)	1.11[20]	5.73[26]

In conclusion, the advantage of using a catalyst is not only in reducing the activation energy to obtain NH_2 radical species, but also in prolonging the lifetime of NH_2. This is why SCR can provide higher than 80% NO removal and is widely used in industry.

2.2.2 Selective non-catalytic reduction (SNCR)

Compared to SCR technology, SNCR is a cheaper method [21-24] for NO removal. The most important advantage of SNCR is that it works in the absence of catalyst, so it leads to approximately 40% reduction on DeNOx cost. However, as the NO reduction rate is only 30-60% of the SCR process it cannot provide sufficient NO reduction to satisfy the more and more restrictive NOx emission standards being applied in industry. Although SNCR does not use a catalyst, ammonia is used in both SCR and SNCR technologies. Because of the absence of a catalyst in SNCR, the probability of NH_2 formation is much lower than that in SCR. Although the general chemical reaction is the same for SCR and SNCR, as shown in (2-1), the formation of NH_2 is limited by the shortage of OH and O.

As shown in

Figure **2-2**, the main reaction producing NH_2 is the oxidation of NH_3 by O or OH radicals based on equations (2-2) and (2-3), but there is a self-limiting process which prevents a self-sustaining chain reaction. There are two reaction pathways between resulting NH_2 and NO. The pathway in (2-4) forms N_2H and OH, which are both able to provide additional O and OH to sustain the process. The pathway in (2-5) forms the final products N_2 and H_2O vapour, but it leads to no further O or OH production: the reduction process cannot be sustained.

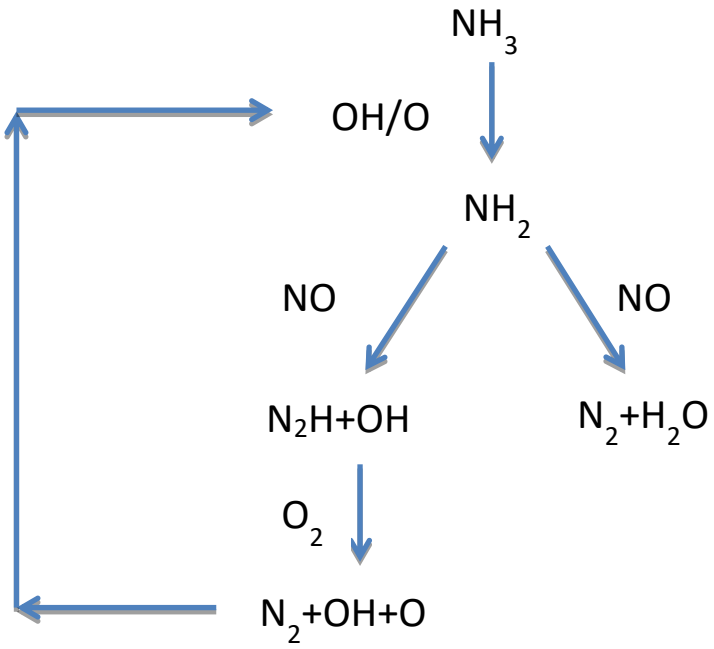

Figure 2-2 Main reaction pathway for NO removal by SNCR technology [21]

$$O + NH_3 \rightarrow OH + NH_2 \quad \textbf{(2-2)}$$

$$OH + NH_3 \rightarrow H_2O + NH_2 \quad \textbf{(2-3)}$$

$$NO + NH_2 \rightarrow N_2H + OH \quad \textbf{(2-4)}$$

$$NO + NH_2 \rightarrow N_2 + H_2O \quad \textbf{(2-5)}$$

As shown in reactions (2-6) and (2-7), a hydrogen atom plays an important role in generating O and OH.

$$N_2H + M \rightarrow H + N_2 + M \quad \textbf{(2-6)}$$

$$H + O_2 \rightarrow O + OH \quad \textbf{(2-7)}$$

where: M can be any gas molecule in the system.

However, NH_3 will react with H according to (2-8) and, once an H atom is used in the reaction with NH_3 rather than O_2, it produces species which are less reactive and NH_2 formation drops significantly. The self-sustaining chain reactions cannot be realised [21].

$$H + NH_3 \rightarrow NH_2 + H_2 \quad \textbf{(2-8)}$$

Another possible reason limiting SNCR for DeNOx is that whereas the NH_2 formed is in the free state, in SCR the NH_2 is attached on the surface of the catalyst where restrained NH_2 has a longer lifetime and higher opportunities to react with NO.

These two possible reasons lead to low NO removal efficiency in a range from 30% to 60% in SNCR. In addition, because there is no catalyst to reduce the activation energy for the reaction between NH_3 and NO, SNCR's working temperature needs to be above 800^{o}C compared to 350^{o}C to 450^{o}C working temperature in SCR.

2.2.3 Electron beam (EB) for DeNOx

EB technology for DeNOx was developed in the 1990s. Highly energetic electrons play the most important role in EB technology. The energy level of electrons is in the range from 700 to 800 keV. This technology has been applied in three power plants listed in Table 2-2.

Table 2-2 Main parameters of industrial EB installation for NO removal [25]

Parameters (Unit)	Chendu TPP China (1998)	Hangzhou TPP China (2003)	Pomorzany EPS, Poland (2002)
Flue gas flow rate (Nm^3/h)	300,000	305,400	270,000
Flue gas temperature (^oC)	150	145	140
NOx concentration (ppm)	410	205	300
NOx removal (%)	18	55	70
Energy efficiency (g/kWh)	45.1	69.8	71.1
EB sources	800keV 320 kWx2	800keV 320kWx2	700keV 260kWx4

As shown in Table 2-2, the working temperature of electron beam technology is approximately 150^{o}C, which is lower than those required for SCR (350-450 ^{o}C) and SNCR (> 800 ^{o}C). However, in EB systems the NO removal efficiency ranges from 18% to 70%, which implies that the efficiency of this technology for NOx removal is related to the condition of the flue gas. The concentration of particles, water vapour and oxygen in the flue gas can limit the distance that energetic electrons can travel, so the effective treatment area can be reduced.

In terms of the mechanism for EB technology for DeNOx, the most important process is gas molecule dissociation by energetic electrons. However, the electrons are more likely to collide with high concentration background gas molecules, such N_2, O_2 and H_2O vapour, than low concentration NO. Reactive species, e.g. N, O, O_3, HO_2 and OH, are generated from collisions and these then react with NO as shown in Figure 2-3 [26]. Since most reactive species are reactive oxygen species (ROS), i.e. O, O_3, HO_2 and OH, the DeNOx process follows oxidation pathways instead of reduction pathways. However, ammonia is still needed to absorb gas phase nitric acid. The reaction product, ammonium nitrate, is a useful economic by-product as it acts as a chemical fertiliser for agriculture [27].

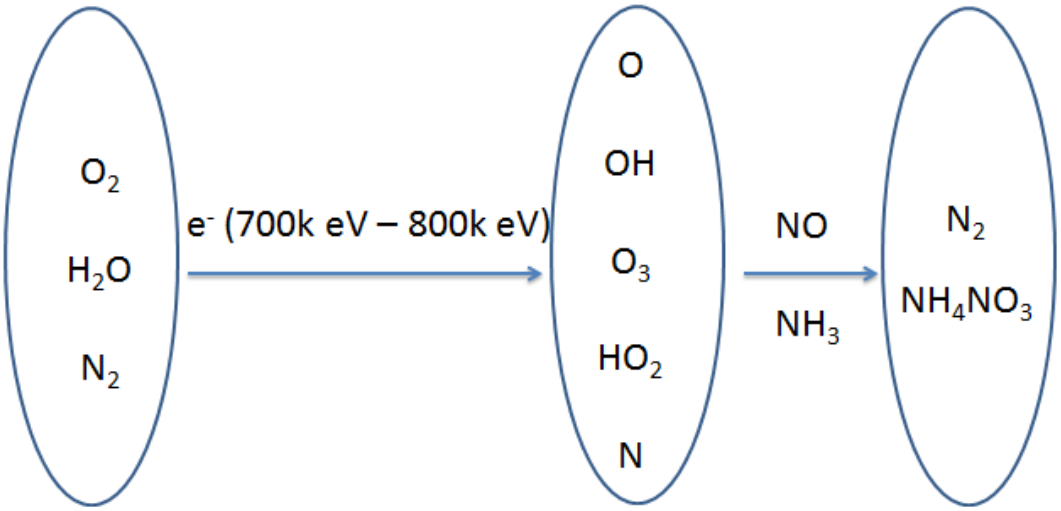

Figure 2-3 Electron beam technology reactions for NOx removal

According to the data from Chengdu TPP power plant in Table 2-2, the electron density is in the range of 10^{10} to 10^{11} /cm^3. In dielectric barrier discharge (DBD), the electron density is in the range of 10^{14} to 10^{15}/cm^3, as will be discussed later and shown in Table 2-12. The electron density in EB technology is 10^4 times lower than that in DBD, so EB is a relatively weak ionization process compared to DBD. The main problems of EB technology are inconsistent efficiency of NO removal, which depends on the condition of the flue gas, and the high installation cost of the electron beam source, because of radiation concerns. This is why the development of electron beam technology for DeNOx has stagnated in the 21st Century.

2.2.4 Ozone oxidation

Ozone oxidation technology was registered by Linde as low temperature oxidation (LoTOx) technology. It was commercialized for DeNOx in petroleum refineries, where the temperature of the flue gas is usually lower than 150^{o}C. The SCR technology cannot be used in such low temperature conditions, because the catalyst is inactive. Meanwhile, under higher temperatures, LoTOx technology cannot be used because of fast O_3 dissociation, as shown in Table 2-3. For instance, the half-life of O_3 at 250^{o}C is only 1.5 seconds, but it can extend to 1.5 hours at 120^{o}C, the extended half-life gives greater chance of useful DeNOx reactions.

Table 2-3 Half-life of ozone at different temperatures [28]

Temperature (^{o}C)	**Half-life**
-50	3 months
-35	18 days
-25	8 days
20	3 days
120	1.5 hours
250	1.5 seconds

Ozone is a strong oxidant which can be used for NO oxidation and the final product is N_2O_5 by the series of reactions shown in equations (2-9) to (2-11).

$$NO + O_3 \rightarrow NO_2 + O_2 \quad \textbf{(2-9)}$$

$$NO_2 + O_3 \rightarrow NO_3 + O_2 \quad \textbf{(2-10)}$$

$$NO_2 + NO_3 \rightarrow N_2O_5 \quad \textbf{(2-11)}$$

The overall reaction is shown in (2-12). The molar ratio of NO:O_3 is 1:1.5 to oxidize two NO molecules to one of the water soluble gas N_2O_5.

$$2NO + 3O_3 \rightarrow N_2O_5 + 3O_2 \quad \textbf{(2-12)}$$

N_2O_5 can react with wet scrubber molecules such as NaOH to generate $NaNO_3$ in reaction (2-13). In addition to N_2O_5, NO_2 can react with NaOH, as shown in (2-14), which leads to a reduction of O_3 usage.

$$N_2O_5 + 2NaOH \rightarrow 2NaNO_3 + H_2O \quad \textbf{(2-13)}$$

$$2NO_2 + 2NaOH \rightarrow NaNO_2 + NaNO_3 + H_2O \quad \textbf{(2-14)}$$

Zhang Jia et al. [29] published the results of an investigation into O_3 injection with a NaOH solution wet scrubber for DeNOx in which more than 90% of NOx removal was obtained at a NO to O_3 molar ratio of 1:1. In general, for DeNOx by O_3 injection with wet scrubber, the molar ratio of NO to O_3 is from 1:1 to 1:1.5, depending on the temperature, residence time and type of wet scrubber [29-32].

LoTOx technology for NO removal is used in industries where the flue gas temperature is lower than 150^{o}C. Nowadays, the energy efficiency of commercial oxygen-fed ozone generators is approximately 150 g/kWh [33-35]. For a petroleum refinery with a flue gas containing 400 ppm of NO at a flow rate of 120,000 m^3/h, the NO output is 64.3 kg/h. Given that 1.5 O_3 molecules is needed to react with, and remove, 1 NO molecule, the O_3 usage is 154.3 kg/h. This requires the power rating of O_3 generator to be 1030 kW.

2.2.5 Laboratory scale technologies

2.2.5.1 Non-thermal plasma with additional hydrocarbon

A challenge for direct non-thermal plasma treatment is conditions of low NO concentration, i.e. in ppm range. One of the main reasons is the short lifetime of reactive species generated by a non-thermal plasma, which leads to a low chance of chemical reaction between reactive species and NO. Thus it is important to produce a long lifetime reactive species by non-thermal plasma. This is analogous to ozone oxidation technology, because when the flue gas temperature is lower than 150°C, O_3 has a long enough lifetime to react with the low concentration NO in the flue. However, the difference between ozone oxidation and this technology is where the oxidant is generated. For ozone oxidation, O_3 is generated in an externally located ozone generator. For this technology, the oxidant is directly generated in the flue gas. The generation process needs the help of propene, a member of the alkene class of hydrocarbons [36-40]. The function of propene is to react with the short lifetime reactive species such as O and OH to generate intermediate species, such as C_3H_5, C_3H_6OH, whose organic group are called R. These then react with O_2 to form oxidant RO_2 as shown in Figure 2-4. RO_2 can selectively react with NO to generate RO and NO_2 [38].

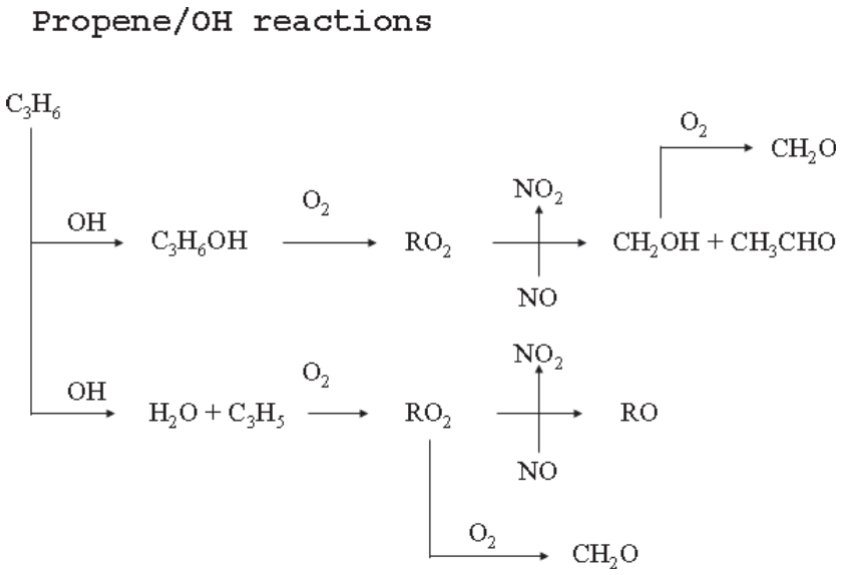

Figure 2-4 Schematic diagram of the chemical reaction mechanism of NO oxidation by propene under non-thermal plasma treatment [38]

However, there are two major problems for this technology. One is the high use of costly propene, in order to obtain full NO oxidation the molar ratio of NO to C_3H_6 is 1:1 [37]. The other problem is the formation of organic radicals, such as CH_2OH and CH_3CHO, which are toxic and need to be fully oxidized to CO_2 to avoid secondary contamination. Therefore, this technology is not commercialized.

2.2.5.2 Activated Carbon NO absorption

Activated carbon is a porous material with an enormous surface area. The surface area of one gram of activated carbon can be larger than one thousand square-metres. There are many oxygen containing groups, such as –COOH and -C-OH, on the surface of activated carbon. They have the ability to chemically absorb polar molecules, such as H_2O vapour and NOx. However, non-polar molecules such as homonuclear diatomic N_2, O_2 and symmetric-structured CO_2 are not absorbed by activated carbon.

In terms of categories of oxygen functional group on the surface of activated carbon, there are four main groups: the carboxylic group (-COOH), lactone group (-COO-), hydroxylic group (-C-OH) and carbonyl group (-C=O). The most popular method to quantitatively identify the surface oxygen functional groups is Boehm titration [41]. According to the acidic strength of each functional group, different basic chemical solvents can be used, as in Table 2-4, to determine the quantity of each oxygen functional group.

Table 2-4 Oxygen functional groups and their corresponding basic solvents [41, 42]

O-functional group	**-COOH**	**-COO-**	**-C-OH**	**-C=O**
Solvent	$NaHCO_3$ (0.1M)	$NaHCO_3$ (0.1M)	NaOH (0.1M)	$NaOC_2H_5$ (0.1M)

In terms of NO absorption by activated carbon, one challenge is its low selectivity between H_2O vapour and NO. As shown in Table 1-1, concentration of H_2O vapour in flue gases is much higher than that of NOx. If some of the surface oxygen functional groups interact with H_2O vapour rather than NOx, this reduces the NOx absorption by activated carbon.

In addition, as the amount of absorbed NO on the surface of activated carbon increases, the absorption ability is reduced. Once the NO concentration in the flue gas leaving the absorbent is higher than the emission standard, the activated carbon needs to be replaced.

The used activated carbon needs to be regenerated for continuous use. The regeneration method for activated carbon is called thermal desorption, as it uses high temperature to heat the activated carbon. With increased temperature, stronger vibration of the absorbed NO molecules can cause it release from the surface of activated carbon. When all of the absorbed NO molecules are released, the regenerated activated carbon can be used again. However, the weight of activated carbon is much heavier than that of the absorbed gases, 5 g of activated carbon is needed to absorb about 3.5 mL NO, whose equivalent weight is 4.68 mg. Heating the activated carbon is the main energy consumption during the NO desorption process as, for thermal desorption, the temperature of activated carbon has to reach approximately 150^{o}C to desorb all of the absorbed NO from the carbon surface, [43, 44]. Theoretically, using the heat capacity values in Table 2-5, the energy to heat 5g activated carbon to 150^{o}C from room temperature (20^{o}C) is about 604.5 J. That means the theoretical energy efficiency for thermal desorption of NO is 27.87 g/kWh. If the heat loss into the surroundings is also considered, the actual value should be even lower than that.

Table 2-5 Heat capacities of gas phase H_2O vapour, NO [45] and NO_2 [46] and solid state activated carbon [47]**.**

Species	Specific heat [kJ/(kg*K)] at STP
H_2O	1.93
NO	0.995
NO_2	0.8066
Activated carbon	0.93

Therefore, there are two challenges limiting NO absorption technology. One is how to selectively absorb NO and the other one is how to effectively remove NO from the activated carbon.

2.2.6 Discussion

When comparing the four industrial DeNOx technologies in Table 2-6, even though EB and SNCR technologies are cheaper, they cannot provide an acceptable NOx removal efficiency to meet the current NOx emission standards. Neither of these technologies is currently widely used nowadays. As a result of high NOx removal efficiencies, SCR and LoTOx technologies are commonly used, despite the high cost.

Table 2-6 Comparison of EB [48], SCR, SNCR and LoTOx [49] technologies for DeNOx

	Volume Capability	**Advantages**	**Disadvantages**	**NOx removal**	**Cost**
EB	Low or Medium	*****Economic by-product *****Works at low temperature	*****Low reduction rate *High ammonia use	18-70%	Medium
SCR	High	*****High removal *****Less secondary pollution	*****High temperature *****Catalyst usage	80-95%	High
SNCR	High	*****No catalyst needed *****Low cost	*****High temperature *High ammonia use and slip problem *****Low reduction rate	30-60%	Low
LoTOx	Medium	*****Stable and high removal *****Easy to operate *****Works at low temperature	*****High cost of ozone generator	80-95%	High

As shown in Table 2-6, although SCR and LoTOx are the two most commonly used technologies for NOx removal in different industry sectors. If the flow rate of flue gas is between 500,000 and 1,000,000 Nm^3/h (Nm3 is cubic metres in normal condition), usually, SCR is the first choice, especially, for large scale coal-fired power plants in the range from

300 to 600MW. LoTOx technology is usually used in relatively smaller scale industry sectors such as petrochemical refineries and combined heat and power plants (natural gas or bio fuel burning) where the flue gas flow rate is normally less than 100,000 Nm^3/h.

Because the main cost of SCR technology comes from the catalyst and reductant used, it is not possible to compare its deNOx energy efficiency with that of LoTox technology. Operational costs of SCR and LoTOx are compared in Table 2-7.

Table 2-7 SCR and LoTOx DeNOx technologies for 1 ton of NOx removal

Technologies	Cost for 1 ton of NOx
SCR	$2103-2704 [17]
LoTOx	$1700-1950 [50]

The operational cost of SCR in Table 2-7 is for a boiler with 75MW capacity. In this circumstance, the cost of LoTOx is cheaper than that of SCR, but when the boiler capacity increases to 300MW or higher, the cost of SCR dramatically reduces, as shown in Figure 2-5 which shows the relationship between boiler capacity and the DeNOx cost for the generation of 1kWh electricity.

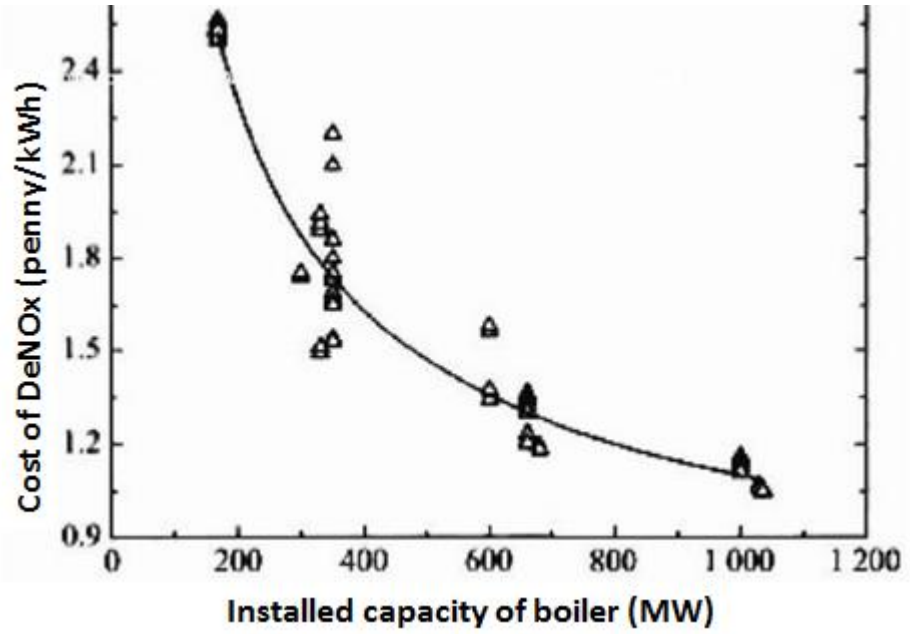

Figure 2-5 Relationship between cost of DeNOX and installed capacity of boiler [51]

From this, it can be seen that when the boiler capacity increases from 300MW to 600MW, the cost of DeNOx reduces from 1.8 penny/kWh to 1.3 penny/kWh, which is approximately

28% reduction in the cost of DeNOx. The cost reduces further if the boiler capacity increases to 1000MW. Therefore, according to different circumstances, i.e. the flue gas temperature, flue gas flow rate and boiler capacity, the best decision can be made between LoTox and SCR for NO removal.

2.3 Non-thermal plasma technologies for NO removal

2.3.1 Introduction

Plasma, the fourth state of matter, is ionized gas which consists of various species including electrons, atoms, molecules and ions. The density of positive ions and negative electrons is approximately equal, so plasma is an electroneutral state. There are two kinds of plasma which are identified by the temperature of heavy particles (including atoms, molecules and ions) and light electrons. One is thermal plasma where the temperature of heavy particles and light electrons is the same. An arc discharge is a thermal plasma and the temperature of both heavy particles and light electrons can reach approximately 11,600 K (1 eV). However, for non-thermal plasma, the temperature of electrons is much higher than that of heavy particles. The temperature of heavy particles is close to the ambient temperature, but the electron temperature is in the range of 10,000 to 200,000 K, corresponding to an energy range of 1 to 20 eV. These highly energetic electrons play an important role in gas ionization and dissociation processes. There are various methods to generate a non-thermal plasma, such as corona discharge, dielectric barrier discharge, glow discharge, radio frequency and microwave discharge [52]. Some of the most commonly used atmospheric pressure non-thermal plasma technologies for DeNOx are discussed in this section [53-57].

Table 2-8 N_2, O_2, H_2O vapour [58] and NO [59] ionization energy by energetic electron.

Reactions	Ionization energy (eV)
$\boldsymbol{N_2 + e \rightarrow N_2^+ + 2e}$	15.6
$\boldsymbol{O_2 + e \rightarrow O_2^+ + 2e}$	12.06
$\boldsymbol{H_2O + e \rightarrow H_2O^+ + 2e}$	13.0
$\boldsymbol{NO + e \rightarrow NO^+ + 2e}$	9.26

In addition to gas ionization, gas dissociation is also caused by energetic electrons. The dissociation energy of a molecule is usually less than its ionization energy, as shown Table 2-9. Although the dissociation energy of NO, at 6.536 eV, is close to that of O_2 and H_2O, direct NO dissociation is rare because of its low concentration (a few hundred ppm). Energetic electrons mainly collide with the high concentration molecules, i.e. O_2, H_2O vapour and N_2. The dissociation energy of N_2 is much higher than that of O_2 and H_2O, so O_2 and H_2O dissociation is more common than N_2 dissociation. Kogelschatz et al. [60] found that the concentration of O is approximately 100 times higher than that of N in a mixture of

20% O_2 and 80% N_2 using DBD discharge. As the main gases which dissociate are O_2 and H_2O and these produce O and OH, which are effective reactive species for NOx removal, this procedure shows promise for DeNOx.

Table 2-9 Dissociation energy for N_2, O_2 H_2O [58] and NO [61] dissociation.

Reactions	Dissociation energy (eV)
$\mathbf{N_2+e \rightarrow N(^4S)+N(^2D)+e}$	12.181
$\mathbf{O_2+e \rightarrow O(^3P)+O(^3P)+e}$	5.166
$\mathbf{O_2+e \rightarrow O(^1D)+O(^3P)+e}$	7.132
$\mathbf{H_2O+e \rightarrow O+OH+e}$	5.173
$\mathbf{NO+e \rightarrow N(^4S)+O(^3P)+e}$	6.536

where: P/S/D represent the different excited or metastable state of atomic N or O.

2.3.2 Chemical kinetics of NO removal by non-thermal plasma

For each chemical reaction, the reaction rate is an important parameter to indicate the change of reactants and product concentrations. There are two parameters which affect the reaction rate. One is reaction rate constant and the other is concentration of reactants, e.g. the reaction rate of the second order reaction A+B→C+D can be expressed as (2-15).

$$reaction\ rate = k[A][B] \tag{2-15}$$

where,
k is reaction rate constant, unit: $cm^3/(mol*s)$;
$[A]$ is concentration of reactant A, unit: $molecule/cm^3$;
$[B]$ is concentration of reactant B, unit: $molecule/cm^3$.

The reaction rate constant k is defined by the Arrhenius equation, as shown in (2-16).

$$k = A\left(\frac{T}{298K}\right)^n e^{-\frac{Ea}{RT}} \tag{2-16}$$

where,
T is the absolute temperature, unit: K;
A is the pre-exponential factor, determined by frequency of collisions;
E_a is the activation energy for the reaction, unit: $J* mol^{-1}$;
n is the temperature factor;
R is the universal gas constant 8.314472×10^{-3} kJ/(mole*K).

For non-thermal plasma NOx removal, chemical reactions between NOx and reactive species are important. Because of different reactive species, the products generated vary with different chemical reaction pathways.

In terms of an NO, N_2 and O_2 system, oxygen reactive species O and O_3 are the most important for NOx removal, as shown in Figure 2-6. However, the effect of O and O_3 on NO oxidation needs to be discussed.

$NO/N_2/O_2$ system without H_2O

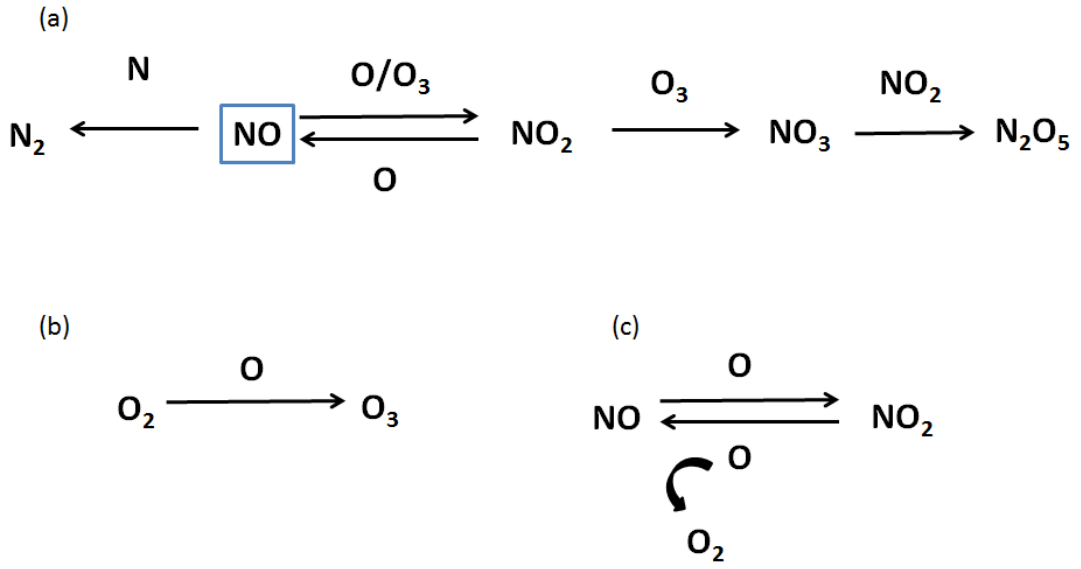

Figure 2-6 Chemical reaction pathway of NOx removal (a), chemical reaction pathway of O_3 formation (b) and chemical reaction pathway for O destruction by NO and NO_2 (c) in $NO/N_2/O_2$ system.

Table 2-10 Chemical reactions for NO oxidation in $NO/N_2/O_2$ system

Reaction	k_{298K} ($cm^3mol^{-1}s^{-1}$)	Ref	
$\boldsymbol{O + O_2 + M \rightarrow O_3 + M}$	1.48×10^{-14} ①	[62]	(2-17)
$\boldsymbol{O + NO \rightarrow NO_2}$	3.01×10^{-11}	[62]	(2-18)
$\boldsymbol{O + NO_2 \rightarrow NO + O_2}$	9.74×10^{-12}	[62]	(2-19)
$\boldsymbol{O_3 + NO \rightarrow NO_2 + O_2}$	1.81×10^{-14}	[62]	(2-20)
$\boldsymbol{O_3 + NO_2 \rightarrow NO_3 + O_2}$	3.52×10^{-17}	[62]	(2-21)
$\boldsymbol{NO_2 + NO_3 + M \rightarrow N_2O_5 + M}$	6.92×10^{-11} ①	[63]	(2-22)

where: ①: the reaction rate constant has changed from 3rd order to 2nd order by multiplying the concentration of M which is 2.462×10^{19} cm^{-3}.

In (2-17) and (2-22) M is a third reactant, whose function is to absorb extra energy from the reaction. M can be any molecule in the gas system, e.g. for O_3 formation in air, M can be O_2 or N_2. As shown in Table 2-10, the reaction rate constant for O_3 formation by the reaction between O_2 and O is 1.48×10^{-14} $cm^3mol^{-1}s^{-1}$. This is 2034 and 658 times lower than that for

the reaction between NO and O and the reaction between NO_2 and O, respectively. Thus, in a gas mixture with the same concentrations of NO, NO_2 and O_2, the O generated by non-thermal plasma predominantly reacts with NO or NO_2. O_2 is difficult to react with O. For the reactions between NOx and O, O is consumed by the reactions (2-23) and (2-24). Firstly, NO is oxidized to NO_2 by O, but then NO_2 is reduced to NO by O again. During this process as shown in Figure 2-6 (c), NO is unchanged, but two O are destroyed and converted to one O_2 as shown in reaction (2-25).

$$\boldsymbol{O + NO \rightarrow NO_2} \quad (2\text{-}23)$$

$$\boldsymbol{O + NO_2 \rightarrow NO + O_2} \quad (2\text{-}24)$$

The overall reaction:

$$\boldsymbol{O + O \xrightarrow{NOx} O_2} \quad (2\text{-}25)$$

Therefore, NO cannot be completely oxidized by O, because of the side reaction between NO_2 and O. However, as mentioned earlier, the reaction rate is dependent on the reaction rate constant and reactants' concentration. If the concentration of O_2 is much higher than that of NOx which can compensate for the lower reaction rate constant, it is possible to make the reaction between O_2 and O more important than that between NOx and O. O_3 is generated as oxidant rather than O and results in oxidation of NO to NO_2, NO_3 and N_2O_5 without the side reaction, as shown in (2-20)-(2-22). The product of NO oxidation by O_3 is dependent on the ratio of NO:O_3. If the molar ratio of NO:O_3 is 1:1, NO is fully oxidized to NO_2. If the molar ratio of NO:O_3 can reach 1:1.5, NO can be fully oxidized to N_2O_5.

In addition, if H_2O is introduced into the gas mixture of NO, N_2 and O_2, it produces another DeNOx reactive species, OH, for a totally different chemical reaction pathway compared to O and O_3. OH oxidizes NO and NO_2 to HNO_2 and HNO_3 by (2-26) and (2-27) in Table 2-11 without any side reaction as shown in Figure 2-7 (a).

Table 2-11 Chemical reactions for NO oxidation by OH reactive species

Reactions	k_{298K} ($cm^3mol^{-1}s^{-1}$)	Ref	
$\boldsymbol{OH + NO + M \rightarrow HNO_2 + M}$	1.72×10^{-11}	[64]	(2-26)
$\boldsymbol{OH + NO_2 + M \rightarrow HNO_3 + M}$	6.4×10^{-11}	[62]	(2-27)

where: the meaning of M is the same as mentioned in Table 2-10.

The presence of OH not only changes the chemical reaction pathway for NO removal, but also limits the formation of O and O_3 as shown in Figure 2-7 (b) and (c).

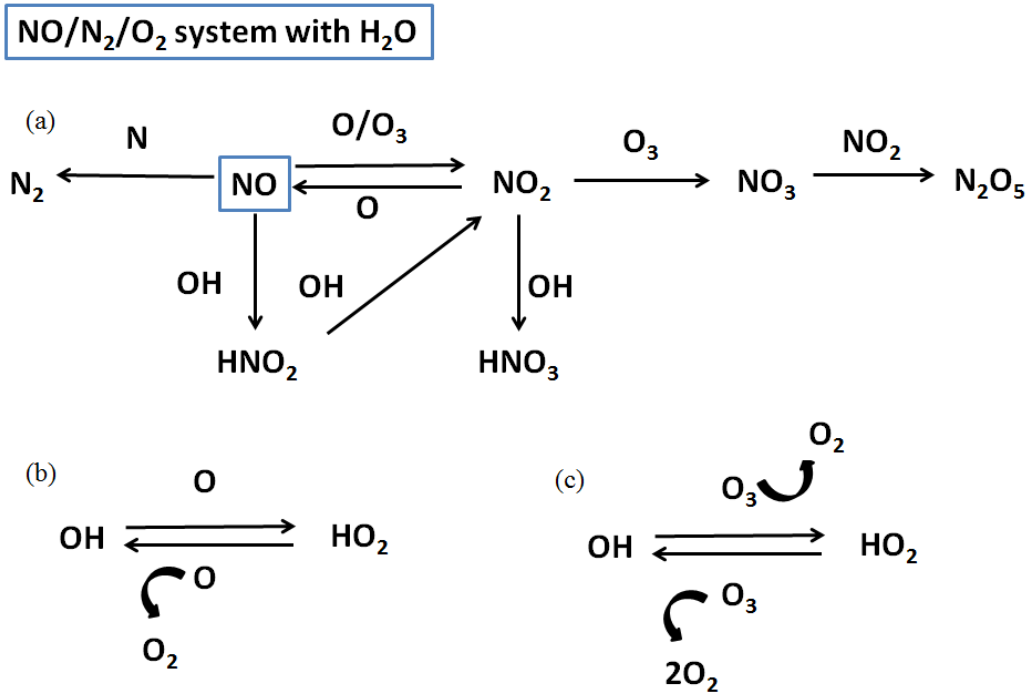

Figure 2-7 Chemical reaction pathway for (a) NOx removal, for O and O_3 destruction by OH and HO_2 in (b) and (c) respectively in $NO/N_2/O_2/H_2O$ system

In terms of O, it can react with OH to produce HO_2, and then HO_2 reacts with O again to produce OH. The overall process leads to two O atoms generating one O_2 molecule, as shown in (2-28) to (2-30).

$$\boldsymbol{O + OH \rightarrow HO_2} \quad (2\text{-}28)$$

$$\boldsymbol{O + HO_2 \rightarrow OH + O_2} \quad (2\text{-}29)$$

The overall reaction:

$$\boldsymbol{O + O \rightarrow O_2} \quad (2\text{-}30)$$

Similarly, for O_3, reactions with OH shown in (2-31) and (2-32) result in two strongly oxidant O_3 molecules converting to three O_2 molecules in (2-33).

$$\boldsymbol{O_3 + OH \rightarrow HO_2 + O_2} \quad (2\text{-}31)$$

$$\boldsymbol{O_3 + HO_2 \rightarrow OH + 2O_2} \quad (2\text{-}32)$$

The overall reaction:

$$\boldsymbol{O_3 + O_3 \xrightarrow{NOx} 3O_2} \quad (2\text{-}33)$$

In general, NO can be converted to N_2, NO_2 and HNO_2 by reactive species N, O or O_3 and OH, respectively, as shown in Figure 2-8. The issue of reactive species O is that it can cause the regeneration of NO by reacting with NO_2. However, when O reacts with O_2 to form O_3, O_3 does not have the side reaction to generate NO. Therefore, in a gas mixture system, it is important to identify the oxidant for NO removal. As mentioned before, the reaction rate is dependent on the reactant concentration and the reaction rate constant. Although the reaction rate constant for the reaction between O and NO is about 10^3 times higher than that for the reaction between O and O_2, the concentration of O_2 is much higher than that of NO in the gas mixture. Whether O or O_3 is the dominant reactive species is dependent on the specific circumstances. In addition, N is able to reduce NO to N_2, but it is more difficult to form N than it is to generate other reactive species, such as O, O_3 and OH, due to the high dissociation energy shown in Table 2-9. Once water vapour is introduced into the gas mixture, OH can bring another reaction pathway to remove NO. The reaction rate constant between OH and NO is of the same order as that between O and NO. These reactions are useful information to support the analysis of NO removal in the following chapters.

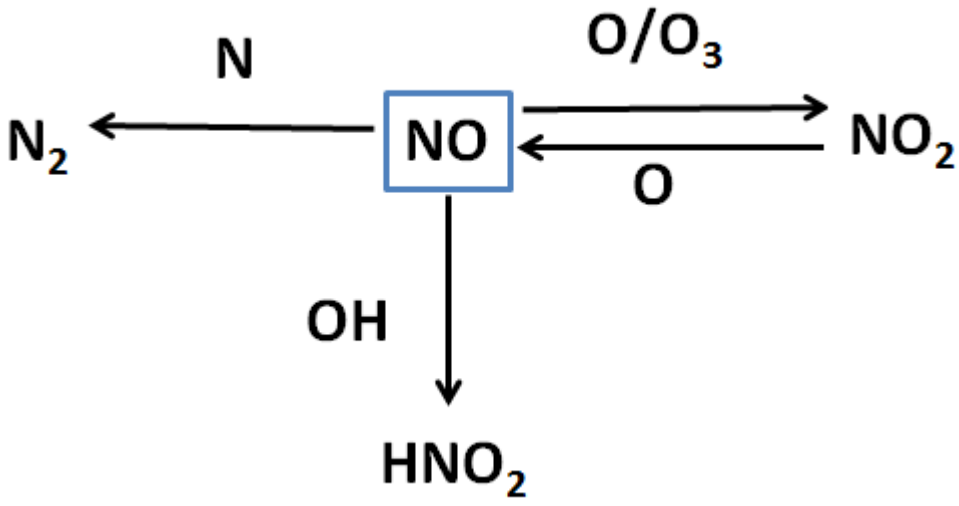

Figure 2-8 NO removal by different reactive species

2.3.3 Atmospheric pressure non-thermal plasma for DeNOx

2.3.3.1 Dielectric barrier discharge (DBD)

Dielectric barrier discharge, as one of the most commonly used non-thermal plasma technologies, has been researched for over one hundred years. The first configuration was designed by Siemens in 1857 for ozone generation experiments [65]. Given DBD reactor properties, it is easy to scale up the size of a DBD reactor for treatment of large quantities of gas [66]. The most successful industrial application using DBD is ozone generation [67, 68] but it has also been investigated for NO removal by many researchers [69-73]. The most ideal solution for NO removal is to dissociate NO directly to form N_2 and O_2 by energetic electrons which are generated by DBD, but the challenge is that the initial concentration of NO is usually a few hundred ppm in the flue gas, so it is difficult for energetic electrons to collide with NO directly. In most cases, energetic electrons collide with background high concentration gases such as O_2, H_2O vapour and N_2. When gas dissociation happens, various reactive species are produced including atomic O, O_3, OH and atomic N which can react with NO by different chemical reaction pathways as outlined earlier.

In order to initiate the process of gas discharge, the applied voltage has to be higher than the breakdown voltage under certain gas pressure and distance, as shown in the Paschen curve in Figure 2-9. Sohst [74] and Schroder [75] provided an empirical formula (2-34) for calculating breakdown voltage under uniform electric field for air at 20^{o}C condition .

$$V_b = 6.72\sqrt{pd} + 24.36(pd) \quad \textbf{(2-34)}$$

where:
V_b is breakdown voltage in kV
p is the gas pressure in bar
d is the gap size in cm

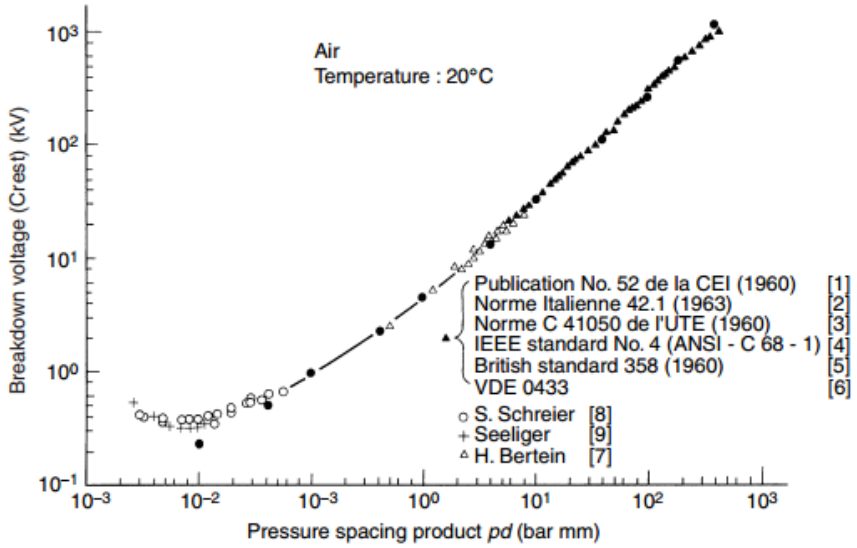

Figure 2-9 Paschen curve for air at 20°C condition[76].

In air under normal temperature and pressure conditions, the density of ions is approximately 10^2-10^3 cm^{-3} [77, 78]. However, when a discharge is initiated in air, the density of electrons and ions dramatically increases in the discharge channel, as the electron density can reach 10^{14}-10^{15} cm^{-3} [79], the charge density is increased by more than 10^{12} times. In order to initiate a gas discharge, a seed electron is required and the applied voltage has to be sufficient. Seed electrons come from gas ionization by cosmic rays or local radiation from the earth. When the applied voltage is higher than the minimum breakdown voltage, seed electrons can obtain enough energy from the electric field to ionize gas molecules and then a conductive discharge channel can be formed. Using (2-34), for a one cm gap under atmospheric pressure at 20°C, the applied voltage has to reach 31.08kV to make the discharge happen.

Two dielectric barrier discharge configurations are shown in Figure 2-10. Both of them are widely used for non-thermal plasma generation. There is no sharp point for the reactor, so they are working on uniform electric field condition and the breakdown voltage follows the Paschen curve in Figure 2-9. Under atmospheric pressure, dielectric barrier discharges work in the filamentary mode in air and the characteristics of filamentary discharge are introduced in Table 2-12.

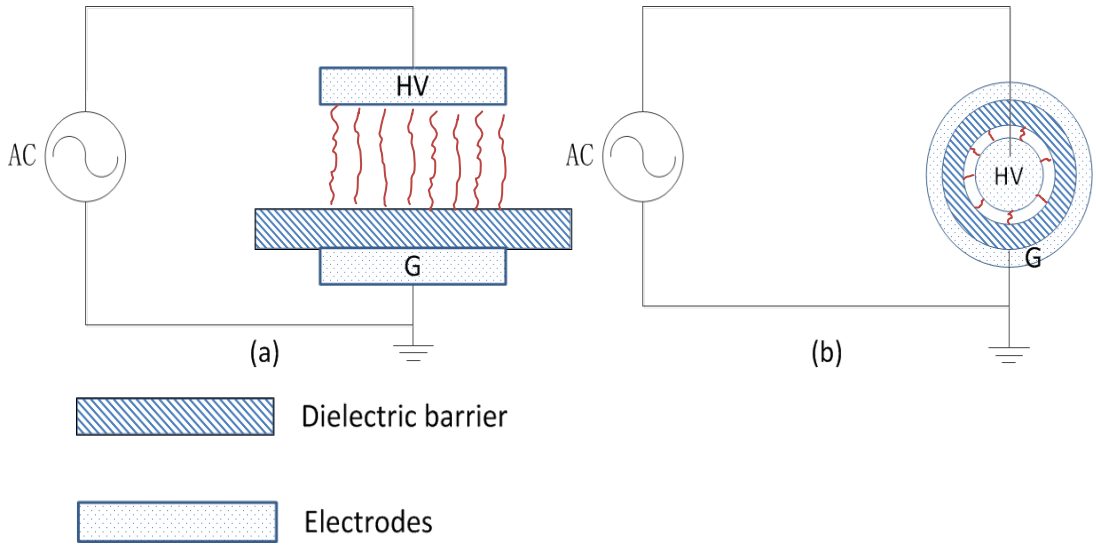

Figure 2-10 DBD configurations (a) plate to plate and (b) cylindrical form

Table 2-12 General characteristics of atmospheric pressure dielectric barrier discharges [79] [80]

	Random filamentary mode
Conditions	1 atm in air/oxygen
Gap size	1mm
Peak current density	100-1000A/cm^2
Current pulse duration	1-10 ns/filament
Filament radius	0.1mm
Total charge transfer	0.1-1 nC/filament
Peak electron density	10^{14}-10^{15} cm^{-3}
Electron energy	1-10 eV

Under the gas mixture of N_2, O_2, NO with or without H_2O for DeNOx, dielectric barrier discharge works in a filamentary mode. The advantage of a cylindrical configuration is that the electrical field is uniform for the whole gas discharge area, but for the plate to plate configuration, if isolation work is not done very well, corona discharge can initiate at the edge of the plate. The advantage of the plate to plate configuration is that it is easy to change the structure of the electrode from plate to mesh or multipoint. These configurations produce a non-uniform field which can make it easier to create electrical discharges.

Song et al.[81] used a cylindrical dielectric barrier discharge reactor, as shown in Figure 2-11, for NOx removal from a diesel engine, i.e. the gas contained particulate matter and hydrocarbons. A 15.5 kHz AC power supply was used to produce the plasma. At 50% engine load condition, the initial NOx concentration was 476 ppm, under different applied voltages the amount of NOx removed was from 238 ppm to 310 ppm and its energy efficiency was from 1.8 to 14.4 g/kWh.

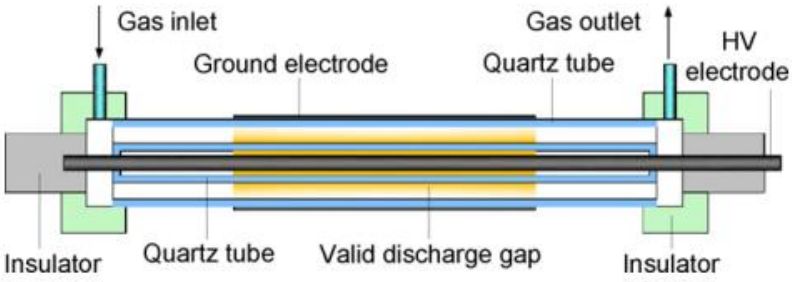

Figure 2-11 The configuration of a cylindrical dielectric barrier discharge reactor [81]

As discussed above, an advantage of the plate to plate configuration is that the shape of electrode can be easily changed from one to another. Takaki et al. [82] investigated the effect of DBD electrode shape on NOx removal using the arrangement in Figure 2-12 (a). The high voltage electrode was a plane covered by an alumina dielectric barrier, but the ground electrode used three different configurations as shown in Figure 2-12 (b). The gas mixture contained N_2, O_2 and NO, the volume ratio of N_2 to O_2 was 9 to 1 and NO concentration was 200 ppm. A radio frequency AC power supply (10 kHz) was used to energize plasma. The multipoint configuration provided the best NO removal results. For 70 ppm NO removal, its energy efficiency was 12 g/kWh, however, for 200 ppm NO removal, the corresponding energy efficiency was dramatically reduced to 2 g/kWh.

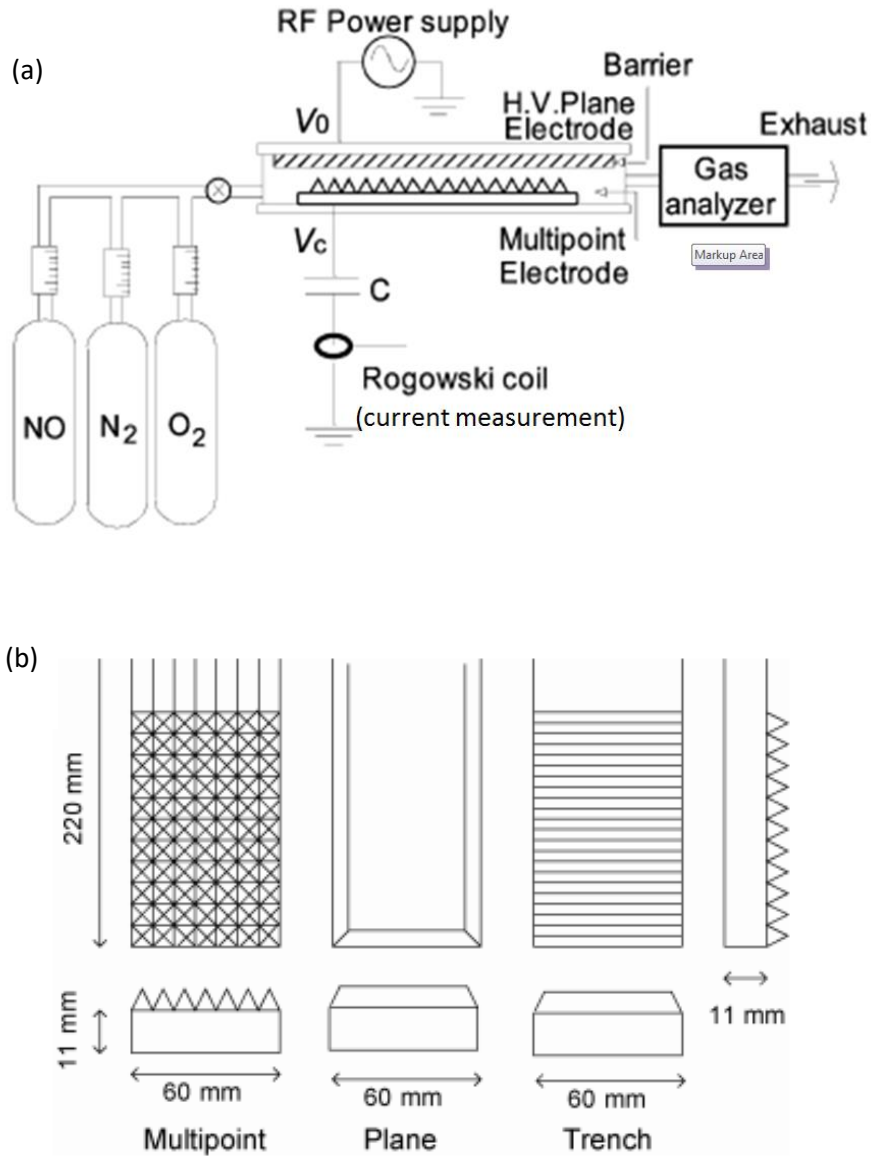

Figure 2-12 Experimental setup and electrode configuration [82]

According to the research discussed above, the energy efficiency of dielectric barrier discharge for NOx removal is less than 15 g/kWh. Although the electron density of DBD is 10^{14} to 10^{15}/cm^3, which is 10^4 times higher than that of an electron beam, the discharge energy is too concentrated in narrow discharge channels of ~0.1 mm radius. In addition, because of the short lifetime of reactive species and as they cannot diffuse quickly into the surroundings, they can only initiate local reactions. The low NOx removal energy efficiency leads to the difficulty in commercial use of direct DBD treatment for NOx removal at present.

2.3.3.2 Packed bed dielectric barrier discharge

Some researchers have, rather than using a dielectric to cover the surface of electrodes, filled the discharge volume with dielectric balls [83-86]. The size of dielectric balls is in the range from 1 to 5 mm. This system is called packed bed dielectric barrier discharge, see Figure 2-13, discharges occur because the dielectric balls distort the electric field. Commonly used dielectric ball materials are γ-alumina, barium titanate ($BaTiO_3$) and titanium dioxide (TiO_2), because they have very high relative permittivity, e.g. $BaTiO_3$'s relative permittivity is from 1,200 to 10,000. When dielectric balls fill the discharge space, because of high equivalent capacitance of dielectric balls, most of voltage is applied to the gas gaps. The spherical shape of a dielectric ball causes distortion of the electric field and discharge is easily initiated at the contact points on the surface of dielectric balls. In addition, some dielectric materials which can be considered to be photocatalytic materials, such as TiO_2, have the potential to promote the discharge process: when UV light with a wavelength shorter than 387nm irradiates the surface of TiO_2, an electron - hole pair can be generated. The presence of this electron and hole promotes the formation of reactive species such as O and OH [87, 88], so the presence of photocatalytic TiO_2 can probably promote NO removal process.

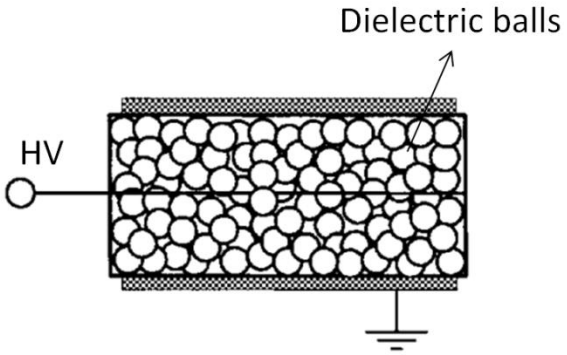

Figure 2-13 Configuration of packed bed dielectric barrier discharge [83]

Mok et al. [57] used glass beads as the dielectric ball in a DBD reactor and with an initial NO concentration of 300ppm. After packed bed DBD treatment, the NO concentration was reduced to 40 ppm and the NO removal energy efficiency reached 16.7 g/kWh. Kim et al. [83] used two combinations of types of dielectric balls. One was a combination of γ-alumina and $BaTiO_3$ (5:1 in volume) and the other one was a combination of γ-alumina and TiO_2 (1:1 in volume). A pulsed high voltage source with rise time of 25ns and duration of 2.5ms was

applied to energize plasma. From an initial NO concentration of 550ppm, the most effective NO removal energy efficiency was 16.5 g/kWh for 82% of NO removal.

Packed bed dielectric barrier discharge provides slightly higher energy efficiency for NOx removal, compared to DBD. One characteristic of packed bed DBD is that the discharge usually happens at the surface of the contact point of the dielectric balls. If the dielectric is one form of catalyst which can be activated and promote the formation of reactive species during the discharge process, the NOx removal energy efficiency can be further promoted. However, the packed bed structure brings some problems, e.g. when the flue gas contains particles it is possible that these could block the gas flow and a high pressure drop may occur as a result of the existence of dielectric balls. As a result, it is better to choose a cylindrical dielectric material than a filled packed bed to ensure there is no back pressure in the system.

2.3.3.3 Corona discharge

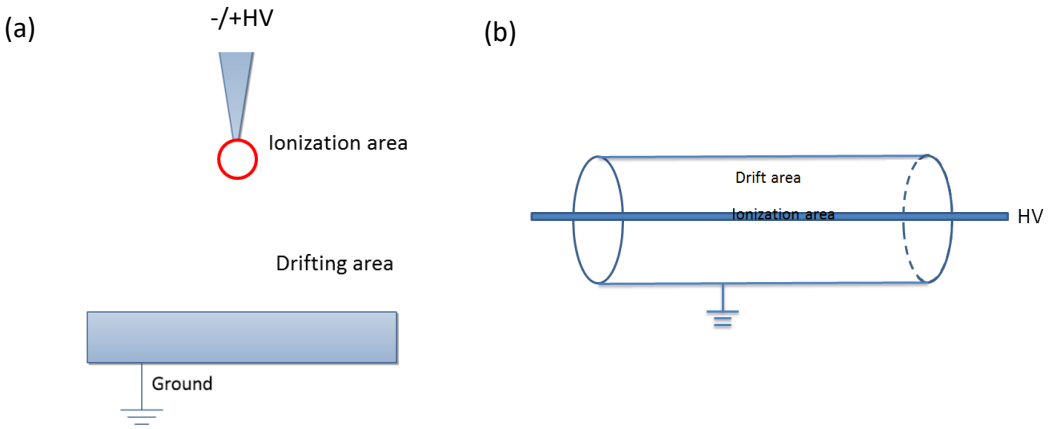

Figure 2-14 Schematic structures of (a) pin-plane and (b) wire-cylinder corona discharge

Because of the asymmetric configuration of two electrodes in the arrangements shown in Figure 2-14 (a) and (b), the electric field is intensively distorted and concentrated at the pin tip or the wire. When the electric field is high enough to initiate gas breakdown, gas ionization firstly happens around the pin and the wire, respectively. As mentioned in Table 2-9, the energetic electron plays an important role to generate reactive species for DeNOx and its generation process occurs around the pin tip or the wire at the voltage in negative polarity, hence the description of negative corona discharge. With the increase of distance from pin or wire, the strength of the electric field drops significantly and, as a result, the electron attachment effect becomes stronger, as shown in Figure 2-15. In order to be a self-sustainable discharge, the ionization coefficient α has to be higher than the electron attachment coefficient η which means the electric field has to be higher than 25kV/cm, otherwise, electrons are going to be attached to electronegative gas molecules such as O_2 and H_2O, and form negative ions which cannot make a further contribution to the ionization process. The effective ionization area is determined by the radius of curvature of the pin and the applied voltage.

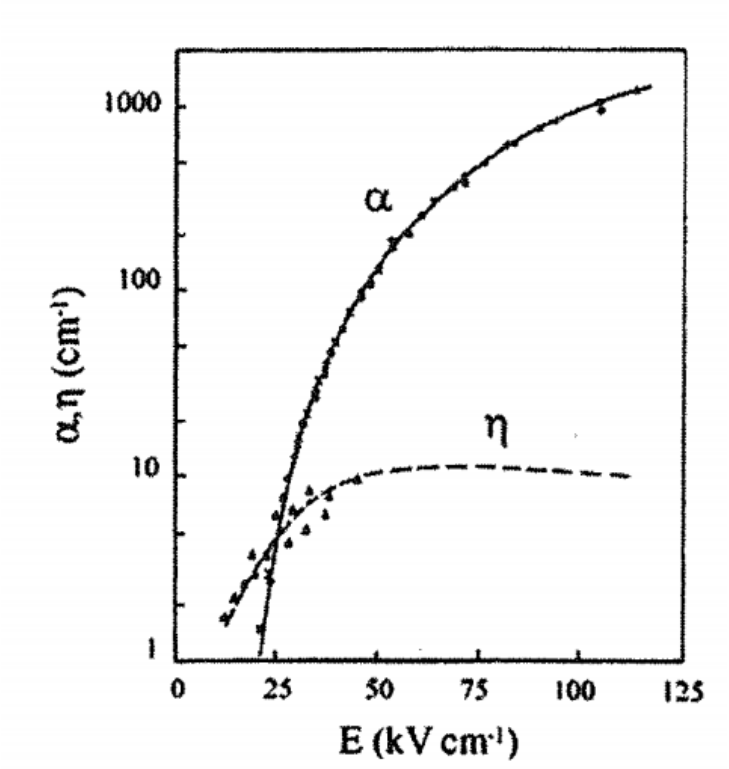

Figure 2-15 Ionization coefficient α and attachment coefficient ŋ at different electric field strengths in dry air [89]

As indicated in Figure 2-16, with increasing applied voltage, negative corona discharge has three discharge modes which are Trichel pulse discharge, pulseless discharge and arc discharge, respectively [90]. At the level when the applied voltage is just high enough to initiate a gas discharge around the pin, pulsed discharges occur. Because most of the voltage potential drop is around the pin, the corresponding discharge area is called the ionization area. The electrons generated in the ionization area move towards the plate, because of their repulsion by the pin of the same polarity and attraction to the plate which is grounded. The electron avalanche and the ionic cloud generated cause a reduction in the electric field between them and the pin. When the total electric field is lower than the breakdown requirement, the discharge extinguishes. When the electrons moves away from the ionization area and then the electric field increases to the level required for breakdown, the next discharge can start again, so the discharges are in pulse mode, which is called Trichel pulse [91]. With increasing applied voltage, the individual discharge current impulses become smaller but the time duration between two pulses is shorter. After a given voltage level the discharge current signals overlap each other and the discharge current reaches a steady state

[92] and becomes constant. This discharge mode is called pulseless discharge. If the applied voltage is further increased, the pulseless discharge cannot be sustained and it converts to arc discharge where the discharge current increases significantly and the energy density in the arc discharge filament is high. At this point the temperature is high enough to produce NO by the Zeldovich's mechanism [3].

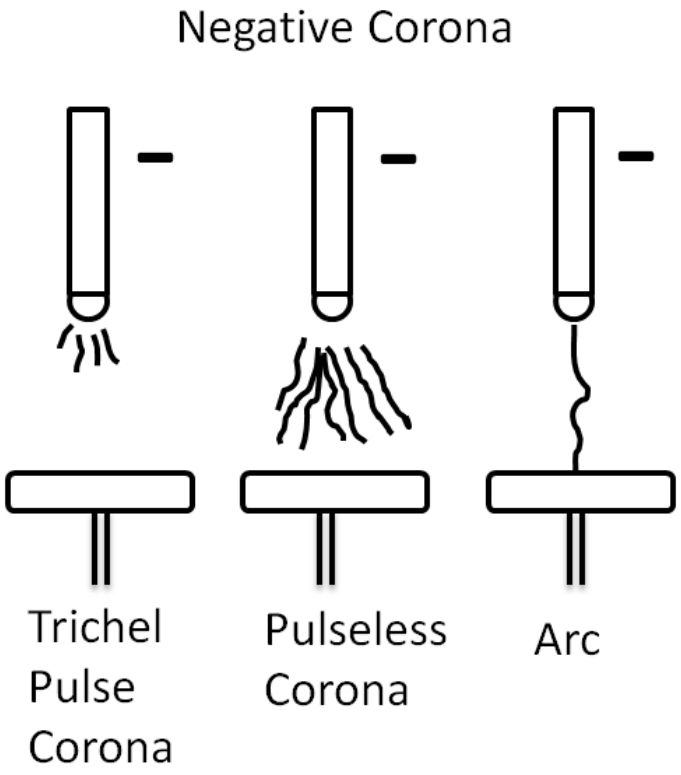

Figure 2-16 The development of negative corona discharge with increasing voltage [90]

In terms of NOx removal by corona discharge, many researchers were focused on reactive species injection from a nozzle, as shown in Figure 2-17. High voltages were directly connected to the nozzle and the reaction chamber was grounded. Gas discharge occurred around the nozzle to generate reactive species, such as O, OH, N and NH_2. Kanazawa et al. [93] investigated the effect of methane (CH_4) shower for NOx removal, because methane could react with O, N and H reactive species to form NH or NH_2 which reduces NO to N_2. The nozzle, whose dimensions are 1.5mm outer diameter, 1.2 mm inner diameter and 5mm long, was energized by DC power supply. A gas mixture of O_2 (19.23%), Ar (3.73%) and CH_4 (0.12%) in N_2 flowed from the nozzle to reaction chamber. At an NO concentration of 200ppm the energy efficiency for NO removal was from 1 to 7 g/kWh. Yan et al. [94]

investigated NOx removal by a similar reactor configuration. The NO removal energy efficiency increased from 5g/kWh when NO concentration was 140ppm to 24g/kWh when NO concentration increased to 421ppm.

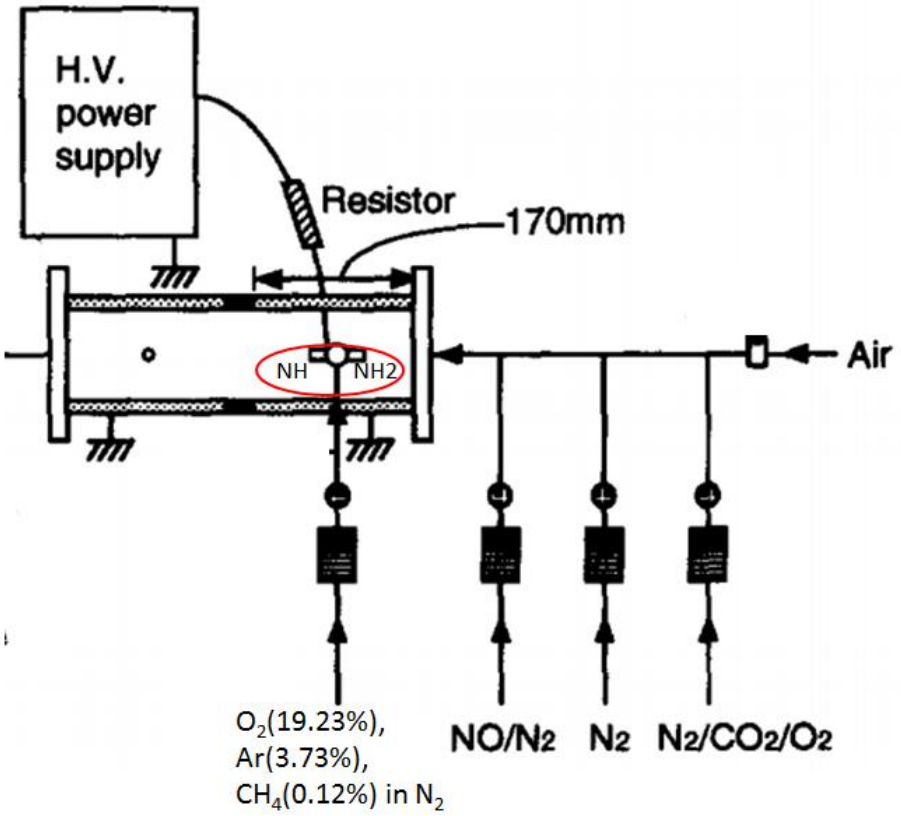

Figure 2-17 Experimental setup for corona discharge DeNOx [93, 94]

For corona discharge, the reactive species injection method is not an efficient way for DeNOx, due to the short lifetime of reactive species. Because the reactive species is injected to a large reactor, it is not possible to spray the reactive species into a large volume. In order to increase the NOx removal energy efficiency, the discharge should cover as large a proportion of the volume of the chamber as possible.

2.3.3.4 Nano second pulsed corona discharge

Pulsed power is able to provide a higher inception voltage compared to other power sources. As shown in Figure 2-18, although the peak voltage of waveform 1 and 2 are the same, the breakdown voltage (V_{b1}) of waveform 1 is larger than that (V_{b2}) of waveform 2. The impulse voltage rise time is shorter and the cross-point between the impulse waveform and V-t

characteristic curve becomes higher [76]: the cross-point represents the breakdown voltage of the system. The benefit of higher breakdown voltage is to increase the relevant electric field across the gas gap, and thus to increase the reduced electric field (E/d) which increases the average electron energy. There is, therefore, a higher proportion of electrons with enough energy to dissociate gas molecules and the energy input is used more efficiently.

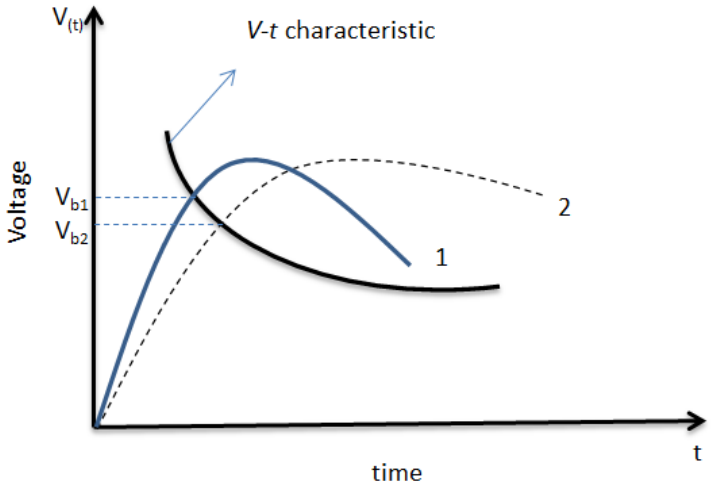

Figure 2-18 Impulse voltage-time characteristics [76]

In addition, nano-second pulsed power can reduce gas heating losses, caused by vibrational and rotational quenching, which happen in the glow-like discharge process, as shown in Figure 2-19. The red colour indicates high heating losses around the wire electrode as longer duration, glow-like discharges occur. In order to limit heating loss, it is important to control the pulse duration within 25 ns.

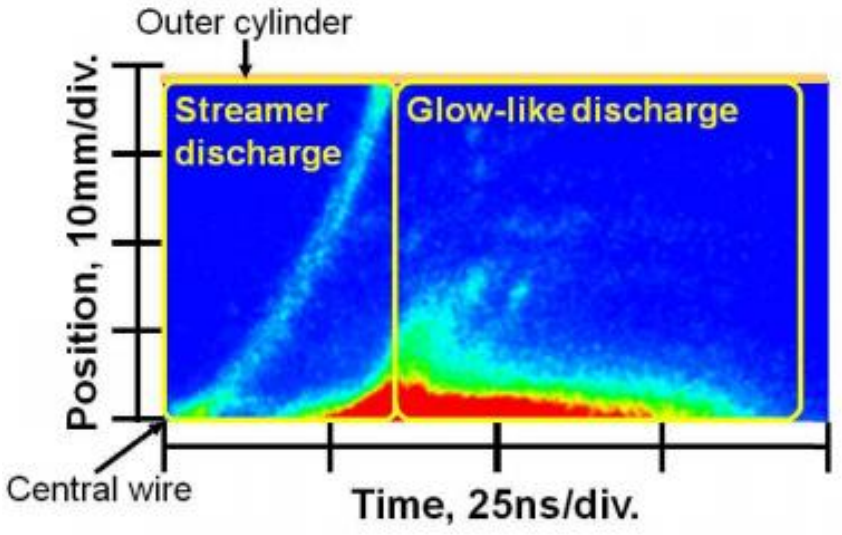

Figure 2-19 A streak image typical of pulsed discharge [95]

Namihira and Wang [95-97] investigated NOx removal using pulsed power in a wire-cylinder configuration. A HV stainless steel wire, 0.5mm in diameter and a copper cylinder with 76mm internal diameter were used as HV and ground electrodes respectively. When the pulse duration was reduced to 5 ns, NO removal energy efficiency was seen to significantly increase, up to 3.75 mol/kWh (112.5 g/kWh), as shown in Figure 2-20.

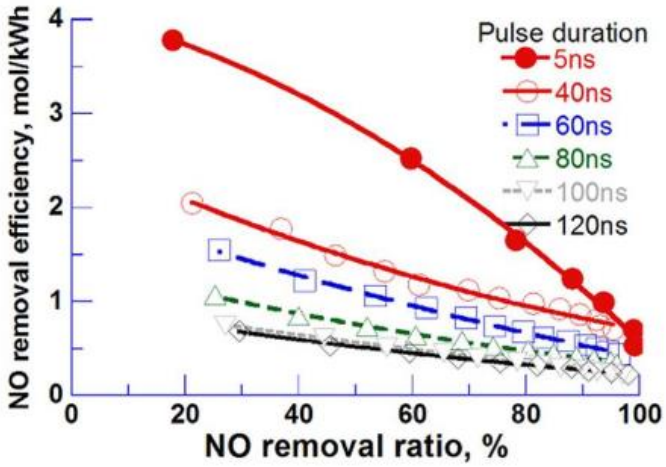

Figure 2-20 The NO removal energy efficiency vs. NO removal ratio for different pulse durations [95]

The problem with using nano-second pulsed corona discharge is the low energy level of pulsed power source, as the energy is transmitted from the capacitance of a pulse forming line. In [97], to generate a 5ns pulse signal a 0.5m pulse forming line, with inductance and capacitance of 140nH/m and 216pF/m, respectively, has a capacitance of only 108pF. If the charging voltage is 50kV, according to the capacitor energy equation $E = \frac{1}{2}CV^2$, the energy level of this pulse generator is only 0.135J. In order to increase the energy level the capacitance has to be increased, however, an increase in capacitance requires an increase in the length of the pulse forming line which leads to an increase in pulse transmission and, hence, in the pulse duration. Therefore, it is not currently possible to make a 5ns pulse power supply with kW level power for industrial application.

2.4 Conclusions

Four current industrial NO removal technologies have been introduced, SCR, SNCR, EB and LoTOx. SCR and LoTOx are the most popular ones, because they can provide higher NO removal efficiency. The drawback of SCR and LoTOx are the use of an additional gas source to support the NO removal process. SCR uses ammonia to reduce NO to N_2 with the help of a catalyst. LoTOx uses O_3 as oxidant to oxidize NO to N_2O_5 which can be easily collected by water or alkaline solution to get nitrite. Both technologies provide good results for NO removal, and at present, the energy efficiency is normally higher than 60 g/kWh.

For non-thermal plasma technology, in terms of chemical kinetics between NOx and reactive species, two reactive species destruction cycles, which convert strong oxidants O and O_3 to O_2, have to be considered. One is O destruction by the cycle of formation of NO and NO_2 and the other is O and O_3 destruction by the cycle of formation of OH and HO_2. Different reactive species can produce different NOx removal pathways. Reactive species O can oxidize NO to NO_2, but only partially due to the side reaction between NO_2 and O to generate NO. Reactive species O_3 can oxidize NO to NO_2 without any side reaction. In addition, if O_3 is still present after all of NO molecules are oxidized to NO_2, further oxidation to N_2O_5 can occur. Reactive species OH oxidizes NO and NO_2 to nitrite acid and nitrate acid, but limits the formation of O and O_3. Four atmospheric pressure non-thermal plasmas have been introduced, dielectric barrier discharge, packed bed dielectric barrier discharge, corona

discharge and nano-second pulsed corona discharge. The advantage of non-thermal plasma is that it can remove NO without the need of catalyst and additional gas source, but the disadvantage of non-thermal plasma technology is the low NO removal energy efficiency, usually less than 30 g/kWh in most non-thermal plasmas except for nano-second pulsed corona discharge. The highest energy efficiency, achieved by 5ns pulse duration pulsed corona discharge, is 112.5 g/kWh, but it is difficult to increase the power level of a pulse power system to satisfy the requirement of industry.

This chapter presented the current NO removal technologies used in industry and laboratory. NO absorption by activated carbon gives another inspiration for NO removal. It is worthwhile investigating further the effect of combining absorption with non-thermal plasma technology to analyse the reduction of NO under higher NO concentration. In addition, direct non-thermal plasma technologies DBD and corona discharge are discussed, including the mechanism and characteristics. Although the NO removal energy efficiency is too low to be commercialised, it is important to quantitatively analyse the NO removal process and explore new ways to improve the energy efficiency. This literature review provides many theories and principles to support the experiments conducted in Chapters 4, 5 and 6 for NO removal by DBD and corona discharge.

Chapter 3 EXPERIMENTAL SETUP AND METHODOLOGY

3.1 Introduction

This chapter presents the information on the experimental arrangements used in this research. As shown in Figure 3-1 there are six parts, including the pneumatic control system, power supply system, electrical signal measurement system, non-thermal plasma treatment system and NOx and O_3 measurement system, each of them will be explained in detail. First aspect to be described is the pneumatic (gas flow) control system, which is important as it allows production of different concentrations of NO, H_2O and O_2. The variation of initial NOx concentration is from 100 ppm to 1000 ppm, that of O_2 is from 0 % to 16.67 % and that of H_2O vapour is from 0% to 2.31%. After that, two power supplies, 0-7 kV 50 Hz AC and 0-20 kV DC, are discussed to specify their application on different non-thermal plasma technology. Third, the electrical signal measurement system which is one of the most important parts in this research is introduced, because it includes the measurement of the applied voltage, discharge current impulse, charge transfer and discharge power by Lissajous figure. Finally, the equipment used to measure gas concentration and the equations used to assess the level of NO removal, NO_2 and O_3 formations and their energy efficiencies are given. These experimental setup and methodologies are important as they provide underpinning knowledge prior to conducting the experiments in Chapters 4, 5 and 6.

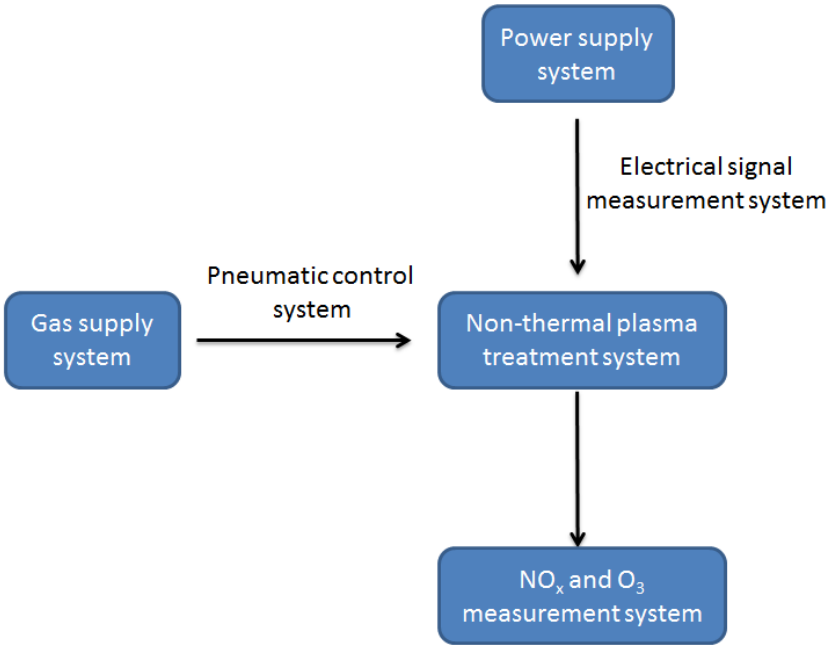

Figure 3-1 Block diagram of the experimental systems

3.2 Pneumatic control system

A schematic diagram of the pneumatic control system, which allows control of the mixture of gases in the test cell, is shown in Figure 3-2. It includes three gas sources, two of them are pure N_2 and O_2 and the last one is a mixture of N_2 and NO where the concentration of NO is 1000 ppm.

Three mass flow controllers from Alicat are normally used to realise the control of NO and O_2 concentrations as shown in Table 3-1. Because NO is defined as a corrosive gas, an anti-corrosive mass flow controller (MCS) is used to control NO gas flow. The other two controllers (MC) are used for non-corrosive gases, namely pure N_2 and pure O_2.

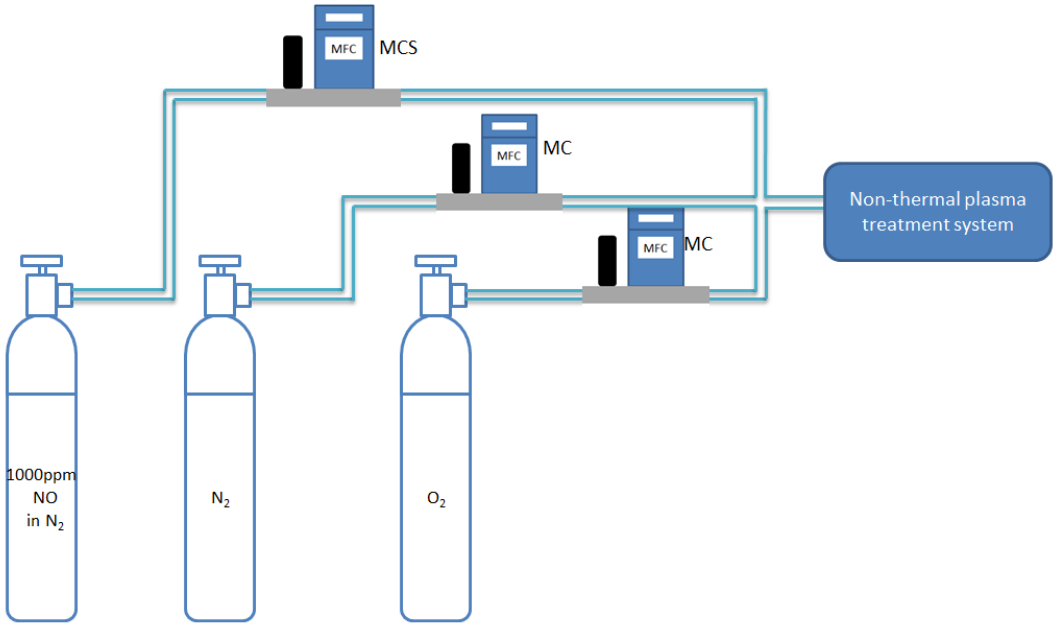

where:

MFC is mass flow controller

Both MCS and MC are the models of Allicat mass flow controllers, MCS is for corrosive gas (including NO) and MC is for non-corrosive gas.

Figure 3-2 Schematic diagram of the pneumatic control system

Table 3-1 Parameters for different model of Alicat mass flow controller

		Controlled gas	Measurement range	Resolution	Accuracy
Mass Flow controller	ALICAT (MCS Series)	NO in N_2	0-10 slpm	0.01 slpm	±0.8% of reading ±0.2% of Full scale
	ALICAT (MC Series)	N_2	0-5 slpm	0.001 slpm	±0.8% of reading ±0.2% of Full scale
	ALICAT (MC Series)	O_2	0-500 sccm	0.1 sccm	±0.8% of reading ±0.2% of Full scale

where:
slpm: standard litre per minute.
sccm: standard cubic centimetre per minute.
1slpm=1000 sccm.

The concentration of NO in the gas entering the plasma can be reduced by the injection of pure N_2 to the mixture of 1000 ppm NO in N_2. The total flow rate for the NO/N_2 gas mixture is held at constant 200 sccm. The concentration of NO under different flow rates of N_2 and NO are controllable from 100 to 1000 ppm as shown in Table 3-2.

Table 3-2 NOx concentrations under different N_2 and NO mixture

FR of 1000ppm NO in N_2 (sccm)	**FR of N_2 (sccm)**	**C_{NO} (ppm)**	**C_{NO2} (ppm)**
200	0	1000	0
120	80	608	0
40	160	206	0
30	170	153	0
20	180	102	0

where:
FR is flow rate;
C_{NO} is the concentration of NO;
C_{NO2} is the concentration of NO_2

The concentration of O_2 is controlled by adding O_2 into the 200 sccm N_2 and NO gas mixture. For instance, for 4.76 % O_2 condition, 10 sccm O_2 is added into the 200 sccm N_2 and NO gas mixture. The total flow rate is changed from 200 to 210 sccm. For 9.09 % and 16.67 % O_2 condition, the total flow rates are increased to 220 and 240 sccm. Before the plasma is

applied, for the 1000 ppm NO condition, the concentrations of NO and NO_2 under different O_2 concentration are shown in Table 3-3. Because O_2 can oxidize NO to NO_2, the concentration of NO decreases and that of NO_2 increases. In addition, the presence of O_2 dilutes the total NOx concentration, so as the O_2 concentration increased from 0 % to 16.67 % the total NOx concentration reduced from 1000 ppm to 817 ppm.

Table 3-3 NO, NO_2 and NOx concentrations under different O_2 concentration

C_{O2} (% vol)	FR of 1000 ppm NO in N_2 (sccm)	FR of O_2 (sccm)	C_{NO} (ppm)	C_{NO2} (ppm)	C_{NOx} (ppm)
0	200	0	1000	0	1000
4.76	200	10	855	102	957
9.09	200	20	756	163	919
16.67	200	40	614	203	817

Adding water vapour into the gas phase is realised by passing gas through a 20°C gas washing bottle, as shown in Figure 3-3. With increasing temperature, the water vapour saturation pressure increases and more water vapour is held in the gas. In this research, the temperature of the laboratory is consistently about 20°C, so the saturated water vapour pressure is 2.338 kPa whose corresponding percentage in volume was 2.31 % (which is the result of 2.338kpa/101kpa), as indicated in Figure 3-4.

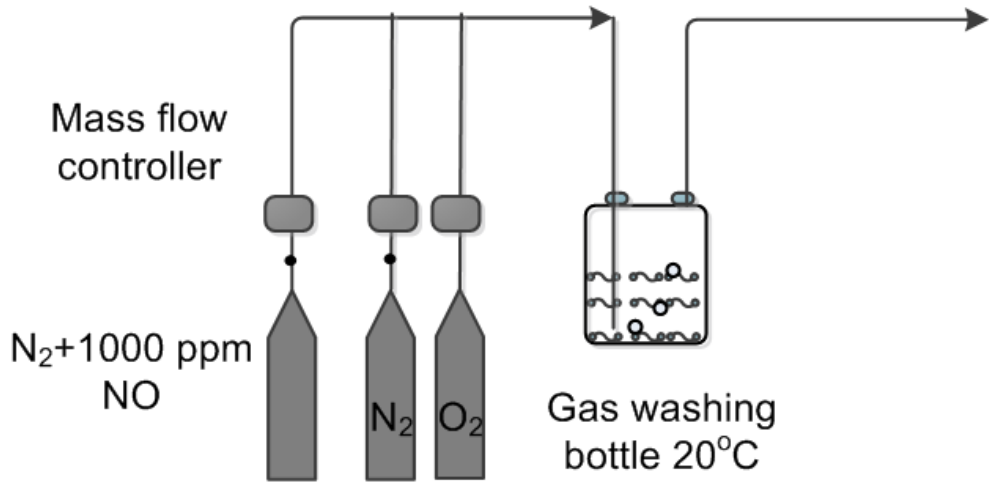

Figure 3-3 Adding water vapour in gas phase process

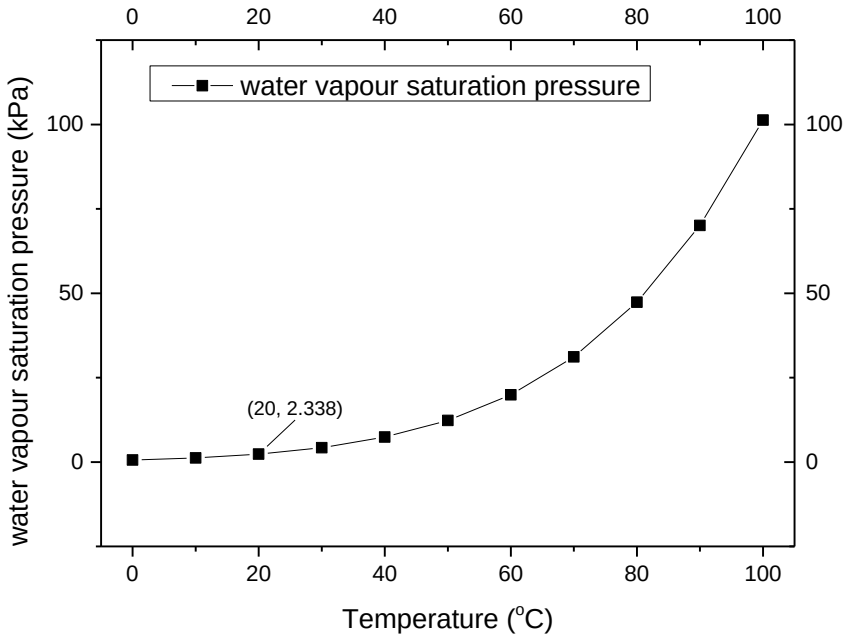

Figure 3-4 The relation between temperature and water vapour saturation pressure [98]

3.3 Power supplies

Two different high voltage power supplies are used in this research. One is a 50 Hz AC power supply which is used to investigate NO removal under DBD, as shown in Figure 3-5. The other one is a DC power supply which is used to investigate NO removal under pin-water negative DC corona discharge, as shown in Figure 3-6.

3.3.1 50 Hz AC power supply system

The 50 Hz AC power supply provides voltages up to 7 kV. It consists of an auto-transformer and a step-up transformer with fixed ratio (240/7000), as shown in Figure 3-5. A 600 kΩ resistor is connected between the AC power supply and the DBD reactor in order to avoid the risk of a short circuit. Details of the DBD reactor, including dimensions and materials, are given in Chapter 4.

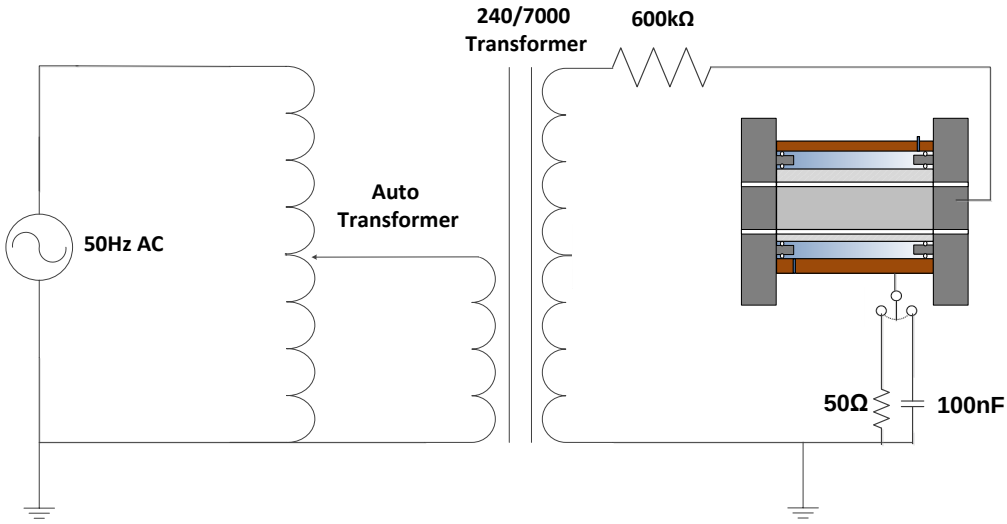

Figure 3-5 Schematic diagram of 240 V/7000 V 50 Hz AC power supply for dielectric barrier discharge

Mains power is connected to the primary side of the auto-transformer and the voltage on the secondary side of the auto-transformer is adjustable from 0 V to 240 V. A step-up transformer with a voltage ratio of 240 V to 7000 V is connected to the secondary side of the auto-transformer. In these experiments, the voltage applied to the reactor is between 4 kV and 7 kV. A 50 Ω resistor and a 100 nF capacitor are used in series with the reactor to measure the discharge current and charge transfer, respectively. The details of how to measurement is made will be given in section 3.4.

3.3.2 DC power supply system

The DC power supply is made by Glassman High Voltage INC from USA and the model used in this research is PS/EJ20R30.OF22. The output voltage can be controlled from 0 kV to 20 kV with a maximum output current of 30 mA. The details of the pin-water corona discharge reactor, including the dimensions and materials, are given in Chapter 5.

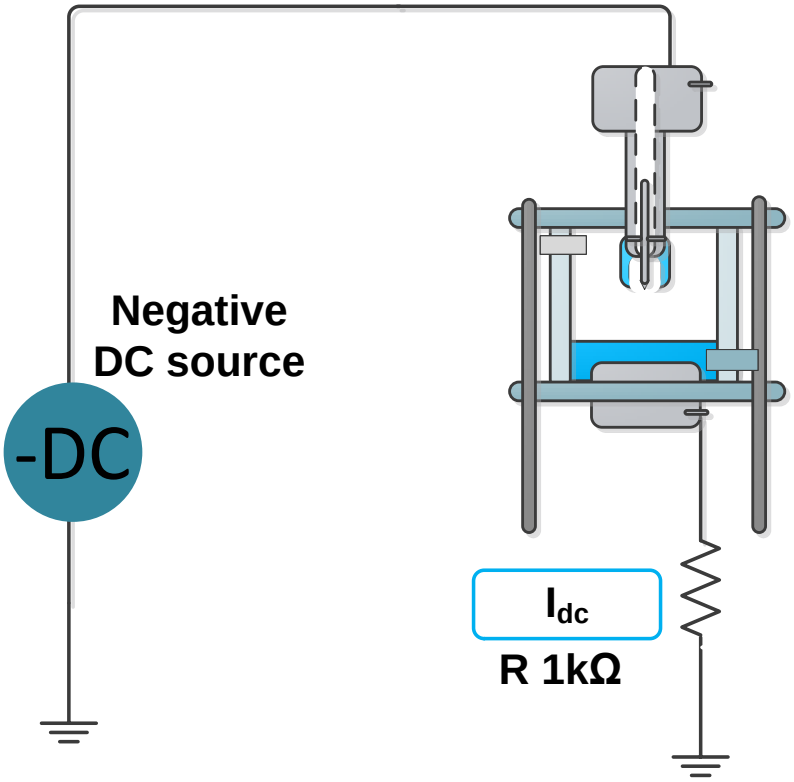

Figure 3-6 Schematic diagram of 20 kV DC power supply for pin-water negative DC corona discharge

One advantage of the DC power supply is its ability to limit the output current. Before switching on the power supply, the maximum output current can be pre-set. To maintain the negative corona discharge in pulseless mode, and avoid the transition to arc discharge, the maximum output current is pre-set to 1 mA. For the corona discharge reactor, a stainless steel pin is used. The reason for choosing a 1 kΩ resistor in the measurement system is that the amplitude of discharge current is very low, resulting in a very low voltage when measured by 50 Ω resistor. In addition, no capacitor is required, because discharge power for corona discharge can be measured by the product of DC voltage and DC current (more details will be given in Chapter 5).

3.4 Electrical signal measurements

3.4.1 Voltage measurement

For voltage measurement, two types of voltage probes are used; one is HV probe "Tektronix P6015A", which can measure up to 20 kV DC and 40 kV for pulsed signals. The other voltage probe is Tektronix TPP100, which is used to measure low voltage signals. The basic parameters of these two probes are shown in Table 3-4.

Table 3-4 Parameters of voltage probes used in this research project

Type	Tektronix P6015A	Tektronix TPP1000
Maximum input voltage	20 kV DC & 40 kV Peak impulse	$300V_{RMS}$
Attenuation	1000:1	10:1
Bandwidth	75 MHz	1 GHz
Rise time	4 ns	<450 ps
System input resistance	100M Ohm	10M Ohm
System input capacitance	3 pF	3.9 pF

3.4.2 Current measurement

Two current measurement methods are used. The method used in the DBD experiments is to measure the voltage across the 50 Ω termination, Figure 3-5, through a coaxial cable (RG405 Z_0=50Ω). The advantage of this measurement is that the nano-second discharge current impulse is transmitted under matched impedance condition, so there is no distortion between the measured current impulse and the actual current impulse. The schematic diagram is shown in Figure 3-7.

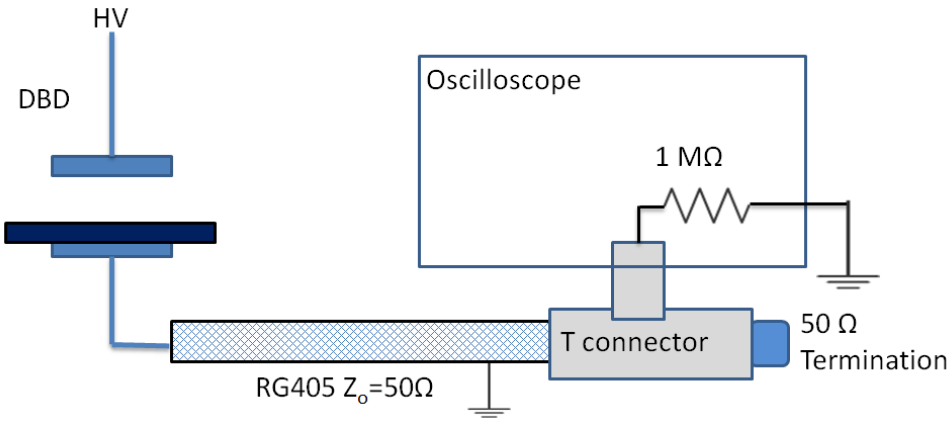

Figure 3-7 Schematic diagram of current measurement by 50 Ω termination

The other method, used for the pin-water corona discharge current measurement, (Figure 3-8) measures the voltage across the 1 kΩ resistor. The reason for using a 1 kΩ resistor instead of a 50 Ω resistor is that a larger resistance increases the amplitude of the measured voltage signal, as discussed in section 3.3.2.

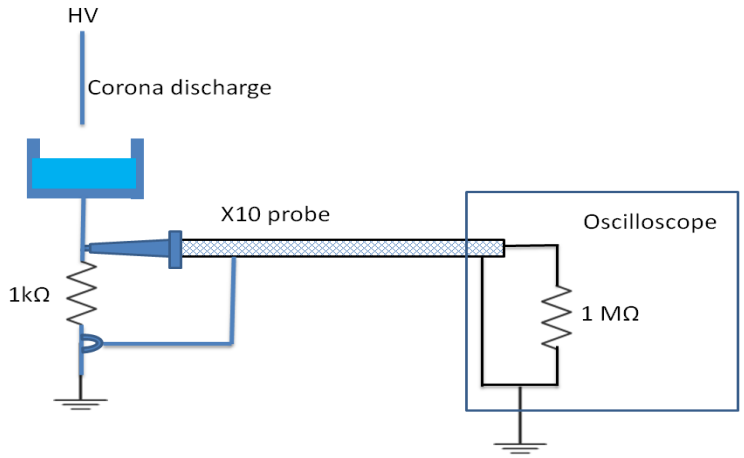

Figure 3-8 Schematic diagram of current measurement by 1 kΩ resistor

3.4.3 Discharge current amplitude distribution

The discharge current amplitude distribution is an important parameter when investigating whether there is any change in reactive species in DBD. An explanation of how to measure the discharge current amplitude distribution is given below. A LeCroy oscilloscope WaveRunner 625 Zi is used for data acquisition. The bandwidth and sampling rate of this oscilloscope are 2.5 GHz and 40 Gs/s respectively. One powerful function of the oscilloscope is to build a histogram of discharge current amplitude distribution. An example of a single discharge current impulse in pure N_2 is shown in Figure 3-9, the oscilloscope will record its amplitude as 2.9 mA.

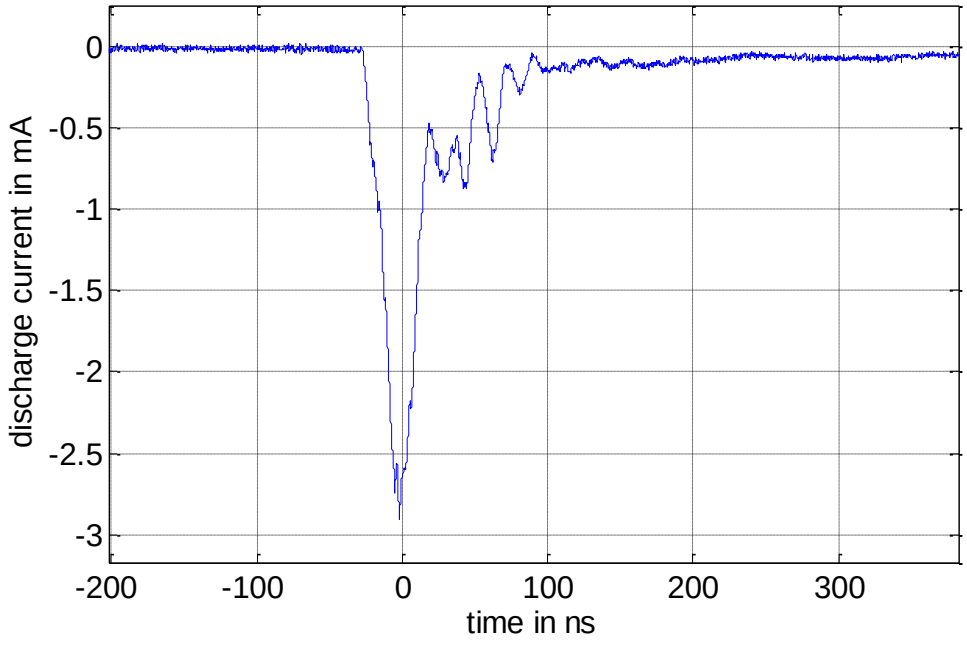

Figure 3-9 A single discharge current impulse waveform at pure N_2 gas condition

At each discharge event above a set magnitude, the trigger level, the discharge current impulse is displayed and the amplitude of this impulse is recorded. This process is repeated 10,000 times for a single data set. A discharge current impulse distribution can be generated from this data, Figure 3-10 is an example taken at 210mL/min N_2 and 7 kV applied peak voltage for negative half period of AC power supply in the DBD reactor. The average current amplitude changes with different gas mixtures, as the discharge energy is related to the gas conductivity. The reactive gas species generated in a discharge can change the

structure of the original discharge. More information on the relationship between the discharge current amplitude and the reactive species is given in Section 4.3.

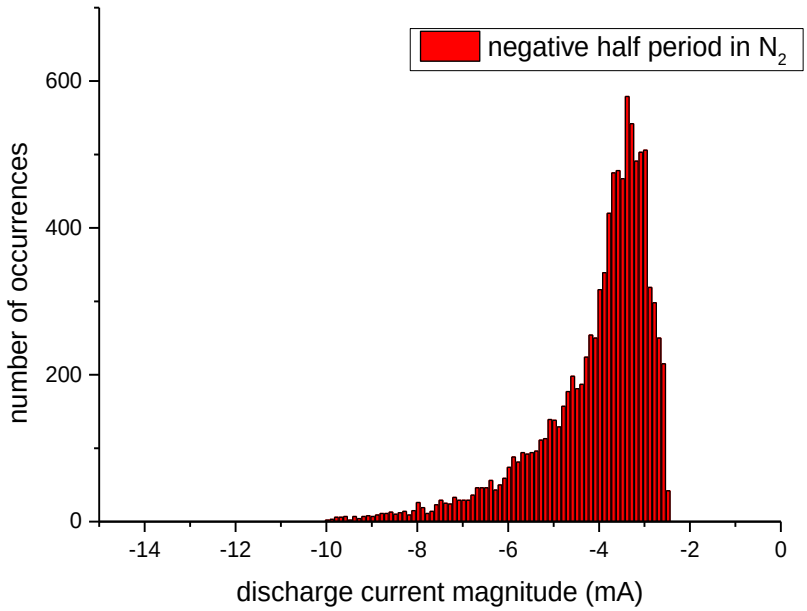

Figure 3-10 Amplitude distribution of 10,000 negative half period discharge impulses in a cylindrical DBD reactor: one dielectric layer, gap 0.35 mm, dielectric barrier thickness 1.5 mm, N_2 at 210mL/min and 7 kV peak applied voltage.

3.4.4 Discharge power calculation

Two methods are used to measure the discharge power. The first one discussed, used for the pin-water negative DC corona discharge, uses the product of voltage and current. The other, for the power calculation in DBD discharges, is based on the Lissajous figure.

3.4.4.1 Product of voltage and current

For DC voltage and current, power can be calculated using equation (3-1):

$$P = V * I \tag{3-1}$$

However, if voltage and current signals periodically change with time then the power can be calculated by (3-2):

$$P = \frac{1}{T} * \int_0^T v_{(t)} * i_{(t)} dt \tag{3-2}$$

where:
T is time period
$i_{(t)}$ is variable current signal with time
$v_{(t)}$ is variable voltage signal with time

As mentioned in Chapter 2, negative corona discharge has different modes with increasing applied voltage. For Trichel pulse discharges, i.e. periodic pulse signals, the power calculation uses (3-2). When discharge converts to pulseless and arc discharge, they are both continuous discharge, so the power can be calculated by (3-1). More description on the waveform of discharge current and voltage will be given in Chapter 5.

3.4.4.2 Lissajous figure of dielectric barrier discharge

One of the most important characteristics of signals in DBD is the Lissajous figure, because it contains many inherent parameters of the DBD reactor. These include the equivalent dielectric capacitance (C_d), gap capacitance (C_g) and total capacitance (C_{tot}), discharge energy and breakdown voltage of the gap (V_b).

In Figure 3-11 the x-axis indicates the voltage being applied to the DBD reactor and the y-axis is the charge transfer, which is measured using an additional capacitor in series connection. One period of the AC voltage waveform is indicated by $A \rightarrow B \rightarrow C \rightarrow D \rightarrow A$.

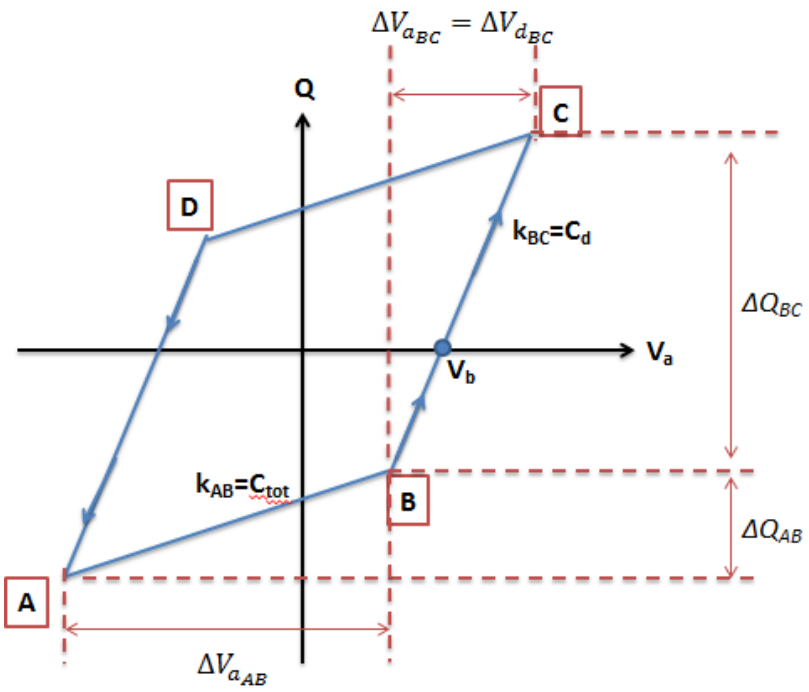

Figure 3-11 A Lissajous figure of DBD for a sinusoidal waveform

A measurement capacitor of 100 nF capacitor is used in this research. This capacitance is much larger than that of the DBD capacitor to reduce the effect of measurement capacitor on voltage sharing. Because the measurement capacitor was connected to the DBD reactor in series, charge transfer in the measurement capacitor was equal to that in total capacitance of the DBD reactor. At Point A, the applied voltage is at its maximum value in negative polarity. During the time period from A to B the applied voltage increases to zero and B to C is the transition to peak positive voltage. The DBD reactor is a pure capacitor and the total capacitance can be calculated by the slope of line AB in Lissajous figure according to (3-3).

$$C_{tot} = \Delta Q_{AB} / \Delta V_{a_{AB}} \quad \textbf{(3-3)}$$

As shown in Figure 3-12, when the applied voltage is lower than the minimum voltage for gas breakdown from t_A to t_B, the applied voltage (V_a), dielectric voltage (V_d) and gap voltage (V_g) are all sinusoidal waves. Once V_a is higher than the minimum voltage for breakdown, V_g becomes constant with the amplitude of V_b during the breakdown period from t_B to t_C, so the change of V_a is equal to the change of V_d. Dielectric capacitance *(C_d)* is calculated by (3-4). A similar argument applies to the positive half period from t_C to t_A.

$$C_d = \Delta Q_{BC} / \Delta V_{d_{BC}} \text{ (where } \Delta V_{d_{BC}} = \Delta V_{a_{BC}}) \quad \textbf{(3-4)}$$

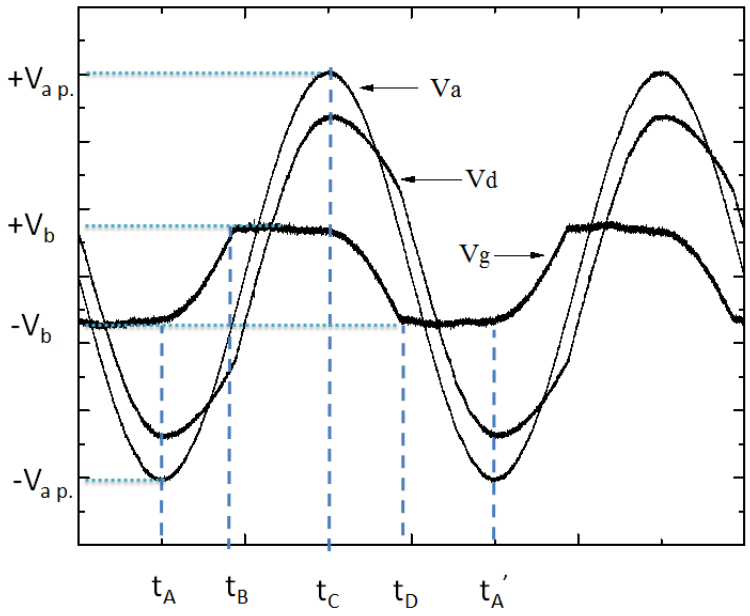

Figure 3-12 Applied sinusoidal voltage and gap voltage waveforms for a DBD

When the values of the total capacitance (C_{tot}) and dielectric capacitance (C_d) are calculated, the gas capacitance (C_g) can be solved from (3-5).

$$\frac{1}{C_{tot}} = \frac{1}{C_g} + \frac{1}{C_d} \qquad \textbf{(3-5)}$$

In addition, in Figure 3-11 the point at which the Lissajous figure crosses the x-axis signifies the breakdown voltage of the gap (V_b). That is the point where the voltage of the measurement capacitor is zero, which means that no net charge is accumulated on the measurement capacitor. As the dielectric capacitor and measurement capacitor are in series, this means that there is no net charge on the dielectric. As the net voltage across the dielectric barrier is zero, the whole applied voltage is applied only to the gas. The reason why the dielectric voltage is zero at the cross point is that there are two separate voltage sources to charge the dielectric capacitor. One is caused by the applied voltage source and the other is caused by the deposited charges which are generated during the previous half cycle of the sinusoidal voltage. At the cross point, the voltages across the dielectric barrier, as generated by the external voltage source and deposited charge, are of the same amplitude but opposite polarity. Therefore, the total voltage across the dielectric is zero and the applied voltage is equal to the voltage across the gap. In addition, the cross point is located in the

discharge time period, so the voltage is the breakdown voltage for the gap. The calculation of discharge power, from Kogelschatz et al. [60], is the product of working frequency, in UK 50Hz, and the discharge energy in one cycle. The principle of discharge energy (E) in one cycle in DBD is based on the charge transfer in gap (ΔQ) and gap voltage (V_g) using (3-6):

$$E = V_g \cdot \Delta Q \tag{3-6}$$

The charge transfer (ΔQ) is calculated from the product of the capacitance (C) and the change of voltage (ΔV) across the capacitor in (3-7):

$$\Delta Q = C \cdot \Delta V \tag{3-7}$$

As highlighted in Figure 3-12, the total charge transfer through the dielectric capacitance during the half cycle from t_A to t_C is given in (3-8):

$$Q_{AC} = C_d \cdot (2V_{a\,p.} - 2V_b) \tag{3-8}$$

The same charge transfer must go through the gap capacitance during the same time period. Because the gap voltage is unchanged during the discharge time period from t_B to t_C, the charge transfer for the gap capacitance can be separated into two parts and the charge transfer during the non-discharge time period from t_A to t_B is given in (3-9):

$$Q_{AB} = C_g \cdot (2V_b) \tag{3-9}$$

The charge transfers during the time periods from t_A to t_C and from t_A to t_B through the gap capacitance are known from (3-8) and (3-9), so the charge transfer during the discharge time period from t_B to t_C can be solved using (3-10):

$$Q_{BC} = Q_{AC} - Q_{AB} = 2C_d \cdot \left(V_{a\,p.} - V_b\right) - 2C_g \cdot V_b \tag{3-10}$$

As both charge transfer and applied voltage are known, the energy transfer for a half period can be calculated using (3-11).

$$E = Q_{BC} \cdot V_b = 2C_d \cdot V_b (V_{a\,p.} - \frac{C_d + C_g}{C_d} \cdot V_b) \tag{3-11}$$

Therefore, the discharge power can be obtained using (3-12):

$$P = 2 \cdot f \cdot E = 4 \cdot f \cdot C_d \cdot V_b(V_{a\,p.} - \frac{C_d + C_g}{C_d} \cdot V_b) \quad \textbf{(3-12)}$$

where:
$f\ is$ the frequency of power supply in Hz;
C_d is the dielectric barrier capacitor in F;
C_g is the gap capacitor and equal to $({C_{tot}}^{-1} - {C_d}^{-1})^{-1}$ in F;
$V_{a\,p.}$is the peak applied voltage in V;
$V_b$is the breakdown voltage of gap in V;
P is the discharge power in W.

3.5 NOx measurement

Concentrations of NO and NO_2 are measured by the thermal scientific Model 42i-HL NOx analyser. Some parameters of the NOx analyser are shown in Table 3-5. The sample flow rate is lower than the actual testing flow rate because the analyser is working with a pump. It can extract the required amount of gas from the main stream of gas flow and carry out the measurements as appropriate. The rest of the gas will bypass the detector and be exhausted.

Table 3-5 NOx analyser specifications

Name	Manufacturer (Part name)	Function	Measurement range	Accuracy	Sample flow rate
NOx analyser	Thermal scientific Model 42i-HL	High concentration NOx measurement	0-5000 ppm	1% of full scale	25 sccm

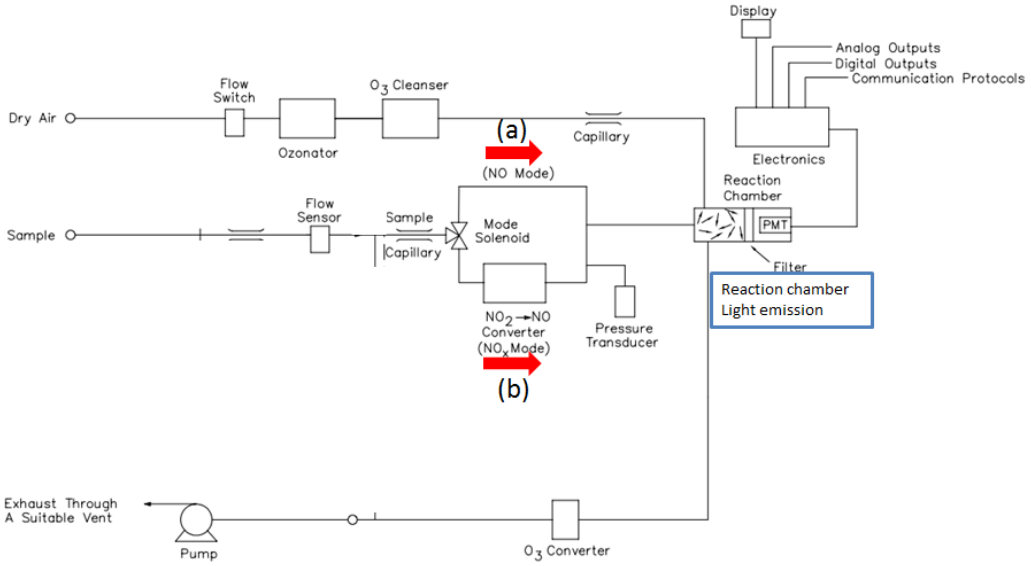

Figure 3-13 NOx analyser schematic flow diagram [99]

The fundamental principle of NOx measurement is to measure the light emission by the reaction between nitric oxide and ozone.

$$NO + O_3 \rightarrow NO_2^* + O_2$$

$$NO_2^* \rightarrow NO_2 + h\nu$$

Following path (a) in Figure 3-13, the emitted light, with a wavelength of about 600nm [100], is detected by photomultiplier tubes. The intensity of light emission corresponds to the NO concentration. NO_2 concentration measurement, following path (b) in Figure 3-13, is based on the same principle for NO measurement, but there is one more process to reduce NO_2 to NO, which is done by molybdenum catalyst at 325 ^oC.

$$2NO_2 \xrightarrow{Mo\ at\ 325^oC} 2NO + O_2$$

When the mixture of NO and NO_2 goes through path (b) into the molybdenum converter chamber, NO_2 is reduced to NO completely. After that, the measured concentration of NO in the reaction chamber represents the sum of NO and NO_2 concentrations, so the difference between total NOx concentration and NO concentration is NO_2 concentration. Therefore, although the concentration of NO_2 is not directly measured, it can be effectively calculated. For NO removal, two important parameters are considered: one is the NO removal and the other is the NO removal energy efficiency, as discussed below.

3.5.1 NO removal and NO_2 formation

In this research, because O_2 is able to oxidize NO at atmospheric pressure and room temperature conditions, some NO is converted to NO_2 without non-thermal plasma treatment. With the increase of O_2 concentration in the gas mixture, more NO is oxidized to NO_2. The initial concentrations of NO and NO_2 under different O_2 concentration were shown in Table 3-3. Therefore, NO removal is based on the difference between the initial NO concentration and the NO concentration after non-thermal plasma treatment. In terms of NO_2, because most of the reactive species are oxidants, the concentration of NO_2 is usually increased. Therefore, the recording of NO_2 formation is based on the difference between the NO_2 concentration after non-thermal plasma treatment and the initial NO_2 concentration. The definitions of NO removal and NO_2 formation are shown in (3-13) and (3-14).

$$R_{NO} = C_{NO\ i.} - C_{NO\ t.} \quad \textbf{(3-13)}$$

$$F_{NO2} = C_{NO_2\ t.} - C_{NO_2\ i.} \quad \textbf{(3-14)}$$

where:
R_{NO} is the NO removal in ppm;
F_{NO2} is the NO_2 formation in ppm;
$C_{NO\ i.}$ is the initial NO concentration in ppm;
$C_{NO_2\ i.}$ is the initial NO_2 concentration in ppm;
$C_{NO\ t.}$ is the NO concentration after non-thermal plasma treatment in ppm;
$C_{NO_2\ t.}$ is the NO_2 concentration after non-thermal plasma treatment in ppm.

3.5.2 NO removal energy efficiency

At standard conditions (0°C and 1 atm), the molar volume (M_v) of any gas is constant.

$$M_v = 22.4\ L/mol \tag{3-15}$$

As highlighted in Section 3.2, the flow rates of all the gases is controlled by mass flow controllers (from Alicat), and the setting of the flow rate is based on the same condition (0°C and 1 bar). Although the laboratory temperature is around 20°C, the mass flow controller has an inbuilt function to take into consideration of the effect of temperature. Therefore, the value of molar volume used in (3-16) is 22.4 mL/min.

$$\eta_{NO} = \frac{\frac{FR}{22.4} * R_{NO} * M_m * 6 * 10^{-5}}{P} \tag{3-16}$$

where:
FR is flow rate at 0°C and 1atm condition in sccm;
R_{NO} is the NO removal in ppm;
M_m is molar mass of NO, 30 g/mol;
P is non-thermal plasma discharge power in W;
η_{NO} is NO removal energy efficiency in g/kWh.

3.6 Ozone measurement

Ozone, O_3, concentration has been considered in this research, because it is a reference in identifying the dominant reactive species between atomic O and O_3 for NO oxidation under different gas conditions. As highlighted in Chapter 2 when discussing the chemical kinetics of NOx removal, both O_3 and O can oxidize NO to NO_2, but they react differently with NO_2. O acts to reduce NO_2 to NO, so it can limit NO removal as a result of this side reaction. O_3 can further oxidize NO_2 to NO_3 without any side reaction for NO oxidation. For O_3 measurement, a comparison with discharge in a reference gas where NO does not exist is used. For instance, for 16.67% O_2 in N_2 without NO, O_3 formation is 394 ppm for 7kV peak applied voltage. However, for 16.67% O_2 with 1000 ppm NO in N_2, the NO oxidation rate is only 148 ppm, not the expected 394 ppm if O_3 is the oxidant. According to the difference in NO removal in the gas mixture where NO exists and the O_3 formation in the reference gas, the dominant reactive species for NO oxidation can be identified quantitatively.

In this research, O_3 concentration is measured using a BMT 964 ozone analyser, information about the O_3 analyser is listed in

Table 3-6. In the tests in this work, before using the analyser, at least half hour is given to warm up and a zero calibration is completed.

Table 3-6 Ozone analyser specifications [101]

Name	***Manufacturer (Part name)***	***Function***	***Measurement range***	***Resolution***	***Accuracy***
Ozone analyser	BMT (964)	Low ozone concentration measurement	0-20 g/Nm^3	0.01g/ Nm^3	0.4% of measurement + 0.1% of scale

where: g/Nm^3 represents g/m^3 in normal condition (20^{o}C, 1atm)

Ozone measurement is based on the light absorption by O_3 at 254 nm UV light. A low pressure mercury lamp is used as the 254nm light source. When a known concentration of O_3 passes through the absorption cell, part of the UV light is absorbed by O_3. At the end of the absorption cell, see Figure 3-14, there is a photodiode to receive the remaining UV light. The initial UV light intensity at the photodiode, I_0, is known. According to the Beer Lambert law, the corresponding O_3 concentration can be calculated using equation (3-17).

$$I = I_0 \cdot e^{-A \cdot C_{O_3}} \quad \textbf{(3-17)}$$

where:
I_0 is the light intensity from the mercury lamp;
I is the light intensity received by the photodiode;
A is constant;
C_{O3} is the concentration of O_3.

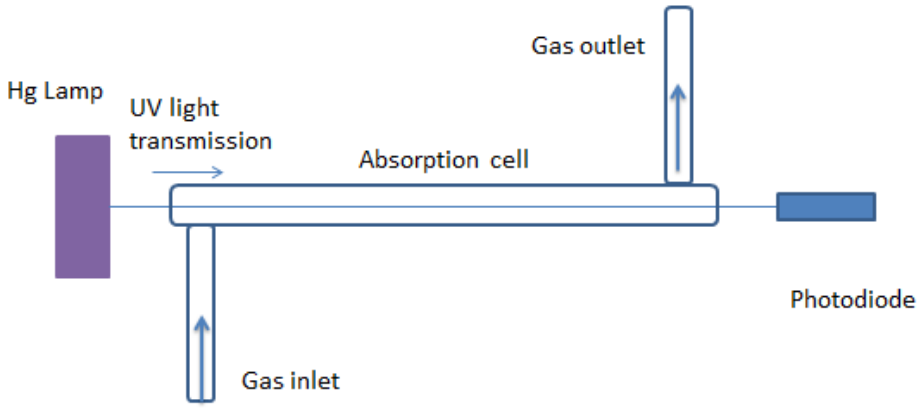

Figure 3-14 Schematic diagram of the ozone analyser

3.7 Conclusion

In this chapter, the use of a pneumatic control system to get different initial concentrations of NO, O_2 and H_2O in the gas mixture has been explained. This is the fundamental to conducting the experiments in the following chapters, as it allows quantitative analysis of the dominant reactive species for NO removal. The electrical signal measurement also provides important information to evaluate the performance of different non-thermal plasma technologies for NO removal, e.g. the measurement of the Lissajous figure and the discharge current impulse distribution. The Lissajous figure provides information on gap capacitance, dielectric capacitance and total capacitance, and on the breakdown voltage and the discharge power. In addition, this chapter provides the general equations for the calculation of NO removal and energy efficiency which are important parameters to determine the applicability of non-thermal plasma technologies in this research.

Chapter 4 DIELECTRIC BARRIER DISCHARGE FOR NO REMOVAL

4.1 Introduction

As explained in Chapter 2, DBD has been investigated by other researchers [40, 73, 81, 82] who highlighted the importance of the reactive species such as O, O_3, OH and N for NO removal, but there has been no quantitative conclusion to identify which reactive species are more important. According to the chemical kinetics for NO removal, different reactive species bring different reaction pathways, so confirming the dominant reactive species is worthwhile. In this chapter, a cylindrical DBD reactor was used for NO removal. The advantage of the cylindrical configuration is that, because the dielectric is a closed loop, there is no dielectric boundary and this avoids the occurrence of corona discharge on sharp edges in the reactor. The discharges which do occur can happen uniformly in the gas gap.

Reactions in five different NO concentration levels were analysed and the effect of O_2 for each NO concentration level was investigated. According to the change of NO concentration, a series of experiments were conducted to determine the dominant reactive species for NO removal under different initial NO, O_2 and H_2O concentrations. In addition, under different gas conditions, the characteristics of discharge were found to be different, especially in respect to the amplitude of discharge current impulse. The average discharge current amplitude was analysed and compared for different gas mixtures and the relationship between the average discharge current amplitude and reactive species will be discussed.

4.2 Experimental setup and procedures

The DBD reactor used in this work is shown in Figure 4-1. The total length of the reactor was 170 mm. An inner stainless steel rod with 6.3 mm diameter was used as the high voltage electrode. A Pyrex tube with outer and inner diameters of 10 mm and 7 mm was used as the dielectric barrier. The gas gap between the stainless steel (SS) rod and the Pyrex tube was 0.35mm. The outmost copper tube with outer and inner diameters of 28 mm and 26 mm was the grounding electrode. The gap between the Pyrex tube and the copper tube was filled with conductive tap water which became part of the grounding electrode. Both ends of the copper

tube were sealed by PVC cap with O-ring to avoid water leakage. Finally, the copper electrode was connected to ground.

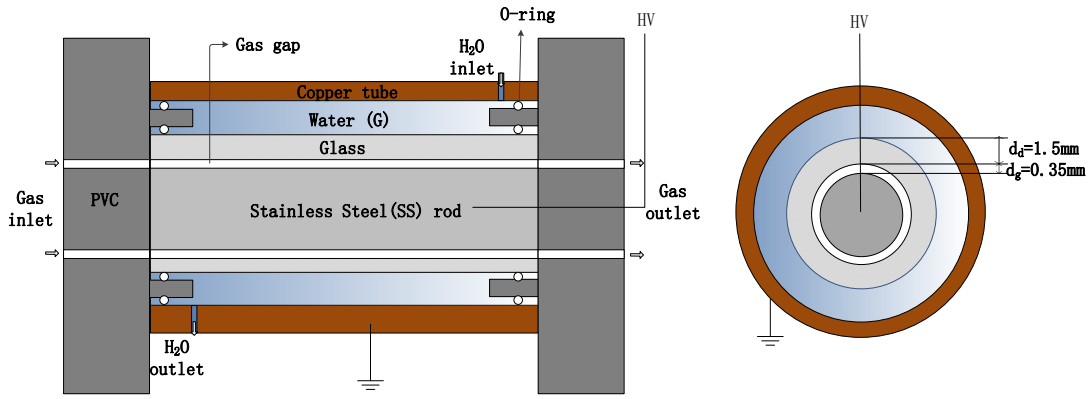

Figure 4-1 Front and side view of the DBD reactor.

The experimental setup, indicating reactor vessel and electrical, thermal and analytical instruments applied, is shown in Figure 4-2. A 50 Hz AC power supply (maximum output voltage was 7 kV at peak) was used to energize the DBD rector. Reactor temperature was controlled by thermal static circulator (LKB Bromma 2219 MultiTemp II) which provided constant temperature water flowing between reactor and circulator and the gas temperature was taken as being controlled by the reactor temperature. Three different test temperatures were chosen, i.e. 44, 62 and 81^{o}C, for the experimental series.

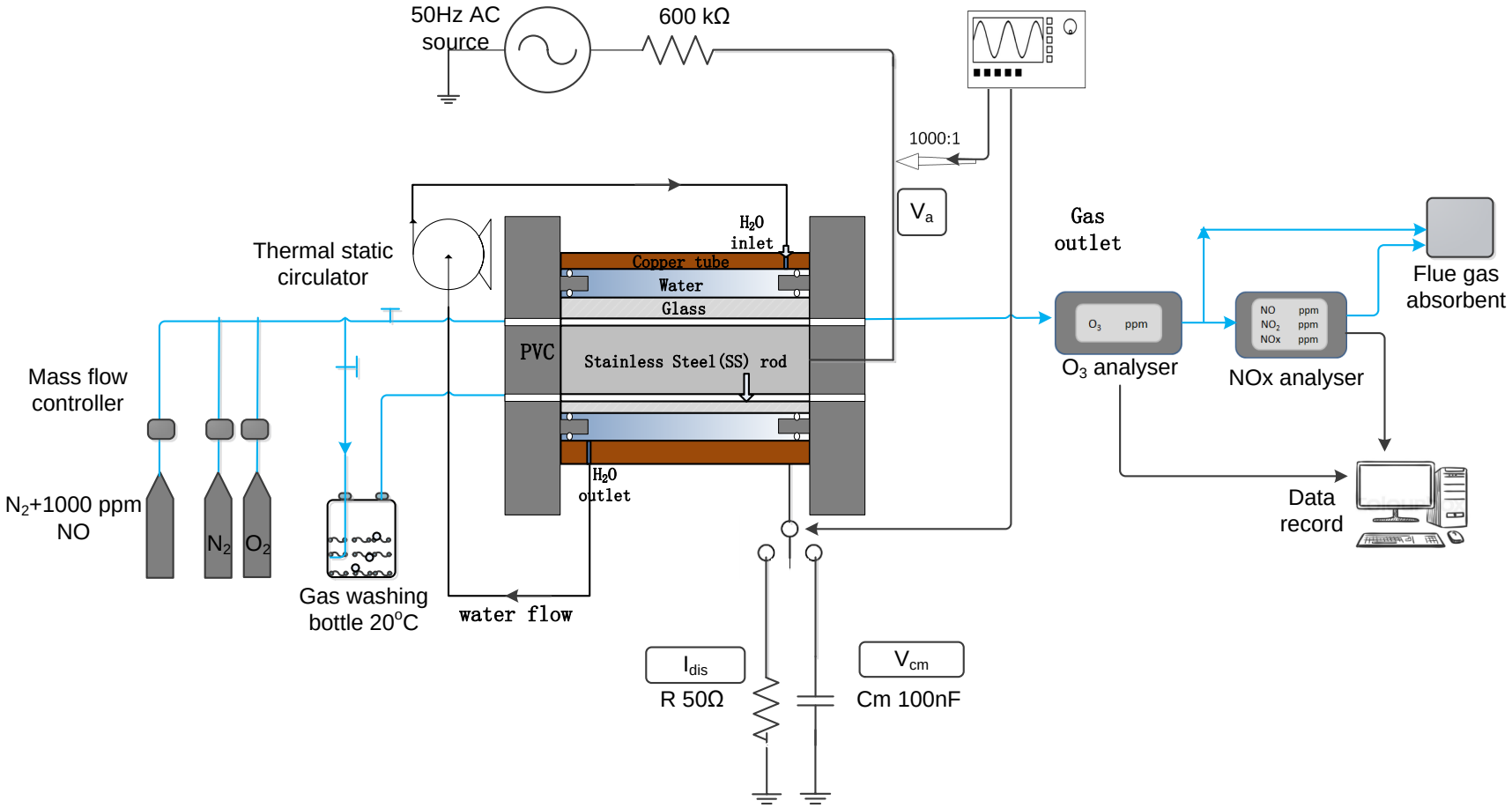

Figure 4-2 Schematic diagram of experimental setup

In respect of the chemical kinetics of NO removal, as mentioned in Chapter 2, when using atomic O there is a side reaction between NO_2 and O which generates NO, but if the oxidant is O_3, there is no such side reaction and NO_2 can be further oxidized to N_2O_5. The formation of O_3 is based on the reaction of O_2 and O, so O generated by a non-thermal plasma can react with both NO and O. The reaction rate constant between O and NO is about 1000 times higher than that between O and O_2, but the reaction rate is determined by the reaction rate constant and each reactant concentration, as discussed in section 2.3.2. Although the reaction rate constant cannot be changed, the concentration of each reactant can be manipulated. Therefore, in order to obtain different concentrations of NO, N_2 was used to dilute an initial NO concentration of 1000 ppm. Different O_2 flow rates were chosen into the gas mixture to change the O_2 concentration. This was defined as five levels of NO concentration, i.e. high, upper-medium, medium, lower-medium and low concentration NO. The various gas concentrations under different O_2 concentration are shown in Table 4-1.

- **High concentration NO**: initial NO was between 614 ppm and 1000 ppm.
- **Upper medium concentration NO**: initial NO was between 426 and 550 ppm.
- **Medium concentration NO**: initial NO was between 158 ppm and 189 ppm.
- **Lower medium concentration NO**: initial NO was between 126 ppm and 150 ppm.
- **Low concentration NO**: initial NO was between 84 ppm and 101 ppm.

Although the total gas flow rate of 200 sccm flow rate for NO and N_2 was constant, the pure N_2 gas flow rate was determined by the required NO concentration. For instance, for a required NO concentration of 600 ppm, the flow rate of 1000 ppm NO in N_2 was 120 sccm and that of pure N_2 was 80 sccm. Similarly, variation in gas flow rates were developed for 200 ppm, 150 ppm and 100 ppm NO condition.

In terms of O_2 concentration, as shown in Table 4-1, the flow rate of O_2 varied from 0 to 40 sccm. However, because O_2 has the potential to oxidize NO to NO_2, some NO became NO_2 before DBD treatment. In practical situations, the range of NO concentration is from 200 ppm to 600 ppm, but in order to investigate the chemical reaction pathways for NO removal, the NO concentration range was expanded from 84 ppm to 1000 ppm, where 84 ppm was at the low concentration NO condition, and 1000 ppm at high concentration NO condition.

Table 4-1 NO, NO_2 and NOx concentration at different conditions prior to non-thermal plasma being applied

C_{NO} range definition	C_{O2} (% vol)	FR of N_2 (sccm)	FR of 1000ppm NO in N_2 (sccm)	FR of O_2 (sccm)	C_{NO} (ppm)	C_{NO2} (ppm)	C_{NOx} (ppm)
High C_{NO}	0	0	200	0	1000	0	1000
	4.76	0	200	10	855	102	957
	9.09	0	200	20	756	163	919
	16.67	0	200	40	614	203	817
Upper Medium C_{NO}	4.76	80	120	10	550	41	591
	9.09	80	120	20	486	80	566
	16.67	80	120	40	426	101	527
Medium C_{NO}	4.76	160	40	10	189	13	202
	9.09	160	40	20	176	15	191
	16.67	160	40	40	158	21	179
Lower medium C_{NO}	4.76	170	30	10	150	8	158
	9.09	170	30	20	140	11	151
	16.67	170	30	40	126	16	142
Low C_{NOx}	4.76	180	20	10	101	14	115
	9.09	180	20	20	93	10	103
	16.67	180	20	40	84	9	93

4.3 Discharge characteristics of DBD

4.3.1 Lissajous figure of DBD

As shown in Figure 4-3, it was found that with the increase in applied voltage, the Lissajous figures expanded following the same slopes for both the discharge and non-discharge time periods. The spikes, which exhibited on the positive and negative slopes of the Lissajous figure, are caused by rapid charge transfer during discharge events.

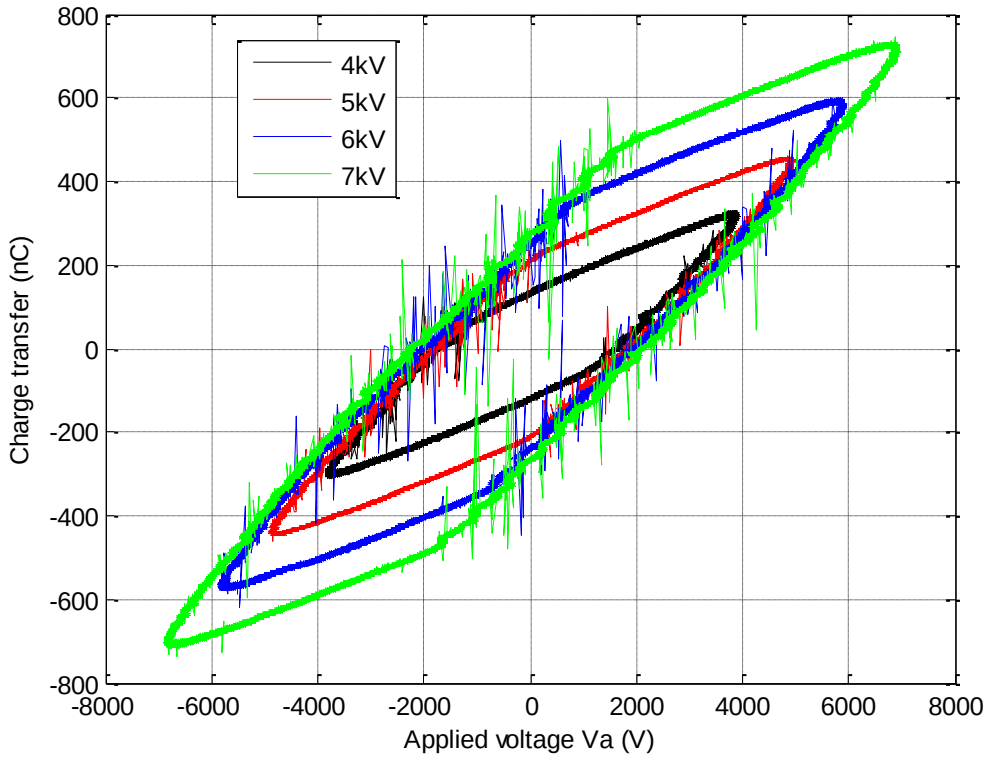

Figure 4-3 the Lissajous figures under different peak applied voltage from 4 kV to 7 kV at 4.76% O_2 and high concentration NO in N_2 condition

As discussed in Chapter 3, the total capacitance (C_{tot}), dielectric capacitance (C_d) and gap capacitance (C_g) can be calculated by Equations (4-1) to (4-3).

$$C_{tot} = \Delta Q_{AB} / \Delta V_{a_{AB}} \quad \textbf{(4-1)}$$

$$C_d = \Delta Q_{BC} / \Delta V_{d_{BC}} \text{ (where } \Delta V_{d_{BC}} = \Delta V_{a_{BC}}) \quad \textbf{(4-2)}$$

$$\frac{1}{C_{tot}} = \frac{1}{C_g} + \frac{1}{C_d} \quad \textbf{(4-3)}$$

According to measurements of the Lissajous figures in Figure 4-3, the total capacitance, dielectric capacitance and gap capacitance are 58.8 pF, 155.25pF and 94.13pF respectively. Using that data the discharge power under different applied voltage can be calculated, based on Equation (4-4), and the results for a range of applied voltages are shown in Table 4-2.

$$P = 2 \cdot f \cdot E = 4 \cdot f \cdot C_d \cdot V_b (V_{a\,p.} - \frac{C_d + C_g}{C_d} \cdot V_b) \quad \textbf{(4-4)}$$

Table 4-2 Power injection to DBD reactor under different applied voltage

Applied voltage at 50Hz (kV)	Power injection to DBD reaction (mW)
4	71
5	116
6	171
7	250

4.3.2 Distribution of impulse current amplitude of DBD

In addition to the information that can be obtained from the Lissajous figure, the discharge current amplitude measurement is another important parameter to be considered. In order to have an accurate measurement, the sampling rate and record length are taken as large as possible. The sample length is 1 Mega samples and the corresponding sampling rate is 100 Ms/s. For the histogram measurement of discharge current amplitude distribution, the sample length is 20 k samples and the sample rate is 20 Gs/s. In order to obtain an accurate discharge current amplitude distribution, a total of 10,000 samples were recorded. A 7 kV 50 Hz AC power supply was used to energize this DBD reactor. For discharge current measurement, it was measured through a coaxial cable (RG405 Z_0=50Ω) with a 50Ω termination as discussed earlier. The discharge voltage and current waveforms, and discharge current amplitude distribution for negative half periods are discussed below. Because there is no significant difference for the positive half periods, they are listed in Appendix A.

4.3.2.1 Current amplitude distribution in the mixture of N_2, O_2 and NO

For 4.76% O_2 and high concentration NO in N_2 condition, i.e. 855 ppm NO concentration, the voltage and current waveforms are shown in Figure 4-4. In order to quantitatively analyse the amplitude of discharge current, a statistical analysis was conducted to calculate the average discharge current amplitude of the 10,000 discharge current impulse samples.

In order to avoid triggering of data collection by noise, the trigger has to be slightly lower than 0mA to trigger the proper discharge impulse. When the trigger was placed between 0 and -25mA, due to an oscillation which sometimes accompanied the main discharge impulse, some positive discharge impulses caused data collection to be triggered. That is why the discharge current distribution of the negative half cycle, as shown in Figure 4-5, has a gap between 0 to -25 mA. In addition, although it was found that the maximum discharge impulse can reach -400mA, after the average of 10,000 discharge impulse samples were calculated, the average discharge current was found to be -125.66mA.

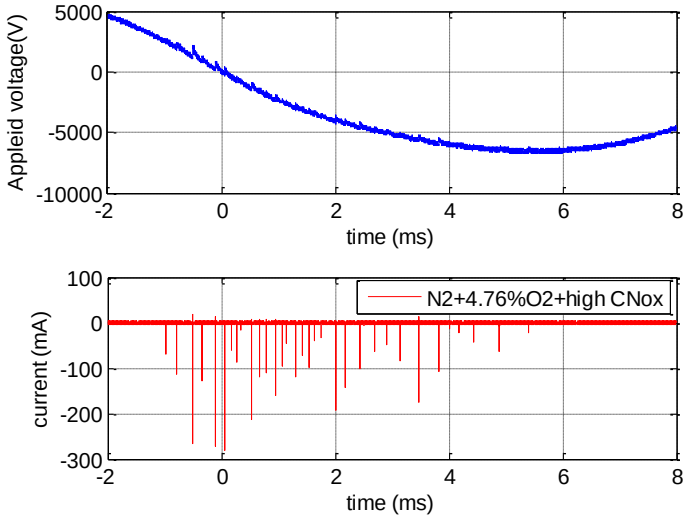

Figure 4-4 Voltage and current waveforms for 210mL/min of 4.76% O_2 and high concentration NO in N_2 at 7 kV peak applied voltage for negative half period (10,000 discharge current impulses were measured)

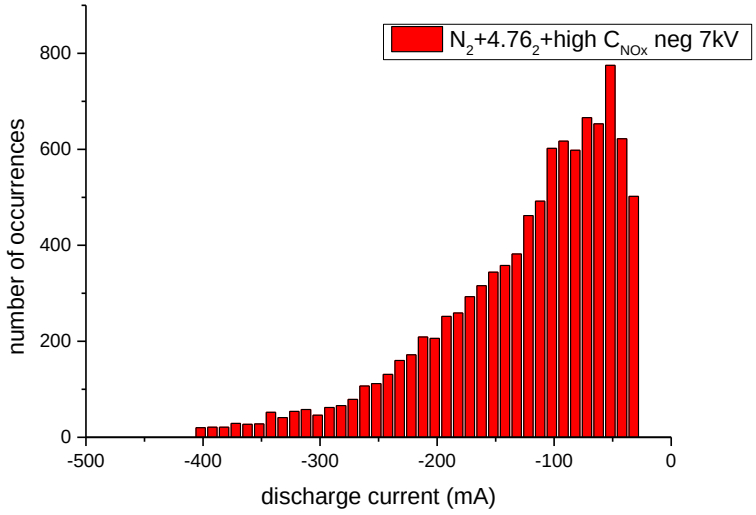

Figure 4-5 Discharge current amplitude distribution for 210mL/min of 4.76% O_2 and high concentration NO in N_2 at 7 kV peak applied voltage for negative half period (10,000 current impulses were measured)

4.3.2.2 Current amplitude distribution in the mixture of N_2, O_2 NO and H_2O

A gas mixture of 4.76% O_2 and high concentration NO in N_2 flowed through a 20°C gas washing bottle, adding 2.31% H_2O vapour to the gas mixture. The discharge current amplitude was significantly reduced when water vapour was added, see Figure 4-6.

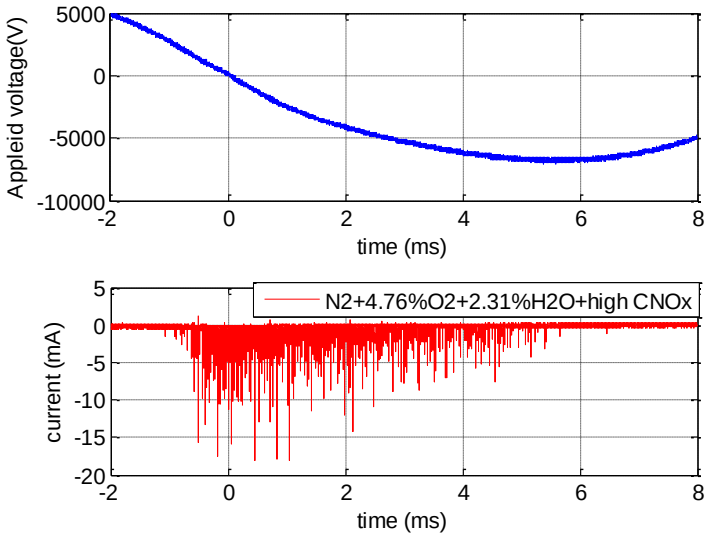

Figure 4-6 Voltage and current waveforms for 210 mL/min of 4.76% O_2, 2.31% H_2O vapour and high concentration NO in N_2 at 7 kV peak applied voltage for negative half period (10,000 current impulses were measured)

Comparing the results from these tests it was found that when 2.31% H_2O vapour was added to the gas mixture, the discharge current amplitude was significantly reduced. As shown in Figure 4-7, the maximum current was less than -20 mA and the average current was calculated to be -5.848 mA. The missing data between 0 and -2.5 mA is due to the trigger setting. A comparison between these two conditions is given in Table 4-3.

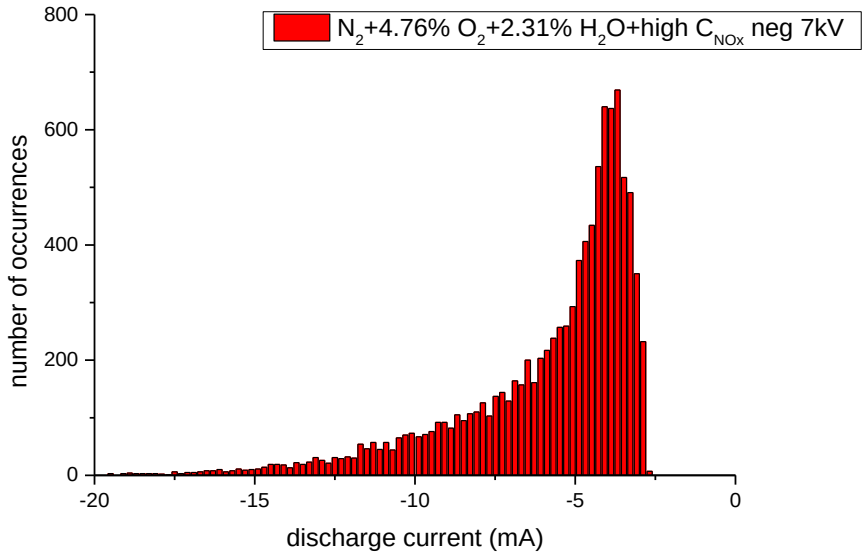

Figure 4-7 Discharge current amplitude distribution for 210 mL/min of 4.76% O_2, 2.31% H_2O vapour and high concentration NO in N_2 at 7 kV peak applied voltage for negative half period (10,000 current impulses were measured)

Table 4-3 Average impulse current at 4.76% O_2 and high concentration NO in N_2 condition with or without 2.31% H_2O vapour

	4.76% O_2 and high concentration NO	**4.76% O_2, 2.31% H_2O and high concentration NO**
Average current amplitude	-125.66 mA	-5.848 mA

4.3.2.3 Impulse current amplitude distribution in N_2 and mixtures of N_2 and O_2

In order to determine why there was such a significant difference in discharge current amplitude when 2.31% H_2O vapour was added to the gas mixture of NO, O_2 and N_2, another two gas conditions, pure N_2 and a mixture of 4.76% O_2 in N_2, were investigated. The voltage and current waveforms and the discharge current amplitude distribution of discharges in N_2 are shown in Figure 4-8 and Figure 4-9, respectively. The average current for N_2 discharge condition was -4.075 mA, which was less than that in 4.76% O_2 and high concentration NO with or without 2.31% H_2O vapour (Table 4-3).

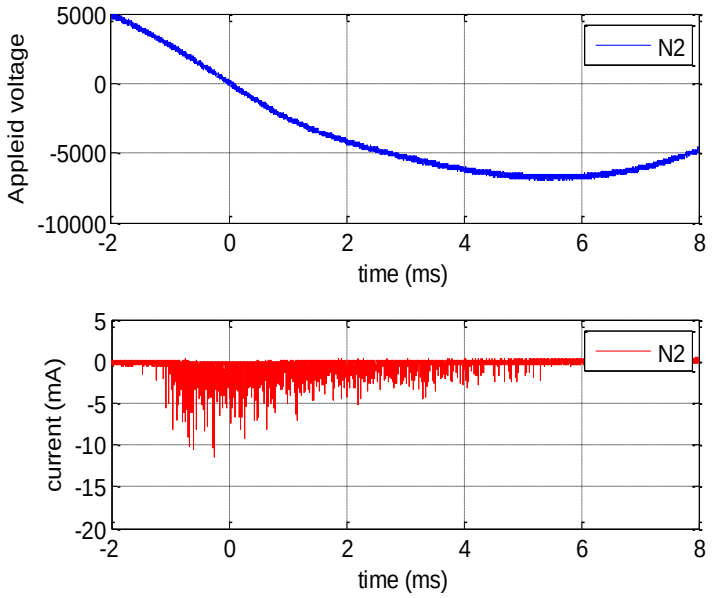

Figure 4-8 Discharge voltage and current waveforms for 210 mL/min N_2 at 7 kV peak applied voltage during negative half period (10,000 current impulses were measured)

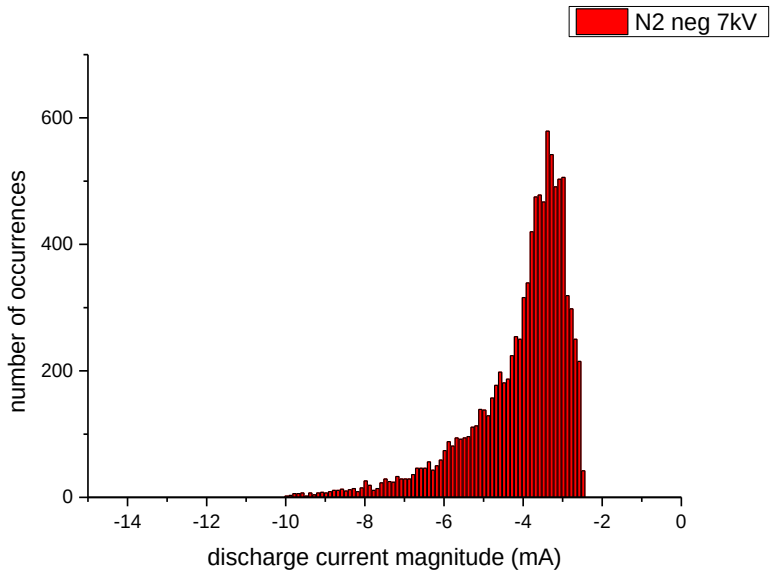

Figure 4-9 Discharge current amplitude distribution at 210mL/min N_2 and 7 kV peak applied voltage for negative half period (10,000 current impulses were measured)

When 4.76% O_2 was added to pure N_2, the discharge current increased significantly compared to that in pure N_2 (Figure 4-10). The maximum current amplitude increased significantly from -10 mA to -165 mA: average current amplitude increased from -4.075mA to -56.77 mA.

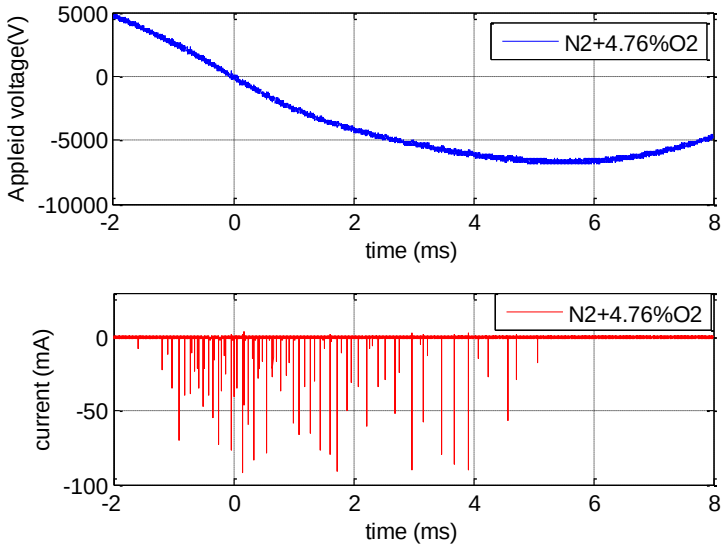

Figure 4-10 Discharge voltage and current waveforms for 210 mL/min of 4.76% O_2 in N_2 at 7 kV peak applied voltage for negative half period (10,000 current impulses were measured)

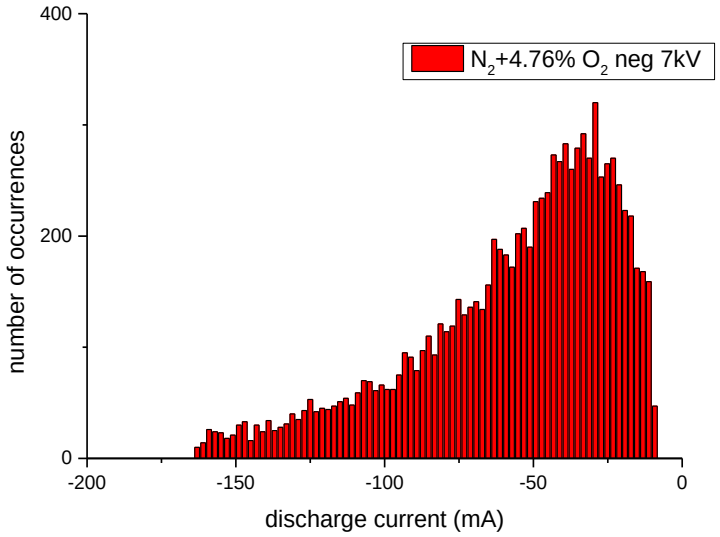

Figure 4-11 Discharge current amplitude distribution for 210mL/min of 4.76% O_2 in N_2 at 7 kV peak applied voltage for negative half period (10,000 current impulses were measured)

4.3.2.4 Discussion of discharge current amplitude under different gas mixtures

The average discharge current amplitude for four different gas mixtures are shown in Table 4-4. When O_2 and a mixture of O_2 and NO were added respectively to pure N_2, the value increased to -56.77 mA and -125.66 mA from -4.075 mA. However, when H_2O vapour was added to the gas mixture of NO, O_2 and N_2, the effect of O_2 and NO was reduced and the average current amplitude was reduced to -5.848 mA, close to the value in pure N_2. Therefore, the amplitude of discharge current, which varied from a few mA to over one hundred mA, depended on the components of the gas mixture.

Table 4-4 The average discharge current amplitude for four different gas mixtures

	N_2	**4.76% O_2 in N_2**	**4.76% O_2+ high concentration NO in N_2**	**4.76% O_2+2.31% H_2O +high concentration NO in N_2**
Average current	-4.075 mA	-56.77 mA	-125.66 mA	-5.848 mA

As shown by the Lissajous figures in Figure 4-12, there was no clear difference in the total charge transfer for the four different gas mixtures. This suggests that more discharge filaments of smaller discharge current amplitude developed, in agreement with visual inspection of the discharge data shown in Figure 4-13: note the change in vertical scale.

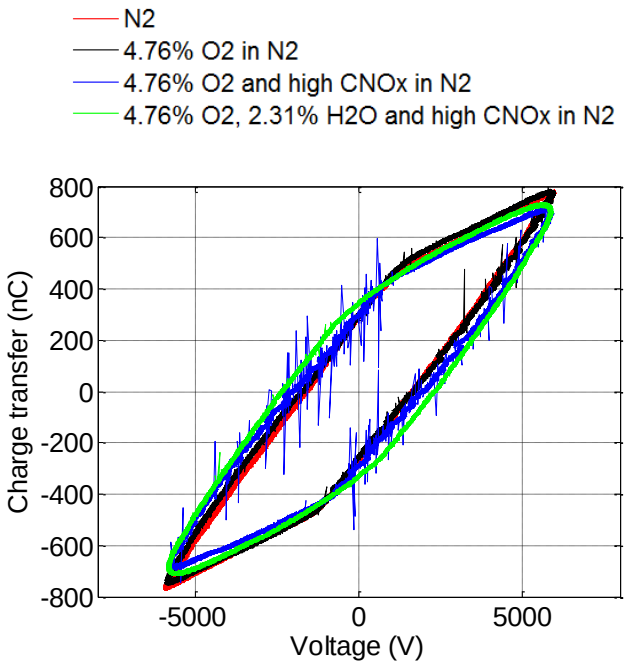

Figure 4-12 Lissajous figures for four different gas mixtures

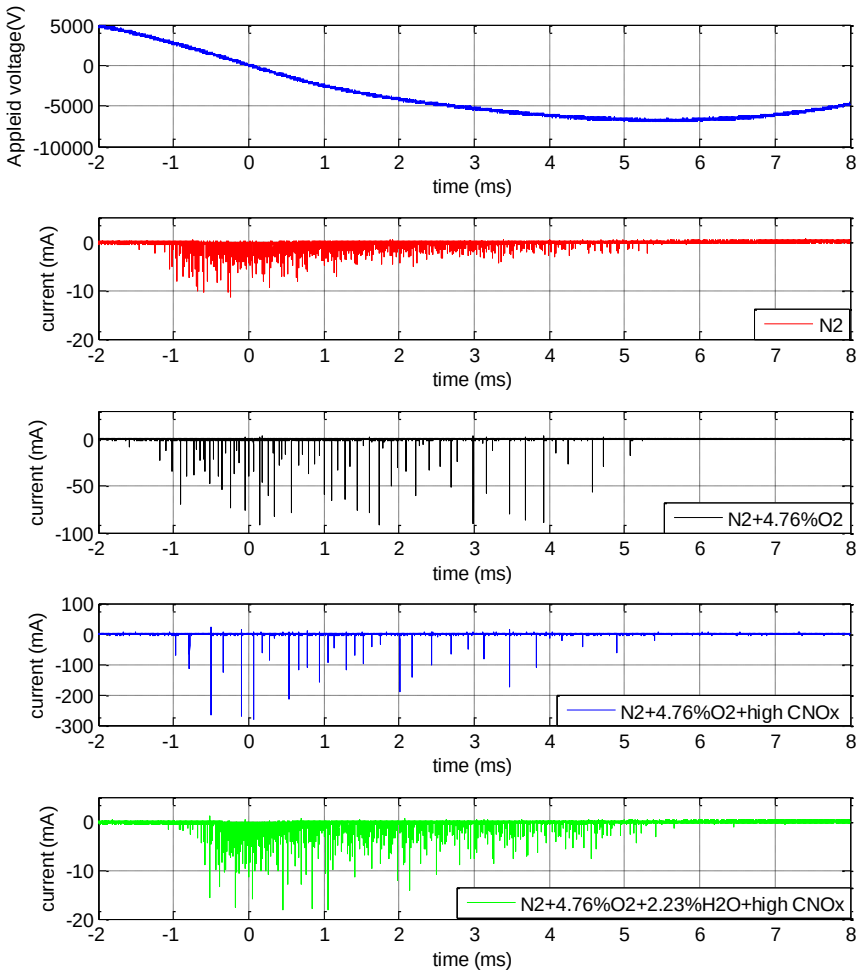

Figure 4-13 Discharge currents for four different gas mixtures at 7 kV peak applied voltage.

In addition, it was found that the breakdown voltage increased with the addition of O_2, NO and H_2O vapour to N_2, see Table 4-5 and Figure 4-14.

Table 4-5 Breakdown voltages for four different gas mixtures

	N_2	**4.76% O_2 in N_2**	**4.76% O_2+ high concentration NO in N_2**	**4.76% O_2+ 2.31% H_2O high concentration NO in N_2**
Breakdown voltage (V)	1637	1704	1995	2315

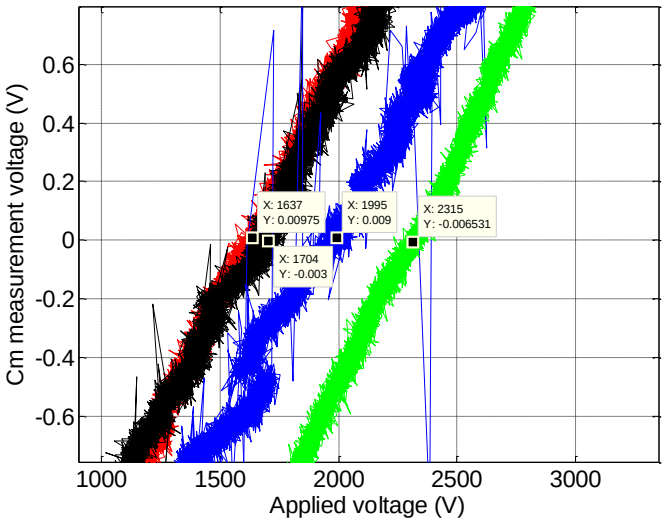

Figure 4-14 Breakdown voltage for four different gas mixtures

A possible reason for the small discharge current amplitude in N_2 is that there were many metastable and excited states of N_2 in the gap as a result of the discharges. These were the source for generating seed electrons for gas discharge, being much easier to ionize and to produce free electrons in comparison to the ionization of ground state N_2: the ionization energy of ground state N_2 is approximately 15.6 eV [102], while an electron colliding with $N_2(a'^1\Sigma_u^-)$ (a metastable state of N_2) requires only 7.03 eV to initiate the ionization. Some energy levels of metastable and excited states of N_2 are shown in Table 4-6. When there are many metastable N_2 molecules, discharge occurs in a Townsend-like discharge mode, where the density of charges in a filament is low and the distortion of local electric field is not significant [103], so the discharge current amplitude is small.

Table 4-6 Some metastable and excited states of N_2 and their correspond energy level.

Species	**state**	**Energy (eV)**
N_2	$A^3\Sigma_u^+$ (metastable)	6.22
N_2	$B^3\Pi_g$ (excited)	7.39
N_2	$a'^1\Sigma_u^-$ (metastable)	8.57
N_2	$C^3\Pi_u$ (excited)	11.05

However, as shown above, in experiments when 4.76% O_2 was added to N_2, discharge current amplitudes increased significantly and the average current amplitude increased from -4.075 mA to -56.77 mA. One possible reason for the change of discharge current magnitudes is related to the high quenching rate of O_2 to metastable states of N_2 shown in Table 4-7. Basically, O_2 can quickly react with N_2's excited and metastable states and so there is less chance for these excited states of N_2 to generate atomic N, because they are quenched by O_2 and NO and used to dissociate O_2. Brandenburg [104] stated that the lifetime of N_2's excited and metastable states are reduced significantly by the presence of O_2, e.g. 1000 ppm of O_2 would effectively reduce the lifetime of N_2's metastable states, so 4.76% O_2 would be expected to significantly reduce the number of N_2 molecules metastable states. With the decrease in N_2 atoms in metastable states, gas ionization would become more difficult and require a higher electric field. This is one possible explanation for the increase of breakdown voltage from 1637 V to 1704 V. In turn, under higher electric field the density of charges in a discharge filament would be high enough to distort local electric fields, which caused an abrupt increase in the discharge current amplitude [104].

For 4.76% O_2 and high concentration NO in N_2 condition, where 855 ppm NO existed in the gas mixture, the effect of NO is similar to, but even stronger than, that of O_2, because the quenching effect of NO on N_2's metastable states is higher than that of O_2. The quenching rate of NO is an order higher than O_2 for metastable states of nitrogen $N_2(A^3\Sigma_u)$ and $N_2(a'^1\Sigma_u^-)$ (Table 4-7). The presence of NO significantly changes the average discharge current amplitude from -56.77 mA to -125.66 mA (Table 4-4) and the corresponding breakdown voltage increased from 1704 V to 1995 V (Table 4-5).

Table 4-7 Quenching effect of O_2 and H_2O and NO on N_2's metastable states [105].

Reactions	A ($cm^3 \cdot s^{-1}$)
$N_2(A^3\Sigma_u) + O_2 \rightarrow N_2 + O_2$	1.3-2.5 $\times 10^{-12}$
$N_2(A^3\Sigma_u) + H_2O \rightarrow N_2 + H + OH$	5.0 $\times 10^{-14}$
$N_2(A^3\Sigma_u) + NO \rightarrow N_2 + NO(A^2\Pi^+)$	7.0 $\times 10^{-11}$
$N_2(a'^1\Sigma_u^-) + O_2 \rightarrow N_2 + O(^3P) + O(^3P)$	2.8 $\times 10^{-11}$
$N_2(a'^1\Sigma_u^-) + NO \rightarrow N_2 + O(^3P) + N(^4S)$	3.6 $\times 10^{-10}$
$N_2(a'^1\Sigma_u^-) + H_2O \rightarrow N_2 + OH + H$	3.0 $\times 10^{-10}$

However, when 2.31% H_2O vapour was introduced to the gas mixture, the discharge current reduced from -125.66 mA to -5.848 mA. Although H_2O vapour has the ability to quench N_2's excited states, H_2O electron attachment ability played a more important role in limiting the amplitude of discharge current. As shown in Table 4-8, the electron attachment cross section of H_2O is more than six times higher than that of O_2 and NO. It can capture free electrons to limit the development of discharge filament, which leads to a higher breakdown voltage (Table 4-5). Under this condition the breakdown voltage was further increased, to 2315 V, because of the confinement of free electrons. Negative ions generated as a result of electron capture did not contribute to additional ionization, so the amplitude of the discharge current was small.

Table 4-8 Gas species' corresponding peak values for an electron attachment cross section

Gas species	Peak cross section	Reactions
H_2O [106]	6×10^{-18} cm^{-2}	$e^- + H_2O \rightarrow OH + H^-$
O_2 [107]	1.4×10^{-18} cm^{-2}	$e^- + O_2 \rightarrow O + O^-$
NO [108]	1.1×10^{-18} cm^{-2}	$e^- + NO \rightarrow N + O^-$

4.4 Effect of oxygen on NO removal

As shown in Table 2-2, practical flue gases have an O_2 concentration of 4.5%, approaching the concentration of O_2 used in this experiment, from 4.76%. In order to analyse the effect of O_2 on NO removal, O_2 concentration was further increased to 16.67%. In this series of experiments no water vapour was added to the gas mixture and, as the dew point of cylinder gas was -40^{o}C and the gas temperature was controlled at 44^{o}C, the water vapour effect can be ignored. The NO removal and energy efficiency were investigated under different applied voltages. During the DBD process O_2 played an important role in generating O and O_3, two important reactive oxygen species for NO removal. In order to quantitatively analyse the effect of O_3 for NO removal, a reference experiment was conducted by using a mixture of N_2 and O_2 but without NO: it provides a reference level of O_3 formation.

4.4.1 O_3 formation in reference gas without NO

For the reference experiment, the gas mixture consisted only of N_2 and O_2. The aim of measuring O_3 formation in the reference gas condition was to probe which of the reactive

species, O and O_3, was more important for NO removal. As discussed in Chapter 2, both O and O_3 can oxidize NO to NO_2, but O causes a side reaction to produce NO as a result of the reaction between NO_2 and O. O_3 does not cause any side reaction for NO removal. Therefore, if NO removal is close to the O_3 formation in the reference gas, O_3 is the dominant reactive species for NO removal. The flow rates of N_2 and O_2 under different O_2 concentration are shown in Table 4-9. The O_3 formation curves for different O_2 concentration under different applied voltage, seen in Figure 4-15, indicate a linear relationship between applied voltage and O_3 formation for all three O_2 concentrations. The increase of O_3 formation with increasing applied voltage was faster when the concentration of O_2 was higher. The volumes of O_3 formed were 143 ppm, 253 ppm and 394 ppm, for 4.76%, 9.09% and 16.67% O_2 respectively at an applied voltage of 7kV. It should be noted that data points with error bars in this chapter are the average of 5 results and the error bar is the standard deviation of these results.

Table 4-9 Flow rates of N_2 and O_2 for different O_2 concentration

C_{O2} (% vol)	FR of N_2 (sccm)	FR of O_2 (sccm)
4.76	200	10
9.09	200	20
16.67	200	40

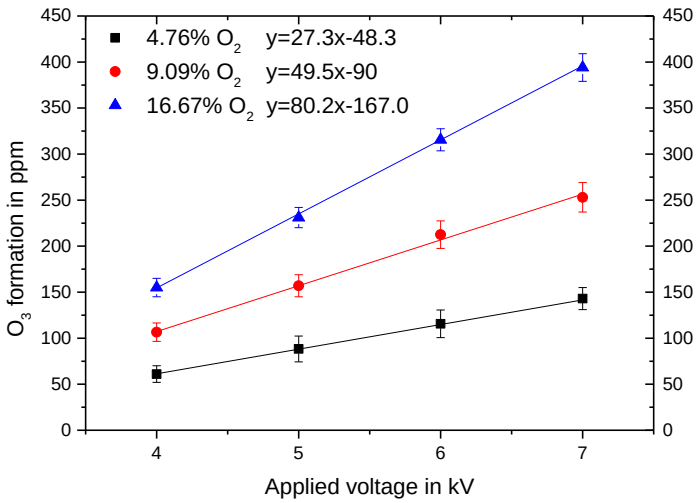

Figure 4-15 O_3 formation under different applied voltage

In addition, an O_3 formation curve under different O_2 concentration for a peak applied voltage of 7kV and a corresponding discharge power of 0.25 W is shown in Figure 4-16. Under this level of discharge power, the side reaction between O and O_3 is negligible, providing a linear relationship between O_3 formation and O_2 concentration.

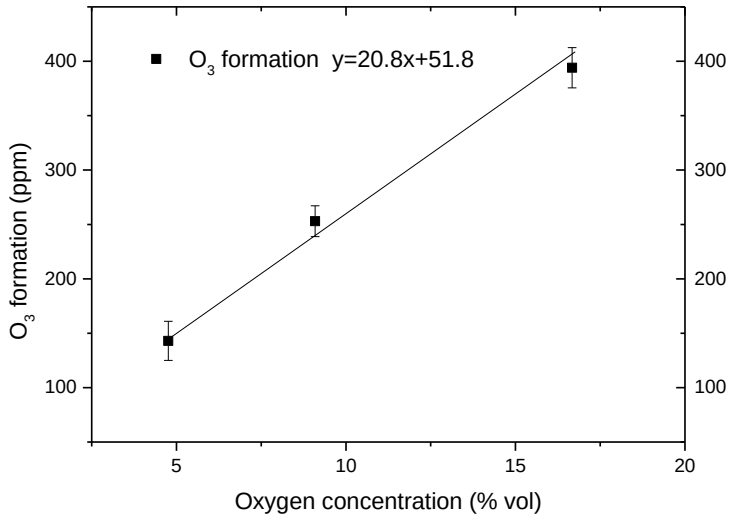

Figure 4-16 O_3 formation under different O_2 concentration at 7 kV peak applied voltage under the mixture of O_2 and N_2

4.4.2 High concentration NO condition

The initial concentrations of NO and NO_2 under different O_2 concentration are shown in Table 4-10. During the discharge process under different O_2 concentration, no O_3 was measured from the output of the DBD reactor.

Table 4-10 NO, NO_2 and NOx concentrations for high concentration NO condition before DBD treatment

C_{O2} (% vol)	FR of 1000ppm NO in N_2 (sccm)	FR of O_2 (sccm)	C_{NO} (ppm)	C_{NO2} (ppm)	C_{NOx} (ppm)
4.76	200	10	855	102	957
9.09	200	20	756	163	919
16.67	200	40	614	203	817

For 4.76% O_2 and high concentration NO in N_2 condition, NO and NO_2 concentrations changed as the applied voltage increased from 0 kV to 7 kV, Figure 4-17. Because there was no discharge below 4kV, there was no change in NO and NO_2 concentration for applied

voltages in the range of 1kV to 3kV. For applied voltages in the range of 4kV to 7kV the concentration of NO gradually reduced from 855 ppm to 642 ppm, indicating that 213 ppm NO had been removed. The concentration of NO_2 increased from 102 ppm to 247 ppm which indicated the formation of 145 ppm NO_2. The 68 ppm difference between NO removal and NO_2 formation would be caused by atomic N reducing NO to N_2. As shown in Figure 4-18, with the increase of applied voltage from 4 kV to 7 kV, the NO removal increased from 111 ppm to 213 ppm,

According to equation (4-5), the energy efficiencies under different applied voltages can be calculated.

$$\eta_{NO} = \frac{\frac{FR}{22.4} * R_{NO} * M_m * 6 * 10^{-5}}{P} \quad \textbf{(4-5)}$$

The discharge power (P) under different applied voltages was shown in Table 4-2. Because the flow rate (FR) is 210 mL/min and the molar mass of NO (M_m) is 30g/mole, for the range of the removal rates (R_{NO}), i.e. 111ppm, 146 ppm, 177 ppm and 213 ppm, the NO removal energy efficiency was calculated to be 25 g/kWh, 20.98 g/kWh, 17.19 g/kWh and 13.2 g/kWh, respectively see Figure 4-18.

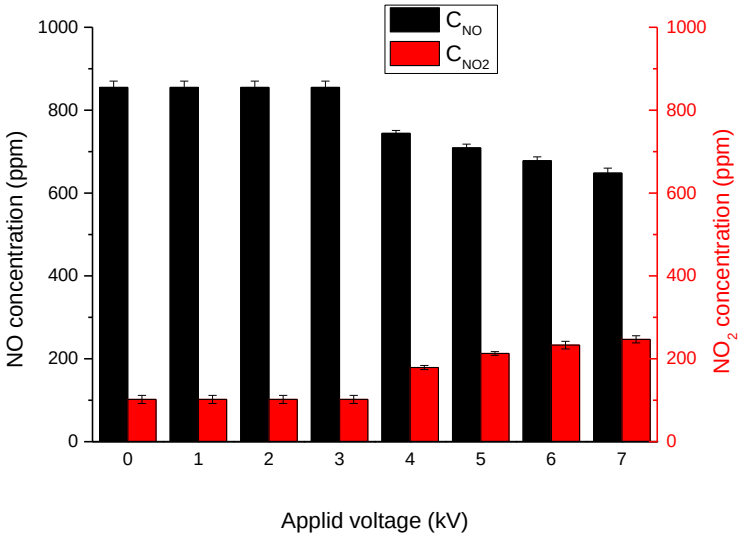

Figure 4-17 NO and NO_2 concentrations at different applied voltage at 4.76% O_2 high concentration NO in N_2 condition

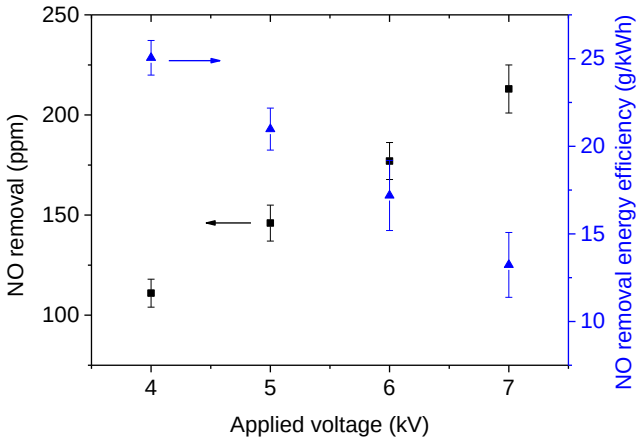

Figure 4-18 NO removal and energy efficiency at different applied voltage under high concentration NO, 4.76% O_2 in N_2 condition

In order to consider the effect of O_2 concentration on NO removal, two additional oxygen concentrations of 9.09% and 16.67% were investigated at a high concentration NO condition. For a 9.09% O_2 condition, with the increase in applied voltage from 4 kV to 7 kV, although the amount of NO removed increased from 96 ppm to 168 ppm, the NO removal energy efficiency reduced from 22.67 g/kWh to 11.98 g/kWh, see Figure 4-19. For 16.67% O_2 condition, with the increase of applied voltage from 4 kV to 7 kV, NO removal increased from 83 ppm to 148 ppm but NO removal energy efficiency reduced from 19.79 g/kWh to 10.4 g/kWh, see Figure 4-20. The general trend of NO removal and energy efficiency was similar to that for 4.76% O_2, i.e. less efficient with increasing O_2 concentration.

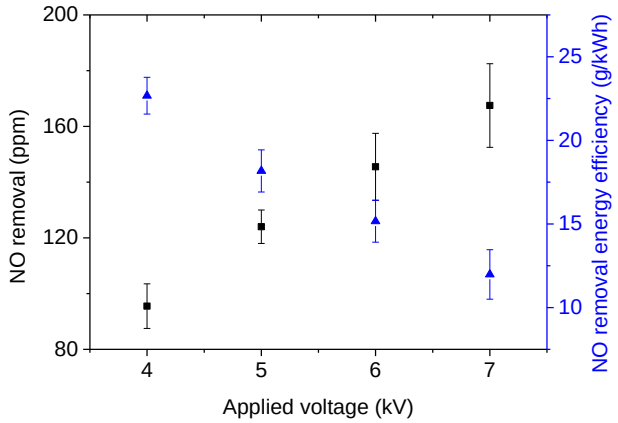

Figure 4-19 NO removal and corresponding energy efficiency at different voltage under high concentration NO, 9.09% O_2 in N_2 condition

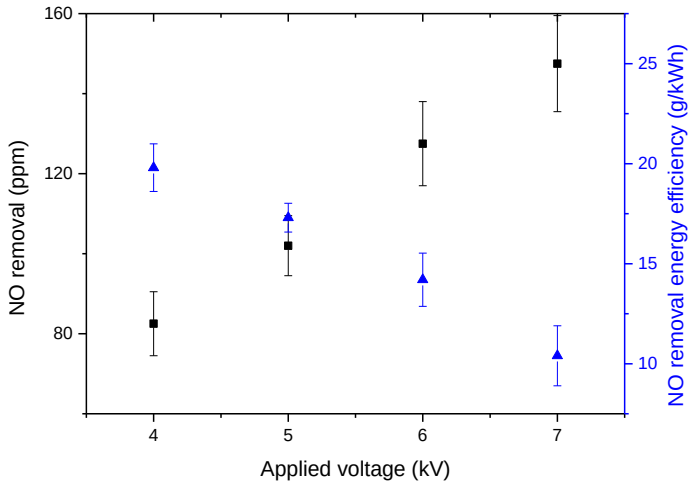

Figure 4-20 NO removal and corresponding energy efficiency at different voltage under high concentration NO, 16.67% O_2 in N_2 condition

As shown in Figure 4-21, it was found that both the NO removal and energy efficiency curves were shifted downwards with increasing O_2 concentration.

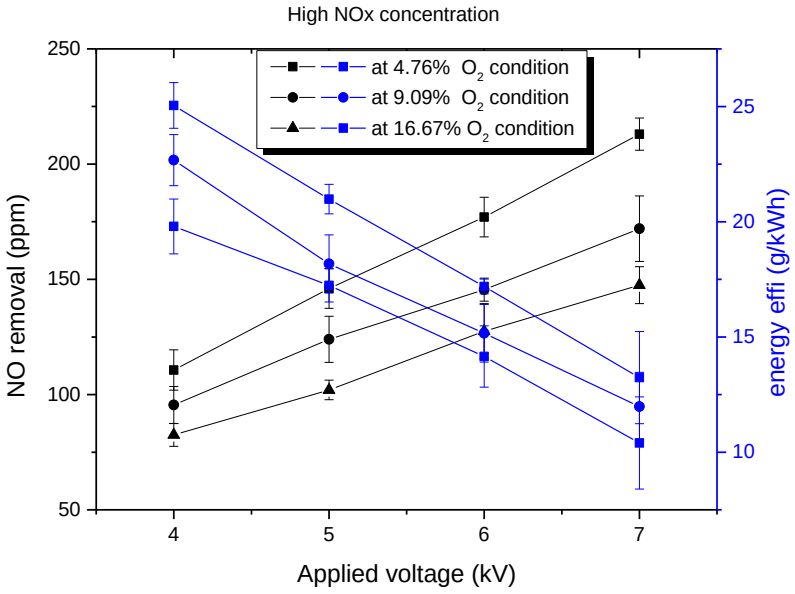

Figure 4-21 Effect of O_2 concentration on NO removal and energy efficiency at high concentration NO condition

In order to determine the reason for this, a comparison between NO removal and NO_2 formation was made at 7 kV peak applied voltage, Figure 4-22. It was found that NO removal was reduced with increasing O_2 concentration, but NO_2 formation was nearly constant. As mentioned before, there was an additional reaction pathway (4-6) for NO removal by N which led to the difference between NO removal and NO_2 formation. However, according to the trend shown in Figure 4-22, N became difficult to generate with increasing O_2 concentration, so the reason why NO removal reduced was the reduction in N formation.

$$\boldsymbol{N + NO \rightarrow N_2 + O} \tag{4-6}$$

This was probably related to the quenching effect of O_2 on the metastable states of N_2. As discussed before, the dissociation energy for N_2 was 12.181eV, so electrons needed to have at least 12.181 eV to dissociate a ground state N_2. The energy requirement for an electron to dissociate N_2 ($A^3\Sigma_u^+$) metastable state reduced to 5.961 eV. While the energy of the electrons was mainly in the range of 1 to 10 eV, see Table 2-15, it was easier to dissociate metastable state N_2, rather than the ground state N_2. However, because of the quenching effect of O_2, many metastable states of N_2 transferred their energy to O_2 and become ground state N_2. The possibility of obtaining N was less for higher O_2 concentration.

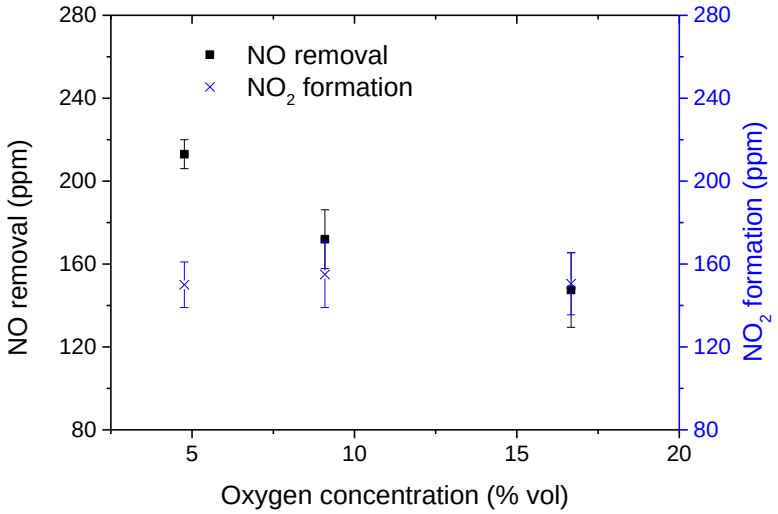

Figure 4-22 NO removal and NO_2 formation at different O_2 concentration under high concentration NO condition, 7 kV peak applied voltage.

For a constant NO_2 formation under different O_2 concentrations at high concentration NO condition, a comparison was made between O_3 formation in the reference gas and the NO_2

formation at the high concentration NO condition in Figure 4-23. If O_3 is the dominant reactive species for NO oxidation at high concentration NO condition, then NO_2 formation should increase rather than being constant with increasing O_2 concentration. As this was not the case, one possible reason could be that NO oxidation is caused by O rather than O_3. The side reaction between NO_2 and O to form NO could limit the NO_2 formation, as discussed in Chapter 2 chemical kinetics for NOx removal.

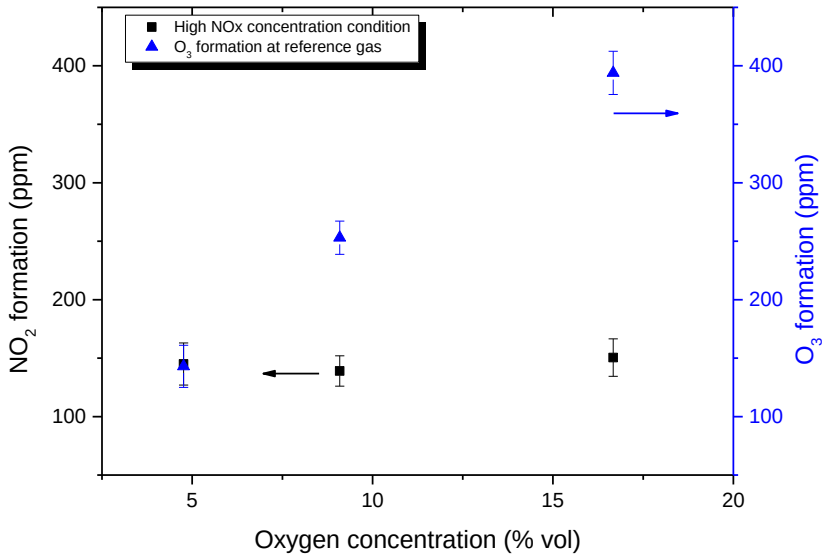

Figure 4-23 Comparison between NO_2 formation in high concentration NO condition and O_3 formation in reference gas condition at 7 kV peak applied voltage

The reason why O was the dominant oxidant at high concentration NO condition could be verified by analysing the reaction rate. The reaction rate constant between atom O and O_2, in Figure 4-24, was 2034 and 658 times lower than that of the reaction between O and NO, and the reaction between O and NO_2 respectively. The total concentration of NO and NO_2 was approximately 1000 ppm, but the concentration of O_2 was in the range of 4.76% to 16.67%, i.e. about 47.6 to 166.7 times higher than that of NOx. However, O would be expected to react with NOx rather than O_2, i.e. O would be the dominant oxidant for NO oxidation under a high concentration NO condition.

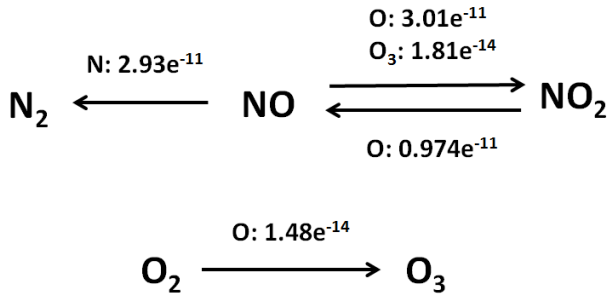

Figure 4-24 The chemical reaction pathways and reaction rate constants for NO removal

In addition, the relationship between the output concentration of NO and NO_2 was considered. If O is uniformly distributed in the gas gap for NO oxidation, according to the reaction rate constant shown in Figure 4-24, the ratio of NO to NO_2 concentration is expected to be 1:3. However, as shown in Table 4-11, the measured NO and NO_2 concentrations after DBD treatment were 648 ppm and 247 ppm at 4.76% O_2 condition. The corresponding ratio was 1:0.381, i.e. much higher than 1:3. When the concentration of O_2 increased to 16.67%, the concentration of NO and NO_2 became 466 ppm and 353 ppm respectively and the ratio was 1:0.758, i.e. still higher than 1:3. This suggests that O was not present throughout the whole gas gap. As mentioned before, the discharge is in the filamentary mode under atmospheric pressure and the lifetime of O is in tens of μs, so O can only exist in the discharge filament, where the ratio of NO to NO_2 should 1:3, but the effective volume was much smaller than the whole reactor volume. The ratio of NO to NO_2 concentration was larger than 1:3, i.e. the chemical equilibrium between NO and NO_2 may be achieved in the discharge filament but not achieved in the whole reactor.

Table 4-11 NO and NO_2 concentration at 0 kV and 7 kV peak applied voltage

C_{O2} (% vol)	$V_{a\,p.}$ (kV)	$C_{(NO)}$ (ppm)	$C_{(NO2)}$ (ppm)	Ratio C_{NO}/C_{NO2}
4.76%	0	855	102	1:0.119
	7	648	247	1:0.381
9.09%	0	756	163	1:0.216
	7	588	302	1:0.514
16.67%	0	614	203	1:0.331
	7	466	353	1:0.758

4.4.3 Upper medium concentration NO condition

In order to further analyse the dominant reactive species at a lower NO concentration condition, experiments on upper medium concentration NO were conducted. The initial concentrations of NO and NO_2 for upper medium concentration NO condition are shown in Table 4-12. The initial NO concentration was diluted to the required concentration by adding N_2. Some NO was oxidized to NO_2 by O_2, and NO_2 concentration increased with increasing O_2 concentration. As shown in Figure 4-25, there was no significant difference for the NO removal and energy efficiency under difference O_2 concentrations. For peak applied voltage of 4kV approximately 90 ppm of NO was removed with 22g/kWh energy efficiency. When the peak applied voltage increased to 7kV, the NO removal was 150 ppm with 12g/kWh energy efficiency.

Table 4-12 NO, NO_2 and NOx concentrations for upper medium concentration NO condition before DBD treatment

C_{O2} (% vol)	FR of N_2 (sccm)	FR of 1000ppm NO in N_2 (sccm)	FR of O_2 (sccm)	C_{NO} (ppm)	C_{NO2} (ppm)	C_{NOx} (ppm)
4.76	80	120	10	550	41	591
9.09	80	120	20	486	80	566
16.67	80	120	40	426	101	527

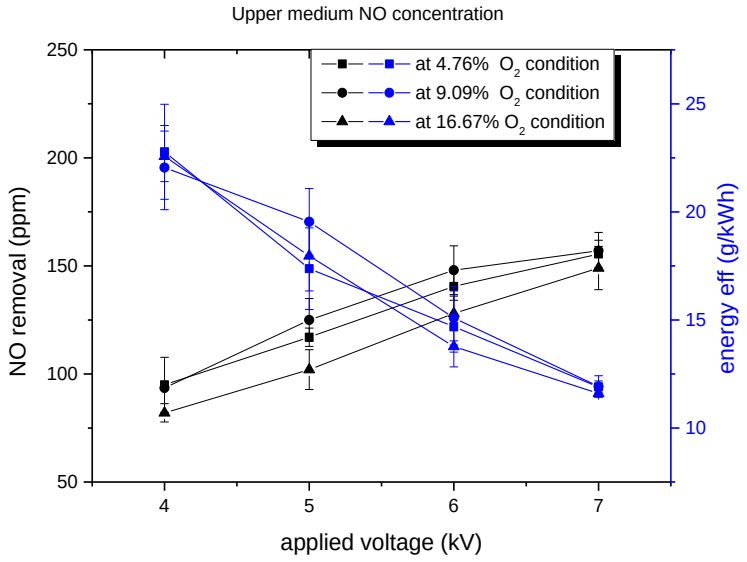

Figure 4-25 NO removal and energy efficiency for upper medium concentration NO condition at 4.76% O_2 condition, 9.09% O_2 condition and 16.67% O_2 condition

As discussed before in comparing the NO removal and energy efficiency between high and upper medium concentration NO conditions, with increasing O_2 concentration the amount of NO removed was reduced, because of the reduction of N formation at a high concentration NO condition. However, according to Figure 4-25, NO removal was nearly unchanged at upper medium concentration NO condition. This suggests that N had difficulty in reacting with NO at this upper medium concentration: the difference between NO removal and NO_2 formation is less than 20 ppm for the three O_2 concentrations, as shown in Figure 4-26. As shown in Table 4-13, the ratio of C_{NO} to C_{NO2} was consistently much higher than 1:3, so the chemical equilibrium between NO and NO_2 was not achieved.

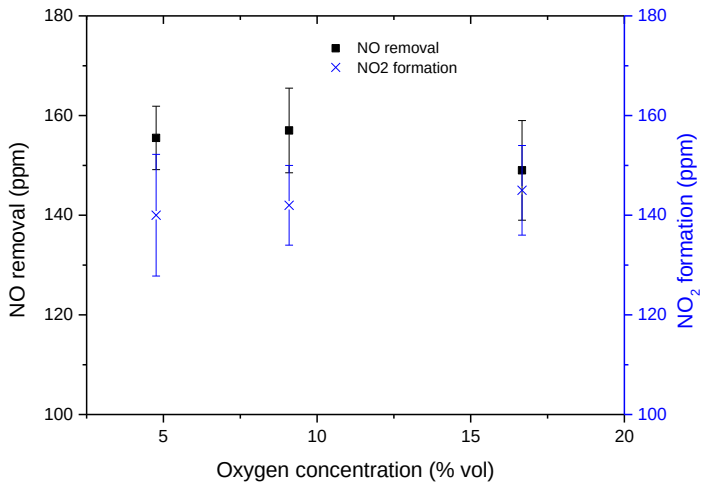

Figure 4-26 NO removal and NO_2 formation at different O_2 concentration at upper medium concentration NO condition, 7 kV peak applied voltage

Table 4-13 NO and NO_2 concentration at 0 kV and 7 kV peak applied voltage

C_{O2} (vol)	$V_{a\,p.}$ (kV)	$C_{(NO)}$ (ppm)	$C_{(NO2)}$ (ppm)	Ratio of C_{NO}/C_{NO2}
4.76%	0	550	41	1:0.075
	7	395	181	1:0.458
9.09%	0	486	80	1:0.165
	7	329	222	1:0.675
16.67%	0	426	101	1:0.237
	7	277	246	1:0.888

A comparison was made between O_3 formation in the reference gas and NO_2 formation in upper medium concentration NO condition, see Figure 4-27. NO_2 formation was nearly constant and did not follow the trend of O_3 formation in the reference gas, so it was proved that O is the dominant reactive species at upper medium NOx condition.

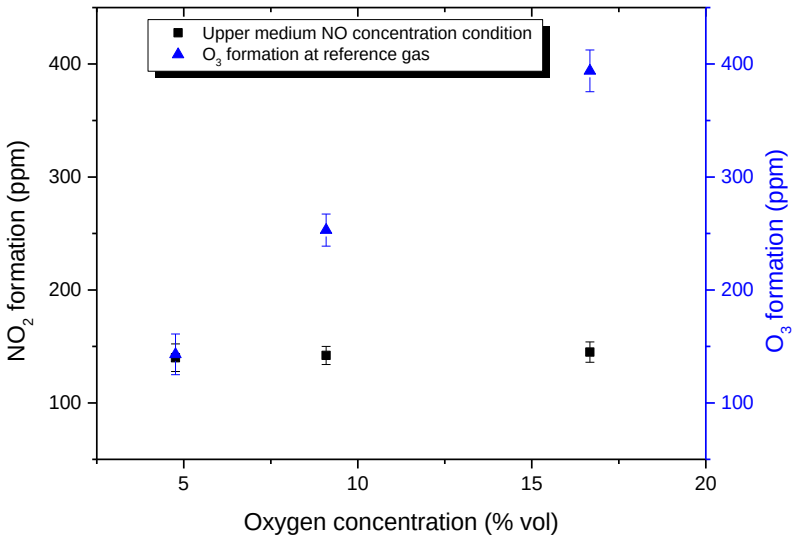

Figure 4-27 Comparison between NO_2 formation in upper medium concentration NO condition and O_3 formation at reference gas condition 7 kV peak applied voltage

4.4.4 Medium concentration NO condition

The initial concentrations of NO and NO_2 for medium concentration NO condition are shown in Table 4-14. For medium concentration NO, the NO removal and energy efficiency curves are shown in Figure 4-28. With increasing applied voltage, NO removal increased but NO removal energy efficiency decreased. This was the same trend as high and upper medium concentration NO conditions, however, it was found that with increasing O_2 concentration, the NO removal and energy efficiency were both increased in medium concentration NO condition, see Figure 4-28. When the peak applied voltage was 7kV, the NO removal and energy efficiency were 109 ppm and 7.92 g/kWh at 4.76% O_2 concentration condition, but they increased to 155 ppm and 14.77 g/kWh when O_2 concentration increased to 16.67%. One possible reason was that some O had the chance to react with O_2 to generate O_3 which can oxidize NO without any side reaction.

Table 4-14 NO, NO_2 and NOx concentrations for medium concentration NO condition before DBD treatment

C_{O2} (% vol)	FR of N_2 (sccm)	FR of 1000ppm NO in N_2 (sccm)	FR of O_2 (sccm)	C_{NO} (ppm)	C_{NO2} (ppm)	C_{NOx} (ppm)
4.76	160	40	10	189	13	202
9.09	160	40	20	176	15	191
16.67	160	40	40	158	21	179

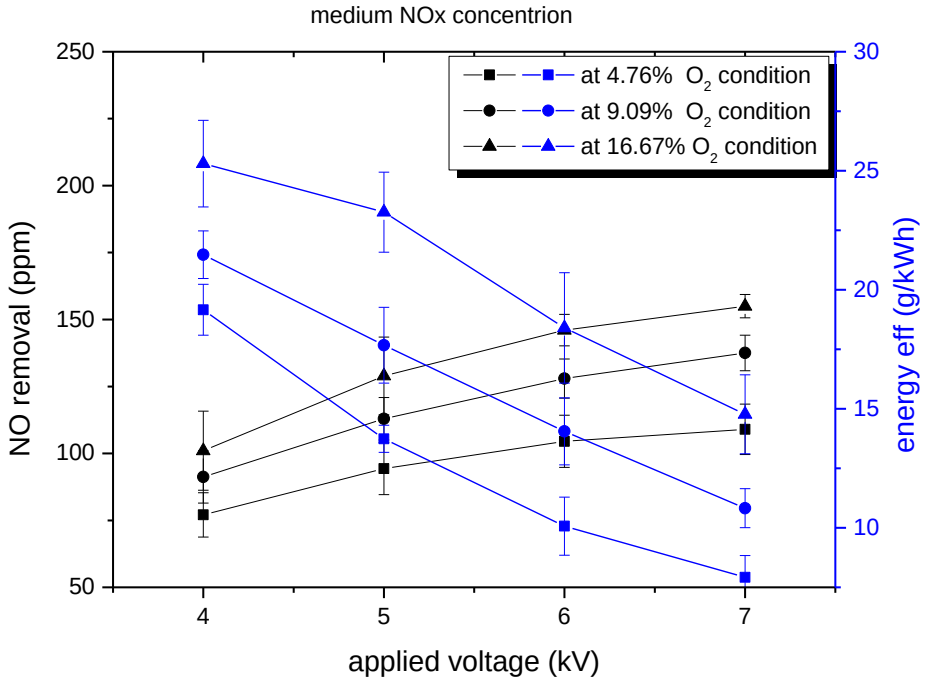

Figure 4-28 NO removal and energy efficiency for medium concentration NO condition at 4.76% O_2 condition, 9.09% O_2 condition and 16.67% O_2 condition

In order to analyse whether there is O_3 generated to oxidize NO, a comparison was made between O_3 formation in the reference gas and NO_2 formation at medium concentration NO condition. Figure 4-29 indicates that there was a drop in NO_2 formation when O_2 concentration increased from 9.09% to 16.67%. In addition, according to the concentrations of NO and NO_2 shown in Table 4-15, it was found that the ratio of NO concentration (42 ppm) and NO_2 concentration (144 ppm) was 1:3.43 at 9.09% O_2 condition, which was close to 1:3. If O_2 concentration further increased to 16.67%, the ratio became 1:130 which was much less than 1:3. If O is the reactive species for NO oxidation, at the chemical equilibrium condition, the ratio of NO concentration and NO_2 concentration cannot be lower than 1:3. However, as the actual ratio was 1:130, this suggests that another reactive species, O_3, was generated which can break the chemical equilibrium between NO and NO_2. In addition, for an O_2 concentration of 16.67%, the total concentration of NO and NO_2 reduced from 179 ppm to 133 ppm as the peak applied voltage increased from 0 kV to 7 kV. Firstly, as discussed for high concentration NO, the contribution of N to reduction of NO at 16.67% O_2 condition was negligible. A possible reason was that part of NO_2 was further oxidized to N_2O_5, the amount of which could not be measured. Comparing the NO removal at medium

NO concentration condition and O_3 formation at reference gas condition: for 4.76% O_2 condition, O_3 concentration in the reference gas was 143 ppm and NO removal was 101 ppm at medium NO concentration condition; for 9.09% O_2 condition, O_3 concentration in reference gas was 253 ppm and NO removal was 134 ppm at medium NO concentration condition. This suggests that even though O_3 oxidizes NO and NO_2, the contribution was not dominant. Therefore, NO oxidation was part of the synergistic effect of O and O_3 in medium concentration NO condition.

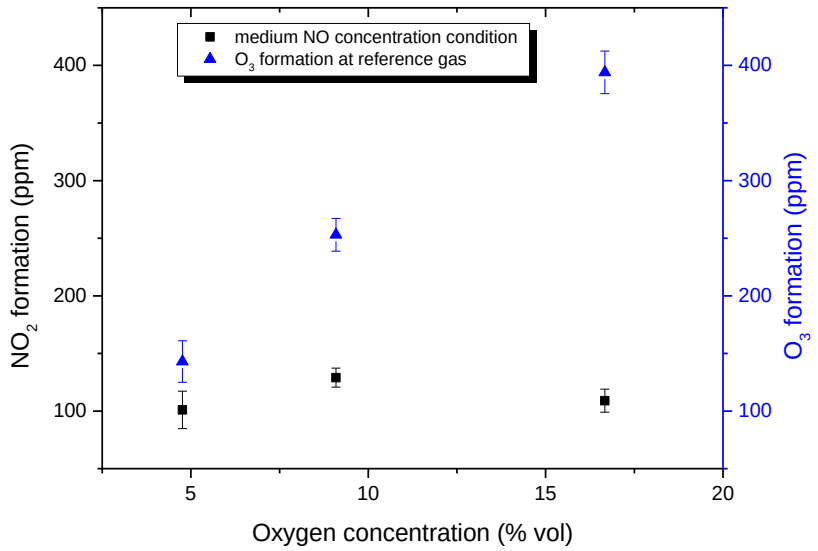

Figure 4-29 Comparison between NO_2 formation in medium concentration NO condition and O_3 formation in reference gas condition at 7 kV peak applied voltage

Table 4-15 NO and NO_2 concentration at 0 kV and 7 kV peak applied voltage

C_{O2} (vol)	$V_{a\,p.}$ (kV)	$C_{(NO)}$ (ppm)	$C_{(NO2)}$ (ppm)	Ratio of C_{NO}/C_{NO2}
4.76%	0	189	13	1:0.069
	7	88	114	1:1.295
9.09%	0	176	15	1:0.085
	7	42	144	1:3.429
16.67%	0	158	21	1:0.133
	7	1	130	1:130

The NO removal at different initial gas concentrations but with consistent 4.76% O_2 is illustrated in Figure 4-30. NO removal increased but energy efficiency decreased with increasing applied voltage: reduction in NO concentration made it was more difficult to maintain the same NO removal efficiency. At higher initial concentration of NO while under the same applied voltage, more NO was removed and higher energy efficiency was achieved Figure 4-30 (b). As shown, at 7 kV peak applied voltage, the energy efficiency reduced from 13.2 g/kWh, 11.9 g/kWh to 8.2 g/kWh respectively for high, upper medium and medium concentration NO conditions.

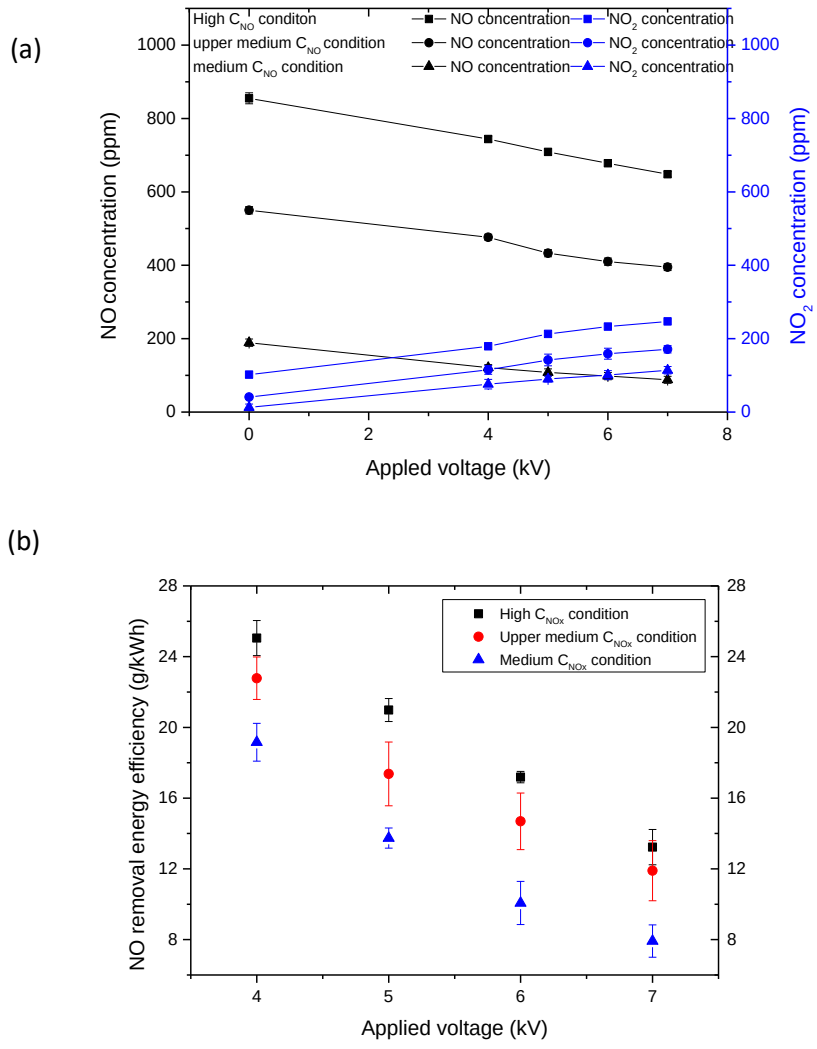

Figure 4-30 (a) NO removal and NO_2 formation and (b) energy efficiency at different applied voltage at 4.76% O_2 condition for high (solid square), upper medium (solid circle) and medium (solid up triangle) concentration NO conditions

4.4.5 Lower medium concentration NO condition

The initial concentrations of NO and NO_2 for lower medium concentration NO condition are shown in Table 4-16. As shown in Figure 4-31, for 4.76% O_2 condition, NO removal increased and energy efficiency decreased with increasing applied voltage: at 7 kV peak applied voltage, NO concentration reduced from 150 ppm to 46 ppm.

Table 4-16 NO, NO_2 and NOx concentrations for lower medium concentration NO condition before DBD treatment

C_{O2} (% vol)	FR of N_2 (sccm)	FR of 1000ppm NO in N_2 (sccm)	FR of O_2 (sccm)	C_{NO} (ppm)	C_{NO2} (ppm)	C_{NOx} (ppm)
4.76	170	30	10	150	8	158
9.09	170	30	20	140	11	151
16.67	170	30	40	126	16	142

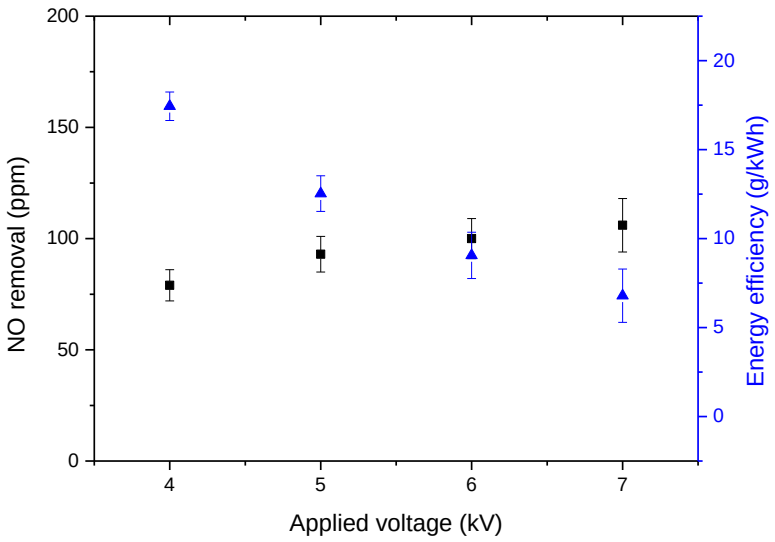

Figure 4-31 NO removal and energy efficiency at 4.76% O_2 and lower medium concentration NO in N_2 condition

For 9.09% O_2 condition, as mentioned before, there is no discharge before the applied voltage increased to 4kV. It was found that when the applied voltage increased to 6kV, NO was nearly fully oxidized. Based on the earlier investigations, that meant O_3 was generated for NO oxidation, as O cannot oxidize NO in such high concentration due to the side reaction

between NO_2 and O: for O_3, there is no side reaction. When the applied voltage was increased to 7 kV, NO_2 concentration reduced from 142 ppm to 100 ppm, see Figure 4-32. During this experiment, no O_3 was measured, indicating that all generated O_3 was used up.

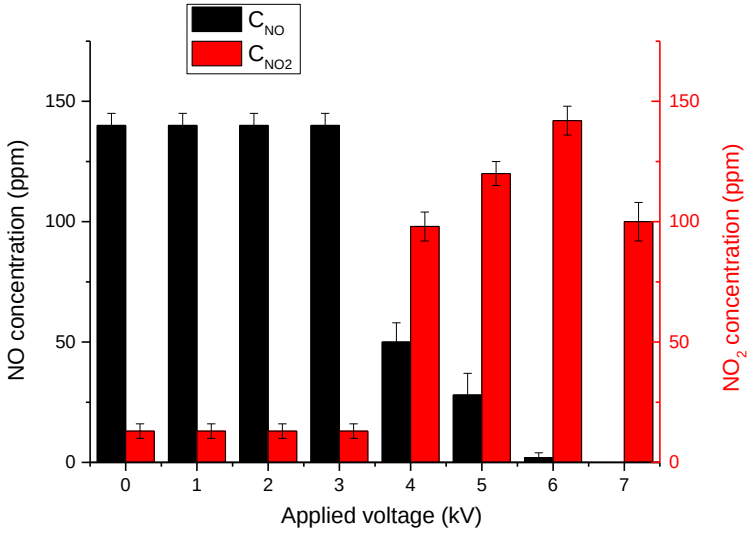

Figure 4-32 NO and NO_2 concentration at different applied voltage under 9.09% O_2 lower medium concentration NOx in N_2 condition

For 16.67% O_2 condition, as seen in Figure 4-33, NO was fully oxidized at 5 kV, as evidenced by the zero NO content. This was 1kV less than the value for 9.09% O_2 condition to fully oxidize NO. When the applied voltage increased to 6kV, NO_2 was fully oxidized and O_3 was measured at the output of DBD reactor.

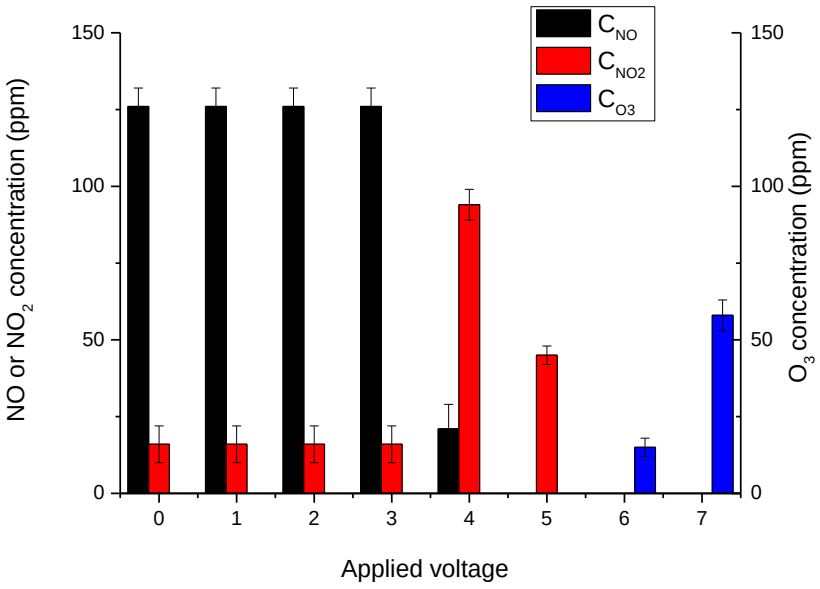

Figure 4-33 NO and NO_2 concentration at different applied voltage under 16.67% O_2 lower medium concentration NOx in N_2 condition

Because O_3 can be measured only after all of NO and NO_2 have fully oxidized to N_2O_5, it was necessary to consider how to quantitatively analyse how much O_3 was generated in total, Equation (4-7) was used to calculate the equivalent O_3 formation, As highlighted in Chapter 2, and shown in Figure 4-34, there is no side reaction to oxidize NO and NO_2 to N_2O_5 by O_3.

$$C_{equal\ O_3} = \Delta C_{NO\ rem} + \frac{\Delta C_{NO\ rem} - \Delta C_{NO2\ form}}{2} + C_{O3} \quad \textbf{(4-7)}$$

where:

$\Delta C_{NO\ rem}$ represents O_3 usage for NO removal;

$\frac{\Delta C_{NO\ rem} - \Delta C_{NO2\ form}}{2}$ represents NO_2 oxidation to N_2O_5 (including the initial NO_2 and generated NO_2 from NO oxidation) ;

C_{O_3} represents the remaining O_3 measured after all of NO and NO_2 are oxidised to N_2O_5.

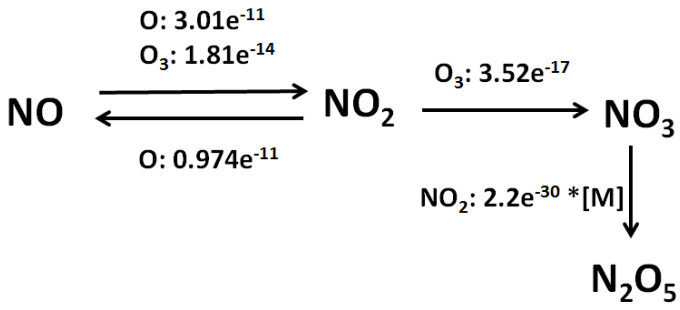

Figure 4-34 Chemical reaction pathways and reaction rate constants for NOx oxidation by O and O_3

For reaction (4-8), M is a third reactant whose function is to absorb extra energy from the reaction. M can be any kind of molecule in the gas mixture. [M] is the concentration of M, at standard condition; [M] is 2.6875×10^{19} cm^{-3}.

$$NO_2 + NO_3 + M = N_2O_5 + M \quad \textbf{(4-8)}$$

In order to analyse the effect of O_2 concentration for NO and NO_2 oxidation, only the condition where the peak applied voltage was 7kV was used: the corresponding NO, NO_2 and O_3 concentration are listed in Table 4-17. According to (4-7), the equivalent O_3 formation can be calculated at a lower medium concentration NO condition.

For 4.76% O_2 condition:

$$C_{equal\ O_3} = 107\ ppm$$

NO was not fully oxidized and there were 43 ppm NO left. No further oxidation for the conversion of NO_2 to N_2O_5. No O_3 was measured.

For 9.09% O_2 condition:

$$C_{equal\ O_3} = 140 + 25.5 = 165.5\ ppm$$

NO was fully oxidized and some NO_2 was further oxidized to N_2O_5. No O_3 was measured.

For 16.67% O_2 condition:

$$C_{equal\ O_3} = 126 + 71 + 58 = 255\ ppm$$

Both NO and NO_2 were fully oxidized to N_2O_5 and there was some O_3 remaining.

Table 4-17 NO, NO_2 and O_3 concentration at 0 kV and 7 kV peak applied voltage

O_2 concentration	Applied voltage	$C_{(NO)}$ ppm	$C_{(NO2)}$ ppm	$C_{(O3)}$ ppm
4.76%	0	150	8	0
	7	43	115	0
9.09%	0	140	11	0
	7	0	100	0
16.67%	0	126	16	0
	7	0	0	58

A comparison was made between equivalent O_3 formation at a lower medium concentration NO condition and O_3 formation at reference gas condition, see Figure 4-35. It was found that the equivalent O_3 formation curve increased with O_2 concentration, but the slope of increase was slower than O_3 formation in the reference gas. However, if the equivalent O_3 formation at medium concentration NO condition was considered, the curve was even flatter than that at lower medium concentration NO condition. This indicates that as the NO concentration reduced, the contribution of O_3 became greater. If O is the dominant reactive species, the equivalent O_3 formation should be the same rather than increasing with increasing O_2 concentration, as seen in Figure 4-35.

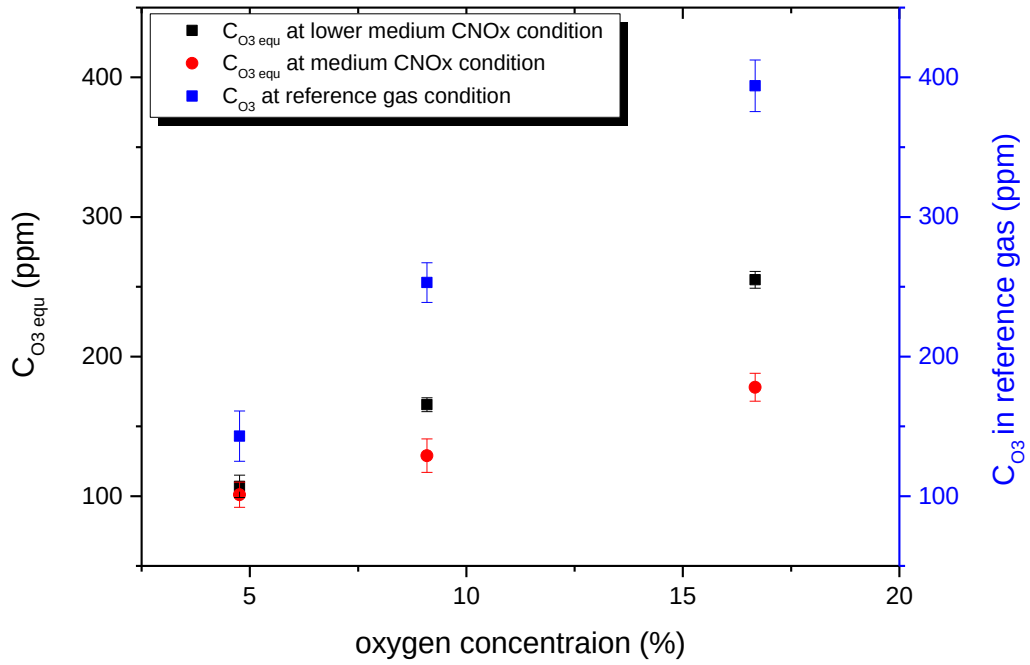

Figure 4-35 Equivalent O_3 formation at medium and lower medium concentration NO condition and O_3 formation at reference gas condition under different O_2 concentration at 7 kV peak applied voltage

4.4.6 Low concentration NO conditions

In order to further promote the effect on O_3 for NOx oxidation, lower concentration NOx was investigated: initial concentrations of NO and NO_2 are listed in Table 4-18. For 4.76% O_2 condition, NO removal increased and energy efficiency decreased with increasing applied voltage. When peak applied voltage increased to 7 kV, NO was fully oxidized, as indicated in Figure 4-36 by the concentration reducing from 101 ppm to 0 ppm.

Table 4-18 NO, NO_2 and NOx concentrations for low concentration NO condition before DBD treatment

C_{O2} (% vol)	FR of N_2 (sccm)	FR of 1000ppm NO in N_2 (sccm)	FR of O_2 (sccm)	C_{NO} (ppm)	C_{NO2} (ppm)	C_{NOx} (ppm)
4.76	180	20	10	101	14	115
9.09	180	20	20	93	10	103
16.67	180	20	40	84	9	93

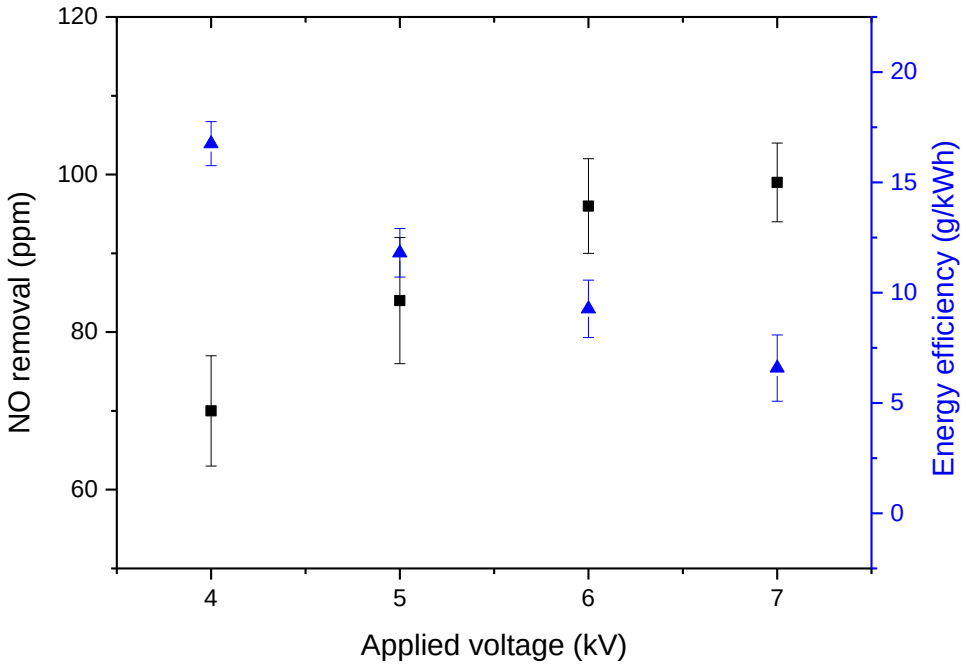

Figure 4-36 NO removal and energy efficiency at 4.76% O_2 and low concentration NO in N_2 condition

For 9.09% and 16.67% O_2 condition, NO was fully oxidized at 4 kV peak applied voltage. When the applied voltage increased to 5kV, NO_2 concentration reduced to zero and O_3 was found. With increasing applied voltage, the concentration of O_3 continued to increase, as shown in Figure 4-37.

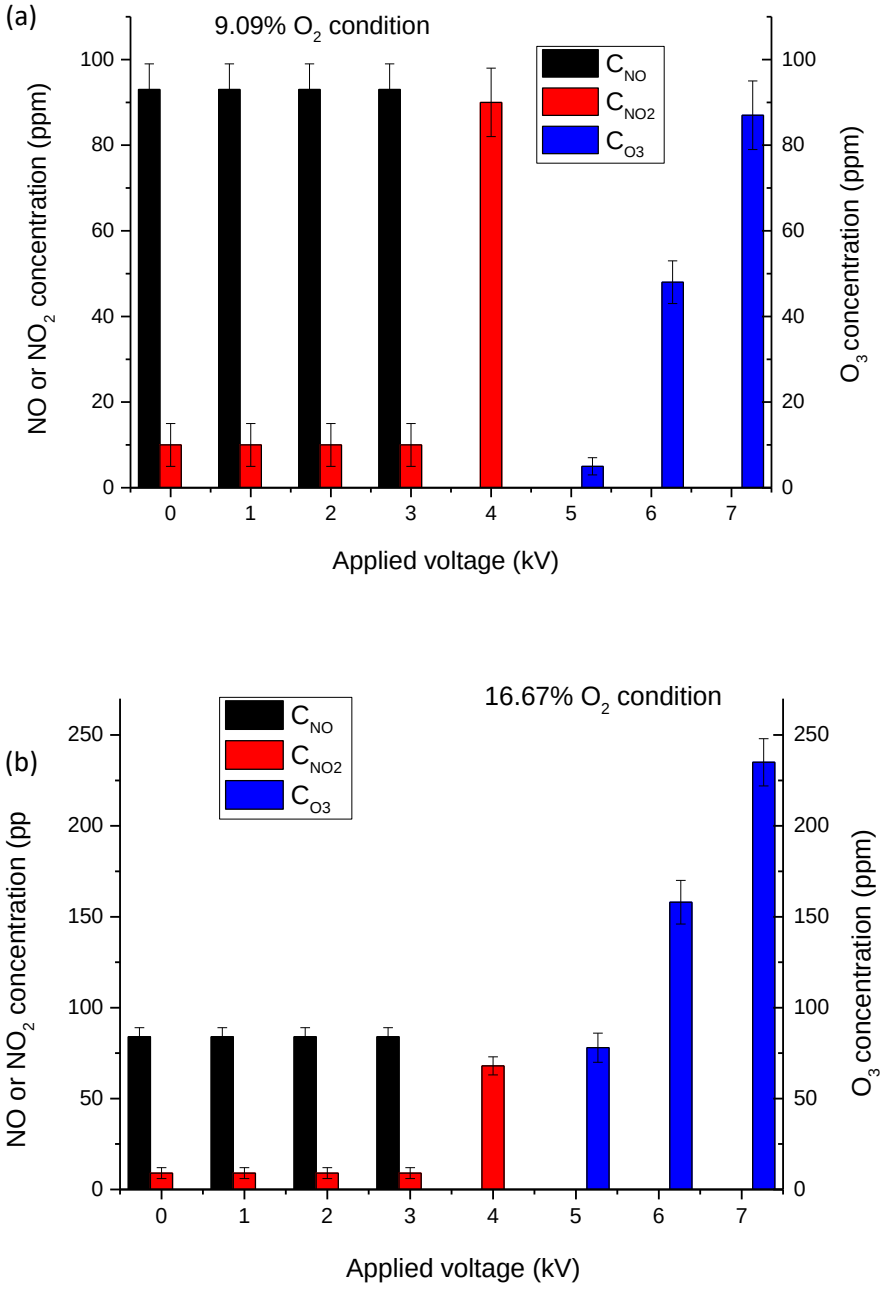

Figure 4-37 (a) NO and NO_2 concentration at different applied voltage under 9.09% and (b) 16.67% O_2 low concentration NOx in N_2 condition

In order to make a comparison, only data from the condition where the peak applied voltage was 7kV were used. The equivalent O_3 formation was calculated and is shown in Table 4-19 and Figure 4-38. The calculated equivalent O_3 production was close to that in the reference gas, so the dominant reactive species was O_3 for NO removal at low concentration NO condition.

Table 4-19 Comparison between calculated equivalent O_3 in low concentration NO condition and O_3 production in reference gas condition at 7 kV under different O_2 concentration.

C_{O2}(%)	$C_{O3\ equ}$ (ppm)	$C_{O3\ in\ reference\ gas}$ (ppm)
4.76	121	143
9.09	230	253
16.67	365	394

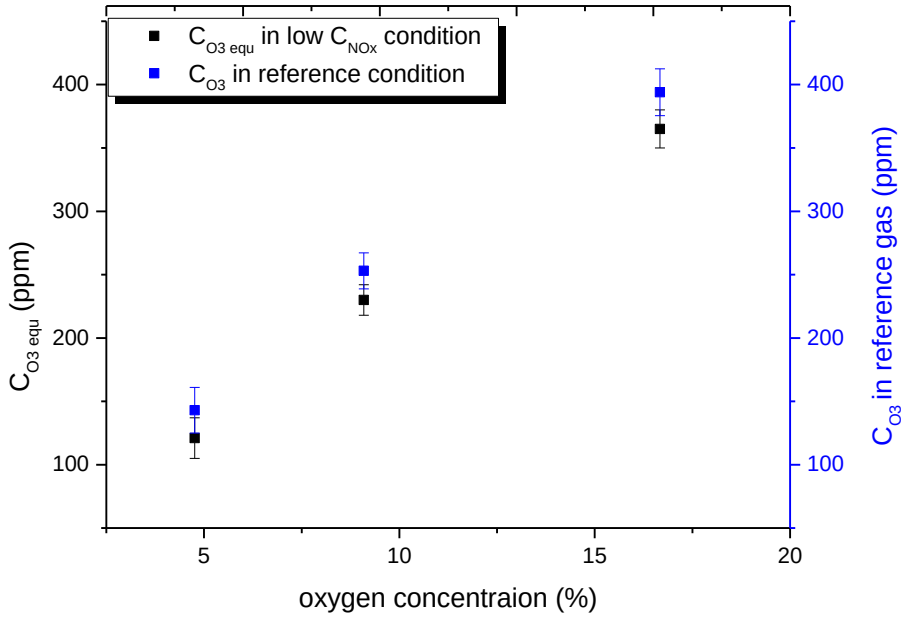

Figure 4-38 Equivalent O_3 formation in low concentration NO condition and O_3 formation in reference gas condition under different O_2 concentration at 7 kV peak applied voltage

4.4.7 Conclusions

In total, five ranges of NO concentration were investigated. Comparing the equivalent O_3 formation curves for different concentration of NO in the gas mixture and in the reference gas, where no NO was in the gas mixture, the dominant reactive species could be identified, see Figure 4-39. The dominant reactive species changed from O to O_3 as NO concentration decreased: for high and upper medium concentration NO, the dominant reactive species for NO oxidation was O; for medium and lower medium concentration NO, both O and O_3 contributed to NO oxidation; for low NO concentration, the dominant reactive species was O_3.

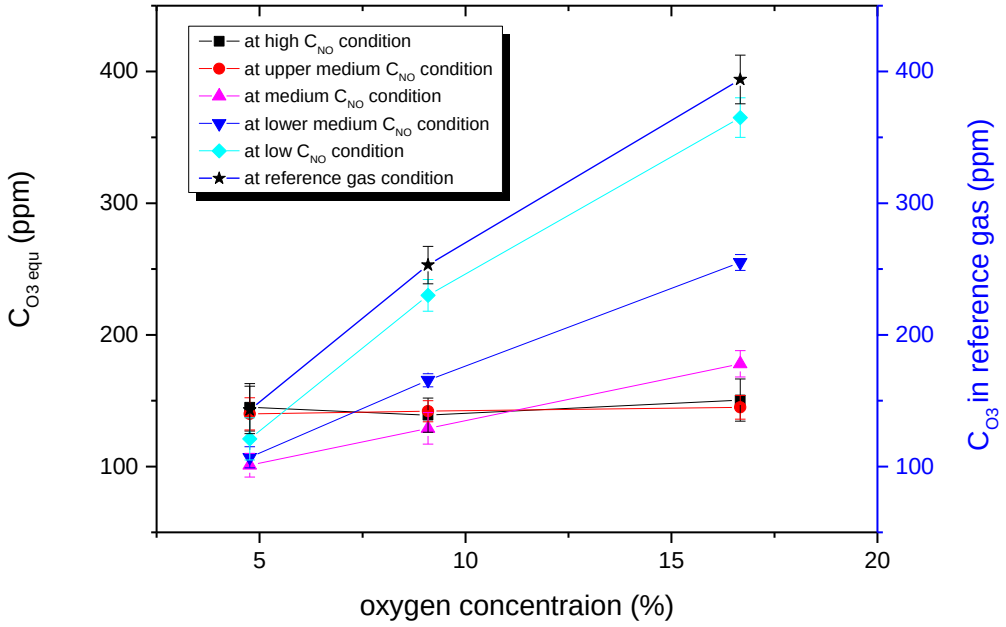

Figure 4-39 Equivalent O_3 formation at five different NO concentration conditions and O_3 formation at reference gas condition under different O_2 concentration at 7 kV peak applied voltage, the gas conditions are as indicated in the key on the figure.

As highlighted in the Literature Review, the concentration of NO in practical flue gases is in the range of 200 ppm to 600 ppm, so, based on the results of the investigation, the dominant reactive species is O and the side reaction can limit the NO removal energy efficiency. In the experiments in this Chapter, the highest NO removal energy efficiency was approximately 25 g/kWh, which is higher than the results obtained by other researchers. Song et al [81]

attained 14.4 g/kWh energy efficiency in a cylindrical DBD reactor and Takaki et al [82] attained 12 g/kWh energy efficiency in a plate-multipoint DBD reactor. However, compared to present industrial DeNOx technologies, LoTox and SCR, the energy efficiency of NO removal by direct DBD technology is still too low to be used. LoTox technology for DeNOx uses O_3 to oxidize NO, but the difference between LoTox and direct DBD treatment is the location that O_3 is generated. For LoTox technology, O_3 is generated in an independent DBD reactor and then injected into the flue gas. The gas source to generate O_3 is pure O_2 rather than the flue gas, so the energy efficiency to generate O_3 can achieve 150 g/kWh [33, 34] which is six times higher than the energy efficiency achieved in this DBD reactor: LoTox does however require the additional gas source. The experimental work so far has not considered the effect of water vapour and this will be explored in the next section.

4.5 Effect of water vapour on NO removal

As mentioned before, O was the dominant reactive species for NO oxidation at high concentration NO condition, but O can bring a side reaction between NO_2 and O to generate NO, which limits the NO removal. Therefore, another reactive species, OH, was used to investigate its potential for NO removal at high concentration NO condition. As shown in Figure 4-40, NO and NO_2 can be oxidized to HNO_2 and HNO_3 by OH. NO_2 is generated by the reaction between HNO_2 and OH.

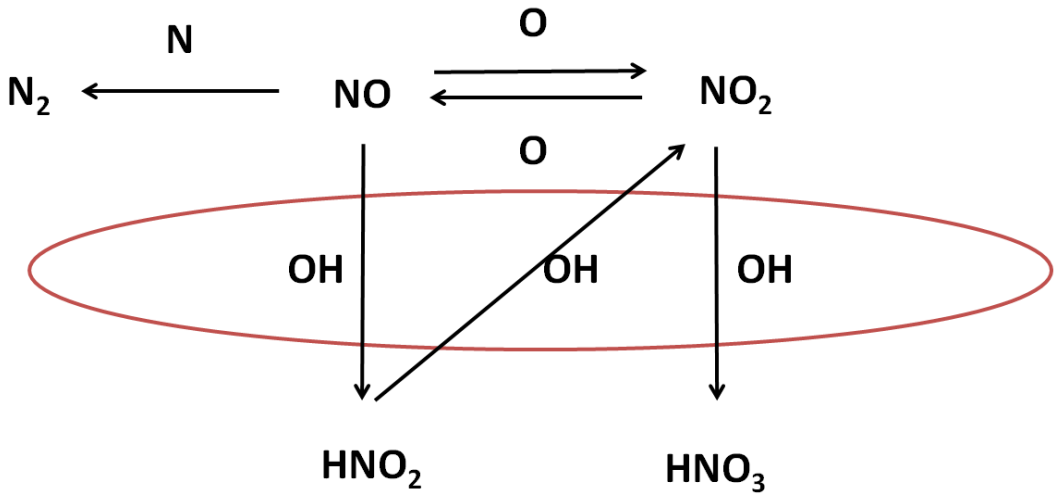

Figure 4-40 Chemical reaction pathway for NO removal by OH [62, 109-111]

In this work, H_2O vapour is introduced into the gas phase by passing a dry gas through a gas washing bottle at 20°C, 2.31% H_2O vapour is added to the gas mixture. The NO removal and energy efficiency results at 4.76% O_2 and high concentration NO in N_2 condition are shown in Figure 4-41. NO removal and energy efficiency in 2.31% H_2O vapour condition was lower than that in zero H_2O condition. When peak applied voltage was 7 kV, NO removal significantly reduced to 151 ppm at 2.31% H_2O vapour condition from 213 ppm at zero H_2O condition. NO removal energy efficiency reduced from 13.23 g/kWh to 10 g/kWh. Luo J et al. [112] presented a similar result for NO removal at 35°C, i.e. the presence of H_2O vapour reduced NO removal and corresponding energy efficiency.

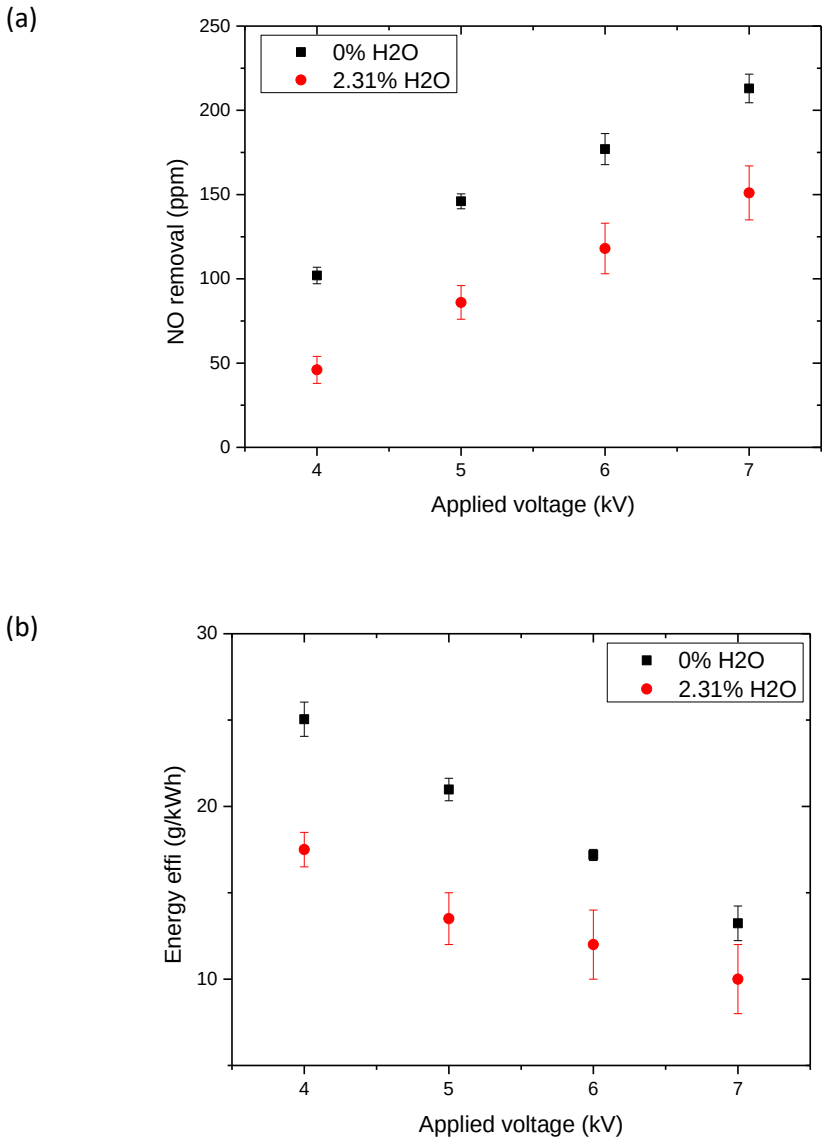

Figure 4-41 (a) NO removal and (b) energy efficiency at zero and 2.31% H_2O vapour for 4.76% O_2 and high concentration NO in N_2 condition, 44°C and 210 sccm total flow rate.

Comparing the moist gas results with dry gas data implies that the presence of 2.31% water vapour reduced NO removal. Although OH has the advantage of reacting with NO without a side reaction, OH also brings some problems for NO removal. As shown in Figure 4-42(a) and Table 4-20, atomic O can react with OH to produce HO_2 and then HO_2 reacts with O again to produce OH. The overall process leads to two O atoms to generate one O_2 molecule.

A similar process exists for the reaction between OH and O_3, as seen in Figure 4-42(b), where two strong oxidant O_3 molecules are converted to three O_2 molecules.

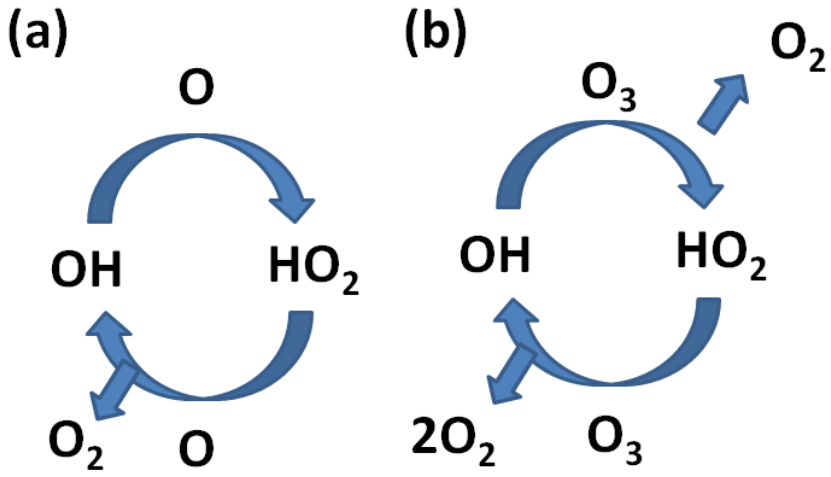

Figure 4-42 OH catalytical react with (a) O and (b) O_3

Table 4-20 H_2O vapour related chemical reaction with O and O_3 [110, 113, 114]

Reactions	Reaction rate constant at 298K $cm^3/(molecule \bullet s)$
$OH + O_3 \rightarrow HO_2 + O_2$	7.25×10^{-14}
$HO_2 + O_3 \rightarrow OH + 2O_2$	2.01×10^{-15}
$OH + O \rightarrow O_2 + H$	3.26×10^{-11}
$O_2 + H \rightarrow HO_2$	3.01×10^{-13}
$HO_2 + O \rightarrow OH + O_2$	5.7×10^{-11}

In order to quantitatively analyse the effect of OH on O and O_3 destruction, a reference gas which consists of 4.76% O_2 and 2.31% H_2O vapour in N_2 was used to evaluate the formation of O_3. Compared to zero H_2O condition, at 7 kV peak applied voltage O_3 formation was reduced from 143 ppm to 46 ppm, see Figure 4-43 (a). The energy efficiency of O_3 production at 7kV was reduced from 17.1 g/kWh to 5.6 g/kWh, Figure 4-43 (b), so the presence of 2.31% H_2O vapour has a significantly negative effect on O_3 formation in dielectric barrier discharge.

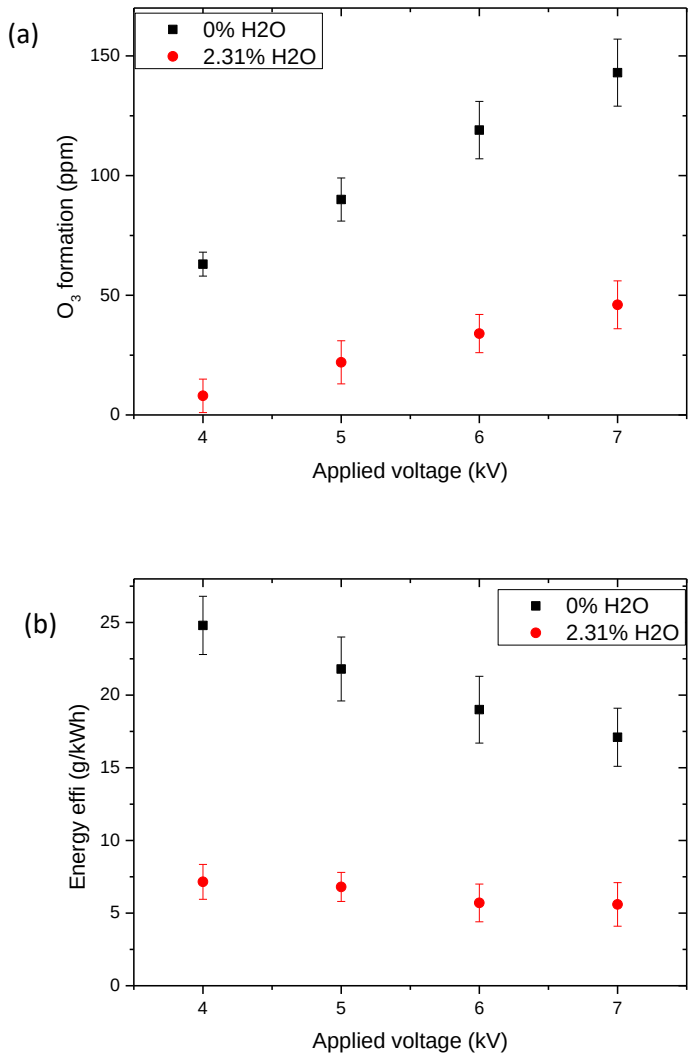

Figure 4-43 (a) O_3 formation and (b) energy efficiency at zero (square) and 2.31% (circle) H_2O for 4.76% O_2 in N_2 condition, 44^oC and 210 sccm total flow rate

For a peak applied voltage of 7kV, 46 ppm of O_3 was formed at reference gas condition, but 151 ppm of NO was removed at 4.76% O_2, 2.31% H_2O vapour and high concentration NO condition. As one O_3 molecule is responsible for removal of one NO molecule, the difference in number of NO removed indicates that 105 ppm NO removal is related to OH.

To further investigate the relationship between O_2 and H_2O for NO removal, different O_2 concentrations were used: the results are shown in Figure 4-44. The difference between NO removal and NO_2 formation does not change significantly as the O_2 concentration increases from 4.76% to 16.67%. The data on NO removal and NO_2 formation are listed in Table 4-21.

The differences between NO removal and NO_2 formation were 91 ppm, 84 ppm and 78 ppm respectively for 4.76%, 9.09% and 16.67% O_2 condition. As discussed in dry and 16.67% O_2 condition, the contribution of metastable N is negligible due to the quenching effect of O_2 on N_2's excited and metastable states. Here the different between NO removal and NO_2 formation is related to OH only.

Table 4-21 NO removal and NO_2 formation at different O_2 concentration at 7kV, on 2.31% H_2O vapour and high concentration NO condition

C_{O2}(%)	NO removal (ppm)	NO_2 formation (ppm)	The difference between NO removal and NO_2 formation (ppm)
0	151	58	93
4.76	151	60	91
9.09	116	32	84
16.67	90	12	78

In addition, it was found that under 2.31% H_2O vapour and high concentration NO condition, there was little difference in NO removal and NO_2 formation at zero and 4.76% O_2 concentration. This implies that the contribution of O to NO oxidation at 4.76% O_2 condition was compensated by the additional OH formation at zero O_2 condition. As O_2 concentration increased to 9.09% and 16.67%, NO removal reduced. In general, an increase of O_2 concentration leads to an increase of O production, so one possible reason for the reduced reaction was that higher O production would limit the reaction between OH and NO, as more OH may react with atomic O, then the effective amount of OH for NO removal would reduce. NO_2 formation was reduced because the chemical reaction between HNO_2 and OH to generate NO_2 was limited because of the shortage of OH.

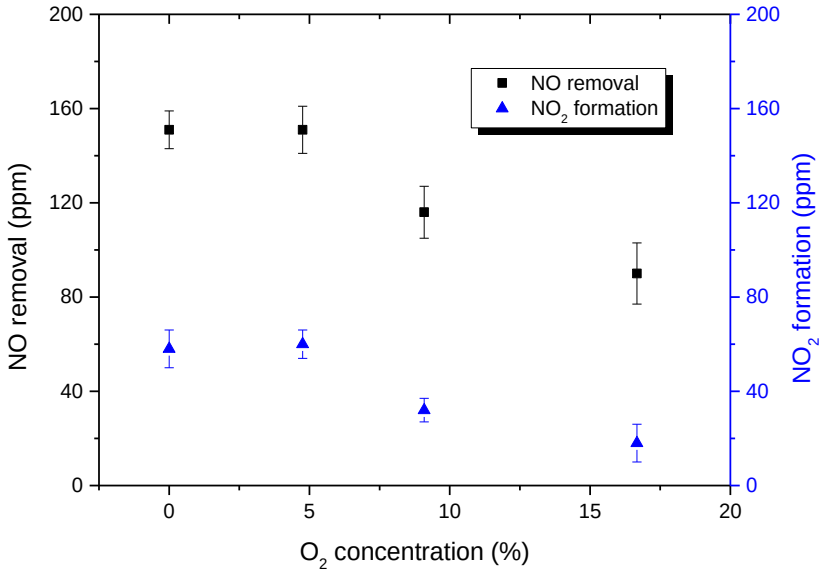

Figure 4-44 NO removal and NO_2 formation at different O_2 concentration at 7 kV peak applied voltage, 2.31% H_2O and high concentration NO condition

4.6 Effect of temperature on NO removal

In this section, the effect of higher temperatures, namely 62°C and 81°C, were investigated for NO removal at high concentration NO condition. The initial concentration of NO, NO_2 and NOx for high concentration NO condition at 62°C and 81°C was the same as the concentration in 44°C, as shown in Table 4-22.

Table 4-22 NO, NO_2 and NOx concentrations for high concentration NO condition before DBD treatment at 62°C and 81°C

C_{O2} (% vol)	Flow rate of N_2 (sccm)	Flow rate of 1000ppm NO in N_2 (sccm)	Flow rate of O_2 (sccm)	C_{NO} initial (ppm)	C_{NO2} initial (ppm)	C_{NOx} Initial (ppm)
4.76	0	200	10	855	102	957
9.09	0	200	20	756	163	919
16.67	0	200	40	614	203	817

From the Lissajous figures at different temperatures at zero H_2O 4.76% O_2 and high concentration NO in N_2 condition, Figure 4-45, it was found that higher temperatures cause an increase in the relative permittivity of the Pyrex which forms the wall of the reaction vessel. This was determined by the increase in aspect of the Lissajous figure which represents dielectric capacitance. In addition, the discharge power increased with temperature, shown as an increase in the Lissajous figure area and reported in Table 4-23. The injected powers for 44°C, 62°C and 81°C temperatures were 0.2506 W, 0.2688 W and 0.3374 W respectively. Some parameters of the DBD reactor under different temperatures, including the capacitance of dielectric and gas gap, are listed in Table 4-23.

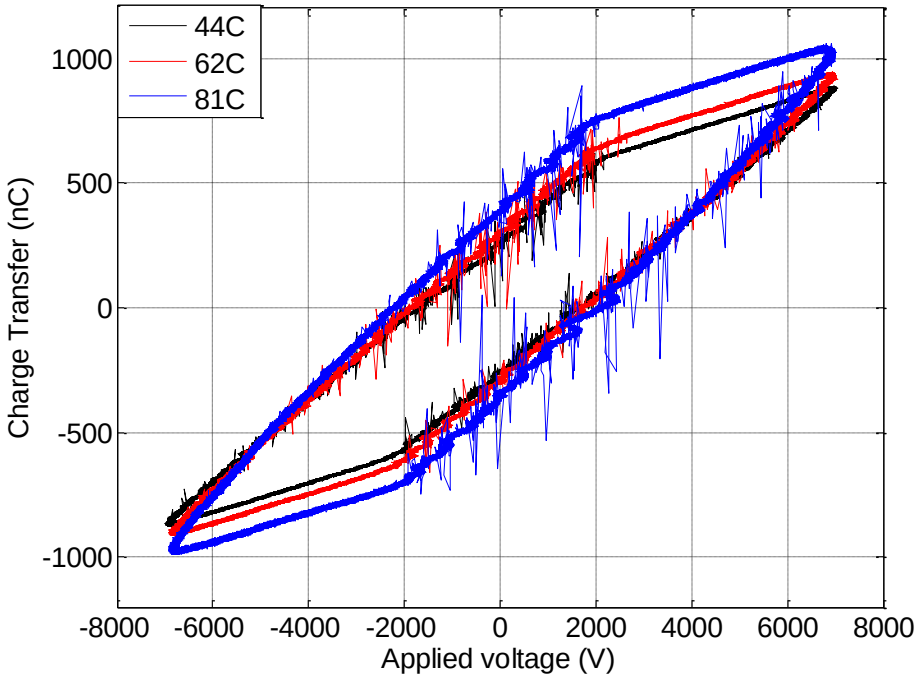

Figure 4-45 Lissajous figure at different temperature, total flow rate was 210sccm on 4.76% O_2 and high concentration NO in N_2 condition at 7kV voltage

Table 4-23 Breakdown voltage, power injection, capacitances of gas, dielectric and total capacitors under different temperatures

V= 7 kV	V_b (V)	P_{dis} (W)	C_{tot} (pF)	C_g (pF)	C_d (pF)
44°C	1606	0.2506	58.6	94.13	155.25
62°C	1851	0.2688	59.48	88.21	182.62
81°C	1990	0.3374	61.56	87.56	207.37

In order to explore the mechanism of NO removal at 62 and 81°C, the reference gas with no NO was used for the O_3 formation measurement. As expected, using the reduced reaction rate constant reported in [115], when the gas temperature increased, O_3 formation was reduced, Figure 4-46. The details of O_3 formation and energy efficiencies under different applied voltage and O_2 concentration are listed in Appendix B.

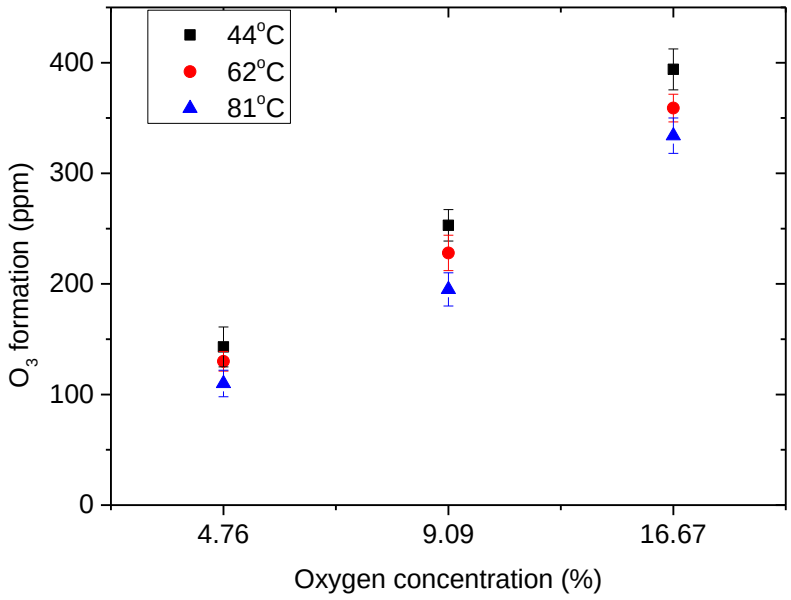

Figure 4-46 O_3 formation at different O_2 concentration for gas temperatures of 44°C, 62°C and 81°C at 7 kV peak applied voltage

At 62 and 81°C, three NOx concentration conditions were used to analyse the change of dominant reactive species for NOx oxidation, these are shown in Table 4-24.

Table 4-24 NO, NO_2 and NOx concentration at high, medium and low concentration NO conditions at 62°C and 81°C

C_{NOx} range definition	C_{O2} (% vol)	FR of N_2 (sccm)	FR of 1000ppm NO in N_2 (sccm)	FR of O_2 (sccm)	C_{NO} (ppm)	C_{NO2} (ppm)	C_{NOx} (ppm)
High C_{NO}	4.76	0	200	10	855	102	957
	9.09	0	200	20	756	163	919
	16.67	0	200	40	614	203	817
Medium C_{NO}	4.76	160	40	10	189	13	202
	9.09	160	40	20	176	15	191
	16.67	160	40	40	158	21	179
Low C_{NO}	4.76	180	20	10	101	14	115
	9.09	180	20	20	93	10	103
	16.67	180	20	40	84	9	93

According to the curves of equivalent O_3 formation in high, medium and low concentration NO conditions and O_3 formation in reference gas condition, the trend of NOx oxidation at 62

and 81°C were similar to those at 44°C, as shown in Figure 4-47. At high concentration NO condition, the dominant reactive species was atomic O. NO oxidation did not increase with the increase of O_2 concentration. At medium concentration NO condition, NO oxidation was slightly increased with the increase of O_2 concentration, but the increase rate was much lower than that for O_3 formation at the reference gas condition. This means that NO oxidation was the synergistic effect of atomic O and O_3. At low concentration NO condition, NO oxidation was mainly a result of O_3, as evidenced by the equivalent O_3 formation curve being close to the O_3 formation curve at the reference gas condition.

(a)

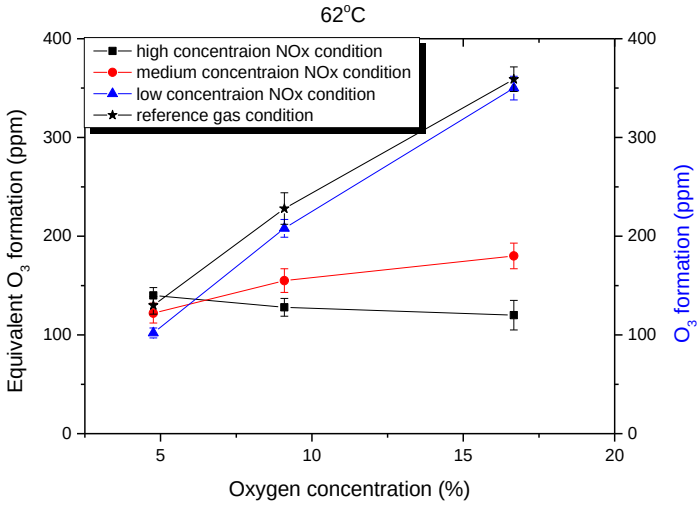

(b)

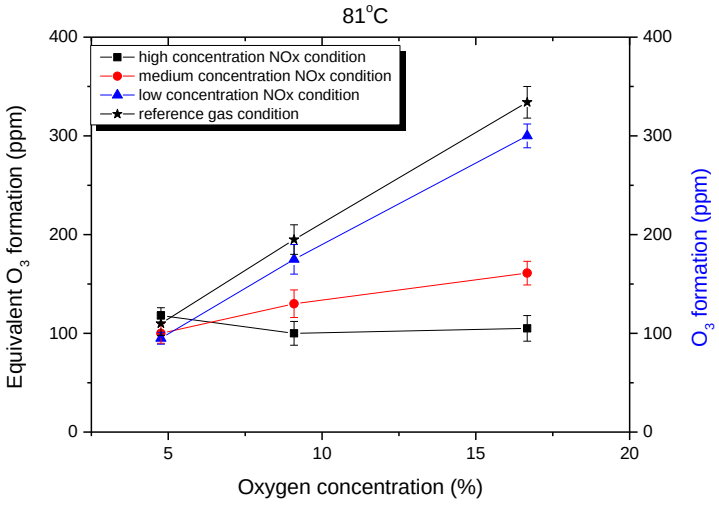

Figure 4-47 Equivalent O_3 formation at high (square), medium (circle) and low (up triangle) NO concentration condition and O_3 formation at reference gas (star) condition at (a) 62°C and (b) 81°C at 7 kV peak applied voltage.

4.7 Synergistic effect of H_2O vapour and gas temperature on NO removal

As highlighted in Section 4.6, 2.31% H_2O vapour reduced the removal of NO at 44^oC. NO removal and energy efficiency were lower than that for zero H_2O vapour. The negative effect of OH on the formation of atomic O was stronger than the positive effect of OH on NO removal.

In order to see the effect of H_2O vapour on the trend of NO removal and NO_2 formation, discharge with 1.21 % H_2O vapour in the gas mixtures was investigated, data is given in Figure 4-48. The concentration of 1.21% H_2O vapour was realised by controlling the percentage of gas going through the gas washing bottle. Given that the total flow rate for 4.76% O_2 condition was 210 sccm, 100 sccm of gas bypassed the gas washing bottle and 110 sccm of gas went through the gas washing bottle, resulting in a 1.21% concentration of H_2O vapour. Under these conditions, it was found that when the temperature increased to 62^oC or 81^oC, NO removal was not reduced but was slightly increased. In addition, the formation of NO_2 reduced and the difference between NO removal and NO_2 formation increased. Given that the difference between NO removal and NO_2 formation was related to OH only, and considering Figure 4-48, this means that the higher temperature at 62 and 81^oC promoted the formation of OH. When the temperature was at 44^oC, H_2O vapour hindered NO removal by competitively collecting atomic O to limit the reaction between atomic O and NO. When the temperature reached 62 or 81^oC, NO removal by OH was more efficient.

One possible reason why higher temperature promotes NO removal is related to the reaction rate constants in Table 4-25. The reaction rate constant between atomic O and OH is more significantly affected by temperature than that of the reaction between atomic O and NO or between OH and NO. At higher temperatures the reaction between atom O and OH is limited by the reduction of reaction rate constants, of at least 17%. However, the reaction between atomic O and NO would be promote as the reaction rate constant increased by 8.97%, so more atomic O and OH were available to react with NO, and NO removal increased.

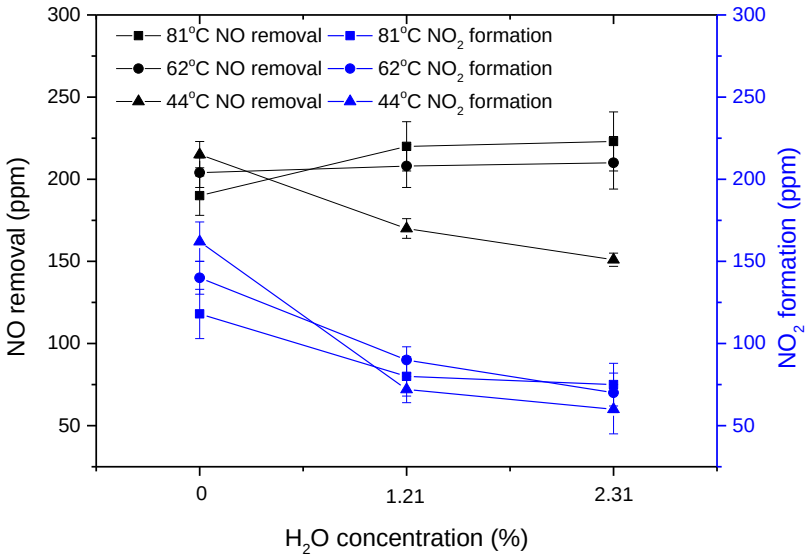

Figure 4-48 NO removal and NO_2 formation at different H_2O concentration 7 kV peak applied voltage and 210 sccm total flow rate. 4.76% O_2 high concentration NO in N_2 condition

Table 4-25 The reaction rate constant at different temperature for chemical reactions

reactions	$k_{at\ 300K}$	$k_{at\ 375K}$	$k_{at\ 400K}$	The change of K
$O + NO \rightarrow NO_2$ [68]	3.01×10^{-11}		3.28×10^{-11}	+8.97%
$OH + NO \rightarrow HNO_2$[116]	1.04×10^{-11}	9.10×10^{-12}		-12.5%
$O + OH \rightarrow O_2 + H$ [113]	3.26×10^{-11}	2.69×10^{-11}		-17.48%
$O_2 + H \rightarrow HO_2$ [113]	3.01×10^{-13}	1.75×10^{-13}		-41.96%
$HO_2 + O \rightarrow O_2 + OH$[117]	5.71×10^{-11}		4.74×10^{-11}	-17%

In order to further distinguish the effect of atomic O and OH at 62 °C and 81°C, different O_2 concentrations were investigated at 2.31% H_2O vapour and high concentration NO in N_2 condition, see Figure 4-49. The general trend of NO removal and NO_2 formation were similar to that at 44°C. At H_2O vapour concentration of 2.31%, NO removals were nearly the

same as those at zero O_2 and 4.76% O_2 conditions. This implies that OH is the dominant reactive species for NO removal. With the increase in the reactor's temperature, the NO removal was increased, but the promotion of NO removal from 62°C to 81°C condition was lower than that from 44°C to 62°C condition. In addition, as shown in Table 4-23, the power injection increased with increase of temperature. It was found that the highest NO removal energy efficiency 12.6 g/kWh, this was achieved at 62°C rather than 81°C.

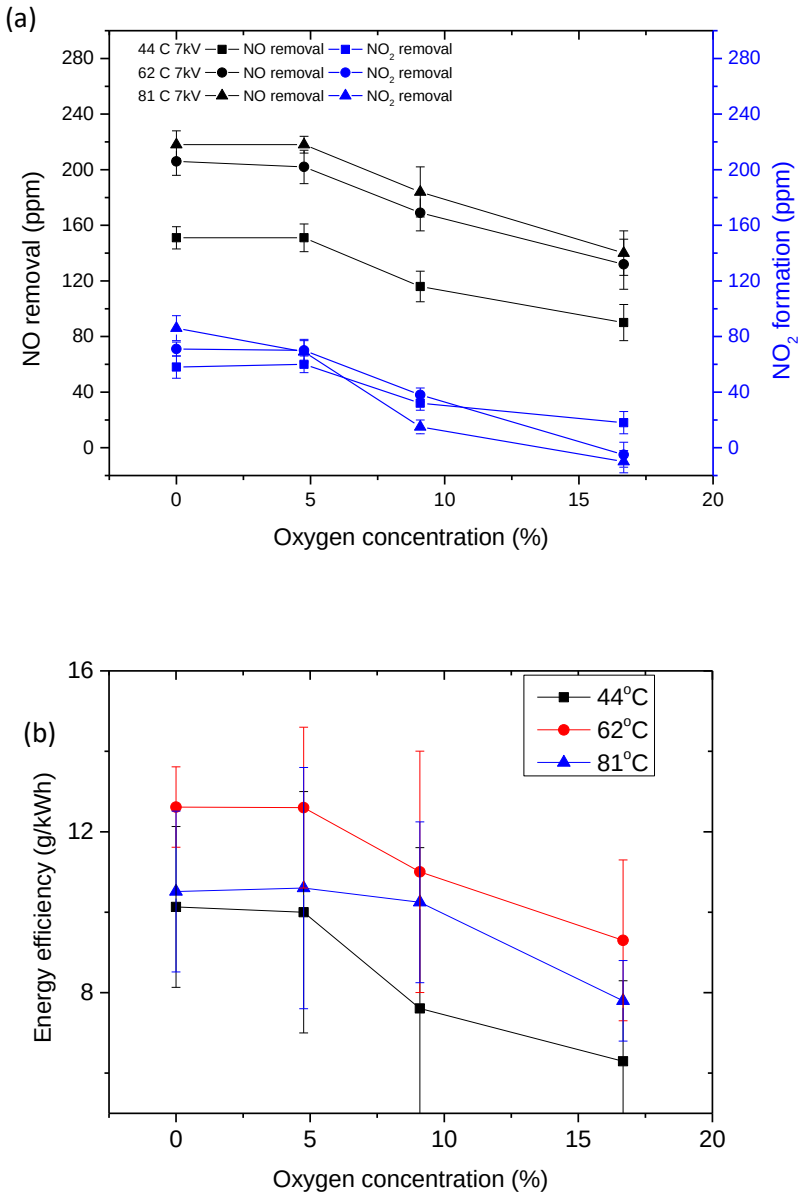

Figure 4-49 (a) NO removal and NO_2 formation and (b) energy efficiency at different O_2 concentration at 44°C (square), 62°C (circle) and 81°C (up triangle); the gas condition was 2.31% H_2O, high concentration NO, and peak applied voltage of 7 kV

4.8 Conclusions

For those discharge characteristics of DBD which were investigated, it was found that because of the quenching effect of O_2 and NO on N_2's metastable states, the presence of O_2 and NO were able to increase the average discharge current significantly, i.e. up to more than one hundred mA from a few mA.

The reduction of N_2's metastable states can limit the formation of N.

Most of the discharge energy is transferred to O_2 and dissociation of O_2 is more significant than that of N_2, so the reactive species for NO removal is O or O_3, rather than N. The effect of H_2O vapour on discharge current was not the same as that of O_2 and NO. Electron attachment played an important role in limiting the discharge development in gases containing H_2O vapour: the average discharge current was reduced to a few mA. Finally, the reduction of N_2's metastable states by the quenching effect of O_2 and NO, and electron attachment effect of H_2O vapour caused an increase in breakdown voltage.

For NO removal, the effects of O_2, H_2O vapour and temperature were extensively investigated under different NO concentration conditions. For a gas temperature of 44^oC: in high and upper medium concentration NO, the dominant reactive species for NO oxidation was O; in medium and lower medium concentration NO, both atomic O and O_3 contributed to NO oxidation; in low concentration NO, O_3 was the dominant reactive species for NO oxidation and could further oxidize NO_2 to N_2O_5 without any side reaction. Compared to situations of zero H_2O condition, when there was 2.31% H_2O vapour in the gas mixture, OH played the dominant role for NO removal, but there was a 30% reduction in the NO removal, from 213 ppm to 151 ppm, and 24.4% reduction in energy efficiency, from 13.5 g/kWh to 10 g/kWh. However, when gas temperature increased to 62^oC and 81^oC, the effect of water vapour promoted NO removal. In terms of the NO removals and energy efficiency, the highest energy efficiency was 25.05 g/kWh with 105 ppm removal rate at 4kV under 44^oC, zero H_2O high concentration NO condition. However, at a 2.31% H_2O vapour and high concentration NO condition, the highest energy efficiency reduced to 12.6 g/kWh with 206 ppm removal rate at 62^oC and 7kVcondition.

In terms of a practical flue gas, the concentration of H_2O vapour was approximately 5%, which is higher than that used in these experiments. Based on the experimental results, if direct DBD technology is used to treat the practical flue gases, the dominant reactive species should be OH. In addition, according to the finding of higher temperature promoting the removal of NO by OH, it is worthwhile investigating the NO removal performance at even

higher temperature, since the temperature of flue gas can be higher than 400^{o}C. In addition, the results discussed are at a condition of 2.31% H_2O content, if the concentration of H_2O vapour was further increased then more OH might be generated. It is worthwhile investigating another type of non-thermal plasma configuration to increase the effect of H_2O. A method of pursuing this is by using liquid water as one of the electrodes. Experiments using this type of electrode are discussed in the next chapter.

In addition, if H_2O vapour can be removed from the flue gas before DBD treatment, the concentration of NO is an important parameter when considering methods to remove NO. When NO concentration is lower than 100 ppm, the direct DBD treatment can be applied. However, if NO is higher than 400 ppm, it is better to use LoTOx technology in order to avoid the side reaction between NO_2 and O which generates NO.

Chapter 5 NEGATIVE DC CORONA DISCHARGE FOR NO REMOVAL

5.1 Introduction

In this chapter, to determine the potential of OH reactive species for NO removal a pin-water configuration corona discharge reactor was investigated. This configuration has uses liquid water as one of the electrodes, discharge on to water acts to generate reactive species OH.

This pin-water corona discharge configuration was usually investigated for degradation of organic compounds in water [118-126], specifically species such as phenol [84, 85] and methylene blue [86], because OH's oxidation potential is higher than that of atomic O and O_3, as shown in Table 5-1.

Based on experience in early stages of experimental work, positive corona discharge too easily converted to arc discharge. This led to the NO formation rather than its removal. As a result, it was determined that it would be better to apply negative polarity discharge to systematically analyse the ability of pin-water corona discharge for NO removal.

Table 5-1 Oxidizing potential for some oxidizing agents [127]

Oxidizing agent	Oxidation potential (V)
F_2	3.06
OH	2.80
O	2.42
O_3	2.08
H_2O_2	1.78
O_2	1.23

However, the arrangement has not been used for NO removal in the gas phase, so in this chapter, the pin-water configuration was investigated for this purpose. The advantage of a water electrode was to provide additional H_2O vapour for generation of OH reactive species: with increasing discharge power more water can be evaporated to give gas phase H_2O. In addition, OH species do not cause side reactions which affect NO removal, Figure 5-1.

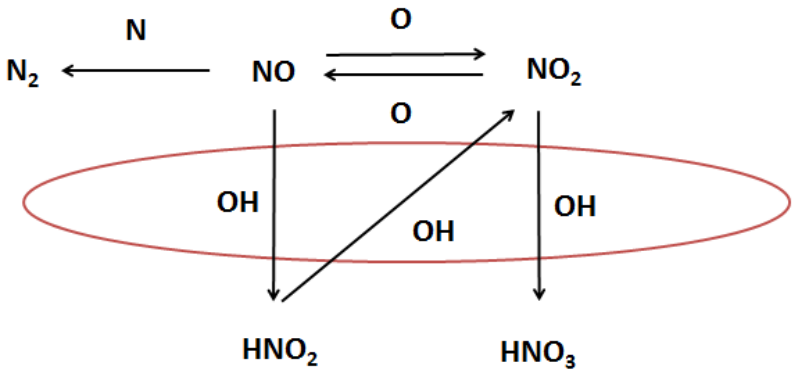

Figure 5-1 The main chemical reaction pathway for NO removal by OH

As highlighted in Chapter 2, three discharge modes can occur under negative electric fields, i.e. Trichel pulse discharge, pulseless discharge and arc discharge. Investigation of NO removal under these three modes is reported in this chapter. In addition, given that the ionization area of corona discharge is around the pin, experiments were conducted to identify the importance of ionization area. In one experiment, the gas flow was controlled to make sure that all gases passed the pin's tip before leaving the reactor. For comparison, the other experiment was conducted under open gas flow condition, where some of the gas could leave the reactor without passing the discharge regime around pin's tip. In addition, the effect of gap discharge and O_2 concentration were analysed in this chapter.

5.2 Experimental setup

A schematic diagram of the experimental setup is shown in Figure 5-2. A negative DC power supply (Glassman HV) was used to energise non-thermal plasma. The signal at the stainless steel pin connected to high voltage was measured using a Tektronix P6015A HV probe. Discharge current was determined by measuring the voltage across a 1kΩ resistor. A Tektronix DPO5104B Digital Phosphor Oscilloscope, with 1GHz bandwidth and 10Gs/s sample rate, was used to record voltage and current signals. Two gases were used, one was pure O_2 and the other one was 1000 ppm NO in N_2. As in the previous experiments, the gas flow rate was controlled by Alicat mass flow devices. Ozone monitor (BMT964) was used to measure O_3 concentration and NOx analyser (Thermo Scientific model 42i-HL) was used to measure NO and NO_2 concentration. Deionised water, from a Milli-Q water purification system, was used as ground electrode. The water conductivity was 6 μS/cm.

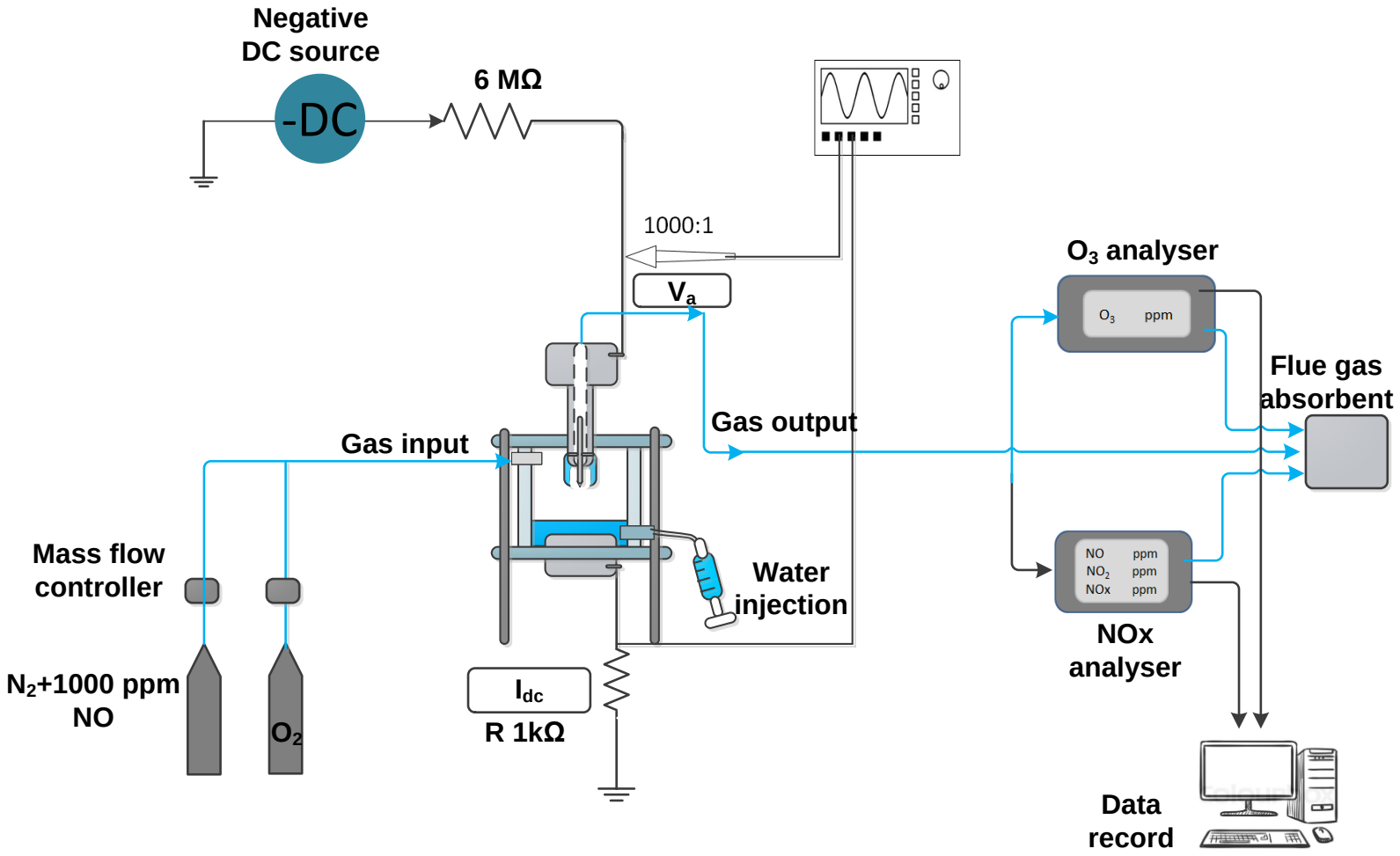

Figure 5-2 Schematic diagram of experimental setup

As outlined above, there were two corona discharge reactor configurations investigated in this chapter. Gas flowed into the reactor vessels through a port in the side of the acrylic tube (OD x ID = 60mm x 50mm), which formed the body of the vessel, and left the reactor through a vent in the centre of the HV electrode. The controlled gas flow configuration in Figure 5-3 (a), used a nylon tube (OD×ID=6mm×4mm) between pin and main electrode. The edge of nylon tube was at the same height as the pin's tip, so all of the gases flowed through the ionization area of the corona discharge and has contact with the plasma before leaving the reaction chamber. In the open gas flow configuration, shown in Figure 5-3 (b), the nylon tube was absent. There was an 18.5mm height difference between the pin's tip and the vent at the bottom of the main electrode, so some gas passed through the gas outlet without making contact with the plasma in the ionization area, which reduced the function of corona discharge for NO removal. The base of the ground electrode was made of stainless steel and a controlled amount of water was inserted into the reactor through the side of the acrylic tube by syringe. The conductivity of water was 6 μS/cm, so the liquid water was a highly resistive electrode. To fix the position of the high voltage stainless steel pin electrode in the centre of the gas outlet, grub screws were applied to opposite sides of the pin. This also ensured good contact between the pin and the power applied to the main electrode.

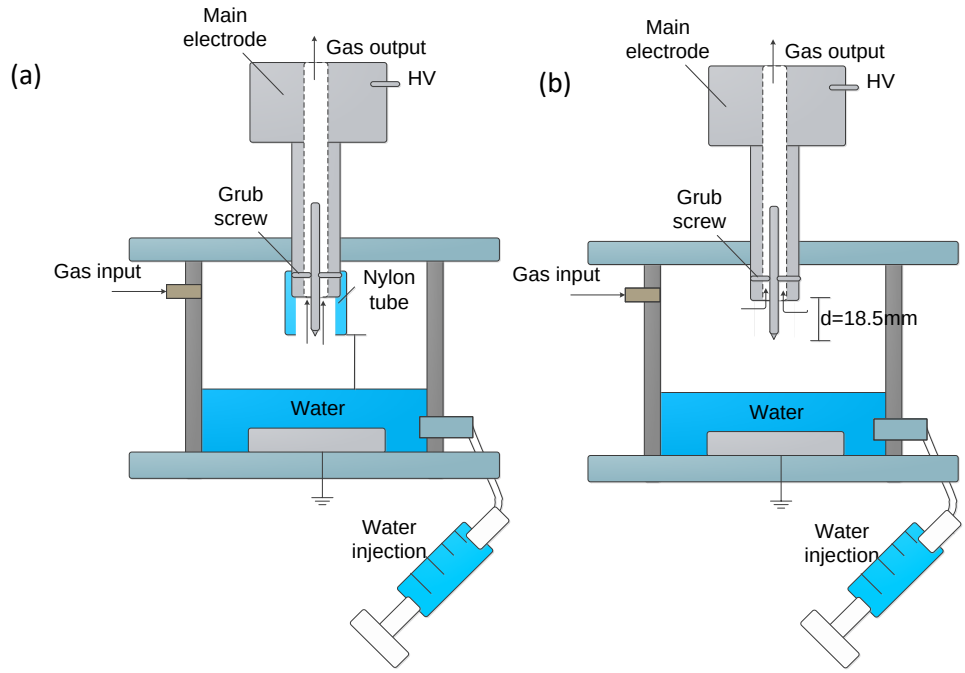

Figure 5-3 Pin-water negative corona discharge reactors: (a) controlled gas flow configuration and (b) open gas flow configuration

In order to investigate the effect of gap discharge between the pin and the water surface, the volume of water injected into the reactor is controlled. Three gap sizes (4mm, 6.5mm and 9mm) are created by injecting 60mL, 65mL and 70mL of water into the reactor, as shown in Figure 5-4.

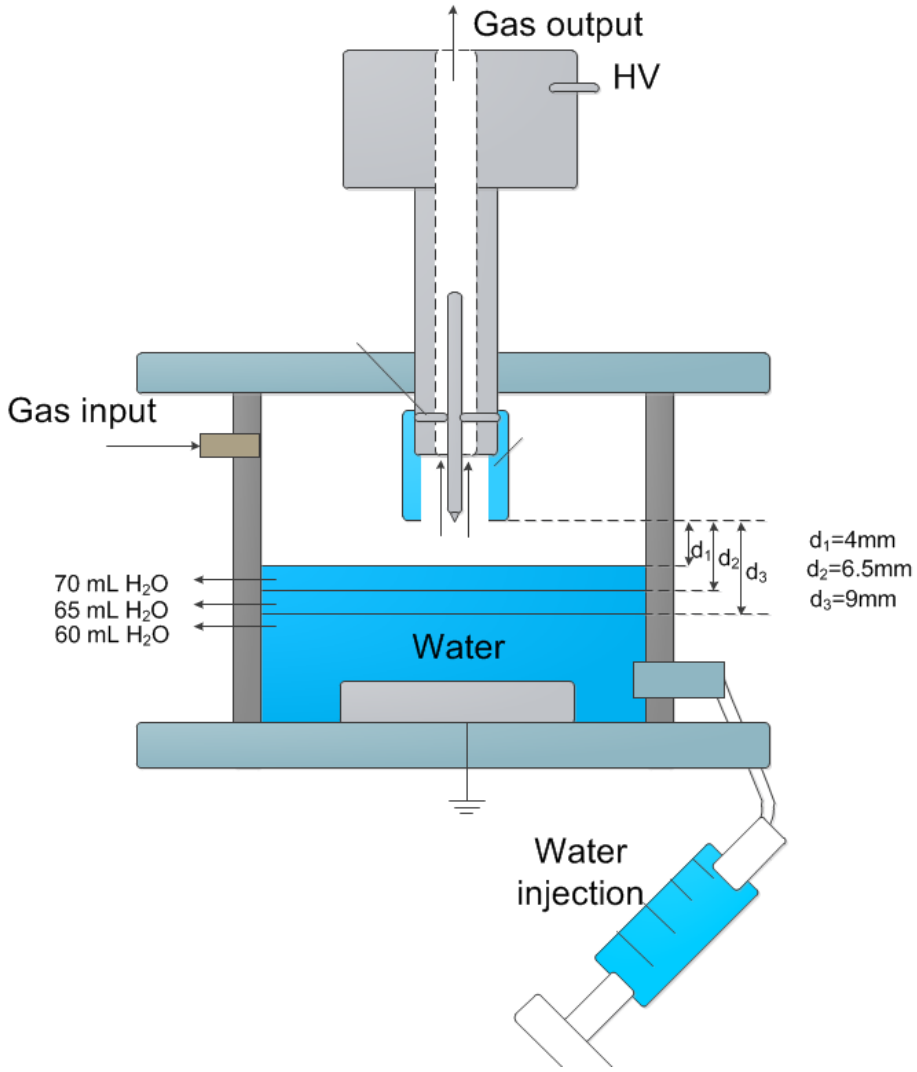

Figure 5-4 Schematic diagram of three different gap distances controlled by the volume of water in the reactor

The variation in concentration of NO and NO_2 under different O_2 concentration in the reactor, prior to the discharge experiments, are shown in Table 5-2. As the O_2 concentration increased from 0% to 16.67%, NO concentration reduced from 1000 to 588 ppm and NO_2 concentration increased from 0 to 190 ppm. Therefore, even without the additional action of discharge, O_2 has the potential to oxidize NO to NO_2.

Table 5-2 NO, NO_2 and NOx concentrations under different O_2 at high concentration NO condition (before corona discharge treatment)

C_{NOx} range definition	**C_{O2} (% vol)**	**Flow rate of N_2 (sccm)**	**Flow rate of 1000ppm NO in N_2 (sccm)**	**Flow rate of O_2 (sccm)**	**C_{NO} initial (ppm)**	**C_{NO2} initial (ppm)**	**C_{NOx} Initial (ppm)**
High C_{NOx}	0	0	200	0	1000	0	1000
	4.76	0	200	10	851	92	943
	9.09	0	200	20	737	154	891
	16.67	0	200	40	588	190	778

For corona discharge, the ionization area was around the pin's tip where the electric field was the strongest. Outside the ionization area, the electric field reduces dramatically and no reactive species are generated. This is the drift area, so called because the electric field in this area is too low to initiate new gas ionization, however, longer lived reactive species generated in the discharge can interact in this region. The lifetime of OH is very short, Ono et al.[87] found that the lifetime of OH in a humid N_2/O_2 mixture was in the range of 10-100 μs, so it had to be used in situ. In order to make use of generated OH by corona discharge, it would be better to direct all of the gases into the ionization area, so controlled gas flow configuration was used.

5.3 NO removal under controlled gas flow configuration

The pin-water corona discharge reactor under controlled gas flow configuration is shown in Figure 5-5. The pin's radius of curvature was 0.3mm in this experiment. The distance between the pin's tip and water surface was 6.5mm, using, as indicated in Figure 5.4, 65mL of water. Between tests the water was removed from the reactor and fresh water was injected.

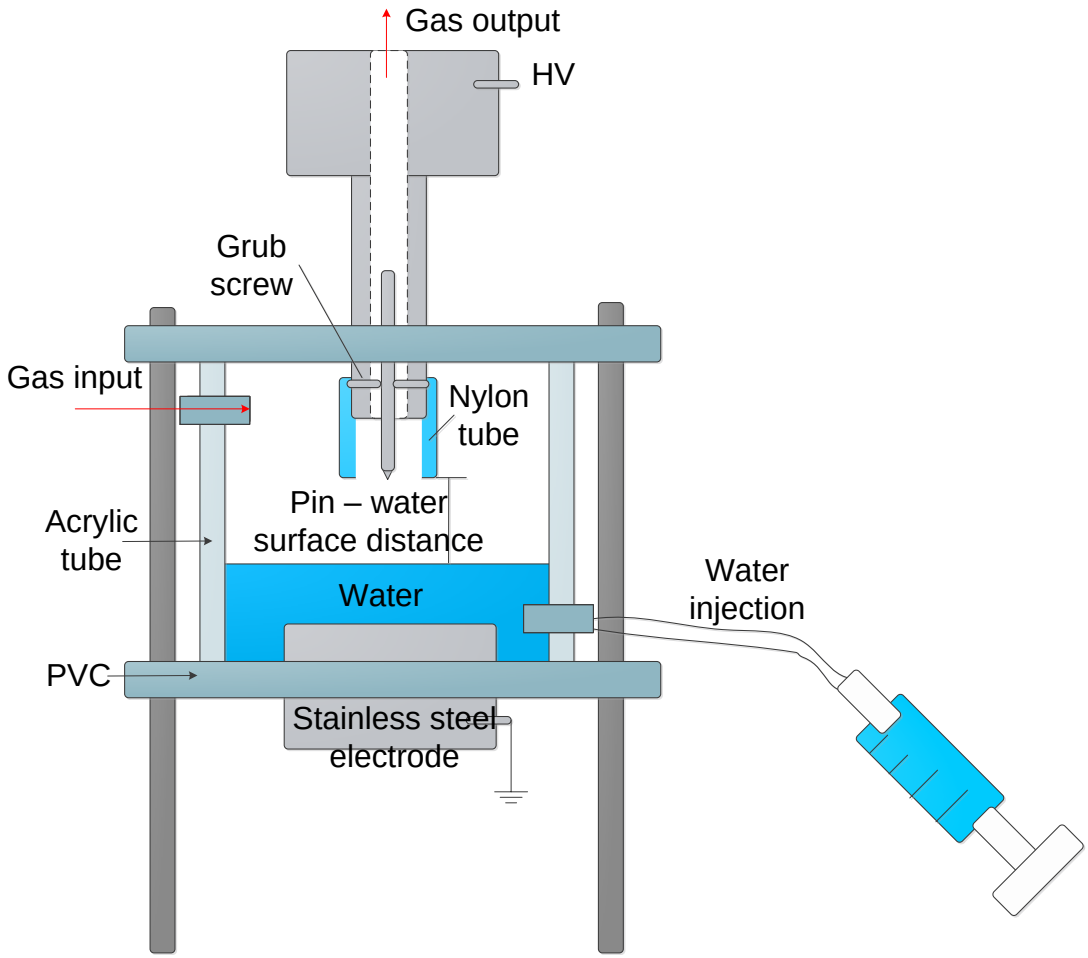

Figure 5-5 The pin-water corona discharge reactor under controlled gas flow configuration

5.3.1 Effect of discharge mode

The discharge mode investigation was conducted at 4.76% O_2 and high concentration NO condition. The first discharge mode for pin-water negative corona discharge was Trichel pulse discharge. The characteristics of Trichel pulse discharge were the same as pin-metal configuration. As the applied voltage increased, the amplitude of impulse current reduced, but the impulse repetition rate increased. However, when the applied voltage reached -5.8kV, as indicated in Figure 5-6 (a), the impulse current started to be continuous. There was a DC current of about -30 μA but, in addition, there were current pulses: the duration of the first pulse was only approximately 70 ns but the amplitude could reach 400 μA, this was followed by a series of smaller discharges lasting about 400ns. When the applied voltage was -8.2kV, the discharge mode changed from Trichel to pulseless discharge, as seen in Figure 5-6 (b), the discharge current was nearly constant with an amplitude of -200 μA. If the applied voltage was further increased, the discharge mode became arc discharge. As shown in Figure 5-6 (c), the applied voltage dropped to -3kV, but the discharge current amplitude increased from - hundred μA to -2mA.

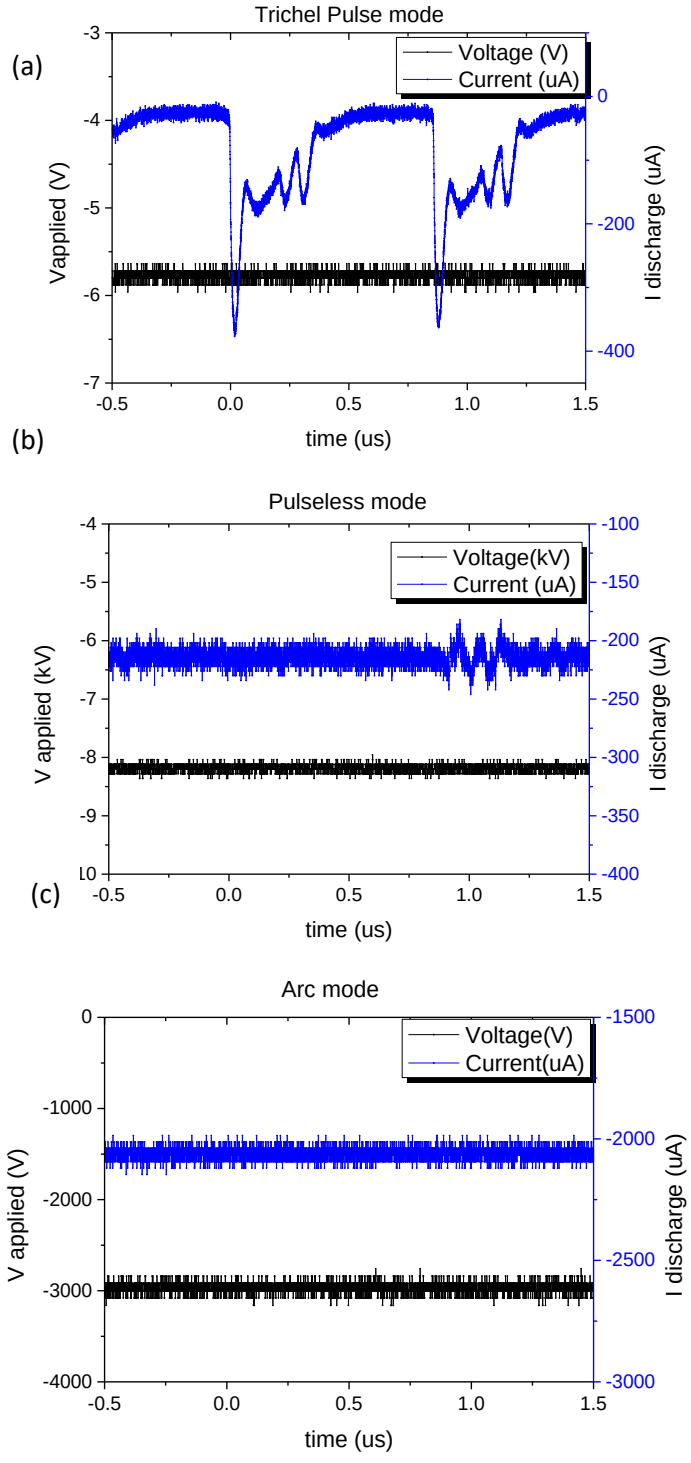

Figure 5-6 The voltage and current waveforms for controlled gas flow configuration, (a) Trichel pulse discharge mode, (b) pulseless discharge mode and (c) arc discharge mode

Photographs of the discharge activity were taken and the following observations were made. First, in the Trichel discharge mode image shown in Figure 5-7 (a), a luminous spot was seen at the pin's tip and a luminous triangle area was observed below the pin and towards the water surface, but the brightness of the triangle area was much weaker than that at the pin's tip. However, at higher applied voltage, the discharge mode became pulseless discharge. The light from the pin tip increased until the nylon tube was glowing and the luminous area below was expanded and brighter than that in the Trichel pulse mode, see Figure 5-7 (b).

(a)

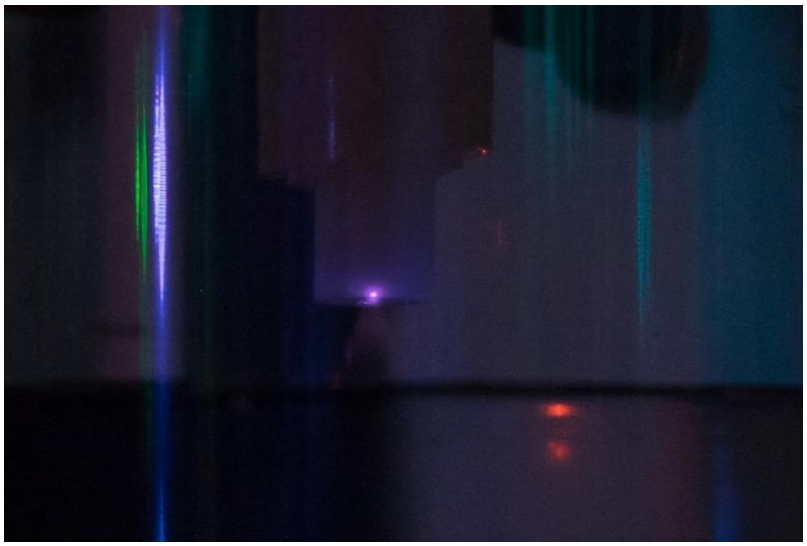

(b)

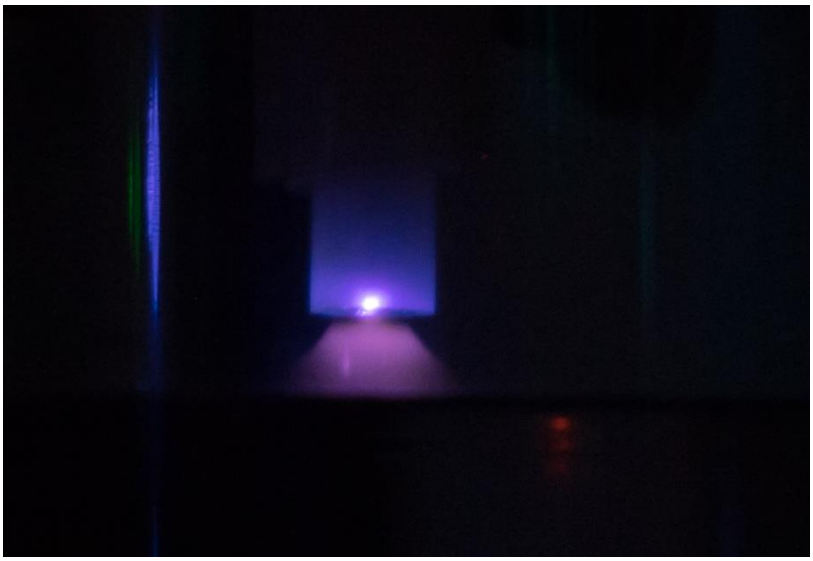

Figure 5-7 Images of pin-water negative corona discharge (a) Trichel pulse discharge and (b) pulseless discharge (exposure time 10s)

In terms of the NO removal and energy efficiency, the initial concentration of NO and NO_2 were 851 ppm and 92 ppm, respectively, see Table 5-2. Under different discharge powers, in both Trichel pulse and pulseless modes the NO removal linearly increased with increasing discharge power, the graphed data of NO removal is shown in Figure 5-8 (a). In addition, the NO removal energy efficiency also increased with increasing power, see Figure 5-8 (b). For discharge powers lower than 0.7 W, when the discharge was in Trichel pulse mode, the energy efficiency increased from 3 to 4.5 g/kWh. For higher discharge power, when the discharge mode was pulseless, the NO removal energy efficiency increased from 5g/kWh up to 6 g/kWh.

In general, with the reduction in NO concentration in the gas mixture, the NO removal energy efficiency tended to reduce. However, in this specific discharge configuration, the NO removal energy efficiency increased with increasing discharge power. There are two possible reasons. One relates to the effective plasma volume. As shown in Figure 5-7, with increasing discharge power, the luminous area expanded from only the region of the pin to the whole gap between the pin and the water surface. The brightness of the discharge around the pin was stronger in the pulseless discharge mode, so the effective ionization area was larger, which led to an increase in the opportunity of contact between NO and non-thermal plasma. Another possible reason was water evaporation. As the discharge power increased, more energy was transferred to the water electrode and the temperature of the water surface was increased, so more H_2O molecules were evaporated from the water's surface. In addition, the temperature in the luminous volume between the pin and the water surface would be increased, and the saturated water vapour pressure would also be increased, see Figure 3-4. As a result, more H_2O vapour could be sustained in the gas phase to generate OH. When the power reached approximately 2W, it was found that the inside wall of the acrylic tube was coated with a layer of water fog. As a result of the increased power, the increase in the ionization area and H_2O vapour concentration in the gas phase led to an increase in NO removal energy efficiency.

As shown in Figure 5-9, it was found that NO concentration was reduced from the initial 851 ppm to 241 ppm at the discharge power of 1.869W. In addition, the NO_2 concentration reduced from 92 ppm to 47 ppm with an increase in discharge power. The reduction rate of NO_2 was much slower than that of NO.

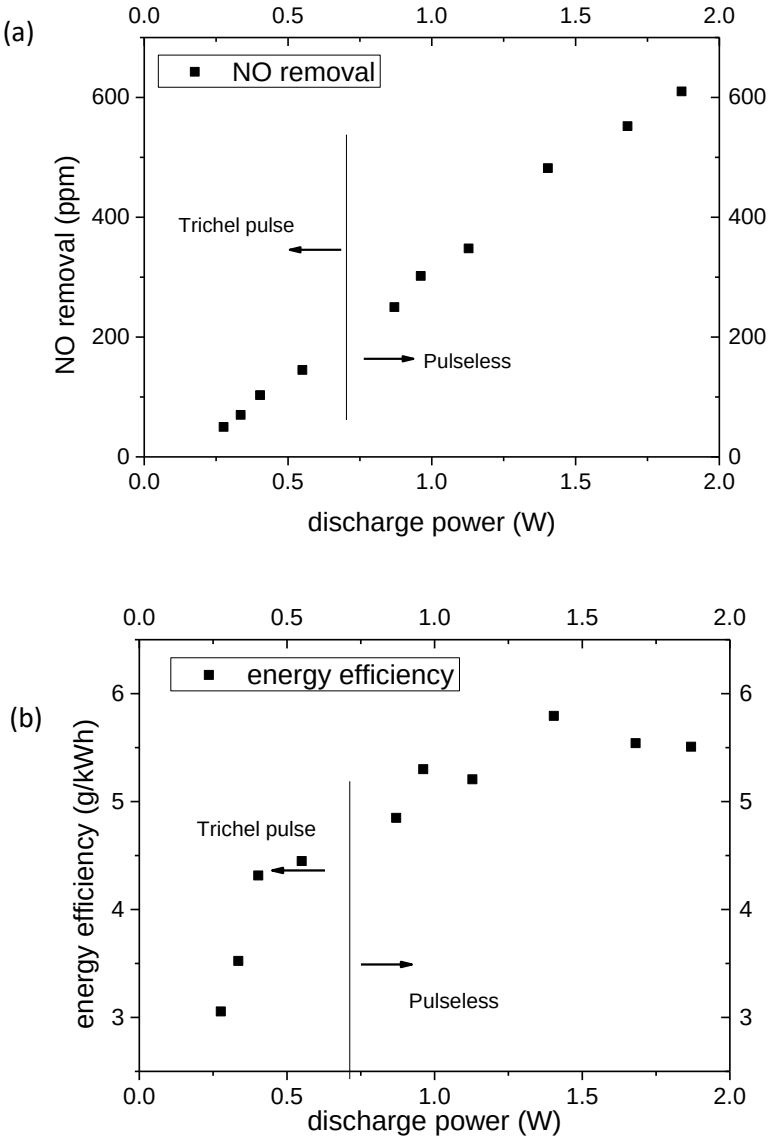

Figure 5-8 (a) NO removal and (b) energy efficiency for controlled gas flow configuration corona discharge at 4.76% O_2 and high concentration NO condition.

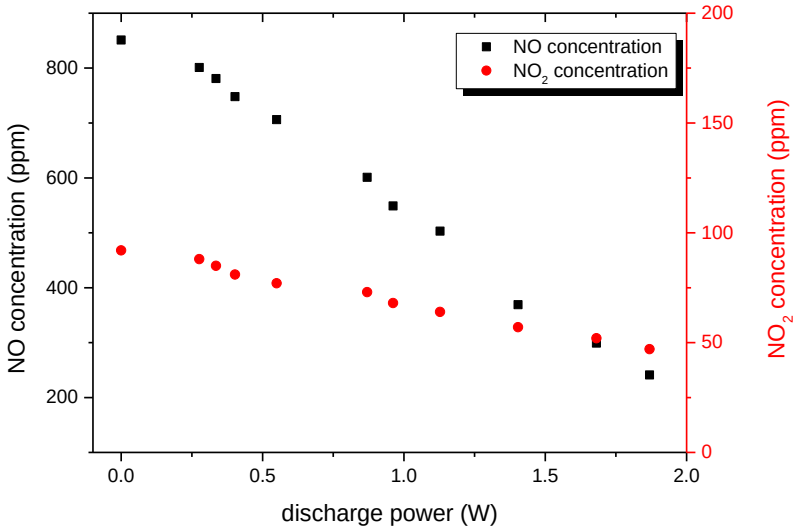

Figure 5-9 NO (square symbol) and NO_2 (circle symbol) concentrations for different discharge power at 4.76% O_2 and high concentration NO conditions

However, if the applied voltage was further increased, the pulseless discharge could not be sustained and was converted to arc discharge and the amplitude of current and voltage was changed to -2050μA and -3kV respectively. The active discharge area shrank into a narrow filament. The actual arc discharge filament was much thinner than that shown in the 10s exposure in Figure 5-10 (a). The reason for that was that the discharge filaments kept moving between pin and water surface, over the course of the 10s exposure all of the discharge filaments images were added together to produce the wide light band in the image.

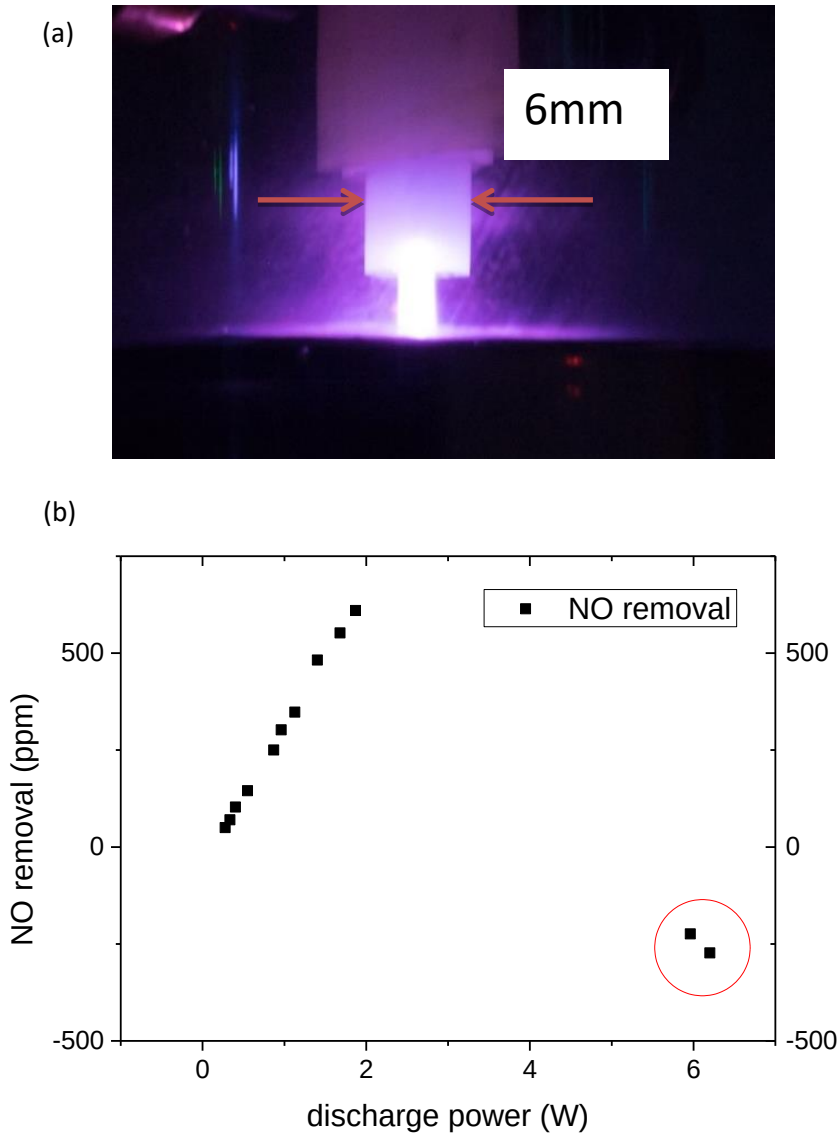

Figure 5-10 (a) Arc discharge image and (b) the corresponding NO removal in the red circle

It was found that NO was generated rather than being removed under arc discharge mode. When the arc discharge power was 6W, it had a negative effect on NO removal, Figure 5-10 shows -200 ppm NO removal, which meant that 200 ppm NO was generated.

Using a 0.25s exposure time, as shown in Figure 5-11, the arc discharge filament was observed to be thinner than that of the pulseless discharge, i.e. the energy density in arc mode was much higher than that in pulseless discharge. The temperature of an arc discharge at atmospheric pressure was reported as being of the order of 10^4K [128].

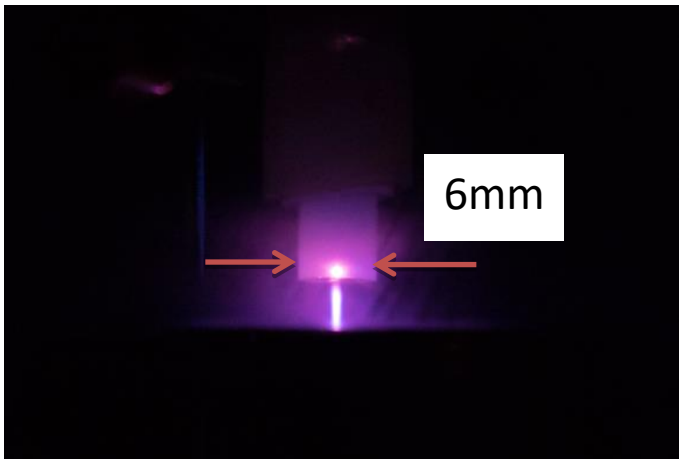

Figure 5-11 Arc discharge image of pin-water negative arc discharge (exposure time 0.25s)

The main reactions in the Zeldovich mechanism for NO formation at high temperature are given in Table 5-3. When the gas temperature is 2400K or higher, the Zeldovich mechanism becomes significant, e.g. during the fossil fuel burning process, gas temperature plays an important role in NO formation. As shown in Figure 5-12, at 1500K the equilibrium NO concentration $[NO]_r$ is 2000 ppm, and the time to reach 1000 ppm ($0.5[NO]_r$) is approximately 1000s, a relatively slow NO formation process. At a gas temperature of 2500K, the equilibrium NO concentration increases to 25000 ppm and the time to reach 12500 ppm is less than 10ms. Therefore, an arc discharge under higher discharge power, which would bring higher gas temperatures, would cause more NO to be generated over a shorter time period.

Table 5-3 Main high temperature NO formation reactions in Zeldovich's mechanism [3, 4].

Reactions	k (at 2400K)
$\boldsymbol{N + O_2 \rightarrow NO + O}$	7.61×10^{-12} (Fast reaction)[129]
$\boldsymbol{O + N_2 \rightarrow NO + N}$	2.21×10^{-17} (Slow reaction)[130]

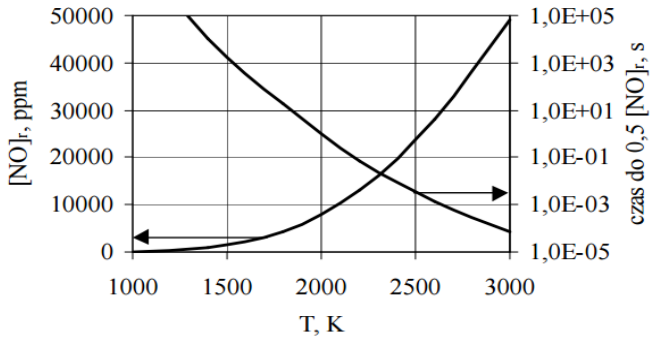

Equilibrium concentration of NO, $[NO]_r$, and time to reach $0,5[NO]_r$ versus the temperature

Figure 5-12 NO equilibrium concentration and the time to reach half of the equilibrium concentration of NO at different temperatures [131]

5.3.2 Effect of pin to water surface distance

As stated above, injecting different amounts of water into the reactor adjusted the distance between the pin and the water surface. For 4mm, 6.5mm and 9mm gap distances, the water volumes injected were 60mL, 65mL and 70mL respectively.

The effect of pin to water surface distance was investigated at 4.76% O_2 and high concentration NO condition in the controlled gas flow reactor. It was found, from the data presented in Figure 5-13, that the NO removal and energy efficiency increased with discharge power for 6.5mm and 9mm gaps. For the 4mm gap NO removal was negative because the discharge was in arc mode, so NO was generated by the Zeldovich's mechanism.

Comparison of NO removal between 6.5mm and 9mm gaps is made in Table 5-4. For the same discharge current of approximately 150 μA, the 6.5 mm gap pin voltage was -7.62 kV while at 9mm it increased to -10 kV: the power injection was greater at 9mm gap but the removal rate was lower. For the 6.5 mm gap and -9.21 kV, the NO removal was 610 ppm with the energy efficiency of 5.51 g/kWh. For the 9mm gap and -11.4 kV, NO removal reduced to 362 ppm with 2.74 g/kWh energy efficiency. The NO removal and energy efficiency results for the 6.5 mm gap were nearly twice those for the 9 mm gap, despite higher energy being injected at the larger gap.

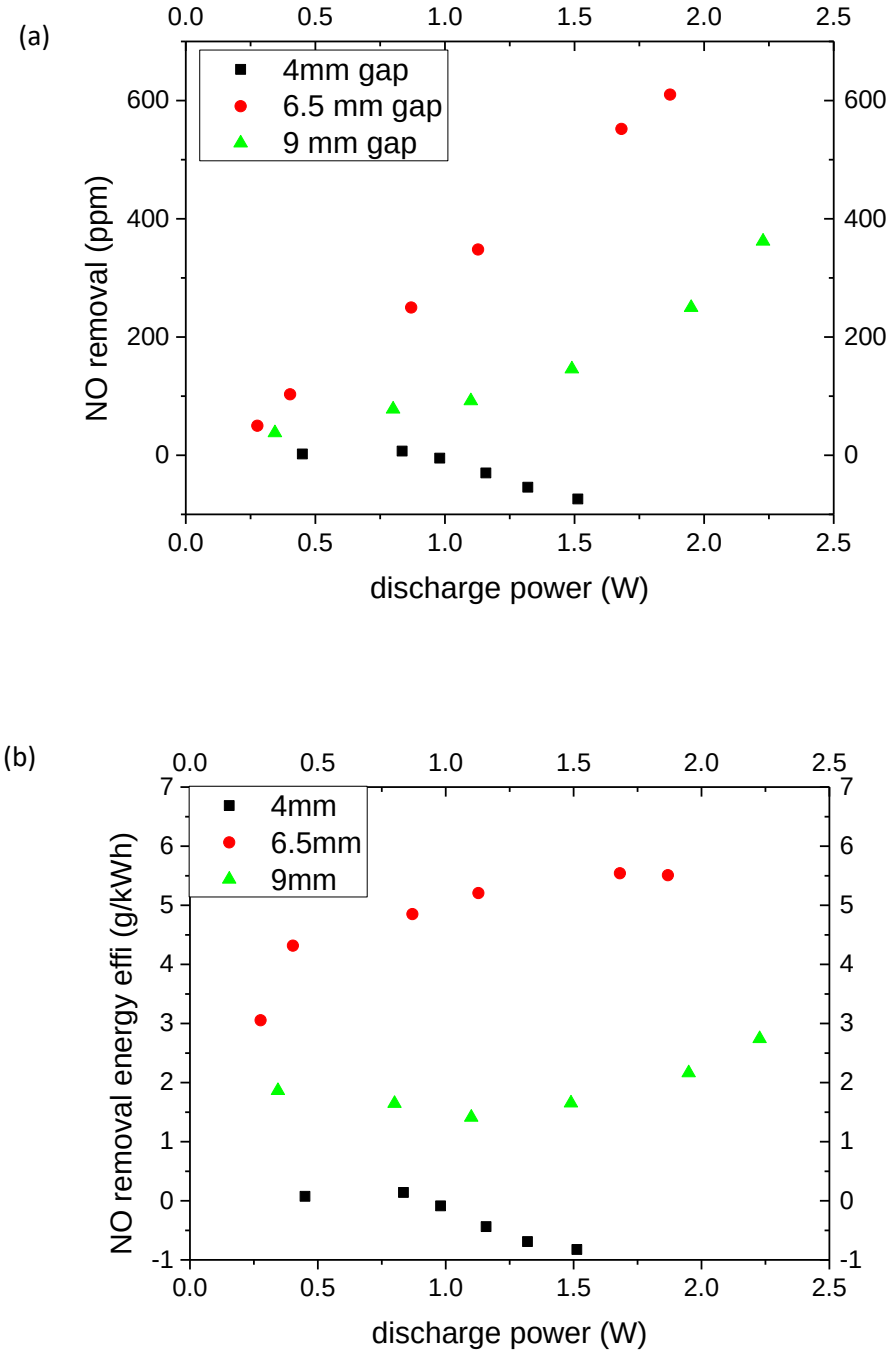

Figure 5-13 Controlled gas flow reactor with 4mm (square), 6.5mm (circle) and 9mm (up triangle) gap distance: (a) NO removal and (b) NO removal energy efficiency against discharge power at 4.76% O_2 and high concentration NO condition.

Table 5-4 Pin voltage, discharge current, power applied, NO removal and energy efficiency for three different gap distances under controlled gas flow condition

Gap size	Vpin (kV)	Current (μA)	Power (W)	NO removal (ppm)	Energy ŋ (g/kWh)
4mm	-1.54	-752	1.16	-30	-0.44
	-1.46	-1036	1.51	-74	-0.83
6.5 mm	-7.62	-148	1.13	348	5.21
	-9.21	-203	1.87	610	5.51
9mm	-10	-149	1.49	146	1.65
	-11.6	-192	2.23	362	2.74

5.3.3 Effect of oxygen

The initial concentration of NO and NO_2 before discharge treatment are listed in Table 5-2. The initial concentration of NO reduced from 1000 ppm to 588 ppm when the O_2 concentration increased from 0% to 16.67%. As shown in Figure 5-14, under the same discharge power, for O_2 concentrations in the range from 0% to 9.09% there was no obvious difference in NO removal, but at an O_2 concentration of 16.67%, the NO removal reduced significantly.

The effect of O_2 concentration on NO removal under wet condition in this discharge reactor was similar to that for DBD conditions which were investigated in Chapter 4. The difference was that the concentration of H_2O vapour in the DBD was fixed at 2.31% by a 20^oC gas washing bottle, but in the pin-water reactor the concentration of H_2O vapour was dependent on the injected discharge power. For NO removal by DBD under the same discharge power condition, the NO removal was the same at 0% and 4.76% O_2 conditions and started to reduce at 9.09% and further reduced at 16.67% O_2 concentration condition. Under pin-water corona discharge conditions, the NO removal started to reduce until the O_2 concentration reached 16.67%. As discussed in Chapter 4, the discharge in high concentration O_2 produced more atomic O in the discharge area and part of the OH reacted with O, rather than NO. For the pin-water corona discharge, one possible reason why the NO removal started to reduce at 16.67% O_2 condition, rather than 9.09% O_2 condition was similar to that at DBD condition, but the balance between the increase in atomic O and the reduction of OH to react with NO was able to sustain the change until 9.09% O_2 concentration. When O_2 concentration

increased to 16.67%, the reduction of OH was higher than the increase of atomic O, so NO removal was reduced. Both atomic O and OH not only reacted with NO, but also with each other. The reaction between atomic O and OH did not consume OH, however, if more and more atomic O and OH were interacting than reacting with NO, the NO removal would reduce.

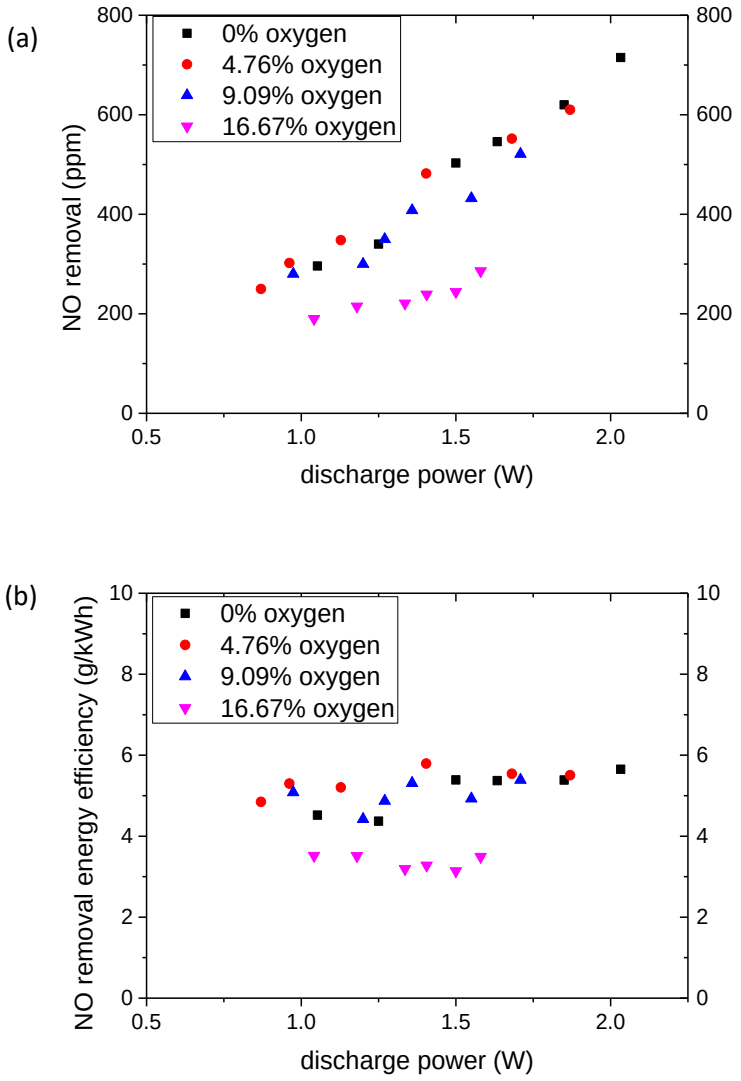

Figure 5-14 O_2 effect on (a) NO removal and (b) energy efficiency at different discharge power for 6.5mm gap: (square) - 0% O_2 condition, (circle) - 4.76% O_2 condition, (up triangle) - 9.09% O_2 condition and (down triangle) - 16.67% O_2 condition O_2

Table 5-5 Pin voltage, discharge current, power applied, NO removal and corresponding energy efficiency for four difference oxygen concentrations under controlled gas flow

O_2 concentration	**Vpin (kV)**	**Current (μA)**	**Power (W)**	**NO removal (ppm)**	**Energy ŋ (g/kWh)**
0%	-7.36	-143	1.05	296	4.52
	-8.8	-231	2.03	715	5.65
4.76%	-7.62	-148	1.13	348	5.21
	-9.21	-203	1.87	610	5.51
9.09%	-8.62	-113	0.97	280	5.08
	-9.6	-178	1.71	521	5.39
16.67%	-10.1	-156	1.58	286	3.49

In terms of the O_2 concentration effect on NO removal under Trichel pulse and pulseless discharge, as shown in

Table 5-5, when O_2 concentration was zero, the highest NO removal was 715 ppm at the discharge power of 2.03 W and the energy efficiency reached 5.65 g/kWh. However, as O_2 concentration increased from zero to 16.67%, NO removal reduced from 715 ppm to 286 ppm and NO removal energy efficiency reduced to 3.49 g/kWh. For 4.76% and 9.09% O_2 concentration, NO removal energy efficiencies were 5.51 and 5.39 g/kWh respectively, but the NO removal reduced to 610 ppm and 521 ppm. In addition, it was found that when O_2 concentration increased from 0% to 16.67%, the maximum discharge current under pulseless discharge mode reduced from -231μA to -156μA while the applied voltage increased from -8.8kV to -10.1kV.

5.3.4 Contribution of ozone for NO removal

In order to analyse the effect of O_3 or atomic O on NO removal in pin-water corona discharge condition, a reference gas was used to measure the concentration O_3 under different discharge power, similar to the method used in the DBD discharge. The reference gas was a gas mixture of 4.76% O_2 in N_2 but with no NO. Because measurement of atomic O was not possible in this experiment, the output O_3 concentration was treated as a probe to indicate how many effective O were generated during the corona discharge process. From the O_3 formation data shown in Figure 5-15 it was found that as the discharge power increased both O_3 formation and NO removal increased but the O_3 formation rate change was much lower than that of NO removal. When the discharge power was 0.4 W, the O_3 formation was 17 ppm while the NO removal achieved 126 ppm, a difference of 109 ppm. When the discharge power increased to 1.7 W, the O_3 formation increased to 138 ppm and

NO removal was 552 ppm, so the difference expanded to 414 ppm. If NO was removed by O or O_3, NO removal should be lower than or close to O_3 formation at reference gas condition, but actually, it was much higher than the O_3 formation. This suggests that OH became more significant for NO removal under the pin-water corona discharge configuration. In addition, as shown in Figure 5-16, OH can catalytically destroy O_3, so the formation of O_3 is limited by the presence of H_2O vapour.

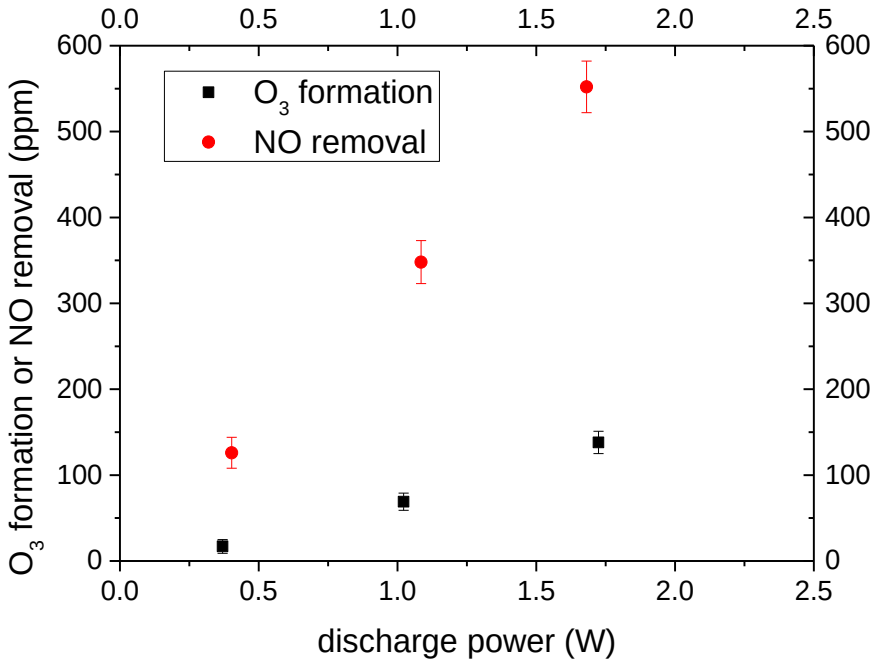

Figure 5-15 O_3 generation (square) in reference gas and NO removal (circle) at 6.5mm gap size, 4.76% O_2 and high concentration NO condition under different discharge power

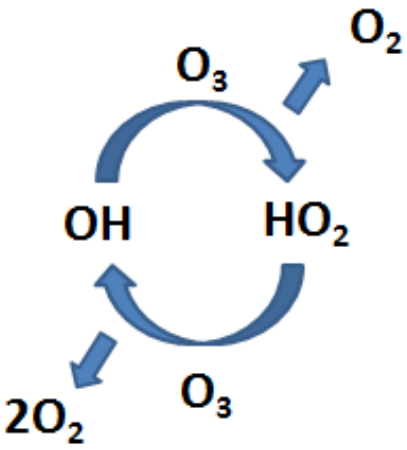

Figure 5-16 OH catalytically convert O_3 to O_2

5.3.5 Comparison between water and metal grounding

In order to investigate further the effect of the water ground electrode on NO removal, the controlled gas flow reactor with no water present was used, i.e. a metal ground electrode. The configuration of controlled gas flow pin-metal corona discharge reactor for this work is shown in Figure 5-17. There was no water in the reaction chamber. Before conducting this experiment, the reactor was cleaned and dried by pure N_2 (dew point is -40^{o}C) for 15 minutes to completely remove H_2O vapour from the reactor. The gap distance was set to 6.5mm and the gas mixture used was 4.76% O_2 and high concentration NO condition, as it was for the experiments in Section 5.3.1. The HV electrode is adjustable so the whole HV electrode, including pin and nylon tube, moved downwards to ensure that the gap distance is fixed 6.5mm and the gas passed between the pin's tip and the nylon tube, into the plasma, before venting.

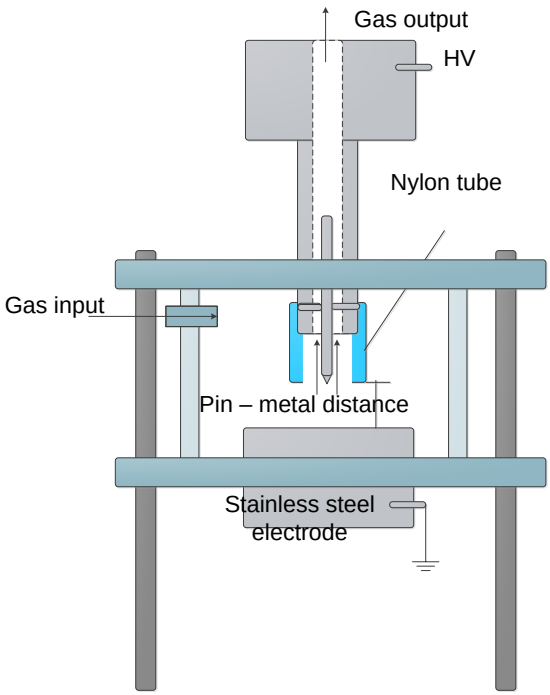

Figure 5-17 Pin-metal corona discharge reactor, controlled gas flow configuration

As shown in Figure 5-18, there were some indications of the important role of a water electrode for NO removal in a corona discharge. First, under pin-metal configuration, the highest discharge power sustained in pulseless discharge mode was 1.30 W, at this power the NO removal was 62 ppm and the NO removal energy efficiency was 0.80 g/kWh. However, under the pin-water configuration, the maximum discharge power sustained in pulseless discharge was 1.87 W, at this power NO removal and energy efficiency were 610 ppm and 5.51 g/kWh which were 9.84 and 6.85 times higher than that at the pin-metal configuration.

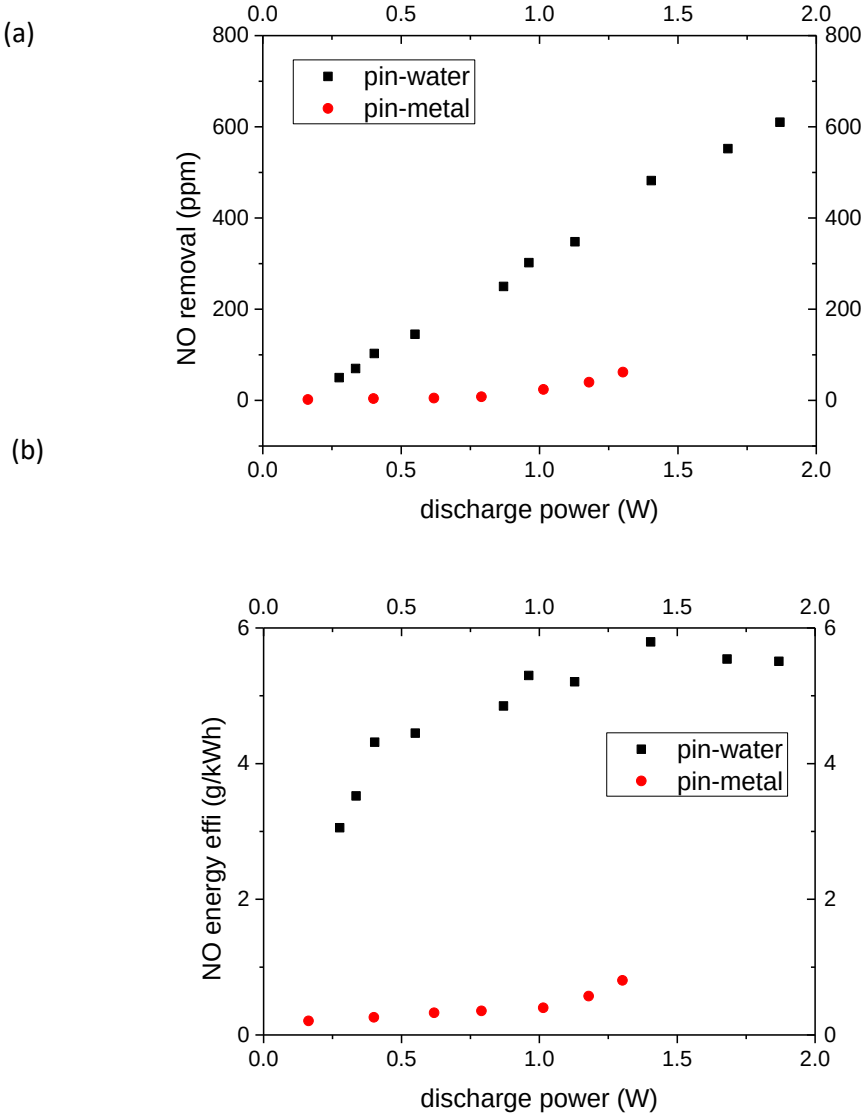

Figure 5-18 (a) NO removal and (b) energy efficiency at different applied power for pin-water (square) and pin-metal (circle) configuration at 4.76% oxygen and high concentration NO condition

The maximum sustainable discharge power in pulseless mode in the pin-metal configuration was lower than that in the pin-water configuration (Table 5-6), i.e. 1.30 W and 1.87 W respectively. In addition, it was found that for pin-metal pulseless discharge the NO removal energy efficiency also increased with increasing discharge power, which indicated the same tendency as the pin-water configuration's results. The reason for that relates to the effective ionization area in discharge. As shown in Figure 5-7, in transition from Trichel to pulseless

discharges, due to increasing voltage, the effective ionization region expanded and this promoted NO removal energy efficiency.

Table 5-6 Pin voltage, discharge current, power applied, NO removal and energy efficiency for pin-metal and pin-water configuration

Conditions	Pin voltage (kV)	Discharge Current (μA)	Power (W)	NO removal (ppm)	Energy ŋ (g/kWh)
Pin-metal	-5.264	-224	1.18	40	0.57
	-5.586	-233	1.30	62	0.80
Pin-water	-7.62	-148	1.16	348	5.21
	-9.21	-203	1.87	610	5.51

The discharge currents for both reactor electrodes were able to reach -200μA, see Table 5-6, but the pin voltage was much higher in pin-water configuration (-9.21 kV) than in pin-metal configuration (-5.586 kV). The increase in voltage probably relates to H_2O vapour's electron attachment ability, as discussed in Chapter 4, the presence of H_2O vapour can significantly increase the breakdown voltage in DBD. With the increase in discharge power, more H_2O vapour evaporated in the gas phase and, as free electrons more easily attach to H_2O vapour, the promotion of ionization process is more difficult. The suppression of ionisation reduces the likelihood of transfer to arc discharge, so the pin voltages can be higher while sustaining pulseless discharge.

The luminous regions between the pin and ground electrode in pin-water and pin-metal configurations are compared in Figure 5-19. As stated above, the pin-water configuration sustained a maximum voltage of -9.21 kV in pulseless discharge, for the pin-metal configuration it was -5.586 kV. For corona discharge, the distortion of electric field was significant and high electrical field existed around the pin. An increase in the applied voltage from -5.586 kV to -9.21 kV would result in the electric field around the pin increasing to almost twice the intensity, so the effective ionization area would expand. It should be noted that the luminance area between the pin and the water surface is not the ionization area, the ionization area is still concentrated around the pin. In the pulseless discharge mode, the luminous area represents the positive column of glow discharge. The electron energy level in this area is about 2 eV [132, 133], although this is much lower than that required for gas dissociation they still have enough energy to excite molecules and produce light. As the pin-

water configuration has a higher maximum applied voltage, -9.21kV, the average electron energy should be higher and produce more light. In addition, it was found that the light intensity at the pin's tip was stronger for the pin-water configuration. Therefore, the advantage of the pin-water configuration is that, due to the higher voltage potential sustained in the pulseless discharge mode, it is not only able to provide reactive species OH, but also to expand the effective ionization area to improve NO removal and energy efficiency.

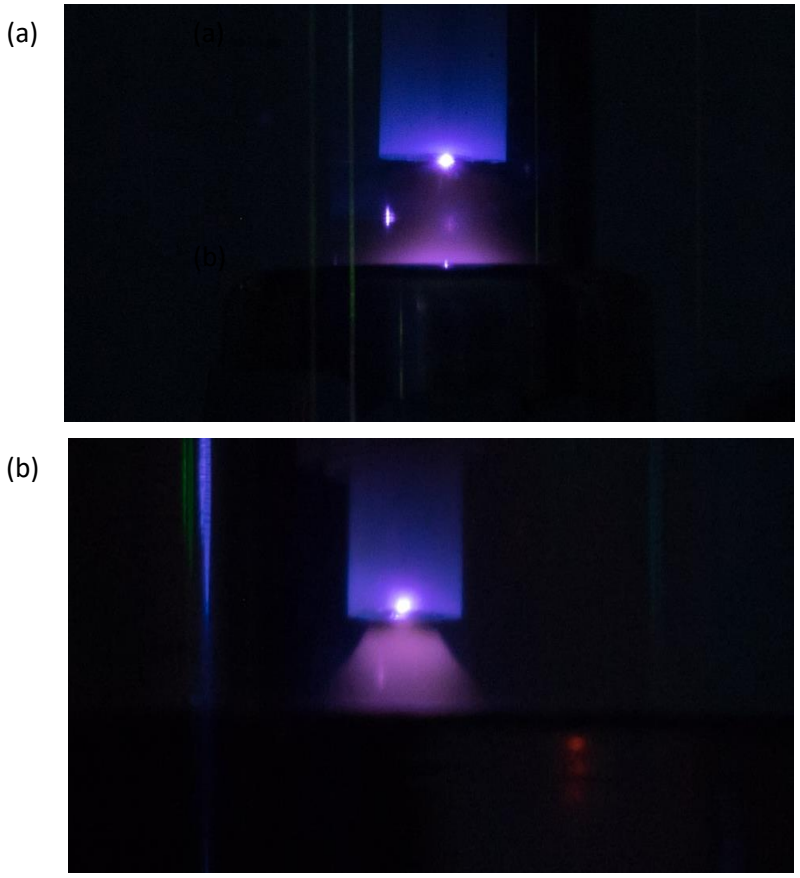

Figure 5-19 Images of (a) a pin-metal discharge at -5.586kV and (b) a pin-water discharge at -9.21kV

5.3.6 Effect of pin's radius of curvature

After investigating the advantage of having water as the grounding electrode, another aspect which was investigated in pin-water configuration with controlled gas flow is the pin tip's

curvature. The pin with 0.3mm radius of curvature was replaced by a pin with 0.5mm curvature. The gap distance was maintained at 6.5mm.

As shown in Figure 5-20, there was no obvious effect on NO removal as the O_2 concentration increased from 0% to 9.09%, but when O_2 concentration increased to 16.67%, NO removal was lower. This was similar to the results obtained for a 0.3mm pin (Figure 5-14), but despite the maximum discharge power in pulseless mode increasing, the energy efficiency with the 0.5mm pin has decreased.

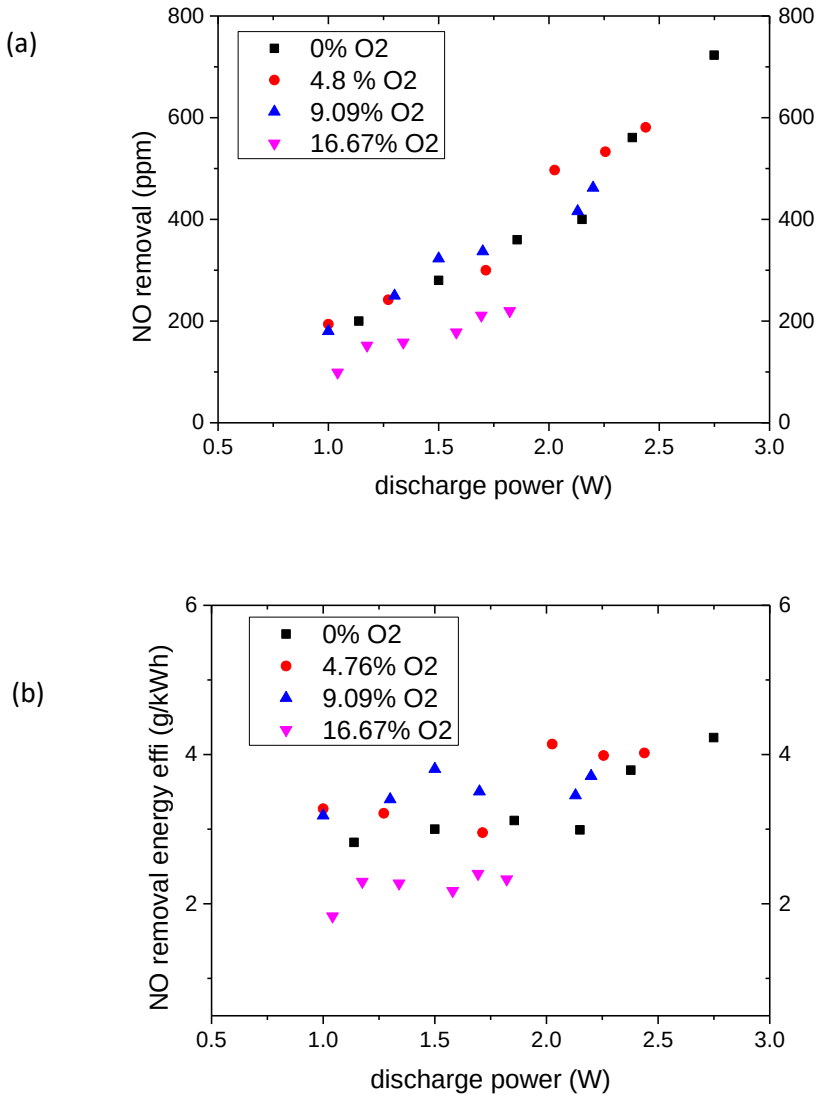

Figure 5-20 (a) NO removal and (b) energy efficiency at different discharge power using a pin with 0.5mm radius of curvature at a 6.5mm gap: gas mixture O_2 content (square) is 0%, (circle) is 4.76%, (up triangle) is 9.09% and (down triangle) is 16.67%

As shown in Table 5-7, O_2 concentration had a negative effect on the highest pulseless discharge current and power. The maximum discharge currents under pulseless discharge were -233 μA, -178 μA, -162 μA and -133 μA for 0%, 4.76%, 9.09% and 16.67% O_2 concentration, respectively. The maximum discharge power before the transition from pulseless discharge to arc discharge were reduced from 2.749W, 2.438W, 2.2W to 1.822 W with the increase of oxygen concentration from 0% to 16.67%.

Table 5-7 Pin voltage, discharge current, power applied, NO removal in ppm and energy efficiency for 3 oxygen concentrations for 0.5mm pin under controlled gas flow condition

Oxygen Concentration	Pin voltage (kV)	Discharge current (μA)	Power (W)	NO removal (ppm)	Energy ŋ (g/kWh)
0%	-7.44	-153	1.14	200	2.82
	-11.8	-233	2.75	723	4.23
4.76%	-11.25	-113	1.27	242	3.21
	-13.7	-178	2.44	581	4.02
9.09%	-12.5	-136	1.7	337	3.50
	-13.58	-162	2.20	462	3.71
16.67%	-13.7	-133	1.82	220	2.33

To compare the effect of radius of curvature of the pin electrode, 0.3mm and 0.5mm, on NO removal and energy efficiencies data are listed in Figure 5-21 and Figure 5-22. It was found that the pin with smaller radius of curvature had a positive effect on NO removal. In terms of NO removal, from Figure 5-21 it was found that the maximum NO removal was similar for both pins, but the energy consumption was less for the pin with 0.3mm radius of curvature. For the pin with 0.3mm radius of curvature for O_2 concentration of 0%, 4.76%, 9.09% to 16.67%, the maximum NO removal values were 715 ppm, 610 ppm, 521 ppm and 286 ppm respectively: for the 0.5mm pin, the equivalent values were 723 ppm, 581 ppm, 462 ppm and 211 ppm. In terms of NO removal energy efficiency, for O_2 concentrations in the range of 0 to 9.09% the 0.3mm pin had an energy efficiency of around 5 g/kWh, for the 0.5mm pin it was around 3.5 g/kWh, which was an approximately 30% reduction. For an O_2 concentration of 16.67%, a similar reduction was found, from 3 g/kWh to 2 g/kWh.

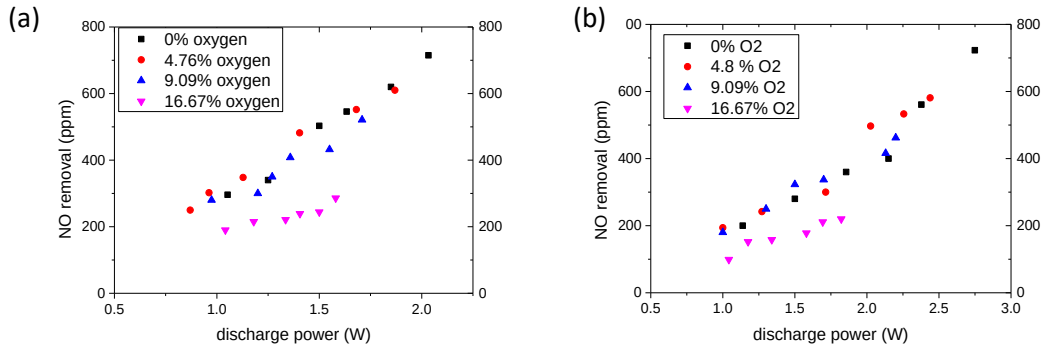

Figure 5-21 NO removal using pins with (a) 0.3mm radius and (b) 0.5mm radius under controlled gas flow-water condition at different O_2 concentration

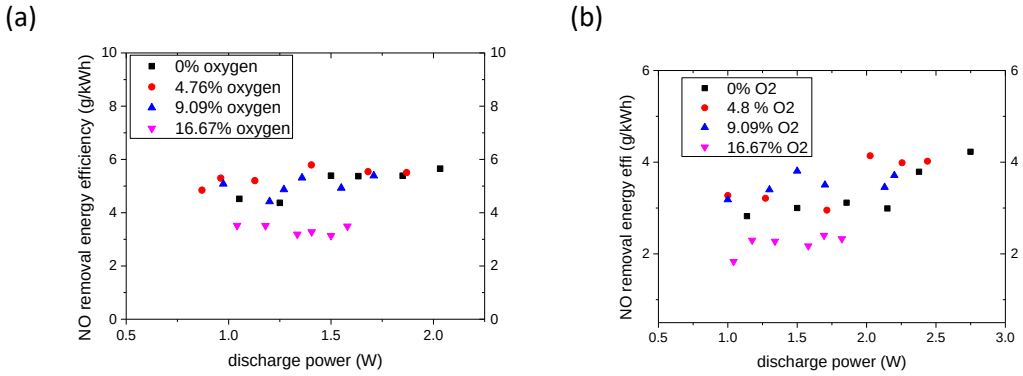

Figure 5-22 NO removal energy efficiency by pins with (a) 0.3mm radius and (b) 0.5mm radius under controlled gas flow-water condition at different O_2 concentration

5.4 NO removal under open gas flow condition

The configuration of the open gas flow pin-water discharge reactor is shown in Figure 5-23. As outlined above, the difference between open and controlled gas flow was set by whether the nylon tube was used or not. For a controlled gas flow condition, the use of the nylon tube guided the gas flow through the ionization area of the corona discharge, because the pin's tip was at the same horizontal level as the nylon tube. For open gas flow condition, as the aperture of the gas outlet was 18.5mm above the pin (d_1), not all of the gas flow was through the ionization area of the corona discharge. The pin's radius of curvature was 0.3mm in this experiment. The effects of the distances between the pin's tip and water surface (d_2) from 4mm, 6.5mm to 9mm were investigated and are reported in this section.

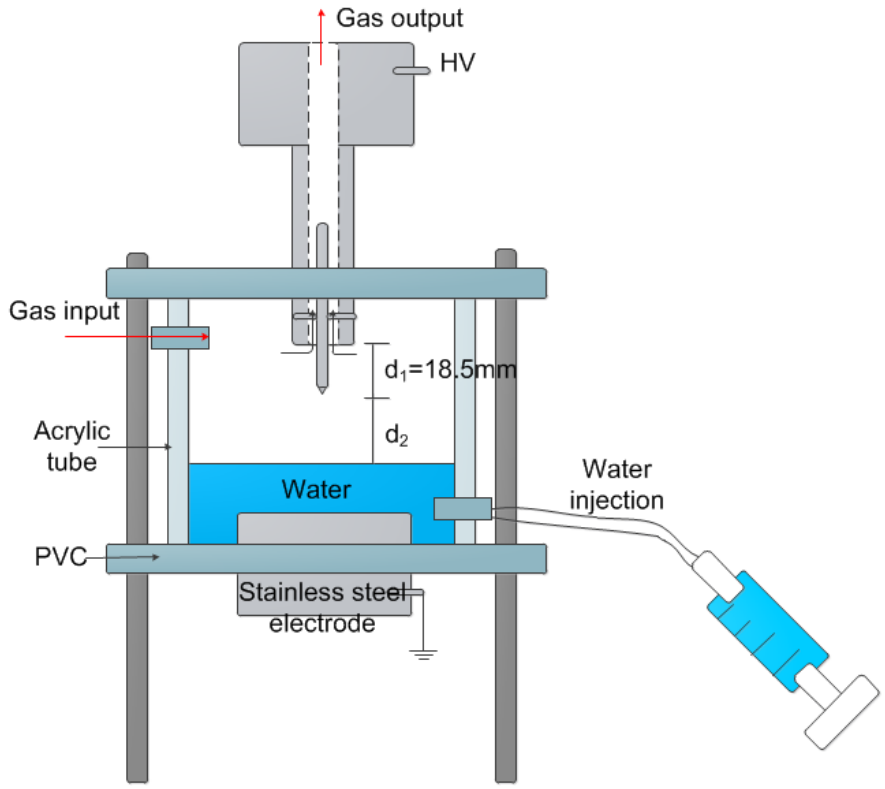

Figure 5-23 The pin-water discharge reactor under open gas flow configuration

5.4.1 Effect of oxygen

For these experiments, in order to compare the results with those from the controlled gas flow study, the distance between pin and water surface was 6.5 mm. NO removal and energy efficiency are shown in Figure 5-24. The effect of O_2 concentration at 16.67% was not as obvious as in the results obtained in the controlled gas flow reactor. For O_2 concentration of 0%, 4.76%, 9.09% and 16.67%, the maximum NO removal values were 365 ppm, 320 ppm, 233 ppm and 58 ppm. The maximum discharge power in pulseless mode reduced from 2.651W, 2.4 W, 1.8 W to 1.435W. The NO removal energy efficiency was lower than 2.5 g/kWh for all of O_2 concentration conditions while under the controlled gas flow configuration the energy efficiency achieved was up to 5.5 g/ kWh. The main reason may relate to the lifetime of OH. As mentioned in [134], the lifetime of OH is under 100μs, therefore NO needs to move through the ionization area to react with OH. For the open gas flow configuration, some NO containing gas flows out of the reaction vessel above the discharge ionization area and has no contact with the plasma, therefore, as expected, the NO

removal results were lower than those under the controlled gas flow configuration. A quantitative comparison between controlled and open gas flow data is made in Section 5.4.2.

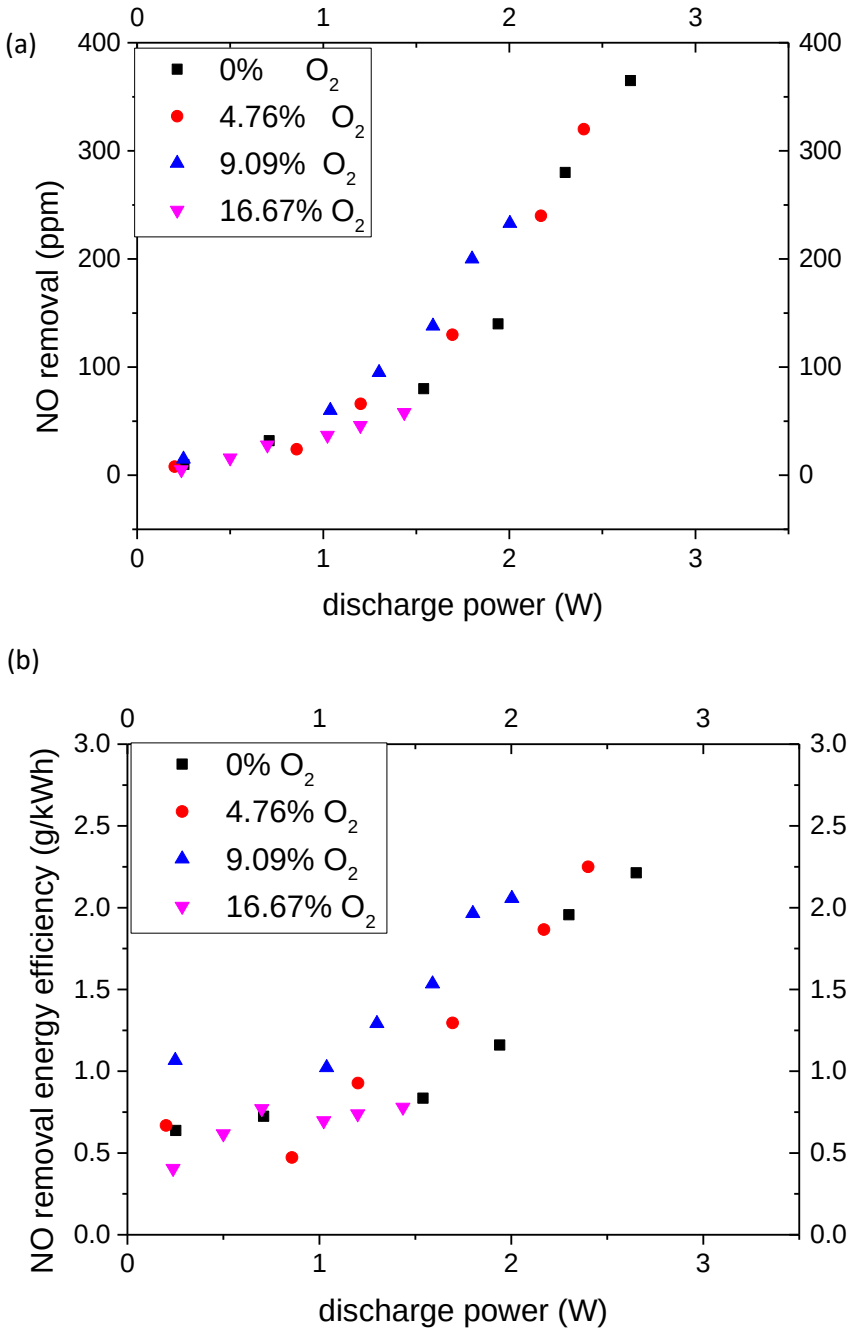

Figure 5-24 (a) NO removal and (b) energy efficiency at different discharge power: 0.3mm radius pin with 6.5mm gap under open gas flow conditions: O_2 concentration key - (square) is 0%, (circle) is 4.76%, (up triangle) is 9.09% and (down triangle) is 16.67% O_2

5.4.2 Comparison between controlled and open gas flow condition

For a zero percent O_2 concentration condition, the maximum NO removal could reach above 715 ppm at 2.03W for controlled gas flow configuration, but for open gas flow configuration, NO removal was reduced to 280 ppm at 2.3W (Figure 5-24), i.e. more than 400 ppm reduction in open gas flow condition. This proves the importance of contact between NO and reactive species to increase the NO removal.

Table 5-8 Pin voltage, discharge current, discharge power, NO removal and energy efficiency for three oxygen concentrations for open gas flow configuration

C_{O2} (% vol)	Pin voltage (kV)	Discharge current (μA)	Power (W)	NO removal (ppm)	Energy ŋ (g/kWh)
0	-6.21	-248	1.54	80	0.83
	-7.07	-375	2.65	365	2.21
4.76	-6.29	-191	1.20	66	0.93
	-8.25	-291	2.4	320	2.25
9.09	-8.21	-194	1.59	138	1.53
	-8.56	-234	2.00	233	2.06
16.67	-9.08	-158	1.43	58	0.78

Comparing the data in

Table 5-5 and Table 5-8 shows that there is a big difference between the controlled gas flow configuration and open gas flow configuration.

At zero percent O_2 concentration condition, the controlled gas flow's maximum discharge current under pulseless mode was -231 μA, but for open gas flow it was -375 μA. The maximum discharge current also increases for O_2 concentrations of 4.76%, 9.09% and 16.67%. When the O_2 concentration was 4.76%, for controlled gas flow configuration, the highest voltage in pulseless mode is -9.21kV with a current of -203 μA, for open gas flow configuration, it is -8.25 kV with a current of -291 μA. The reduction of the transition from pulseless to arc discharge from -9.21 kV to -8.25 kV suggests that the presence of nylon tube can make the transition much easier. In the controlled gas flow configuration, the inner surface of the nylon tube can accumulate negative charges when discharge happens at the pin's tip. As the polarity of accumulated charges is the same as that for the pin, the discharge is more difficult to initiate and the maximum voltage to sustain in pulseless discharge mode is higher, but the discharge current is lower.

In addition, the shapes of the luminous area for open and controlled gas flow configurations were investigated (Figure 5-25). For open gas flow configuration, it was a triangle-shaped luminous area, but for controlled gas flow configuration, it was a bell-shaped luminous area, which nearly covered the cross section of the nylon tube.

(a)

(b)

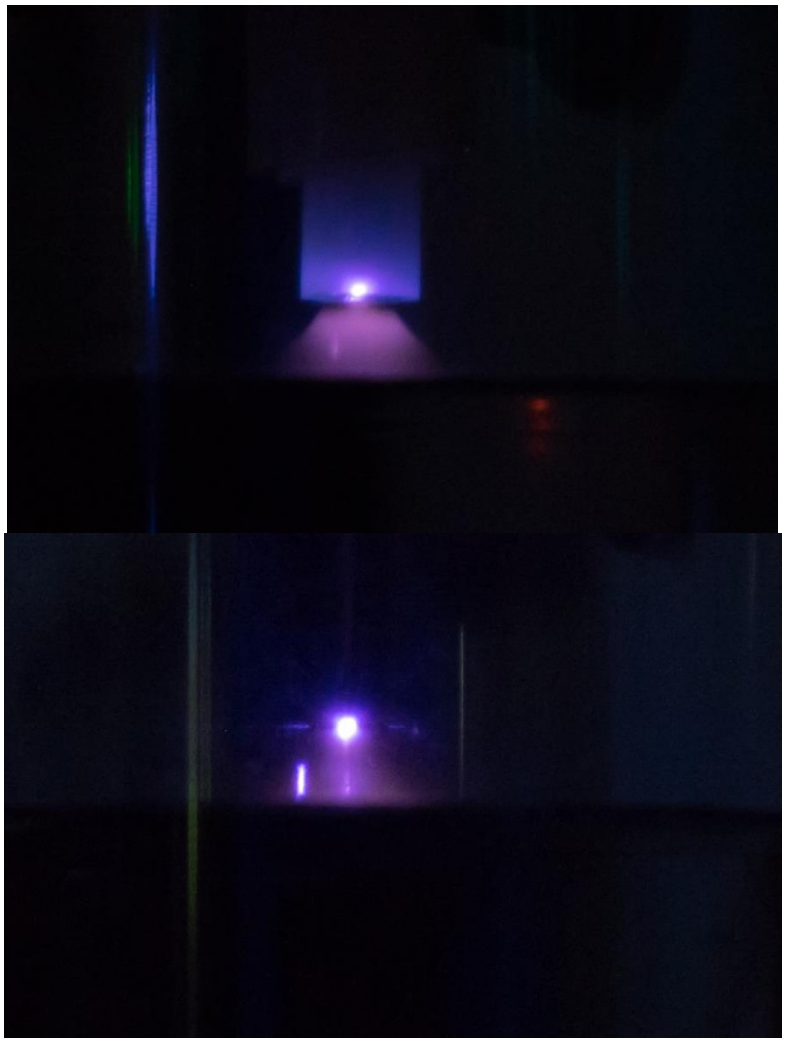

Figure 5-25 Images of pulseless discharge (a) controlled gas flow configuration at -9.21kV and (b) open gas flow configuration at -8.247 kV (exposure time is 10s)

A possible reason for the wider luminous area in the controlled gas flow configuration is as follows: as nylon is a dielectric material, when discharge occurs electrons could move to the nylon tube's surface and stay there, left image in Figure 5-26. With increasing applied voltage, more and more free charges attach to the edge of the nylon tube. As the polarity of deposited charges is the same as that of pin, they broaden the area of high electric field across from the ground water electrode to expand the discharge area. So the nylon tube not

only channels the gas flow through the ionisation region but also expands the equivalent high voltage electrode area.

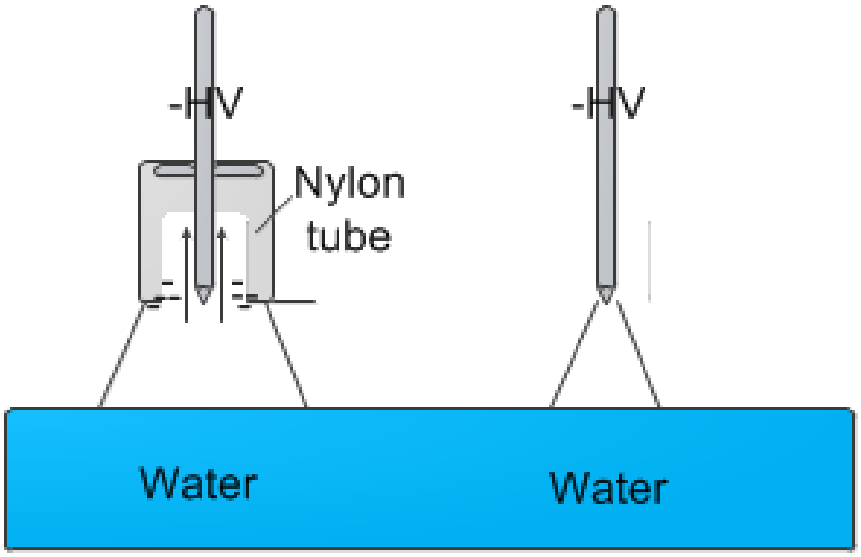

Figure 5-26 Left image - controlled gas flow configuration with charges deposited on the surface of nylon tube and right image - open gas flow configuration, no deposited charge.

5.4.3 Effect of pin to water surface distance

The effect of the gap distance was also examined under the open gas flow condition. Three gap sizes 4mm, 6.5mm and 9mm were investigated and the data are shown in Table 5-9. Comparing the data in Table 5-4 and Table 5-9: for the 4mm gap, under controlled gas flow pulseless corona discharge was not sustained, but for open gas flow configuration, pulseless discharge was realised and the maximum NO removal was 257 ppm with 3.104 g/kWh energy efficiency (Table 5-9). For the 6.5mm gap, the maximum NO removal reduced from 610 ppm in controlled gas flow to 320 ppm in open gas flow. For the 9mm gap, the maximum NO removal reduced from 362 ppm in controlled gas flow to 182 ppm in open gas flow. Although the open gas flow configuration provided a higher current injection, both NO removal and energy efficiency were lower than under controlled gas flow configuration. In terms of NO removal energy efficiency, under controlled gas flow configuration, the highest energy efficiencies were 5.51 g/kWh and 2.74 g/kWh for 6.5 mm and 9 mm gaps, but under open gas flow the highest energy efficiencies reduced to 2.25 g/kWh and 1.32 g/kWh for 6.5mm and 9mm gaps respectively. In open gas flow configuration it was found that the performance was better when the gap was 4mm than that at 6.5mm.

Table 5-9 Pin voltage, discharge current, discharge power, NO removal and energy efficiency for three gap sizes for open gas flow configuration at 4.76% O_2 and high concentration NO conditions

conditions	Pin voltage (kV)	Discharge current (uA)	Discharge Power (W)	NO removal (ppm)	Energy ŋ (g/kWh)
4 mm gap	-4.38	-242	1.06	134	2.13
	-4.92	-284	1.40	257	3.10
6.5mm gap	-7.09	-239	1.69	130	1.30
	-8.21	-294	2.4	320	2.25
9mm gap	-9	-199	1.79	92	0.87
	-10.04	-231	2.32	182	1.32

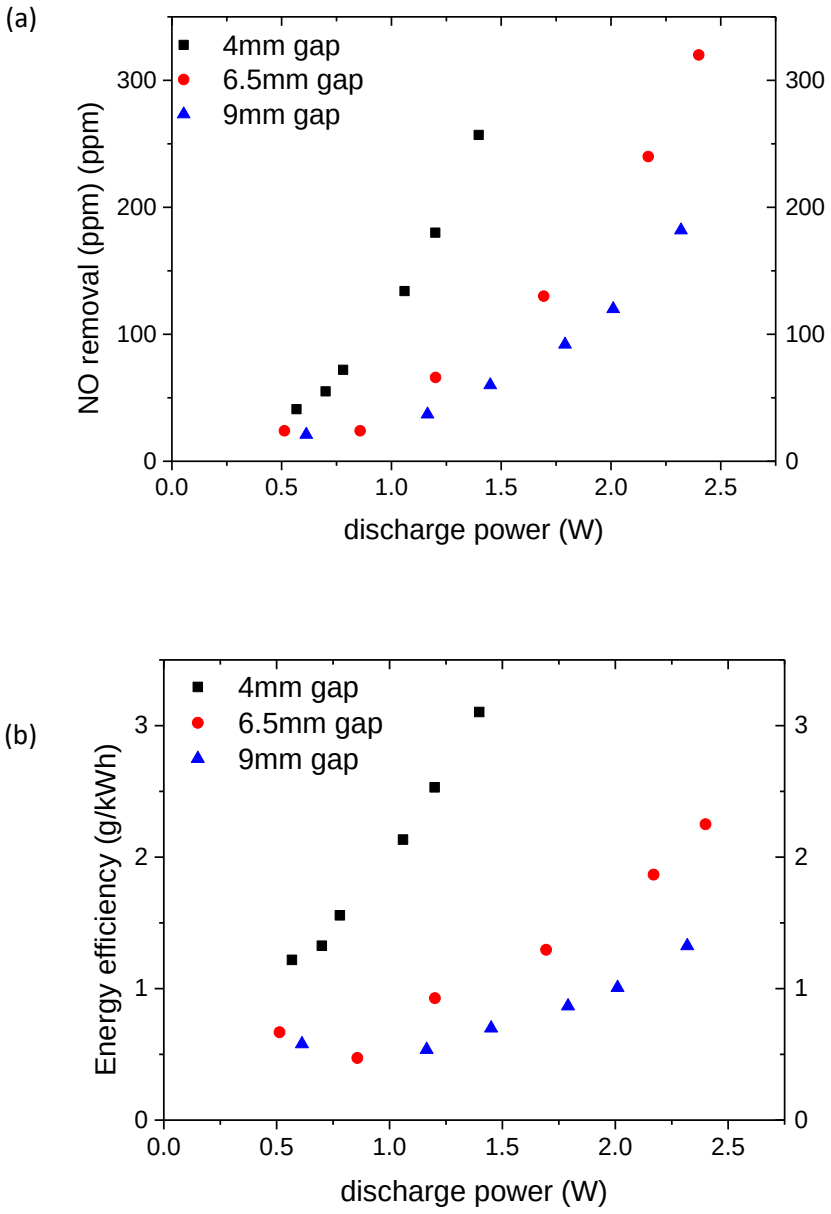

Figure 5-27 Gap distance effect on (a) NO removal and (b) NO removal energy efficiency at different discharge power, open gas flow reactor under 4.76% O_2 and high concentration NO condition: gap distance key - (square) is 4mm, (circle) is 6.5mm, (up triangle) is 9mm

5.5 Conclusions

These experiments investigated the potential of pin-water negative corona discharge for NO removal by reactive species OH, which had no side reaction.

First, it was found that NO removal energy efficiency increased with increasing discharge power. There were two possible reasons proposed. One was the expansion of the ionization area in the transition from Trichel pulse discharge to pulseless discharge. The other was the increase in H_2O concentration in the gas phase: higher concentration of OH led to an increase in the NO removal. In addition, because of the short lifetime of OH, both the NO removal and energy efficiency were higher under the controlled gas flow configuration than under open gas flow configuration. For instance, for the gas containing 4.76% O_2 and an initial NO concentration of 851 ppm, under controlled gas flow the NO removal was 610 ppm with 5.507 g/kWh energy efficiency, but under open gas flow NO removal reduced to 320 ppm with 2.25 g/kWh energy efficiency. This significant difference was determined by the contact between plasma and gases. If the ionization area was far from the gas outlet, part of NO containing gas left the reactor without contacting the OH species in the ionisation region. The effect of oxygen concentration on NO removal was not significant in the range of 0% to 9.09%, but had a negative effect when it increased to 16.67%. NO removal was investigated under Trichel pulse discharge, pulseless discharge and arc discharge modes and it was found that NO removal was realised using Trichel pulse and pulseless discharge modes, but NO was generated in arc mode. As outlined in this Chapter, as a result of increased gas temperature NO generation followed Zeldovich's mechanism. When the arc discharge power reached 6W, it generated 200 ppm of NO.

Second, the pin's radius of curvature affected the NO removal results. For gas containing 4.76% O_2, the pin with 0.3 mm radius of curvature resulted in 610 ppm NO removal with energy efficiency of 5.507 g/kWh, however, for the pin with 0.5mm radius of curvature, NO removal was reduced to 581 ppm with energy efficiency of 4.02 g/kWh. A sharper pin may improve NO removal and energy efficiency.

Third, in order to confirm that OH species had a positive impact on NO removal the effect of water electrodes was investigated using a pin-metal discharge arrangement. The results (Figure 5-18) indicated that the effect of water electrode was positive for NO removal. The water electrode not only provided H_2O vapour to generate OH, but also increased the

maximum voltage which will sustain pulseless discharge, which can increase the ionization area of the corona discharge.

In this chapter, a novel pin-water corona discharge was investigated for NO removal. The new configuration increased the OH species effect on the NO removal reactions, but the energy efficiency is lower than 6g/kWh which is too low to be commercialised. As mentioned before, the pin-water corona discharge has been investigated as a water purification technology, so it is a better choice to combine these two pollutants treatments process together in one reactor to improve its applicability.

Chapter 6 IMPROVING NO REMOVAL BY PRE-CONCENTRATION USING ACTIVATED CARBON

6.1 Introduction

As highlighted in the Literature Review, the concentration of NO in flue gases is usually a few hundred ppm, so the collision between an energetic electron and an NO molecule seldom happens during non-thermal plasma treatment. To improve on the opportunity to have an electron react with NO, it is worth investigating a new method of increasing the concentration of NO in the flue gas. In this chapter, a 2-stage process is presented: low concentration NO (1000ppm) from a flue gas is absorbed onto activated carbon granules and then a thermal desorption process is used to release a high concentration of NO (up to 6%). At 6% concentration level, the NO removal mechanism was investigated quantitatively. It is important to analyse the difference between NO removal under ppm level and percentage level, from the chemical kinetics point of view. The aim of this chapter is to investigate the performance of non-thermal plasma for NO removal when NO concentration is in percentage level.

The Literature Review indicated that activated carbon was one of the most widely used absorbents in collecting a range of chemicals [88, 135, 136] including NOx. Activated carbon is a porous material with higher than 1000 m^2/g specific surface area [27, 137]. There are many oxygen functional groups on the surface of activated carbon, including carboxylic group (-COOH), lactone group (-COO-), hydroxylic group (-C-OH) and carbonyl group (-C=O). These play an important role in low concentration NO absorption.

In this set of experiments, the effects of temperature, gas flow rate and concentration of O_2 and H_2O vapour on the NO absorption process by activated carbon were investigated. After thermal desorption, direct non-thermal plasma treatment of high concentration NO was investigated to determine NO removal and energy efficiency and the dominant reactive species was identified.

6.2 Experimental setup

To create high concentration NO for removal by direct non-thermal plasma treatment, there were three main processes (Figure 6-1). First, there was the low concentration NO absorption process by activated carbon, Figure 6-1(a). Secondly, there was the thermal desorption of NO, Figure 6-1(b): although two methods were tried for the thermal desorption, as discussed in 6.2.3, the figure shows the direct method which was more successful. Finally, after high concentration NO was released from activated carbon, it was treated by DBD directly, Figure 6-1(c). The DBD reactor is a meshed electrode DBD. As explained in Chapter 2, the plate to plate configuration is easier when changing the shape of the electrode. The non-uniform structure of the mesh electrode meant that it was easier to initiate discharge because of the change in electric field distribution. In addition, in Chapter 4 it was found that the maximum power level of cylindrical DBD reactor was 0.25W, which is too low to treat high concentration NO, so a more powerful DBD reactor, up to 1.044W power at 7kV, was used in this chapter.

A schematic diagram of the equipment used in the DBD treatment of desorbed high concentration NO is shown in Figure 6-2. A 50Hz AC power supply (maximum output voltage was 7kV) was used to energize the DBD reactor. As with previous work, the gas flow rates were controlled by Alicat mass flow controllers. A Tektronix P6015A HV probe with a bandwidth of 75 MHz was used to measure the voltage applied to the reactor. A 100nF capacitance was used to measure charge transfer and discharge power by Lissajous figure, a Tektronix DPO5104B Digital Phosphor Oscilloscope with 1GHz bandwidth and 10Gs/s sample rate was used to record electrical signals. NOx analyser (thermal scientific model 42i-HL) was used to measure NO and NO_2 concentration. Finally, all data were recorded and analysed in Matlab and Origin.

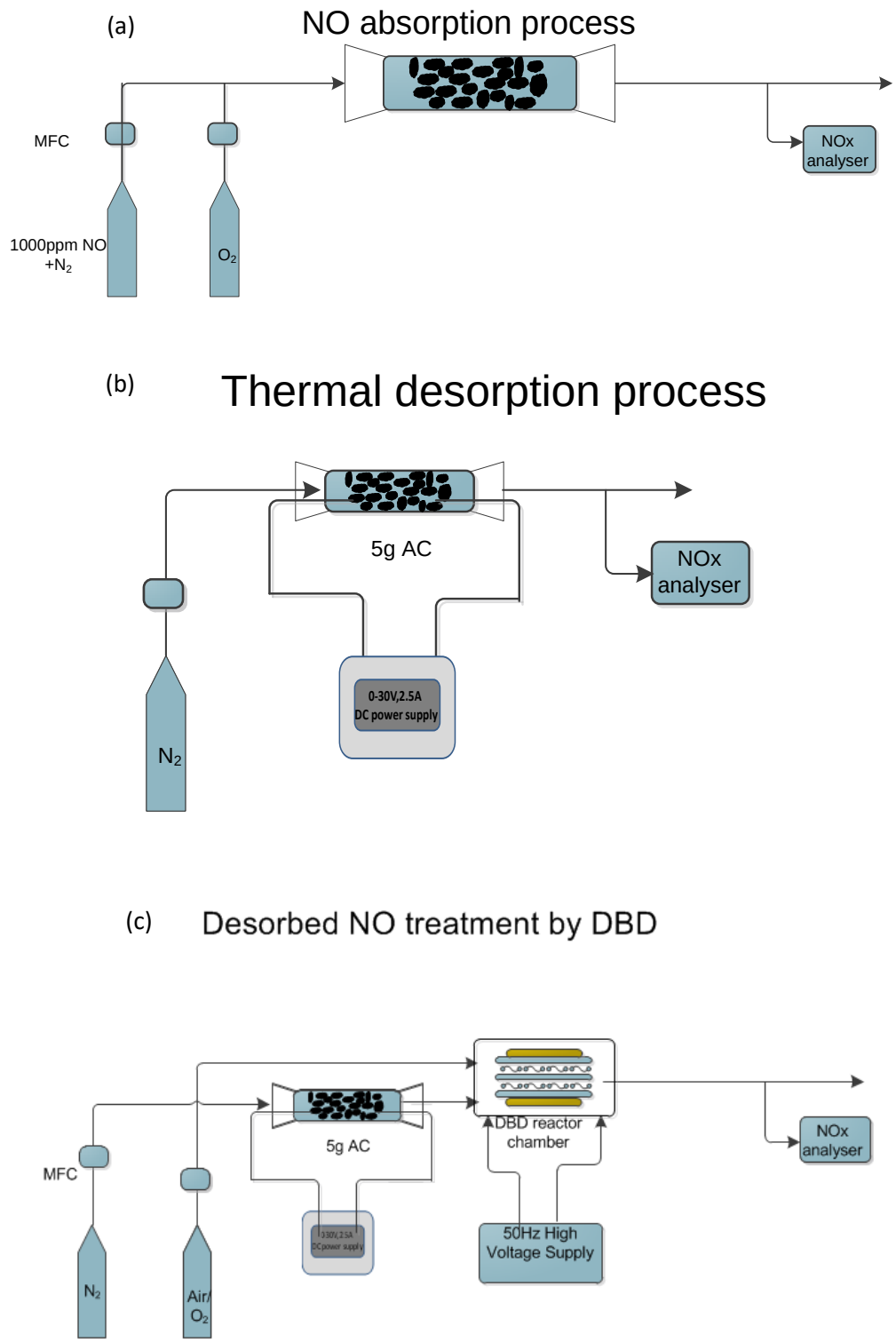

Figure 6-1 Schematic diagram of (a) NO absorption process, (b) thermal desorption process and (c) DBD treatment on desorbed high concentration NO

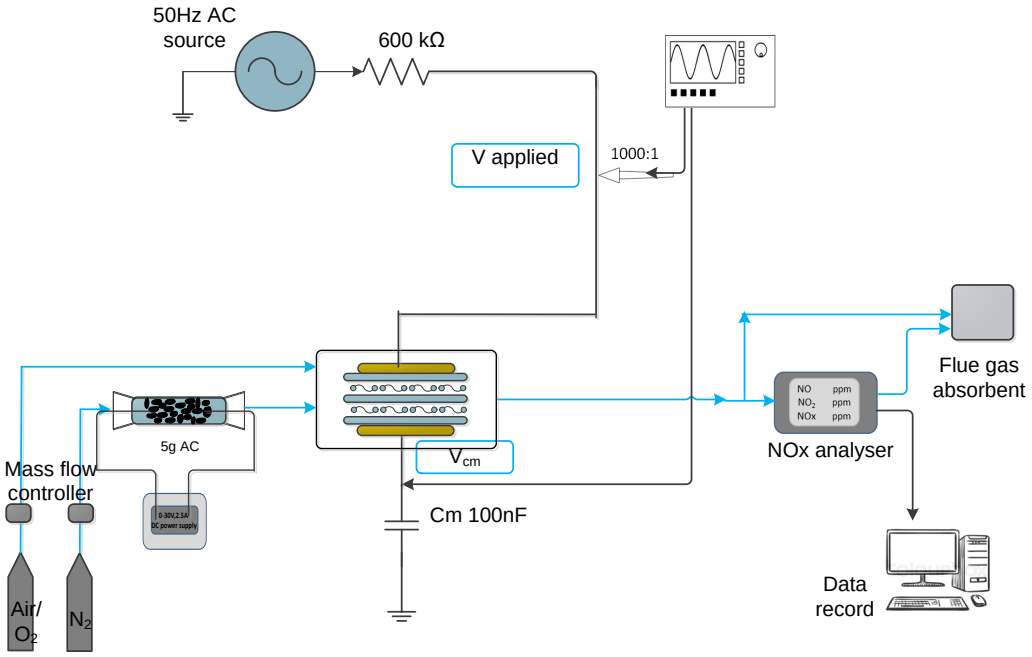

Figure 6-2 Schematic diagram of DBD of thermally desorbed high concentration NO.

In these experiments, five grams of activated carbon was put into a Pyrex tube with dimensions of 15mm x 11mm (OD x ID) and 300mm long. As shown in Figure 6-3, the effective length of the five grams activated carbon in the Pyrex tube was approximately 120mm, both ends of the container were sealed by rubber stoppers and glass wool was used to fix the position of activated carbon inside the tube. In addition, activated carbon is a good conductor, so for the thermal desorption process, a DC power supply was connected to both ends of the activated carbon: two steel pins connect the activated carbon to the DC power supply. The shape of the activated carbon pellet was cylindrical. The diameter was approximately 4mm and the length was in the range of 4mm to 7mm.

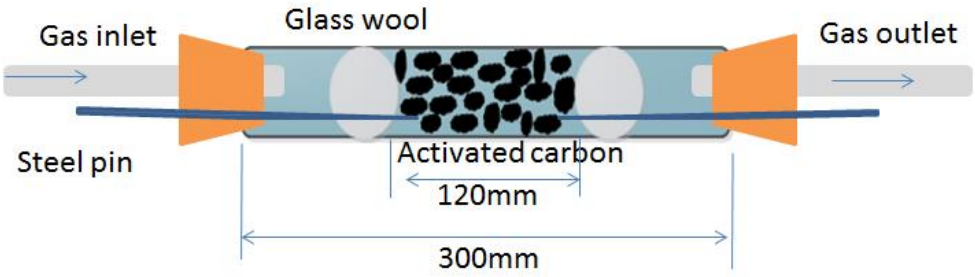

Figure 6-3 Schematic diagram of activated carbon container

6.3 Activated carbon NO absorption

As measured by the Brunauer-Emmett-Teller (BET) method in liquid nitrogen, the specific surface area of activated carbon used in this set of experiments was 1358 m^2/g with pore volume 0.47742 cm^3/g. In this chapter, the success of the absorption-desorption regime is demonstrated. The gas input in this experiment was 1000 ppm NO and the flow rate was 210mL/min. As shown in Figure 6-4, after the process of absorption and desorption, the NO concentration was increased up to 6% and the flow rate reduced to 50mL/min.

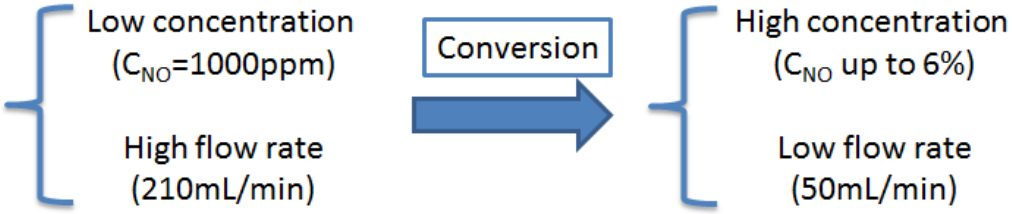

Figure 6-4 Change in gas properties due to NO absorption and thermal desorption processes

6.3.1 Effect of oxygen concentration

As mentioned before, NOx absorption by activated carbon is based on their molecular polarity. The oxygen functional groups on the activated carbon surface can absorb polar molecules. The polarity of gas molecules is related to their dipole moments. For homo-nuclear diatomic molecules such as N_2 and O_2, their dipole moments are zero because of their symmetric molecule structure. Unsymmetrical gas molecules, e.g. H_2O, NO and NO_2 are polar and can be absorbed by activated carbon, dipole moments are given in Table 6-1.

Table 6-1 Molecules dipole moment [138]

Substance in gas phase	Dipole moment $\times 10^{30}$ [C.m]
N_2	0
O_2	0
H_2O	6.2
NO	0.5
NO_2	1.3

The effect of O_2 concentration on NO absorption over 17.5 min absorption process is shown in Figure 6-5. The reason why the absorption time is set to 17.5 min is that when the O_2 concentration was 4.76%, the escaping NO concentration was 35 ppm, which satisfies the 50ppm NOx emission standard,

Table 1-2. When O_2 concentration was reduced to 2.44%, NO concentration slowly increased to 100 ppm after 17.5min absorption process, which meant that more than 90% of NO was absorbed by activated carbon. However, when O_2 concentration was 0%, NO concentration increased to 950 ppm in less than 200s, which meant that there was only 50 ppm NO being absorbed. As the majority of NO escaped the activated carbon when there was no O_2 in the gas flow, O_2 played an important role for NO absorption process.

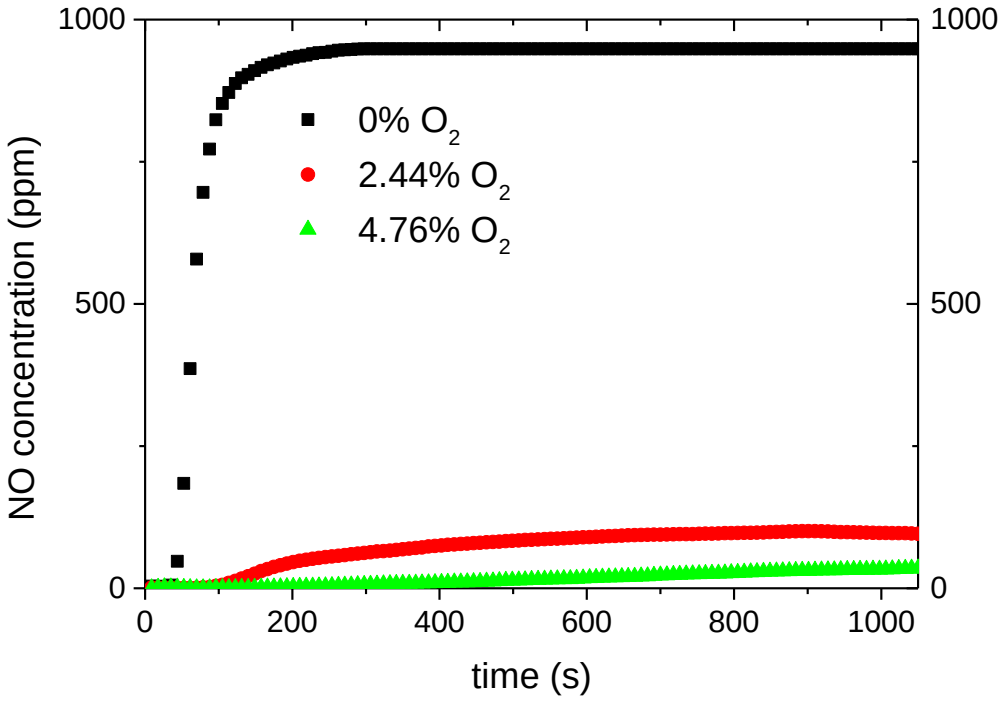

Figure 6-5 NO absorption curve with different oxygen concentration in gas mixture, (square) for 0% O_2, (circle) for 2,44% O_2 and (up triangle) for 4.76% O_2

As indicated in the data in Table 6-2, the total volume of NO at the input to the tube over the 17.5min adsorption process was 3.5mL and the volumes of NO output were 3.31mL, 0.35mL and 0.12mL respectively for 0%, 2.44% and 4.76% O_2 conditions. With the increase in O_2 concentration, more NO could be absorbed by activated carbon.

Table 6-2 The volume of NO absorbed in activated carbon after 17.5min absorption process

1000 ppm NO in N_2	**O_2 flow rate**	**O_2 concentration**	**Volume of NO into**	**NO Adsorbed**	**Peak C_{NO} at outlet of**

flow rate (mL/min)	(mL/min)	(%)	cylinder (mL)	in 17.5min (mL)	absorption tube (ppm)
200	0	0	3.5	0.19	950
200	5	2.44	3.5	3.15	100
200	10	4.76	3.5	3.38	35

In order to investigate why only 50 ppm NO was absorbed by activated carbon when there was no O_2 in the gas mixture, activated carbon's ability to absorb NO_2 was evaluated. As explained in Chapters 4 and 5, O_2 was able to oxidize NO to NO_2 and the dipole moment of NO_2 is 2.6 times higher than that of NO (Table 6-1), so it was important to analyse activated carbon NO_2 absorption ability under 0% O_2. The gas used was 1000 ppm NO_2 in N_2 and the flow rate was 200mL/min. The NOx concentration curves are shown in Figure 6-6.

It was found that although the initial gas was NO_2, the output of NO_2 was nearly 0 ppm, but the output of NO was gradually increasing and the trend in NO increase was similar to that in 4.76% O_2, 1000 ppm NO in N_2 condition. This indicates that in the earlier work the absorbed species was NO_2, rather than NO, because NO_2 can be absorbed at the condition of zero O_2 condition. Therefore, when the input gas was NO, the presence of O_2 was important in converting NO to NO_2 for effective NO absorption.

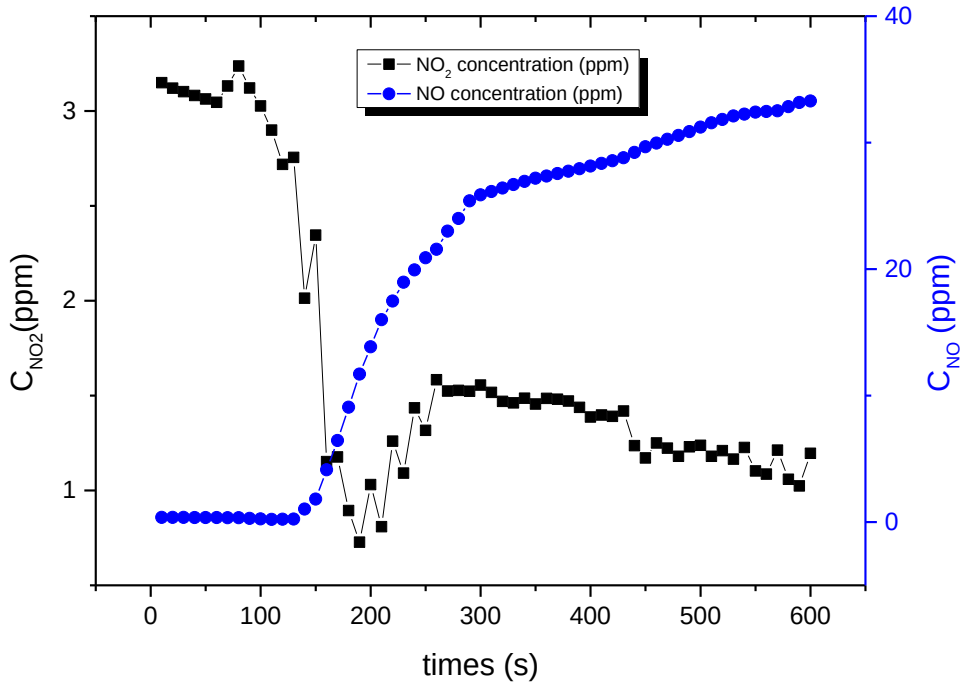

Figure 6-6 NO (circle) and NO_2 (square) concentration curves after going through activated carbon, when the gas was NO_2 (1000 ppm) in N_2 at 200mL/min flow rate.

In addition, Rubel et al. [44] explained the process of NO absorption by activated carbon in the presence of O_2 (Figure 6-7). There are two intermediate states before NO_2 is absorbed on the surface of activated carbon. First, the absorbed NO molecule and O_2 molecule interact to generate a positive NO ion and a negative O_2 ion on the surface of activated carbon. After that, another NO molecule interacts with the negative O_2 ion. The absorbed negative O_2 ion splits into two negative atomic O ions. Each of these reacts with one absorbed positive NO ion to leave two NO_2 attached on the activated carbon surface. The reason why NO is positive but O_2 is negative on the activated carbon surface probably relates to the electron affinity of gases. As shown in Table 6-3, NO has a lower electron affinity than O_2.

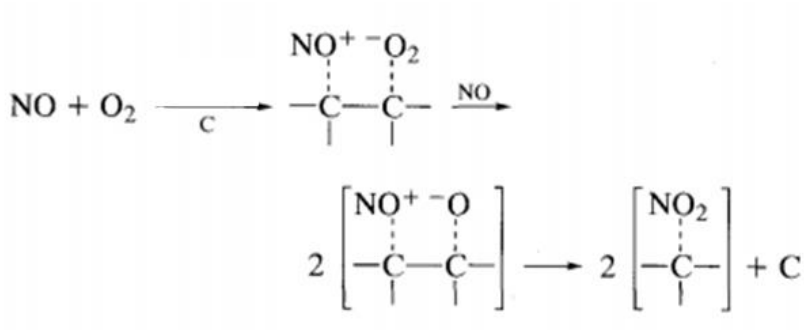

Figure 6-7 NO absorption on activated carbon with the assistance of O2 [44]

Table 6-3 Electron affinity ability of O_2 and NO [139]

Gas species	Electron affinity
NO	0.026 eV
O_2	0.451 eV

6.3.2 Effect of temperature

The effect of temperature on activated carbon NO absorption process was investigated under the condition of 4.76% O_2 1000 ppm NO in N_2 concentration at 210mL/min flow rate. Because activated carbon is a conductive material, two methods were used to increase the temperature. The first used an external water bath: activated carbon was put in a U-shaped Pyrex tube, so it could be immersed into the water bath and the temperature of activated carbon was controlled by the water temperature. The other method was to energise activated carbon by using a DC source (30V 2.5A) directly. The temperature was controlled by applying different DC currents and temperatures were measured by a thermometer. The total resistance of 5g activated carbon was approximately 12.25 Ohms.

For the water bath heating method, the concentration of NO at the output of the tube containing activated carbon for a range of temperatures is shown in Figure 6-8: note that higher values of NO indicate that less is being absorbed by the activated carbon. Higher

temperature of activated carbon made it more difficult to absorb NO, possibly because the vibration of surface oxygen functional group was stronger. As shown in Table 6-4, after 17.5min absorption the stabilised NO concentrations were 360 ppm, 470 ppm and 590 ppm for activated carbon temperatures of 60 °C, 70 °C and 80°C, respectively.

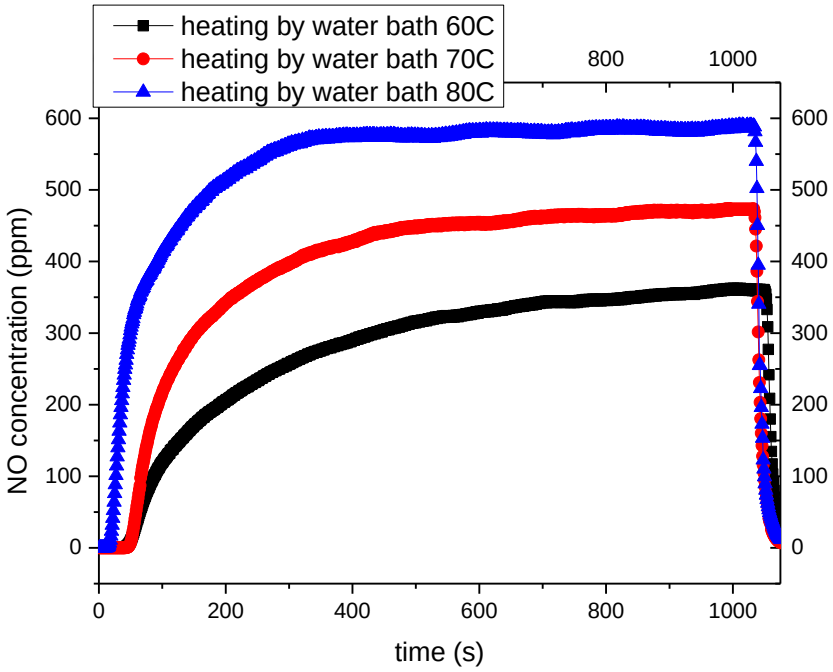

Figure 6-8 Activated carbon NO absorption ability, temperature was controlled by water bath, (square) for 60°C, (circle) for 70°C, (up triangle) for 80°C

Table 6-4 NO concentration under different activated carbon temperature, temperature controlled by water bath

Temperature of activated carbon (°C)	NO concentration (ppm)
60	360
70	470
80	590

For direct energising activated carbon by DC power supply, NO concentration curves at different temperatures are shown in Figure 6-9. The DC current is constant at 0.3A, 0.6A and 0.8A to heat the activated carbon to 60°C, 80°C and 100°C. Since the whole reactor is exposed to the surroundings, the heating loss is significant. Because the temperature control by the DC power supply was more sensitive than by the water bath heating method, the temperature division was increased to 20°C instead of 10°C. Comparing Figure 6-8 and Figure 6-9, it was found that the steady state was achieved more quickly by a direct DC power supply method. One possible reason was the heat was directly generated from activated carbon itself: in the water bath heating method, the heat was first transferred to the Pyrex tube and then absorbed by activated carbon, so it took a longer time to reach the expected temperature.

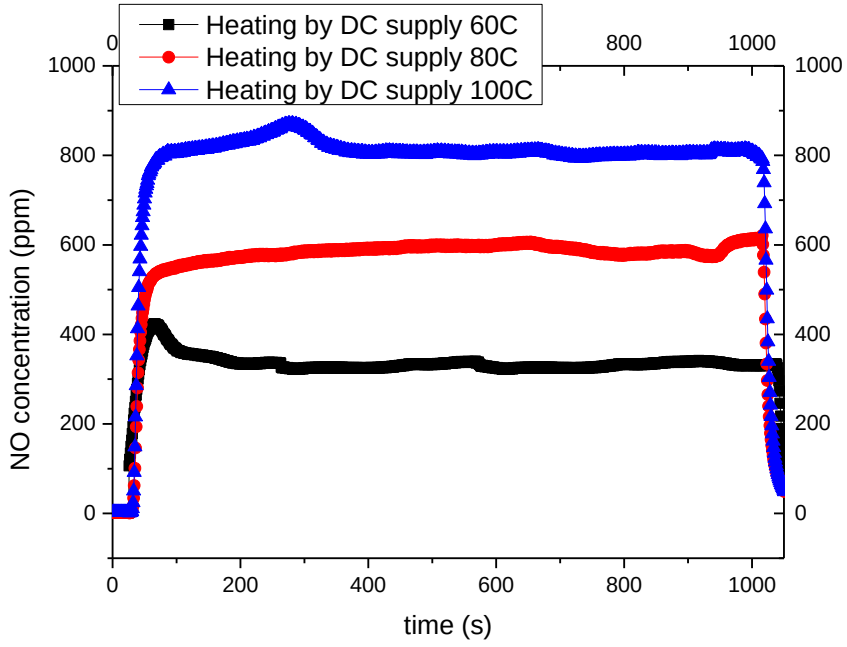

Figure 6-9 Activated carbon NO absorption ability, temperature was controlled by power injected to activated carbon itself, (square) for 60°C, (circle) for 80°C, (up triangle) for 100°C

As shown in Table 6-5, the stabilised NO concentrations were 340 ppm, 580 ppm and 800 ppm respectively for activated carbon temperatures of 60 °C, 80 °C and 100°C, respectively after 17.5min absorption process. Comparing the results for 60 °C and 80 °C from Table 6-4 and Table 6-5, the stabilised NO concentration are very close: for 60 °C the values were 360

ppm and 340 ppm and for 80 ^{o}C they increased to 590 ppm and 580 ppm, respectively. This means that there is no significant difference in activated carbon NO absorption ability by internal or external heating methods. The main difference is the response time needed to reach the stable absorption state. Direct heating by DC power supply is much faster than that by water bath. In addition, it was found that when the temperature increased from room temperature to 100^{o}C, the NO concentration after absorption tube was increased to 800 ppm from 35 ppm. If the temperature is further increased up to 230^{o}C [27], activated carbon can directly convert to NO desorption state. Therefore, in order to maximize the activated carbon NO absorption ability, the temperature of activated carbon is better to be 20^{o}C when the temperature is in the range of 20^{o}C to 100^{o}C for the NO absorption process.

Table 6-5 NO concentration under different activated carbon temperature, temperature controlled by DC source

Temperature of activated carbon (^{o}C)	NO concentration (ppm)
60	340
80	580
100	800

6.3.3 Effect of flow rate

The effect of flow rate on NO absorption process was investigated and the data is presented in Figure 6-10. The concentration of O_2 was 4.76% for all three flow rates. At the higher flow rate, the output NO concentration after the absorption process was higher. This means that less NO was absorbed by the activated carbon, because the residence time of NO in activated carbon was less.

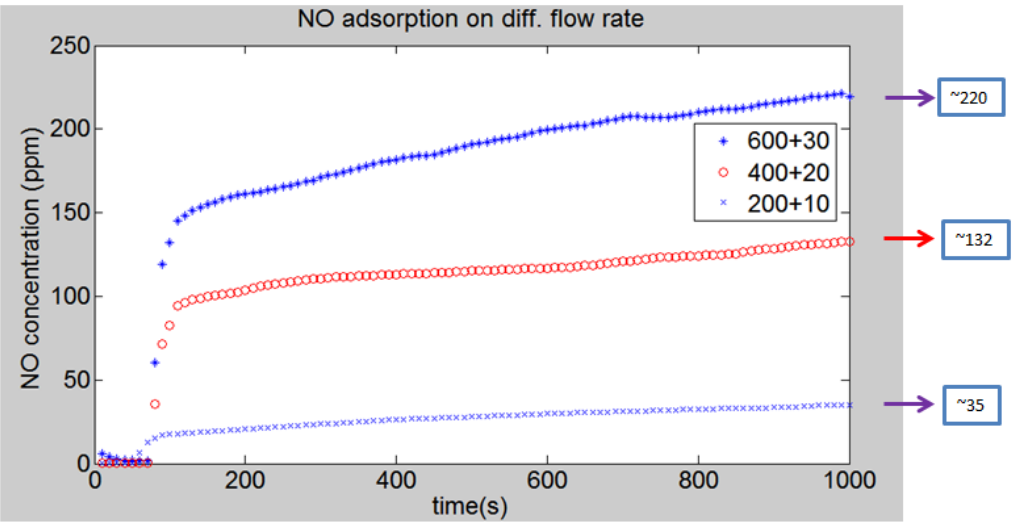

Figure 6-10 Flow rate effect on NO adsorption at condition of 4.76% O_2 and 1000 ppm NO and N_2 in balance, (plus) for 630mL/min flow rate, (circle) for 420mL/min flow rate, (cross) for 210mL/min flow rate

As shown in Table 6-6, NO concentrations after 17.5min absorption process were 35 ppm, 132 ppm and 220 ppm respectively for 210 mL/min, 420 mL/min and 630 mL/min flow rates.

Table 6-6 Flow rate effect on NO absorption ability

Total FR (mL/min)	FR of 1000 ppm NO in N_2 (mL/min)	FR of O_2 (mL/min)	C_{NO} after absorption (ppm)
210	200	10	35
420	400	20	132
630	600	30	220

6.3.4 Effect of water vapour concentration

NO absorption by activated carbon is dependent on the oxygen functional group, because they are able to absorb polar molecules. As shown in Table 6-1, H_2O is a polar molecule with a higher dipole moment than NOx. It is worth investigating the effect of H_2O on the NO absorption process, because H_2O exists with NOx in practical flue gases (Table 2-2). Here, as in earlier experiments, water vapour was added to gas by passing it through a gas washing bottle at 20°C (Figure 6-11). The effect of 2.31% H_2O vapour on NO absorption was investigated and the data are presented in Figure 6-12.

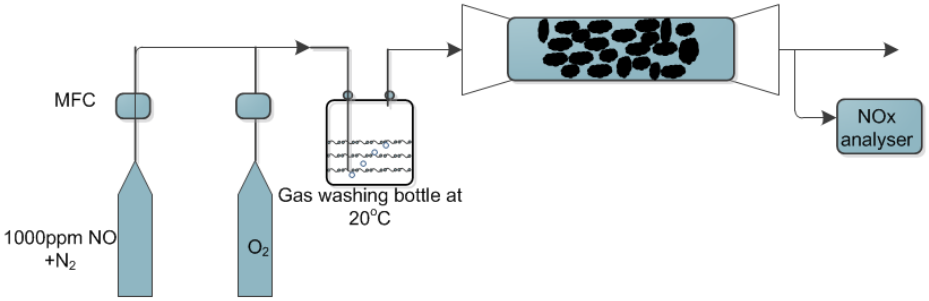

Figure 6-11 NO absorption process with the presence of 2.31% H_2O in the gas mixture

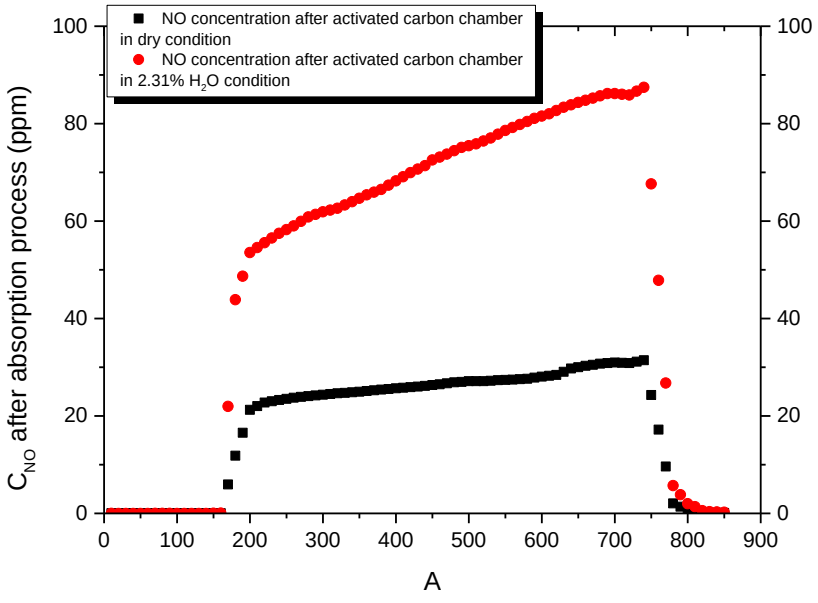

Figure 6-12 NO concentration after going through activated carbon chamber at 0% (square) and 2.31% (square) H_2O vapour condition with 4.76% O_2 and 1000 ppm NO in N_2

It was found that the negative effect of 2.31% H_2O vapour on NO absorption was significant. When 2.31% H_2O vapour was in the gas mixture, NO concentration was increased to 55 ppm quickly. After approximately ten minutes absorption process, NO concentration increased to 88 ppm at 2.31% H_2O vapour condition, compared to 31 ppm at 0% H_2O condition. The final NO concentration increased more than 2.8 times from 31 ppm to 88 ppm, so the selectively of activated carbon on H_2O vapour and NO was poor. For practical flue gases the H_2O vapour concentration was approximately 5% and, as indicated in the results above, the effectiveness of activated carbon for NO absorption would be further reduced. This indicates the difficulty in commercialising the technology of NO absorption by activated carbon.

6.4 Thermal NO desorption process

6.4.1 Characteristic of thermal NO desorption process

As shown in Figure 6-8 and Figure 6-9, no matter where the thermal energy came from (external water bath heating or internal direct DC power supply), the adsorption ability of activated carbon for NO was similar. Therefore, in order to heat activated carbon faster, the direct DC power supply was used (Figure 6-13). In the Pyrex tube there was high resistance at the contact points between captivated carbon pellets. Because O_2 can support combustion, when O_2 took part in the desorption process, the temperature at contact points was high enough to ignite activated carbon. Therefore, only N_2 was used for the desorption process, to avoid the possibility of activated carbon combustion.

The NO absorption process was the same at 4.76% O_2, 1000 ppm NO in N_2 condition. The total gas flow rate was 210 mL/min. After 17.5 minutes of absorption, the volume of absorbed NO was 3.5mL.

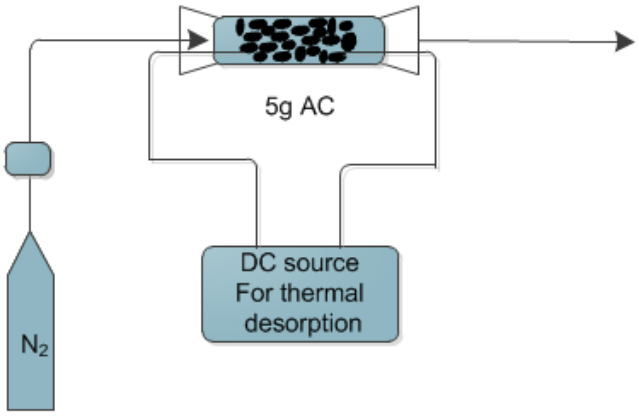

Figure 6-13 Thermal energy directly connected to activated carbon for desorption

For the desorption process, the carrier gas was N_2 at 50mL/min flow rate. In addition, the maximum measurable NOx concentration for Thermo Scientific High Level NOx Monitor 42iHL was 5000 ppm, so a dilution system was added before the desorbed high concentration NO went to the NOx analyser (Figure 6-14). The flow rate of the dilution system was 700 mL/min by N_2. As shown in Table 6-7, it was found that the volume of

desorbed NOx was 3.28mL which was slightly less than the absorbed 3.38 mL. The difference between absorbed NOx and desorbed NOx may have been caused by the activated carbon, which could reduce NO to N_2 by (6-1).

$$C + 2NO \rightarrow N_2 + CO_2 \quad \textbf{(6-1)}$$

Table 6-7 Information about the NO absorption and desorption processes

Input gas mixture	O_2(4.76%vol), NO (1000ppm) in N_2
Flow rate of NO(1000ppm) in N_2	200 mL/min
Flow rate of O_2	10mL/min
Total V_{NO} injected and time	3.5mL in 17.5mins
Desorption gas and flow rate	N_2, 50mL/min
Dilution system gas and flow rate	N_2, 700 mL/min
Total desorbed NO	3.11mL
Total desorbed NO_2	0.17mL
Total desorbed NOx	3.28 mL
Heating system power and time	75 W, 4 mins (2.5A, 30V)

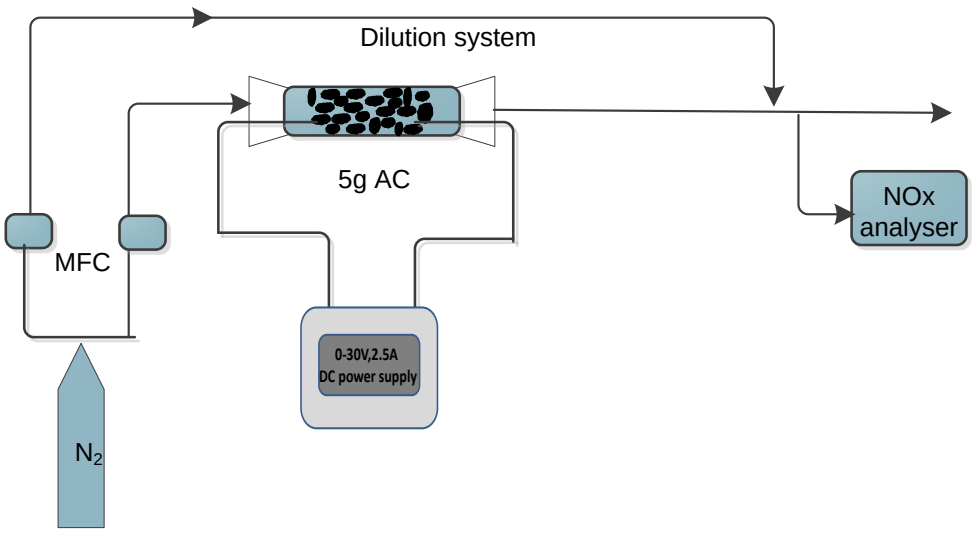

Figure 6-14 Schematic diagram of thermal desorption process with dilution system

A NO concentration curve during the thermal desorption process is shown in Figure 6-15. It was found that the highest NO concentration reached 60000 ppm, equal to 6%. The dilution system ensured that the NO concentration which went through the NOx analyser was lower than 5000 ppm. The time duration for complete NO desorption was approximately 240s.

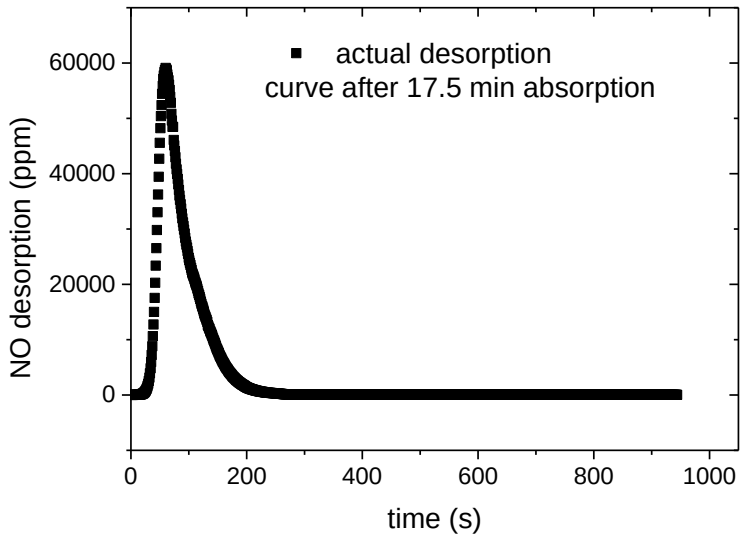

Figure 6-15 NO desorption curve using 50 mL/min N_2 (the effect of dilution has been considered.)

As mentioned earlier, the advantage of the absorption process was to convert low concentration NO in high flow rate to high concentration NO in low flow rate. A comparison between input NO concentration and thermal desorption NO concentration is shown in Figure 6-16. In order to have a clear comparison between input NO concentration and thermal desorption NO concentration, the thermal desorption NO concentration curve was divided by ten. The duration of absorption was 17.5min and the input NO concentration was 1000 ppm, but the output NO concentration was able to reach 60,000 ppm, which is sixty times higher than the input NO concentration. The NO existing time was reduced from 17.5 min to 4 min (240s).

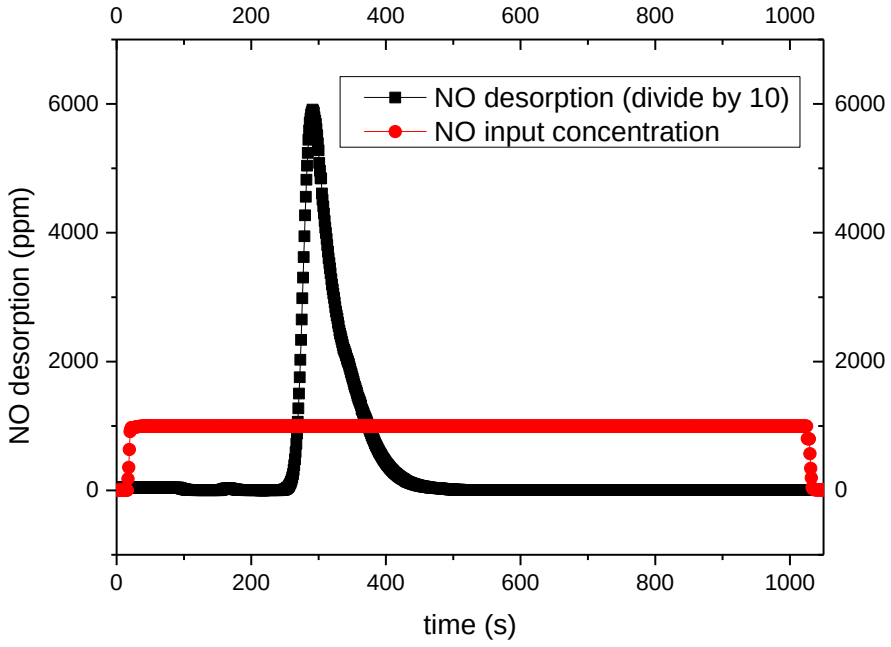

Figure 6-16 The input NO concentration curve (circle) and the output (divided by 10) NO concentration curves during thermal desorption process (square)

6.4.2 Effect of N_2 flow rate

When the flow rate of nitrogen was increased from 50mL/min to 100mL/min, as expected, the peak concentration of desorbed NO was reduced to almost half, from 60,000 ppm to 28,000 ppm (Figure 6-17). In addition, the total existing time of NO at two flow rate conditions was nearly about 240s, because NO desorption was determined by the temperature of activated carbon. When the temperature reached the required temperature for full desorption, all absorbed NO would be released. As shown in Table 6-8, the total desorbed NOx volumes in different desorption flow rates were nearly the same. They were 3.28mL and 3.26mL respectively for 50mL/min and 100mL/min desorption flow rates.

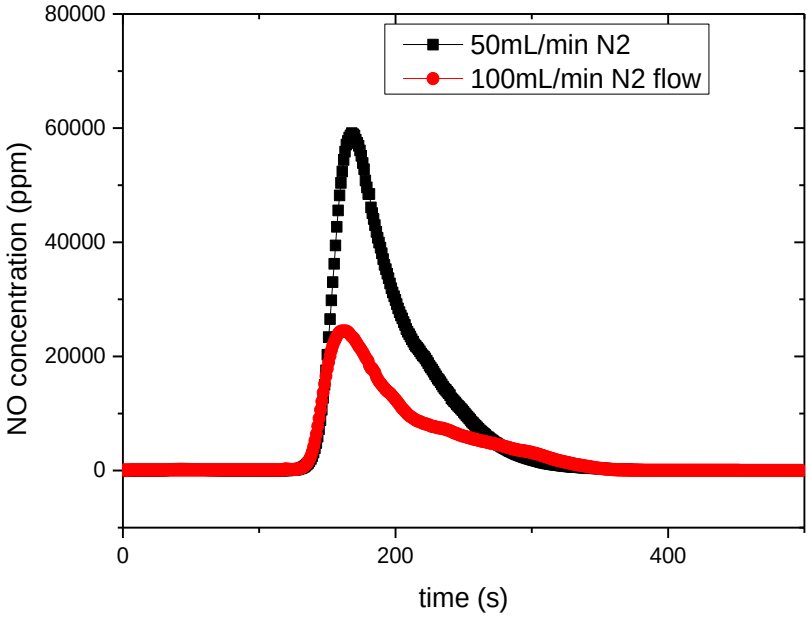

Figure 6-17 NO desorption curve by different nitrogen flow rate (square) 50mL/min, (circle) 100 mL/min

Table 6-8 The volume of NO, NO_2 and NOx by different desorption flow rate

Adsorption NO	Desorption flow rate	Volume of NO	Volume of NO_2	Total volume of NOx
3.5mL NO	50 mL/min	3.11 mL	0.17 mL	3.28 mL
3.5 mL NO	100 mL/min	3.08 mL	0.18 mL	3.26 mL

6.4.3 Effect of DC current amplitude

In terms of thermal energy for desorption, the DC power supply was directly connected to the activated carbon and, according to the thermal NO desorption curve, the total NO desorption time was about 240s. If it is assumed that this time was the connection time for the DC power supply, then the energy can be calculated. As the DC current was 2.5A and the resistance of activated carbon was approximately 12.25 Ohms, then after 240s heating process, the total energy used to desorb 3.28mL NOx was about 18375J. Therefore, the desorption energy efficiency calculated by (6-2) was 0.86 g/kWh for full NOx desorption process.

$$\eta_D = \frac{V_{NO_x} * 30 * 3.6 * 10^6}{22.4 * 1000 * E} = 4821 * \frac{V_{NO_x}}{E} \quad \textbf{(6-2)}$$

where:
η_D is the thermal desorption energy efficiency in g/kWh;
E is the heat energy in J;
$V_{NO_x}$is the volume of desorbed NOx in mL.

As a result of the low thermal desorption energy efficiency needed to fully desorb all absorbed NO in activated carbon, partial desorption was investigated to increase desorption energy efficiency. One possible advantage for partial desorption in this experiment was less heating time. The thermal desorption system was exposed in open air, so the heating losses were higher for longer process times. From Table 6-9, when the heating time was reduced to 13s from 240s, the heating energy was 995J, and there was 0.752mL NO desorbed from activated carbon which was 21.49% of the input NO volume. Desorption energy efficiency increased to 3.644 g/kWh from 0.86 g/kWh for the full desorption process.

Table 6-9 NO desorption by controlling the heating energy to ~1000 J (Absorption time was still 17.5 minutes and the volume of input NO was 3.5mL)

DC current (A)	Heating time (s)	Energy injection (J)	Desorbed NO (mL)	Desorption rate (%)	Thermal NO desorption energy efficiency (g/kWh)
2.5	13	995	0.752	21.49	3.644

In order to investigate the effect of heating time on thermal desorption energy efficiency, four DC currents were used. The total heat energy injected was nearly the same at ~1000J.

As shown in Table 6-10, for applied DC currents of 1A, 1.5A, 2A and 2.5A the volumes of desorbed NO were 0.6mL, 0.67mL, 0.72mL and 0.752mL, respectively. The volume of NO desorbed was calculated by integrating the concentration of NO in time and multiplying by the flow rate. The heating time varied significantly, from 13s to 80s, for consistent 1000J energy injection. It was found that with longer heating time, the desorbed NO volume reduced from 0.752mL to 0.6mL, and corresponding thermal desorption energy efficiency reduced. Therefore, the increased heating time required because of reduced current had a negative effect on the thermal desorption energy efficiency in open air conditions.

Table 6-10 NO desorption when heating energy injection was approximately 1000 J, (Absorption time was still 17.5 minutes and the volume of input NO was 3.5mL)

DC current (A)	Heating time (s)	Energy injection (J)	Desorbed NO (mL)	Desorption rate (%)	Thermal NO desorption energy effy (g/kWh)
1	80	980	0.60	17.14	2.952
1.5	36	992	0.671	19.17	3.261
2	20	980	0.72	20.57	3.542
2.5	13	995	0.752	21.49	3.644

NO desorption curves by different values of current are shown in

Figure **6-18**. For 1A condition, the rate of NO desorption was relatively slower than the other three conditions. The peak value of NO concentration was half of that in the other three DC current conditions, but it had longer time for desorption. For 1.5A, 2A and 2.5A, the difference was not significant, but higher current provided a higher peak value over a short period.

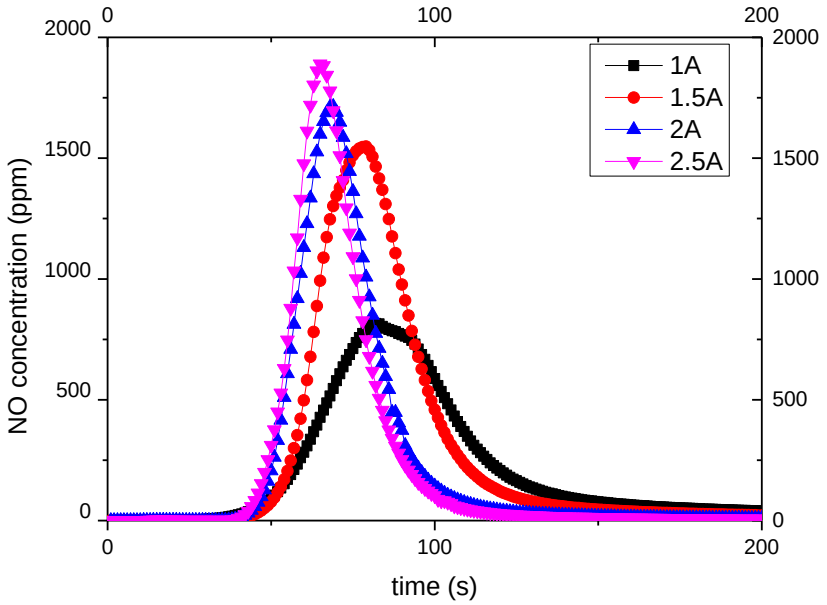

Figure 6-18 Desorption curves at different heating currents, 1A (square), 1.5A (circle), 2A (up triangle) and 2.5 A (down triangle) for approximately 1000J heat energy injection

6.5 Desorbed NO treatment by DBD

The desorbed gas with high concentration of NO was treated by meshed dielectric barrier discharge. The configuration of the meshed DBD reactor is shown in Figure 6-19. Because of the mesh structure, gases were able to directly pass through the discharge area. There were three layers of 0.1mm thickness PVC as dielectric, and two layers of # 28 Stainless steel 304 material meshes, whose parameters were a 0.56mm aperture and 0.35mm wire diameter, between two brass electrodes. The actual meshed DBD reactor is shown in Figure 6-20.

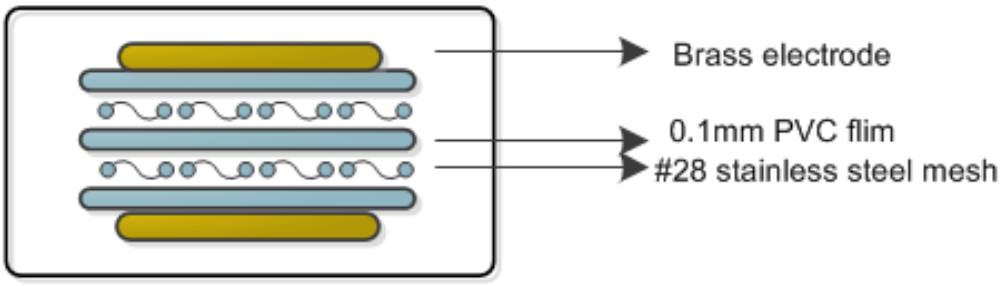

Figure 6-19 Schematic diagram of meshed dielectric barrier discharge reactor configuration

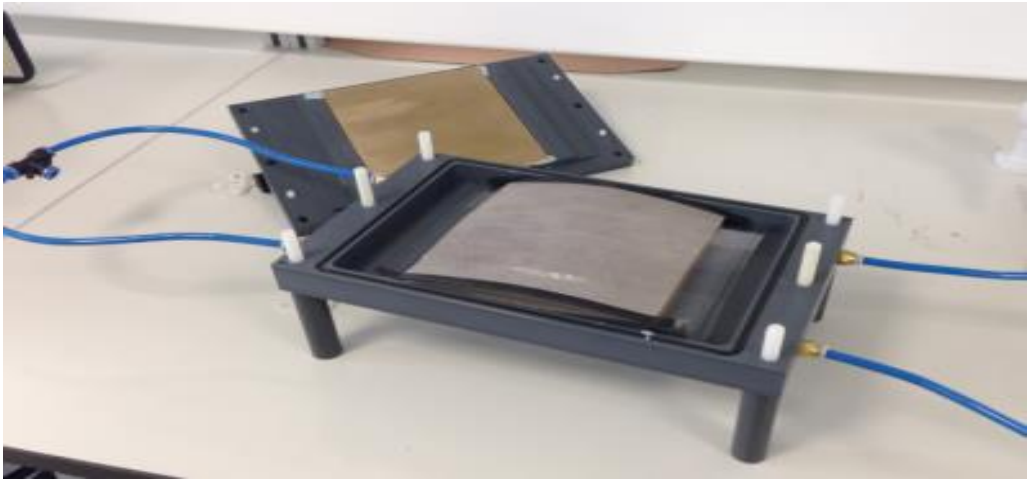

Figure 6-20 Image of meshed dielectric barrier discharge reactor

6.5.1 DBD treatment in nitrogen

As shown in Figure 6-21, during the DBD treatment process, O_2 was not used, so there was no O_3 formation. Because the concentration of NO was increased to 6%, the possibility of NO dissociation by energetic electron and NO reduction by N by (6-3) was increased significantly compared to 1000 ppm NO condition. A 0.5L chamber was placed at the end of the DBD reactor chamber, in order to provide more time for the reaction between reactive species and NO.

$$N + NO \rightarrow N_2 + O \qquad \textbf{(6-3)}$$

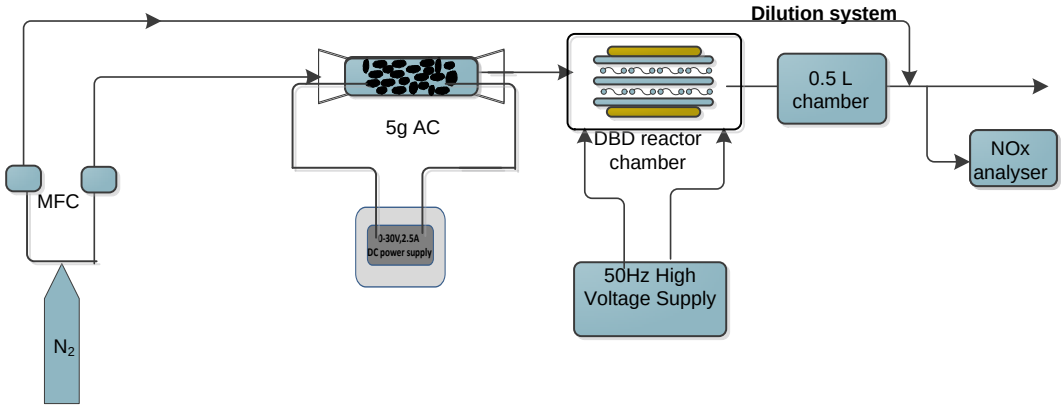

Figure 6-21 Schematic diagram of desorbed high concentration NO treatment by DBD in N_2

Desorption curves for three different N_2 flow rates (50mL/min, 100mL/min and 200mL/min) are shown in

Figure **6-22**. At 50 mL/min N_2 condition, the residence time of gases in the DBD reactor was four times longer than at 200mL/min. The maximum NO concentration was 1670 ppm at 50mL/min of N_2, but was 1306 ppm when the N_2 flow rate was 200mL/min. Therefore, a longer residence time significantly promotes the NO removal process.

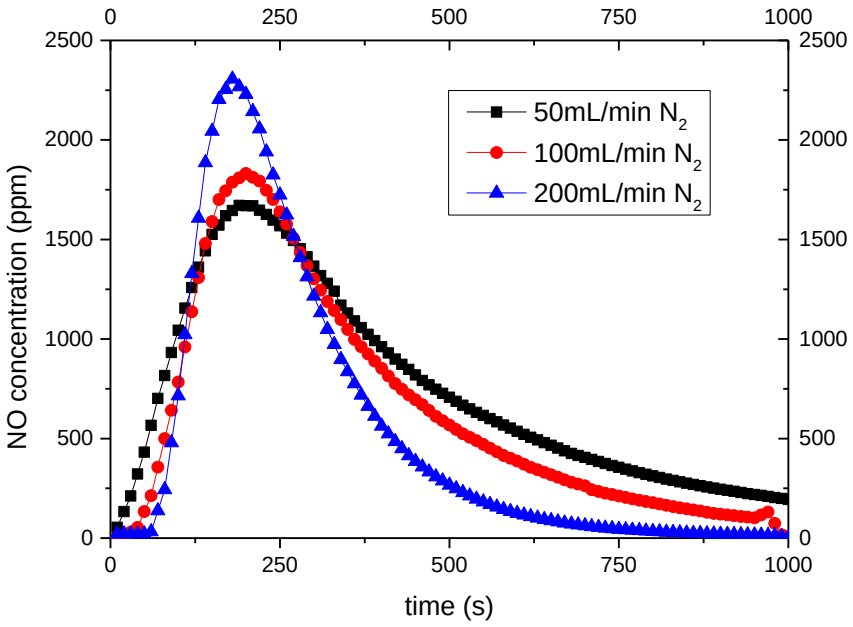

Figure 6-22 NO concentration curves for different N_2 flow rates of 50 mL/min (square), 100mL/min (circle) and 200mL/min (up triangle).

As highlighted in Table 6-8, the initial amount of desorbed NO and NO_2 after thermal desorption process were 3.11 mL and 0.17 mL respectively. Volumes of NO and energy efficiencies under different N_2 flow rates are shown in Table 6-11. The discharge power was constant at about 1.044 W: the DBD treatment time was set to 240s because, as shown in Figure 6-15, the NO existed for 240s in the gas stream. It was found that the highest NO removal energy efficiency (excluding the energy consumption in the thermal desorption process) was 56.82 g/kWh at 50 mL/min N_2 condition. With an increase of N_2 flow rate, the NO removal energy efficiency reduced to 32.51 g/kWh at 200 mL/min N_2 condition.

Table 6-11 N_2 flow rate effect on NO removal by meshed DBD treatment

Flow rate of N_2 (mL/min)	**V_{NO} after DBD treatment (mL)**	**NO removal Energy efficiency excluding heating energy (g/kWh)**	**V_{NO2} after DBD treatment (mL)**
50	0.5474	56.82	0.178
100	1.1063	46.06	0.2061
200	1.8105	32.51	0.2241

In order to investigate the effect of the initial NO concentration on NO removal energy efficiency, gas with 1000 ppm NO in N_2 at 200mL/min condition was investigated under the same discharge power. As shown in Figure 6-23 and Table 6-12, NO concentration was reduced from 1000 ppm to 445 ppm after 1.044W DBD treatment and the corresponding energy efficiency was 8.53 g/kWh. However, as shown in Table 6-11, under the same flow rate of 200mL/min the NO removal energy efficiency achieved was 32.51 g/kWh, which was 3.8 times higher than 8.53 g/kWh. Therefore, if the initial NO concentration was higher, NO could be treated more efficiently by DBD under the mixture of NO and N_2

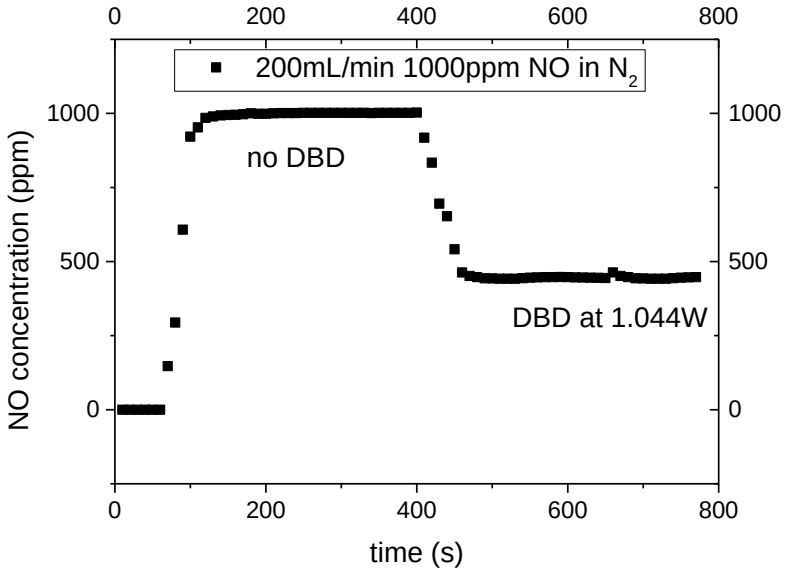

Figure 6-23 NO concentration before and after DBD treatment at 1.044W for 1000 ppm NO in N_2 gas condition

Table 6-12 NO removal and energy efficiency by direct DBD treatment at 1000 ppm NO in N_2 condition

Flow rate of 1000 ppm NO in N_2 (mL/min)	**C_{NO} before DBD treatment (ppm)**	**C_{NO} after DBD treatment (ppm)**	**NO removal energy efficiency (g/kWh)**
200	1000	445	8.53

6.5.2 DBD treatment in a mixture of nitrogen and oxygen

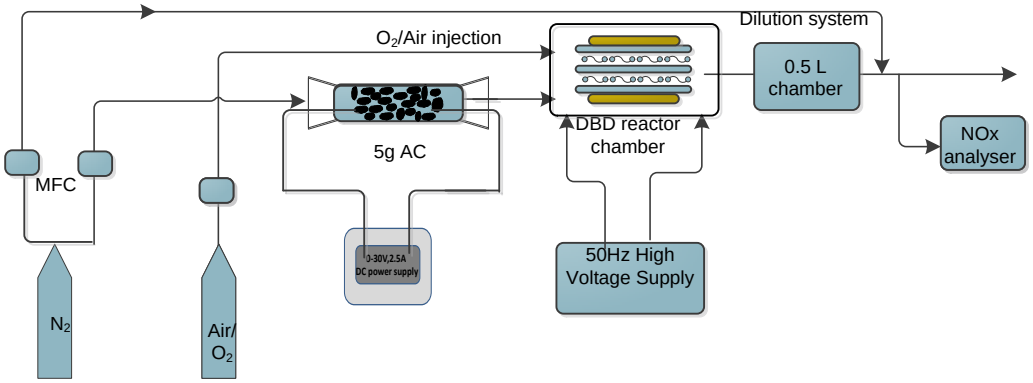

Figure 6-24 Schematic diagram of desorbed high concentration NO treatment by DBD in a mixture of N_2 and O_2

For the NO desorption process, only N_2 can be used, because O_2 can cause the activated carbon to burn. However, for the DBD treatment process, although NO removal under pure N_2 has been investigated, it was thought that adding O_2 to the DBD gas would be advantageous. In this section, NO removal under the mixture of N_2 and O_2 has been analysed: O_2 was added through another gas connection into the DBD reactor, as shown in Figure 6-24. As discussed in Chapter 4, when O_2 was added to the gas the formation of N was reduced significantly, the main reactive species for desorbed NO was taken to be atomic O and O_3. The concentration of O_2 in the gas mixture was controlled by the source of additional gas: the total gas flow rate in the DBD was 100 mL/min. For the NO desorption, N_2 flow rate was 50mL/min, therefore, when 50mL/min air was used, the concentration of O_2 in the DBD gas was 10.5%. When 50mL/min O_2 was used, the concentration of O_2 in the DBD gas increased to 50%. The results of NO and NO_2 concentration curves by DBD treatment with 1.044W discharge power at 10.5% and 50% O_2 concentration conditions are shown in Figure 6-25. It was found that although the initial volume of adsorbed NO was 3.5mL, NO and NO_2 concentration were higher and the NO and NO_2 existing times were longer at 10.5% O_2 concentration condition. As shown in Table 6-13, the volumes of NO were reduced to 0.62 mL and 0.205 mL but the volumes of NO_2 were increased to 1.7 mL and 0.748 mL after the DBD treatment at 10.5% and 50% O_2 concentration conditions. For the same flow rate of 100 mL/min, the volume of NO was 1.1063 mL in the DBD treatment at pure N_2 condition, as shown in Table 6-11. Under the system employed here NO volume reduced to 0.62 mL and 0.205 mL at 10.5% and 50% O_2 in N_2 conditions. Similarly the volume of NO_2 increased

from 0.2061mL to 1.7mL and 0.748mL. Therefore, when there was O_2 in the gas mixture, NO oxidation was more important than NO reduction by N. One possible reason why the volume of NO_2 at 50% O_2 was lower than that at 10.5% O_2 could relate to the conversion of NO_2 to N_2O_3 or N_2O_4 at high concentrations.

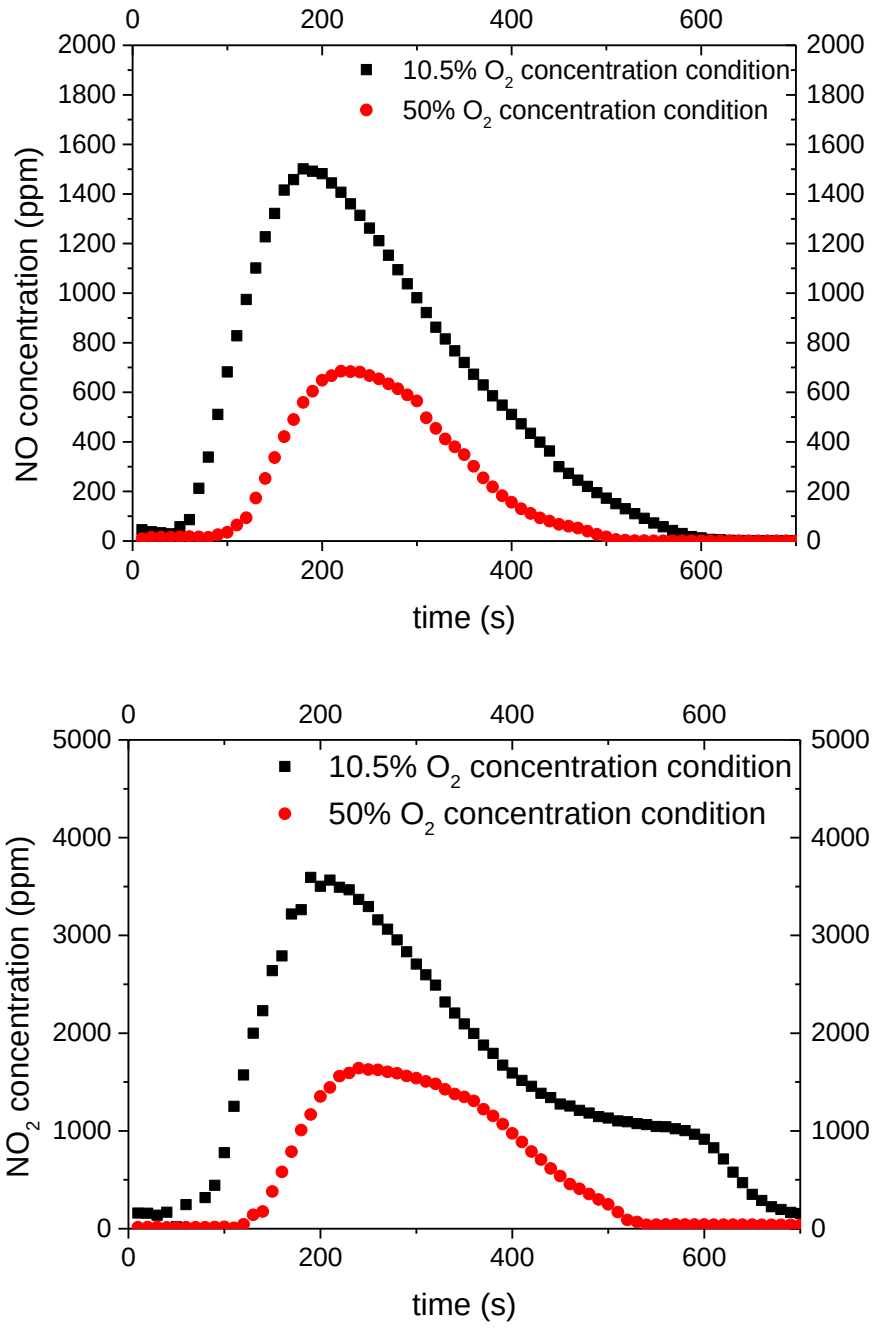

Figure 6-25 NO (square) and NO_2 (circle) concentration curves by DBD treatment with 1.044W discharge power at 10.5% and 50% O_2 concentration conditions

Table 6-13 The volumes of NO and NO_2 after DBD treatment with 1.044W discharge power at 10.5% and 50% O_2 concentration conditions

O_2 concentration (%)	**Volume of NO after DBD treatment (mL)**	**Volume of NO_2 after DBD treatment (mL)**	**Volume of NOx (mL)**
10.5	0.62	1.7	2.32
50	0.205	0.748	0.953

In order to quantitatively analyse the effects of atomic O and O_3 on NO removal, a reference gas was used where there was no NO in the gas mixture. The corresponding O_3 formations are shown in Table 6-14. Concentrations of O_3 at 10.5% and 50% O_2 condition were 1150 ppm and 4920 ppm, respectively. Because there was no cooling system for this DBD reactor, O_3 concentration at the beginning was higher than at the final stable condition (Figure 6-26). In addition, it was found that for 50% O_2, the concentration of O_3 generated at 1.044W discharge power was ten times less than the maximum NO concentration from the desorption process. For 10.5% O_2 concentration condition, the difference was multiplied by 52.

Table 6-14 O_3 formation by DBD at reference gas condition under 1.044W discharge power

O_2 concentration (%)	**Flow rate of O_2 (mL/min)**	**Flow rate of air (mL/min)**	**Flow rate of N_2 (mL/min)**	**O_3 concentration (ppm)**
50	**50**	0	50	4920
10.5	**0**	50	50	1150

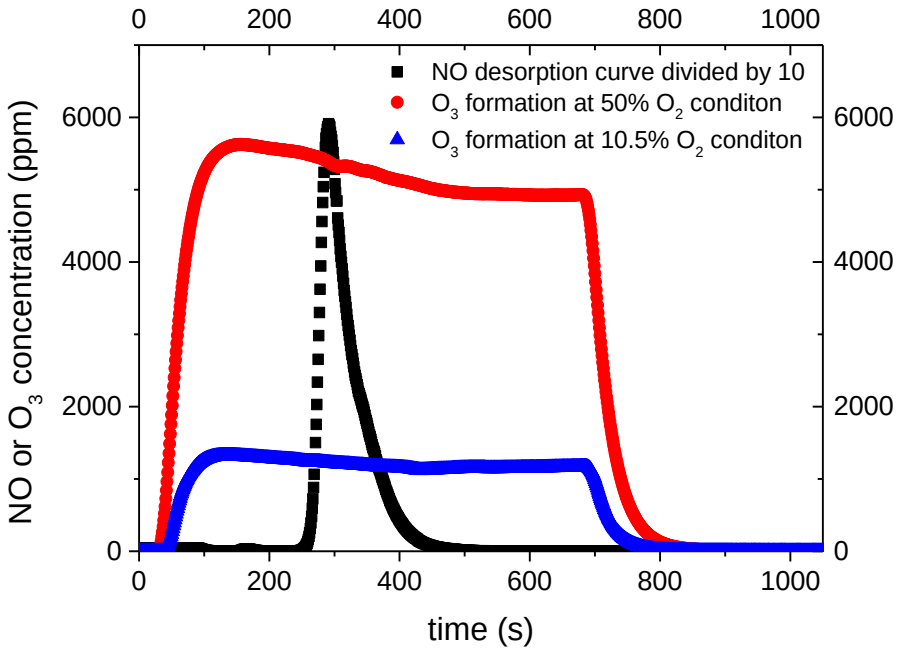

Figure 6-26 NO desorption curve (square) and O_3 formation curves at 10.5% (circle) and 50% (up triangle) O_2 concentration conditions. In order to make them comparable, NO desorption curve reduced by a factor of ten

Because of the concentration of O_3 in the reference gas, the contribution of O_3 for NO removal was supposed to be less than 10%. It is possible to have another oxidant to oxidize NO at high concentration NO condition. As explained in Chapter 4 and 5, O_2 has the potential to oxidize NO, so it is worthwhile reducing the discharge power in order to reduce the formation of reactive species including O and O_3. The maximum voltage of the 50Hz AC power supply used to energize the DBD was 7kV. For applied voltages of 7kV, 6kV, 5kV and 0kV, the corresponding discharge power was 1.044W, 0.75 W, 0.5 W and 0 W. It was found that the volume of NO and NO_2 were almost constant, independent of discharge power. The results are shown in Figure 6-27 and Table 6-15. For the data points with error bars, the data is the average of 3 results and the error bar is the standard deviation of these results.

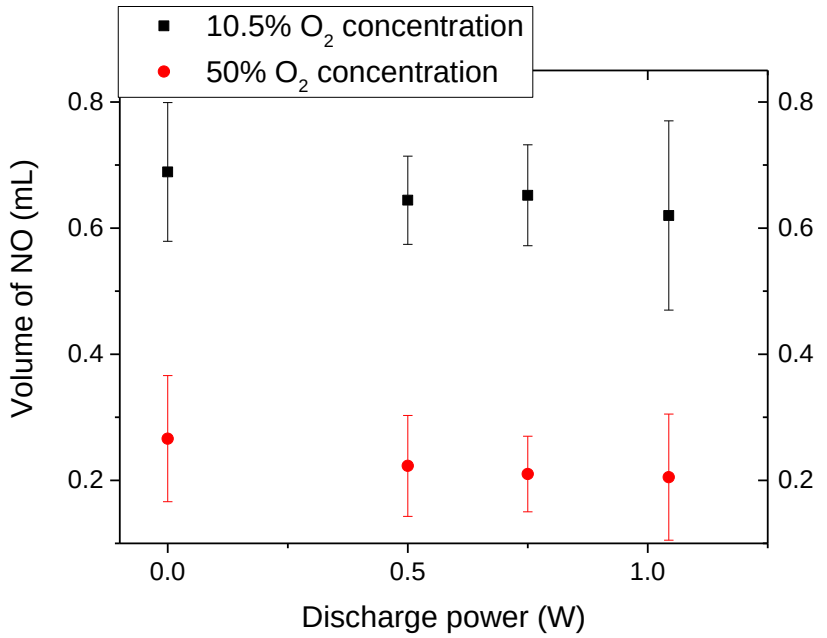

(a)

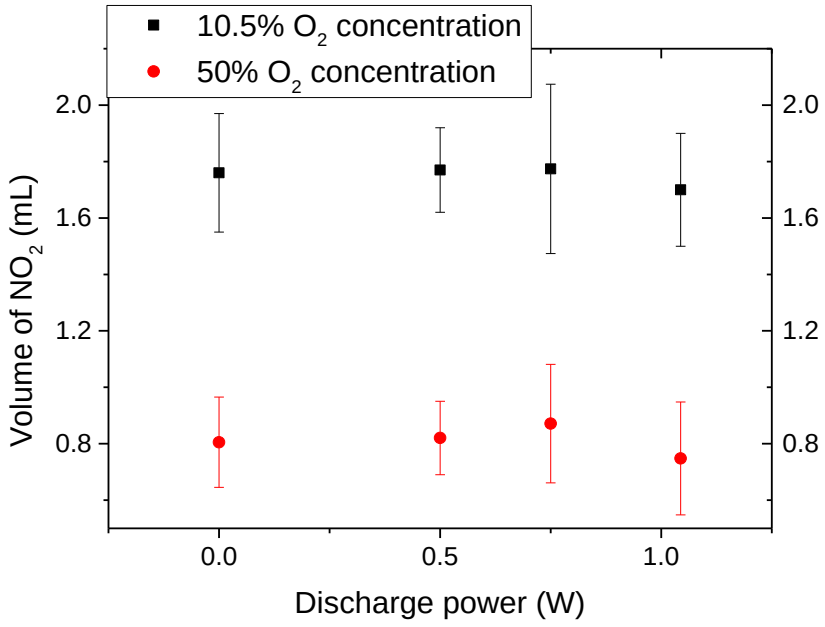

(b)

Figure 6-27 The volume of (a) NO and (b) NO_2 after DBD treatment in 10.5% and 50% O_2 under different discharge power

Table 6-15 The volume of NO and NO_2 under different discharge power at 10.5% and 50% O_2 concentration conditions

O_2 concentration (%)	Discharge power (W)	V_{NO} (mL)	V_{NO2} (mL)
10.5	0	0.69	1.76
	0.5	0.64	1.77
	0.75	0.65	1.77
	1.044	0.62	1.7
50	0	0.27	0.81
	0.5	0.22	0.82
	0.75	0.21	0.87
	1.044	0.21	0.75

As highlighted in Table 6-8, the volume of NO and NO_2 after thermal desorption were 3.11 mL and 0.17 mL, so approximately 95% of NOx was NO. The reaction between NO and O_2 was not significant when NO concentration was in ppm range, but for a high NO concentration (up to 6%), this reaction plays an important role in NO oxidation: the reaction is shown in (6-4). If the NOx concentration increases from 1000 ppm to 6%, an increase of sixty times, the increase of reaction rate is 3600 times (60x60) because it is a second order the concentration of NO. This was the main reason why, without DBD treatment, NO could be oxidized effectively. However it was found that the reduction in NO was much less than the formation of NO_2, which meant that part of NO_2 was converted to other species.

$$NO + NO + O_2 \rightarrow NO_2 + NO_2 [117] \quad \textbf{(6-4)}$$

In addition, for high concentrations of NO and NO_2, reactions (6-5) and (6-6) could happen [62, 110]. The formation of N_2O_3 and N_2O_4 could lead to the reduction in total measured NOx, because they cannot be measured by the NOx analyser. Therefore, although O_2 could be used as the major oxidant for NO oxidation at a high NO concentration, it was difficult to fully oxidize NO by O_2. When NO concentration was reduced to hundreds of ppm, strong oxidants such as O_3 and OH were still needed to completely remove all the NO.

$$NO + NO_2 \rightarrow N_2O_3 \quad \textbf{(6-5)}$$

$$NO_2 + NO_2 \rightarrow N_2O_4 \quad \textbf{(6-6)}$$

6.6 Conclusions

First, an absorption-desorption process using activated carbon has been used to convert low concentrations of NO in a high flow rate to a high concentration in a low flow rate. NO could then be treated more efficiently by non-thermal plasma. During the absorption process, slower flow rates and lower temperatures would promote the NO absorption process and higher amounts of NO would be absorbed by activated carbon. H_2O vapour had a negative effect on the NO absorption process: because of H_2O's larger dipole moment, activated carbon's NO absorption ability was reduced by half. The O_2 molecule plays an important role in NO absorption. Without the existence of O_2 in the gas mixture, only 5% of NO can be absorbed by activated carbon. For 4.76% O_2 condition, more than 95% of NO can be absorbed, but the absorbed species is NO_2 rather than NO.

Secondly, the thermal desorption process allowed the concentration of desorbed NO to be increased to 6% when the flow rate of N_2 was 50 mL/min. The concentration of NO increased 60 times from 1000 ppm to 6%. Because of high energy consumption for full NO desorption, partial desorption was investigated and it was found that under the same heating energy injection, larger DC current with shorter operating time could provide a higher NO desorption and thermal desorption energy efficiency: this may have resulted from lower heat losses to the surroundings.

Thirdly, for the DBD treatment of desorbed NO, when desorbed NO was treated by N_2 alone, higher concentration NO increased NO removal energy efficiency significantly. When O_2 was added to the gas mixture, it was found that high concentration NO could be oxidized by O_2 effectively and the oxidation rate increased with increasing O_2 concentration. When the O_2 concentration was 50%, about 91% of NO can be oxidized by O_2. The contribution of reactive species atomic O and O_3 in DBD treatment was negligible for NO oxidation.

NO absorption and desorption processes do open a new research direction to solve the problem of NO removal. Apart from the energy injection for thermal desorption, it is a very promising development to economically remove NO, because O_2 can effectively oxidize high concentration NO and the cost of O_2 is much cheaper than that of O and O_3. In addition, because of high concentration NO_2 or N_2O_4 generated, it is possible to further improve the treatment procedure by combining with nitric acid production processes, which can offset the cost of this NO removal technology. However, in terms of NO absorption technology for industrial applications, there are still many challenges to be overcome. For practical flue

gases, water vapour always exists, so it is important to improve activated carbon selectivity on NO rather than water vapour. In addition, the energy required for thermal desorption process is too high to be used in industry and a less expensive desorption technology is needed to make it affordable.

Chapter 7 CONCLUSIONS AND FUTURE WORK

7.1 Conclusions

Nitric Oxide (NO) is a gas pollutant which is harmful to both people and the environment, it is important to keep exploring new technologies to remove NO, e.g. to improve efficiency. This research is mainly focused on the use of non-thermal plasma technology for NO removal. It investigated the chemical reaction pathways and mechanisms of NO removal by different non-thermal plasma technologies, including Dielectric Barrier Discharge (DBD) and corona discharge. Chemical kinetics of NO removal by different reactive species including O, O_3, O_2 and OH were analysed theoretically and experimentally.

Under cylindrical DBD, most NO was oxidized rather than reduced, so reactive species O, O_3 and OH are more important than reactive species N for NO removal. However, the question of which reactive species is dominant is dependent on the reaction rate, which is controlled by two parameters, i.e. the reactant concentration and the reaction rate constant. The reaction rate constant between NOx and atomic O is approximately three orders higher than that between O_2 and atomic O to generate O_3, so for different NO and O_2 concentration, the dominant reactive species changed. When the O_2 concentration was in the range of 4.76 to 16.67% and the NO concentration was higher than 420 ppm, most of the atomic O generated from non-thermal plasma reacted with NOx, rather than O_2, so the dominant reactive species for NO removal was O. However, that brings a side reaction between NO_2 and atomic O to generate NO. It was proved that the formation of NO_2 was constant with the increase in O_2 concentration (Chapter 4). However, for NO concentrations of less than 100 ppm, O_3 became the dominant reactive species for NO oxidation, because NO oxidation increased with the increase in O_2 concentration. The equivalent O_3 formation in the gas mixture containing NO is close to the O_3 formation in a reference gas that contained no NO, i.e. O firstly reacts with O_2 to generate O_3, when NO concentration is lower than 100ppm. When NO concentration is in the range of 120 ppm to 190 ppm, there is a synergistic effect of O and O_3. However, when 2.31% H_2O vapour was added to the gas mixture, the dominant reactive species became OH, which reacted with NO without any side reaction but limited the formation of O and O_3 by catalytically converting them to O_2. It was found that NO removal was reduced with increasing O_2 content when 2.31% H_2O vapour was in the gas mixture. One possible reason for that is the occurrence of chemical reaction between OH and O, which reduces the number of OH species which can react with NO. Further investigation

found that an increase in temperature could promote the effect of OH for NO removal, due to a reduction of reaction rate constant between OH and O.

There is always water vapour in the raw flue gas from the combustion of fossil fuel, so the effect of H_2O vapour on chemical reactions is inevitable. Therefore, the dominant reactive species for NO removal in practical flue gas should be OH if direct DBD treatment is used in practice. Based on the trend of the temperature effect in wet condition, a higher temperature may provide a better NO removal performance, but further experiments are needed to prove the validity. If H_2O vapour can be extracted from the practical flue gas, the NO removal technology can be chosen based on the initial NO concentration. When NO concentration is lower than 100 ppm, direct DBD treatment is suitable and cheap. When NO concentration is higher than 420 ppm, LoTOx technology is needed to fully remove NO, because the existence of the side reaction between O and NO_2 will limit the oxidation of NO. Although the dominant reactive species are quantitatively identified under different condition in this research, the energy efficiency is still lower than 30g/kWh. It is necessary to explore a synergistic solution associated with non-thermal plasma technology to improve the NO removal energy efficiency.

In addition to the findings of the transition of the dominant reactive species under different gas conditions, it was found that the filamentary discharge current impulse amplitudes were dependent on the gas compositions. For an applied peak voltage of 7kV, at 100% N_2 the average discharge current amplitude was -4.075 mA, but when 4.76% O_2 was added to the N_2 the value increased to -56.77 mA. If a mixture of 4.76% O_2 and 1000 ppm NO was added to N_2, it further increased to -125.66 mA. However, when 2.31% H_2O vapour was added to the mixture of O_2, NO and N_2, it significantly reduced to -5.848 mA. In addition, when O_2, NO and H_2O vapour were added to N_2 one by one, the gap breakdown voltage increased. The main reasons for these changes were the quenching effect of NO and O_2 on metastable states of N_2 and H_2O's electron attachment ability. First, metastable states of N_2 played an important role in generating seed electron and kept the density of charges low in discharge filaments in Townsend-liked discharges, so the discharge current amplitude is low in N_2. However, the presence of NO and O_2 would eliminate these metastable states. In their absence, the charge density increased and the discharge converted to a streamer-like discharge, so the average discharge current amplitude and the breakdown voltage were higher than that in N_2. Because the quenching effect of NO is stronger than O_2, the average discharge current amplitude at 4.76% O_2 and 1000 ppm NO in N_2 was higher than at 4.76%

O_2 in N_2. However, when 2.31% H_2O vapour was added to the mixture of NO, O_2 and N_2, the average discharge current significantly reduced from -125.66 mA to -5.848 mA. A possible reason was that when H_2O vapour was added, the quenching effect of NO and O_2 was not dominant, but the electron attachment on H_2O was more important. Once electrons attach to form negative water vapour ions, they are not useful in stimulating gas ionization. Discharge processes become limited, so discharge current reduced and higher breakdown voltages resulted.

Because there is no side reaction between OH and NO, non-thermal plasma discharge using liquid water as one electrode was applied to investigate the potential of OH for NO removal. The main purpose of the liquid water electrode is to generate more OH, water evaporation becomes stronger with increasing discharge power. Under the pin-water configuration, three modes of negative DC discharge occurred under increasing voltage, namely Trichel pulse discharge, pulseless discharge and arc discharge. Under Trichel pulse discharge, only the gas around the pin tip was luminous. The NO removal and energy efficiency is low. With increasing applied voltage, initially the amplitude of discharge pulses reduced but the discharge frequency increased, at higher voltage the discharge current became DC and the discharge converted to pulseless mode. In pulseless discharge the whole volume between the pin and the water surface was luminous. The NO removal and energy efficiency were continuously increasing which was different from the DBD treatment process. In DBD, with the increase of discharge power, NO removal was increased, but NO removal energy efficiency was reduced. Two possible reasons are that with the increase in applied voltage, the effective ionization area was increased and the concentration of H_2O in the gas phase was also increased, which can generate more OH to remove NO. However, once the discharge mode converted to arc, the mechanism changed completely, non-thermal plasma became thermal plasma and NO was formed by the Zeldovich mechanism.

In this electrode system a similar trend to that in the DBD was found. Under wet condition, the increase of O_2 concentration also caused the reduction of NO in corona discharge. The difference is that for DBD, the NO removal started to reduce when the O_2 concentration increased to 9.09%. For the pin-water negative corona discharge, it started to reduce when the O_2 concentration reached 16.67%. One possible reason for the reduction of NO removal with increasing O_2 concentration is that the reaction between O and OH was promoted but the reaction between OH and NO was limited. At 4.76% O_2 and high NO concentration, although 610 ppm of 851 ppm NO (72% NO removal efficiency) was removed by corona

discharge, the energy efficiency was only 5.5 g/kWh. For DBD, although only 210 ppm of 855 ppm NO (24.6% NO removal efficiency) was removed, the energy efficiency was 13.2g/kWh. The difference between DBD and pin-water discharge is the energy injection. The energy injection in DBD was only 0.25W, but for pin-water discharge, it was 1.87W. The discharge energy is concentrated on the pin only, so the energy efficiency is low. For direct non-thermal plasma treatment, it is better to use a low energy density discharge configuration like DBD to improve the energy efficiency, the energy density of corona discharge is too high to use commercially.

After the investigation of direct non-thermal plasma treatment for NO removal in less than 1000 ppm concentration, NO removal in higher concentration (up to 6%) was investigated, because it could increase the possibility of a collision between energetic electron and NO. Firstly, activated carbon was used to absorb low concentration NO (1000 ppm) from the gas mixture. Activated carbon as a porous material has an enormous surface area and oxygen functional groups on the surface play important roles for NO absorption. Analysis of the absorption ability under different O_2 concentrations showed that the absorbed species was NO_2 rather than NO. When there was no O_2 in the gas mixture, only 50 ppm from 1000 ppm NO was absorbed. For an O_2 concentration of 4.76%, 965 ppm NO was absorbed.

Comparing NO concentration before and after activated carbon NO absorption and thermal desorption processes, it was shown that NO concentration could be increased from 1000 ppm at a flow rate of 210 mL/min to a peak concentration of 6% at 50 mL/min. However, there was one serious problem for thermal desorption process, the thermal desorption energy efficiency was only 0.86g/kWh.

For the DBD treatment process on the desorbed high concentration NO, two gas mixtures were investigated. One was desorbed high concentration NO with N_2. Without the activated carbon NO absorption and thermal desorption processes, under 200 mL/min flow rate and 1.044W discharge power, the NO removal energy efficiency was only 8.53 g/kWh for 1000 ppm NO condition. For the 6% NO at the same experimental conditions, the NO removal energy efficiency increased to 32.51 g/kWh. There was nearly 4 times increase in NO removal energy efficiency, if the energy injection for thermal desorption process was ignored. Another advantage of NO absorption technology was that the gas desorption flow rate can be reduced. If the flow rate reduced to 50mL/min from 200mL/min, the energy efficiency increased to 56.82g/kWh from 32.51g/kWh.

Other gas mixtures of high concentration NO with N_2 and with two O_2 concentrations were investigated. One was 10.5% O_2 and the other one was 50% O_2. It was found that NO removal was nearly the same for DBD powers in the range of 0W to 1.044W. In this system NO could be oxidized by O_2 effectively, without the need for the stronger oxidants O and O_3: as the cost of generating O and O_3 could be saved, this could be a promising technology for NO removal. It also had the potential to incorporate the process to form nitric acid, as an economic by-product, to further reduce the overall cost of NO removal. However, there are two challenges for NO removal by activated carbon. One is poor selectivity on NO absorption when H_2O vapour is in the gas mixture and the other is high energy consumption of the thermal desorption process, so it is important to explore new materials or modified activated carbon which has better selectivity on NO and investigate another desorption method, rather than thermal desorption.

7.2 Future work

This research has investigated the mechanism of NO removal by DBD and pin-water negative corona discharge. The characteristics of DBD and pin-water negative corona discharge and chemical kinetics for NO removal were also investigated. In order to have a comprehensive understanding of the NO removal process by non-thermal plasma, the following aspects of the research can be investigated further.

In this research, the chemical kinetic analysis was based on the species of final products and their concentrations. It is important to have a deep understanding of the dynamic analysis from the beginning of discharge to the end. The development of each reactive species during the discharge process was important. Some spectroscopic instruments are important in evaluating the dynamic process, such as Laser Induced Fluorescence (LIF). It is also important to build a dynamic model to evaluate the discharge process and chemical kinetics. In addition, as highlighted in Literature Review, the highest NO removal energy efficiency was 112.5 g/kWh in a wire to cylinder reactor when using 5ns HV pulse voltage [95]. The main function of nano-second pulse was to limit the heat loss process, because the heat loss started to be significant after about 20ns. It is possible to increase the NO removal energy efficiency by using a HV pulse voltage with less than 5ns pulse duration. In corona discharge for NO removal in this research it was found that the contact between NO and OH was important, because of the short lifetime of OH. The general lifetime of reactive species is in μs, so it was valuable to investigate an alternative reactive species which has a longer lifetime. The help from the catalyst may be important in prolonging the lifetime of the reactive species. For example in SCR technology, NH_3 can be absorbed by the catalyst and the active part, NH_2 , would be exposed on the surface to react effectively with NO. Because NH_2 is constrained at the surface of the catalyst, the lifetime is long enough to react with NO, that is why the performance of SCR is much better than that of SNCR. Therefore, non-thermal plasma with a catalyst is a potential technology to explore for NO removal.

When NO concentration was increased to a percentage level, after NO absorption and desorption processes, NO oxidation can be realised by O_2. However, because of the poor selectivity between NO and H_2O for activated carbon, it is important to investigate absorbents to find ones which only absorb NO. In terms of the desorption process, thermal desorption is not practical, following concerns about energy consumption. It is better to investigate alternative desorption technologies such as gas discharge or the change of pressure method where absorption is in high pressure and desorption is in low pressure.

Chapter 8 REFERENCES

[1] Gómez-García MA, Pitchon V, Kiennemann A. Pollution by nitrogen oxides: an approach to NOx abatement by using sorbing catalytic materials. Environment International, 2005; 31(3): 445-67.
[2] Adams M. Nitrogen oxides (NOx) emissions Data and maps, Indicator Specification (Indicator codes: APE 002, European Environment Agency (EEA) 2010.

[3] Zeldovich J. The oxidation of nitrogen in combustion and explosions. Acta Physiochimica URSS, XXI, Academy of Science of the USSR. 1946; 4.
[4] Wünning JA, Wünning JG. Flameless oxidation to reduce thermal no-formation. Progress in Energy and Combustion Science. 1997; 23(1): 81-94.
[5] Biarnes M, and, Esteves J. Nitrogen Oxides: What is NOx? [online] accessed at http://wwwe-instcom/combustion/nitrogen-oxides-nox.
[6] Air pollution from electricity-generating large combustion plants. Copenhagen European Environment Agency EEA Technical report. 2008; 4: ISSN:1725-2237.

[7] S. Penkett SG, C. Plass-Duelmer and I. Galbally. WMO/GAW Expert Workshop on Global Long-term Measurements of Nitrogen Oxides and Recommendations for GAW Nitrogen Oxides Network. World Meteorological Organisation Global Atmosphere Watch 2009; GAW Report No. 195.
[8] Chaloulakou A, Mavroidis I, Gavriil I. Compliance with the annual NO2 air quality standard in Athens. Required NOx levels and expected health implications. Atmospheric Environment. 2008; 42(3): 454-65.
[9] Carslaw DC, Beevers SD. Investigating the potential importance of primary NO2 emissions in a street canyon. Atmospheric Environment. 2004;38(22):3585-94.
[10] Curtis L, Rea W, Smith-Willis P, Fenyves E, Pan Y. Adverse health effects of outdoor air pollutants. Environment International. 2006;32(6):815-30.
[11] Department for Environment FaRA. Nitrogen Dioxide in the United Kingdom Summary. Air Quality Expert Group. 2004.
[12] Chauhan AJ, and, Johnston SL. Air pollution and infection in respiratory illness. British Medical Bulletin. 2003;68(1):95-112.
[13] Odiyi BO, Eniola AO. The Effect of simulated acid rain on plant growth component of Cowpea (Vigna unguiculata) L. Walps. Jordan Journal of Biological Sciences. 2015;8(1):51-4.
[14] Department for Environment, Food and Rural Affairs. "Environmental Permitting Guidance The Large Combustion Plants Directive". [online] Version 3. 2010;Nobel House, London:Available at: https://www.gov.uk/government/uploads/system/uploads/attachment_data/file/69327/pb13635-ep2010combustionplants.pdf p38.
[15] Laboratory NET. "Regulatory Drivers for Existing Coal-Fired Power Plants". US department of energy.[online] available at https://www.netl.doe.gov/research/coal/crosscutting/environmental-control/nox-control/regulatory-drivers
[16] Ministry of Environmental Protection The People's Republic of China. "Emission standard of air pollutants for thermal power plant". GB 13223-2011. 2012:[online] Available at: http://english.mep.gov.cn/standards_reports/standards/Air_Environment/Emission_standard1/201201/t20120106_222242.htm.
[17] (LADCO) TLMADC. Midwest Regional Planning Organization (RPO) Boiler Best Available Retrofit Technology (BART) Engineering Analysis. 2005 March.

[18] Topsoe N-Y. Catalysis for NOx abatement selective catalytic reduction of NOx by ammonia: fundamental and industrial aspects. CATTECH. 1997;1:125.
[19] Topsoe NY, Topsoe H, Dumesic JA. Vanadia/Titania Catalysts for Selective Catalytic Reduction (SCR) of Nitric-Oxide by Ammonia: I. Combined Temperature-Programmed in-Situ FTIR and On-line Mass-Spectroscopy Studies. Journal of Catalysis. 1995;151(1):226-40.
[20] Yuan R-M, Fu G, Xu X, Wan H-L. Bronsted-NH4+ mechanism versus nitrite mechanism: new insight into the selective catalytic reduction of NO by NH3. Physical Chemistry Chemical Physics. 2011;13(2):453-60.
[21] Lyon RK, Hardy JE. Discovery and development of the thermal DeNOx process. Industrial & engineering chemistry fundamentals. 1986;25(1):19-24.
[22] Lyon RK. Thermal DeNOx controlling nitrogen oxides emissions by a noncatalytic process. Environmental science & technology. 1987;21(3):231-6.
[23] Wenli D, Dam-Johansen K, Østergaard K. Widening the temperature range of the thermal DeNOx process. An experimental investigation. Symposium (International) on Combustion. 1991;23(1):297-303.
[24] Kasuya F, Glarborg P, Johnsson JE, Dam-Johansen K. The thermal DeNOx process: Influence of partial pressures and temperature. Chemical Engineering Science. 1995;50(9):1455-66.
[25] Basfar AA, Fageeha OI, Kunnummal N, Chmielewski AG, Licki J, Pawelec A, et al. A review on electron beam flue gas treatment (EBFGT) as a multicomponent air pollution control technology. Nukleonika. 2010;55:271-7.
[26] Chmielewski A. Electron beams for power plant flue gas treatment. Radiation technology for conservation of the environment. 1998:3.
[27] Mochida I, Shirahama N, Kawano S, Korai Y, Yasutake A, Tanoura M, et al. NO oxidation over activated carbon fiber (ACF). Part 1. Extended kinetics over a pitch based ACF of very large surface area. Fuel. 2000;79(14):1713-23.
[28] Batakliev T, Georgiev V, Anachkov M, Rakovsky S, Rakovsky S. Ozone decomposition. Interdisciplinary Toxicology2014. p. 47.
[29] Zhang J, Zhang R, Chen X, Tong M, Kang W, Guo S, et al. Simultaneous Removal of NO and SO2 from Flue Gas by Ozone Oxidation and NaOH Absorption. Industrial & Engineering Chemistry Research. 2014;53(15):6450-6.
[30] Jensen TK, Jørgensen L, Ørtenblad M, Stamate E, Simonsen P, Tobiassen L, et al., editors. NOx reduction obtained by low-temperature plasma generated ozone. International Gas Union research conference; 2008.
[31] Głomba M, Kordylewski W. Simultaneous removal of NOx, SO2, CO and Hg from flue gas by ozonation. Pilot plant studies. Environment Protection Engineering. 2014;40(3).
[32] Jakubiak MP. Pilot-scale studies on NOx removal from flue gas via NO ozonation and absorption into NaOH solution. Chemical and Process Engineering. 2012;33(3):345-58.
[33] OZOTEK. 1KG/H OZONE GENERATOR MODEL: OTH-OXY1000. [online] available at http://www.o3tech.cn/product/large-scale-ozone-generator-1kg.html.
[34] NewlandEntech. NLO 系列大型臭氧发生器（CHINESE）NLO series industrial Ozone generator.
[35] Eden JG, Kim MH, Cho JH, Park SJ. Modular microplasma microchannel reactor devices, miniature reactor modules and ozone generation devices. Google Patents; 2016.
[36] Kefeng S, Yan W, Jie L, Guofeng L, Duan L. Enhancement of NO x abatement by advancing initiation of C 3 H 6 oxidation chemistry with a corona radical shower. Plasma Sources Science and Technology. 2007;16(1):104.
[37] Shin H-H, Yoon W-S. Hydrocarbon Effects on the Promotion of Non-Thermal Plasma NO–NO2 Conversion. Plasma Chemistry and Plasma Processing. 2003;23(4):681-704.
[38] Anthony RM, James TS, Whitehead JC. Modelling of non-thermal plasma aftertreatment of exhaust gas streams. Journal of Physics D: Applied Physics. 2004;37(1):42.

[39] Parker AE, Monks PS, Wyche KP, Balzani-L ööv JM, Staehelin J, Reimann S, et al. Peroxy radicals in the summer free troposphere: seasonality and potential for heterogeneous loss. Atmos Chem Phys. 2009;9(6):1989-2006.
[40] Zhu A-M, Sun Q, Niu J-H, Xu Y, Song Z-M. Conversion of NO in NO/N2, NO/O2/N2, NO/C2H4/N2 and NO/C2H4/O2/N2 Systems by Dielectric Barrier Discharge Plasmas. Plasma Chemistry and Plasma Processing. 2005;25(4):371-86.
[41] Boehm HP. Some aspects of the surface chemistry of carbon blacks and other carbons. Carbon. 1994;32(5):759-69.
[42] Biniak S, Pakuła M, Szymański GS, Świątkowski A. Effect of Activated Carbon Surface Oxygen- and/or Nitrogen-Containing Groups on Adsorption of Copper(II) Ions from Aqueous Solution. Langmuir. 1999;15(18):6117-22.
[43] Guo Y, Li Y, Zhu T, Ye M. Investigation of SO 2 and NO adsorption species on activated carbon and the mechanism of NO promotion effect on SO 2. Fuel. 2015;143:536-42.
[44] Rubel A, Stewart M, Stencel J. Activated carbon for control of nitrogen oxide emissions. Journal of materials research. 1995;10(3):562-7.
[45] Smidth F. Gases-specific heat capacities and individual gas constants. [online] available at: http://catalogconveyorspneumaticcom/Asset/FLS%20Specific%20Heat%20Capacities%20of%20Gasespdf

[46] Elmemesser.ee. Nitrogen dioxide Phyical Properties. [online] available at: http://wwwelmemesseree/assets/media/201127/cd5f65b0b6f022b151d6e35d9eed121epdf.
[47] Wang L, Wang R, Lu Z, Chen C, Wang K, Wu J. The performance of two adsorption ice making test units using activated carbon and a carbon composite as adsorbents. Carbon. 2006;44(13):2671-80.
[48] Markovic V. Electron beam processing of combustion flue gases. IAEA bulletin. 1987;29(2):25-7.
[49] 烟气脱硝技术原理及几种烟气脱硝技术的比较(Chinese)

Flue gas DeNOx technologies principle and a comparison on a few mature DeNOx technologies in industry. [online] http://wwwchinatiansaicom/news/daqizl/593html. 04/06/2016.
[50] Using Non-thermal plasma to Control Air Pollutants. The Clean Air Technology Center(CATC) US Environmental Protection Agency (E143-03(2005 February.
[51] 北极星环保网. 燃煤电厂烟气 SCR 脱硝成本分析与优化(Chinese) Coal fired power plan flue gas SCR DeNOx cost analysis and optimization. 26/12/2016.

[52] Van Veldhuizen E, Rutgers W. Corona discharges: fundamentals and diagnostics. Invited paper, Proc Frontiers in Low Temp Plasma Diagn IV, Rolduc, Netherlands. 2001:40-9.
[53] Oda T, Takahashi T, Yamashita R. Non-thermal plasma processing for VOCs decomposition and NOx removal in flue gas. Journal of Advanced Oxidation Technologies. 1997;2(2):337-45.
[54] Mizuno A, Shimizu K, Matsuoka T, Furuta S. Reactive absorption of NOx using wet discharge plasma reactor. IEEE transactions on industry applications. 1995;31(6):1463-8.
[55] Zhao GB, Garikipati S, Hu X, Argyle MD, Radosz M. Effect of oxygen on nonthermal plasma reactions of nitrogen oxides in nitrogen. AIChE journal. 2005;51(6):1800-12.
[56] Saavedra HM, Pacheco MP, Pacheco-Sotelo JO, Reyes CET, Gomez JAD. Modeling and experimental study on nitric oxide treatment using dielectric barrier discharge. IEEE Transactions on Plasma Science. 2007;35(5):1533-40.

[57] Mok YS, Nam CM, Cho MH, Nam I-S. Decomposition of volatile organic compounds and nitric oxide by nonthermal plasma discharge processes. IEEE Transactions on Plasma Science. 2002;30(1):408-16.
[58] Atsushi K, Ryo O. Two-dimensional simulation of fast gas heating in an atmospheric pressure streamer discharge and humidity effects. Journal of Physics D: Applied Physics. 2014;47(15):155202.
[59] Reiser G, Habenicht W, Müller-Dethlefs K, Schlag EW. The ionization energy of nitric oxide. Chemical physics letters. 1988;152(2-3):119-23.
[60] Kogelschatz U. Advanced Ozone Generation Brown Boveri, Baden, Switzerland.87-120.
[61] Gilmore FR. Potential energy curves for N2, NO, O2 and corresponding ions. Journal of Quantitative Spectroscopy and Radiative Transfer. 1965;5(2):369IN1-89IN3.
[62] Atkinson R, Baulch DL, Cox RA, Jr. RFH, Kerr JA, Rossi MJ, et al. Evaluated Kinetic and Photochemical Data for Atmospheric Chemistry: Supplement VI. IUPAC Subcommittee on Gas Kinetic Data Evaluation for Atmospheric Chemistry. Journal of Physical and Chemical Reference Data. 1997;26(6):1329-499.
[63] Becker E, Rahman M, Schindler R. Determination of the rate constants for the gas phase reactions of NO3 with H, OH and HO2 radicals at 298 K. Berichte der Bunsengesellschaft für physikalische Chemie. 1992;96(6):776-83.
[64] DeMore WB, Sander SP, Golden D, Hampson R, Kurylo MJ, Howard CJ, et al. Chemical kinetics and photochemical data for use in stratospheric modeling. evaluation no. 12. 1997.
[65] Xiong Z, Huang Q, Wang Z, Lu X, Pan Y. On the Electrical Characteristic of Atmospheric Pressure Air/He/O2/N2/Ar Plasma Needle. IEEE transactions on plasma science. 2013;41(7):1746-50.
[66] Kogelschatz U. Dielectric-barrier discharges: their history, discharge physics, and industrial applications. Plasma chemistry and plasma processing. 2003;23(1):1-46.
[67] Lang H, Emi P, Liechti P, editors. Advanced ozone generation technology to solve the oxidation problems of today. Aplicaciones del Ozono en la Produccion de Agua y la Depuracion de Liquidos Cloacales; 1999: AIDIS.
[68] Kogelschatz U, Eliasson B, Hirth M. Ozone generation from oxygen and air: discharge physics and reaction mechanisms. 1988.
[69] Sun W, Pashaie B, Dhali SK, Honea FI. Non-thermal plasma remediation of SO2/NO using a dielectric-barrier discharge. Journal of Applied Physics. 1996;79(7):3438-44.
[70] Moo B, Kushner M, Rood M. Gas-phase removal of NO from gas streams via dielectric barrier discharges. Environmental Science & Technology. 1992;26(4):777-81.
[71] Chang MB, Kushner MJ, Rood MJ. Removal of SO2 and the simultaneous removal of SO2 and NO from simulated flue gas streams using dielectric barrier discharge plasmas. Plasma Chemistry and Plasma Processing. 1992;12(4):565-80.
[72] Penetrante BM, Hsiao MC, Merritt BT, Vogtlin GE, Wallman PH, Neiger M, et al. Pulsed corona and dielectric-barrier discharge processing of NO in N2. Applied Physics Letters. 1996;68(26):3719-21.
[73] Takaki K, Jani MA, Fujiwara T. Removal of nitric oxide in flue gases by multi-point to plane dielectric barrier discharge. IEEE Transactions on Plasma Science. 1999;27(4):1137-45.
[74] H.Sohst. fur Angew Pjysik. 1962;14:620.
[75] G.A.Schoder. fur Angew. Physok 13 p.296. 1961.
[76] Kuffel E, W.S.Zaengl, and, J.Kuffel. High Voltage Engineering Fundamentals. Second edition, Butterworth-Heinemann publishing, Oxford. 2000.

[77] Hirsikko A, Nieminen T, Gagné S, Lehtipalo K, Manninen H, Ehn M, et al. Atmospheric ions and nucleation: a review of observations. Atmospheric Chemistry and Physics. 2011;11(2):767-98.
[78] Laakso L, Hirsikko A, Grönholm T, Kulmala M, Luts A, Parts T-E. Waterfalls as sources of small charged aerosol particles. Atmospheric Chemistry and Physics. 2007;7(9):2271-5.
[79] Becker KH, Kogelschatz U, Schoenbach KH, and, Barker RJ. Non-Equilibrium Air Plasmas at Atmospheric Pressure. Institute of Physics Publishing, London, UK. 2004.
[80] Kogelschatz U, Eliasson B, Egli W. Dielectric-Barrier Discharges. Principle and Applications. J Phys IV France. 1997;07(C4):C4-47-C4-66.
[81] Song C-L, Bin F, Tao Z-M, Li F-C, Huang Q-F. Simultaneous removals of NOx, HC and PM from diesel exhaust emissions by dielectric barrier discharges. Journal of Hazardous Materials. 2009;166(1):523-30.
[82] Takaki K, Shimizu M, Mukaigawa S, Fujiwara T. Effect of electrode shape in dielectric barrier discharge plasma reactor for NOx removal. IEEE Transactions on Plasma Science. 2004;32(1):32-8.
[83] Kim HH, Takashima K, Katsura S, Mizuno A. Low-temperature NO x reduction processes using combined systems of pulsed corona discharge and catalysts. Journal of Physics D: Applied Physics. 2001;34(4):604.
[84] Hoeben WFLM, Veldhuizen EMv, Rutgers WR, Kroesen GMW. Gas phase corona discharges for oxidation of phenol in an aqueous solution. Journal of Physics D: Applied Physics. 1999;32(24):L133.
[85] Grabowski L, Van Veldhuizen E, Pemen A, Rutgers W. Corona above water reactor for systematic study of aqueous phenol degradation. Plasma Chemistry and Plasma Processing. 2006;26(1):3-17.
[86] Malik MA, Ghaffar A, Ahmed K. Synergistic effect of pulsed corona discharges and ozonation on decolourization of methylene blue in water. Plasma Sources Science and Technology. 2002;11(3):236.
[87] Ono R, Oda T. Measurement of hydroxyl radicals in pulsed corona discharge. Journal of electrostatics. 2002;55(3):333-42.
[88] Tamon H, Okazaki M. Influence of acidic surface oxides of activated carbon on gas adsorption characteristics. carbon. 1996;34(6):741-6.
[89] Group LR. Research on long air gap discharges at Les Renardières. Electra. 1972;23.
[90] Chang JS, Lawless PA, Yamamoto T. Corona discharge processes. IEEE Transactions on Plasma Science. 1991;19(6):1152-66.
[91] Sattari P, Gallo C, Castle G, Adamiak K. Trichel pulse characteristics—negative corona discharge in air. Journal of Physics D: Applied Physics. 2011;44(15):155502.
[92] Kondo Y, Miyoshi Y. Pulseless corona in negative point to plane gap. Japanese Journal of Applied Physics. 1978;17(4):643.
[93] Kanazawa S, Chang JS, Round GF, Sheng G, Ohkubo T, Nomoto Y, et al. Removal of NOx from flue gas by corona discharge activated methane radical showers. Journal of Electrostatics. 1997;40:651-6.
[94] Yan K, Kanazawa S, Ohkubo T, Nomoto Y. Oxidation and Reduction Processes During NOx Removal with Corona-Induced Nonthermal Plasma. Plasma Chemistry and Plasma Processing. 1999;19(3):421-43.
[95] Namihira T, Wang D, Akiyama H. Pulsed power technology for pollution control. Acta Physica Polonica A. 2009;115(6):953-5.
[96] Douyan W, Namihira T, and, Akiyama H. Pulsed discharge plasma for pollution control. InTech, Rijeka, Croatia. 2010:265-88.

[97] Wang D, Matsuda M, Matsumoto T, Namihira T, Akiyama H. Energy transfer efficiency of nano-seconds pulsed power generator for nonthermal plasma processing technique. IEEE Transactions on Dielectrics and Electrical Insulation. 2011;18(4):1091-6.
[98] [online], http://www.engineeringtoolbox.com/. available at http://www.engineeringtoolbox.com/water-vapor-saturation-pressure-d_599.html. Accessed 23 Feb 2017.
[99] Scientific TF. Model 42i-High Level User Instruction Manual Chemiluminescence NO-NO2-NOx analyser Part Number 101903-00 P21.
[100] Bates JN. Nitric oxide measurement by chemiluminescence detection. Neuroprotocols. 1992;1(2):141-9.
[101] BMT MESSTECHKNK GMBH, Ozone analyzer BMT 964 Datasheet
[102] Rao SM, Joseph MA, Robert AW, Dariusz D. High-resolution Electron-impact Emission Spectra and Vibrational Emission Cross Sections from 330-1100 nm for N2. The Astrophysical Journal Supplement Series. 2011;196(1):13.
[103] Gherardi N, Gouda G, Gat E, Ricard A, Massines F. Transition from glow silent discharge to micro-discharges in nitrogen gas. Plasma Sources Science and Technology. 2000;9(3):340.
[104] Brandenburg R, Maiorov VA, Yu BG, Wagner HE, Behnke J, Behnke JF. Diffuse barrier discharges in nitrogen with small admixtures of oxygen: discharge mechanism and transition to the filamentary regime. Journal of Physics D: Applied Physics. 2005;38(13):2187.
[105] Atsushi K, Ryo O, Tetsuji O. Behaviour of OH radicals in an atmospheric-pressure streamer discharge studied by two-dimensional numerical simulation. Journal of Physics D: Applied Physics. 2013;46(17):175206.
[106] Itikawa Y, Mason N. Cross Sections for Electron Collisions with Water Molecules. Journal of Physical and Chemical Reference Data. 2005;34(1):1-22.
[107] Itikawa Y. Cross Sections for Electron Collisions with Oxygen Molecules. Journal of Physical and Chemical Reference Data. 2009;38(1):1-20.
[108] Yagi I, Okada S, Matsumoto T, Wang D, Namihira T, Takaki K. Streamer Propagation of Nanosecond Pulse Discharge With Various Rise Times. IEEE Transactions on Plasma Science. 2011;39(11):2232-3.
[109] Atkinson R, Baulch D, Cox R, Hampson R, Kerr J, Troe J. Evaluated kinetic and photochemical data for atmospheric chemistry: Supplement III. International journal of chemical kinetics. 1989;21(2):115-50.
[110] Atkinson R, Baulch DL, Cox RA, Crowley JN, Hampson RF, Hynes RG, et al. Evaluated kinetic and photochemical data for atmospheric chemistry: Volume I - gas phase reactions of Ox, HOx, NOx and SOx species. Atmos Chem Phys. 2004;4(6):1461-738.
[111] Atkinson R, Baulch DL, Cox RA, Hampson RF, Kerr JA, Troe J. Evaluated kinetic and photochemical data for atmospheric chemistry: Supplement IV. Atmospheric Environment Part A General Topics. 1992;26(7):1187-230.
[112] Luo J, Suib SL, Marquez M, Hayashi Y, Matsumoto H. Decomposition of NOx with Low-Temperature Plasmas at Atmospheric Pressure: Neat and in the Presence of Oxidants, Reductants, Water, and Carbon Dioxide. The Journal of Physical Chemistry A. 1998;102(41):7954-63.
[113] Robertson R, Smith GP. Temperature Dependence of O+ OH at 136− 377 K Using Ozone Photolysis. The Journal of Physical Chemistry A. 2006;110(21):6673-9.
[114] Laroussi M, Lu X, Kolobov V, Arslanbekov R. Power consideration in the pulsed dielectric barrier discharge at atmospheric pressure. Journal of Applied Physics. 2004;96(5):3028-30.

[115] Hippler H, Rahn R, Troe J. Temperature and pressure dependence of ozone formation rates in the range 1–1000 bar and 90–370 K. The Journal of Chemical Physics. 1990;93(9):6560-9.
[116] Anastasi C, Smith IWM. Rate measurements of reactions of OH by resonance absorption. Part 6.-Rate constants for OH + NO(+ M)- HNO2(+ M) over a wide range of temperature and pressure. Journal of the Chemical Society, Faraday Transactions 2: Molecular and Chemical Physics. 1978;74(0):1056-64.
[117] Atkinson, R Baulch, D.L. Cox, R.A. Crowlet, J.N. Hampson, R.F. Kerr, J.A. Rossi.M.j and Troe, J. Summary of Evaluated Kinetic and Photochemical Data for Atmospheric Chemistry.
[118] Peter B, Peter G, Joris D, Jan V, Christophe L. Influence of the water surface on the glow-to-spark transition in a metal-pin-to-water electrode system. Plasma Sources Science and Technology. 2008;17(4):045014.
[119] Peter B, Jingjing L, Joris D, Michael GK, Jan V, Christophe L. Dc excited glow discharges in atmospheric pressure air in pin-to-water electrode systems. Journal of Physics D: Applied Physics. 2008;41(21):215201.
[120] Zhao YY, Wang T, Wilson MP, MacGregor SJ, Timoshkin IV, Ren QC. Hydroxyl Radicals and Hydrogen Peroxide Formation at Nonthermal Plasma Water Interface. IEEE Transactions on Plasma Science. 2016;44(10):2084-91.
[121] Peter B, Christophe L. Non-thermal plasmas in and in contact with liquids. Journal of Physics D: Applied Physics. 2009;42(5):053001.
[122] Cserfalvi T, Mezei P. Operating mechanism of the electrolyte cathode atmospheric glow discharge. Fresenius' Journal of Analytical Chemistry. 1996;355(7):813-9.
[123] Gaisin AF, Son EE. Vapor-air discharges between electrolytic cathode and metal anode at atmospheric pressure. High Temperature. 2005;43(1):1-7.
[124] Chen Q, Saito K, Takemura Y-i, Shirai H. Physicochemistry of the plasma-electrolyte solution interface. Thin Solid Films. 2008;516(19):6688-93.
[125] Polyakov OV, Badalyan AM, Bakhturova LF. The Yields of Radical Products in Water Decomposition under Discharges with Electrolytic Electrodes. High Energy Chemistry. 2003;37(5):322-7.
[126] Qiang C, Junshuai L, Kenji S, Hajime S. The characterization of radio-frequency discharge using electrolyte solution as one electrode at atmospheric pressure. Journal of Physics D: Applied Physics. 2008;41(17):175212.
[127] Barrera-Díaz C, Cañizares P, Fernández FJ, Natividad R, Rodrigo MA. Electrochemical Advanced Oxidation Processes: An Overview of the Current Applications to Actual Industrial Effluents. Journal of the Mexican Chemical Society. 2014;58:256-75.
[128] AD. McGraw-Hill Dictionary of Scientific & Technical Terms, 6E. . Retrieved June 22 2017 from https://encyclopedia2thefreedictionarycom/Arc+Discharge. 2003.
[129] Michael JV, Lim KP. Rate constants for the N2O reaction system: Thermal decomposition of N2O; N+NO→N2+O; and implications for O+N2→NO+N. The Journal of Chemical Physics. 1992;97(5):3228-34.
[130] Bose D, Candler GV. Thermal rate constants of the O2+N→NO+O reaction based on the A2′ and A4′ potential-energy surfaces. The Journal of Chemical Physics. 1997;107(16):6136-45.
[131] Nitrogen oxides formation in combustion processes. Department of Mechanical Engineering Wroclaw University of Technology [online] Available at http://fluidwmepwrwrocpl/~spalanie/dydaktyka/combustion_en/NOx/NOx_formationpdf.
[132] Gibson AS, Riousset JA, Pasko VP. Minimum breakdown voltages for corona discharge in cylindrical and spherical geometries. NSF EE REU Penn State Annual Research Journal. 2009;7:1-17.
[133] R.J.Roth. Principles. Industrial plasma engineering. 1995;1(IOP Publishing Ltd).

[134] Mizuno A, Kurahashi M, Imano S, Ishida T, Nagata M, editors. Sterilization using OH radicals produced by pulsed discharge plasma in atmospheric pressure. Industry Applications Conference, 1997 Thirty-Second IAS Annual Meeting, IAS '97, Conference Record of the 1997 IEEE; 1997 5-9 Oct 1997.
[135] Chiang Y-C, Chiang P-C, Huang C-P. Effects of pore structure and temperature on VOC adsorption on activated carbon. Carbon. 2001;39(4):523-34.
[136] Qiang T, Zhigang Z, Wenpei Z, Zidong C. SO 2 and NO selective adsorption properties of coal-based activated carbons. Fuel. 2005;84(4):461-5.
[137] Zhang Z, Atkinson JD, Jiang B, Rood MJ, Yan Z. Nitric oxide oxidation catalyzed by microporous activated carbon fiber cloth: An updated reaction mechanism. Applied Catalysis B: Environmental. 2014;148:573-81.
[138] M.L.McGlashan. Tables of Physical&Chemical COnstans, 3.7.1 Dipole moments and dipole lengths Kaye&Laby Online, National Physical Laboratory.
[139] Rienstra-Kiracofe JC, Tschumper GS, Schaefer HF, Nandi S, Ellison GB. Atomic and Molecular Electron Affinities: Photoelectron Experiments and Theoretical Computations. Chemical Reviews. 2002;102(1):231-82.

Chapter 9 PUBLICATIONS

Conference paper:

- L. Zhou, T. Wang, S. Macgregor, M. Wilson, I. Timoshkin and M. Given, "NO removal and discharge characteristics using dielectric barrier discharge*," 21th IEEE Pulsed Power Conference (PPC)*, 18-22 June, 2017.

Journal Paper:

- L. Zhou, T. Wang, S. Macgregor, Q. Ren, M. Wilson, I. Timoshkin and M. Given "NO removal at different initial concentration of NO O_2 and H_2O and temperature impact" *IEEE Transactions on Plasma Science* (In preparation)

Appendixes

Appendix A - Discharge current waveforms for positive half period under different gas components

(a) For the mixture of N_2, O_2 and NO.

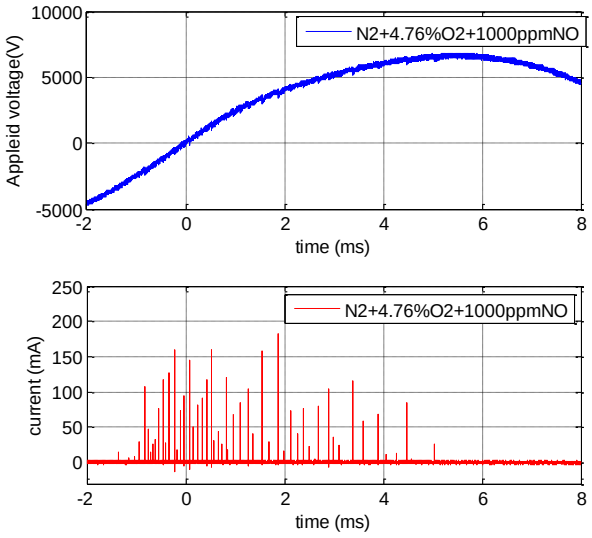

Figure 0-1 Discharge voltage and current waveforms at 210mL/min (4.76% O_2 and high concentration NO in N_2 condition) and 7 kV peak applied voltage for positive half period (10,000 current impulses measured)

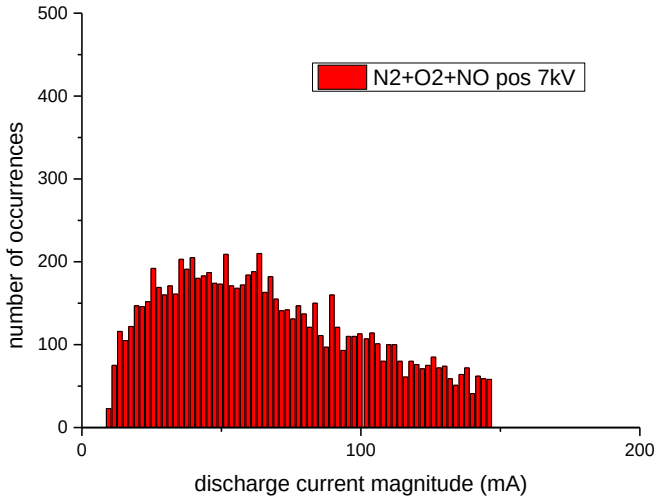

Figure 0-2 Discharge current amplitude distribution at 210mL/min (4.76% O_2 and high concentration NO in N_2 condition) and 7kV peak applied voltage for positive half period (10,000 current impulses measured)

(b) For the mixture of N_2, O_2, NO and H_2O

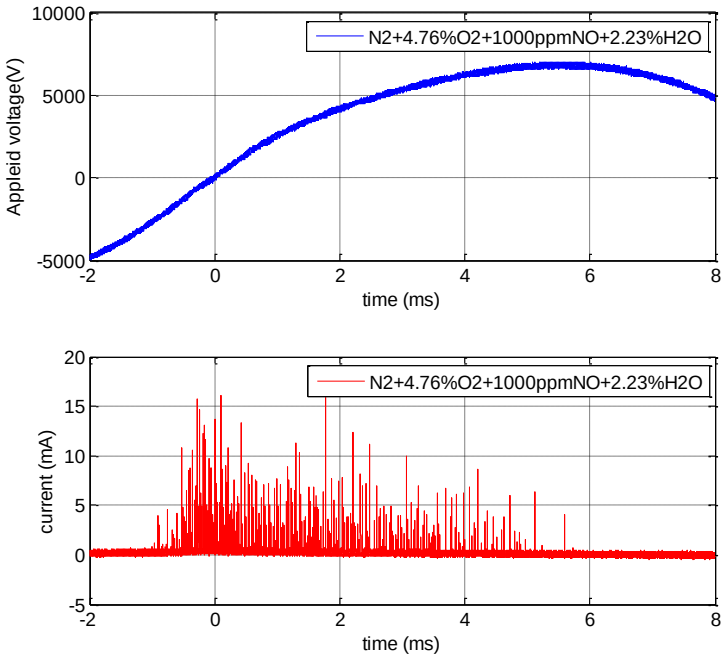

Figure 0-3 Discharge voltage and current waveforms at 210mL/min (4.76% O_2, 2.31%H_2O and high concentration NO in N_2 condition) and 7 kV peak applied voltage for positive half period (10,000 current impulses measured)

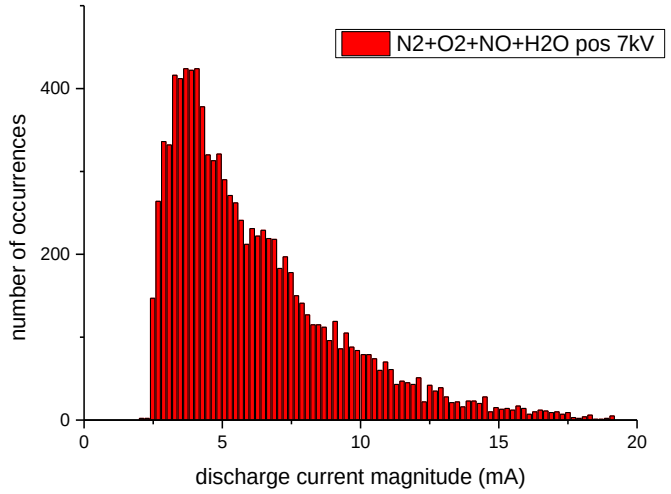

Figure 0-4 Discharge current amplitude distribution at 210mL/min (4.76% O_2, 2.31%H_2O and high concentration NO in N_2 condition) and 7 kV peak applied voltage for positive half period (10,000 current impulses measured)

(c) For N_2 alone.

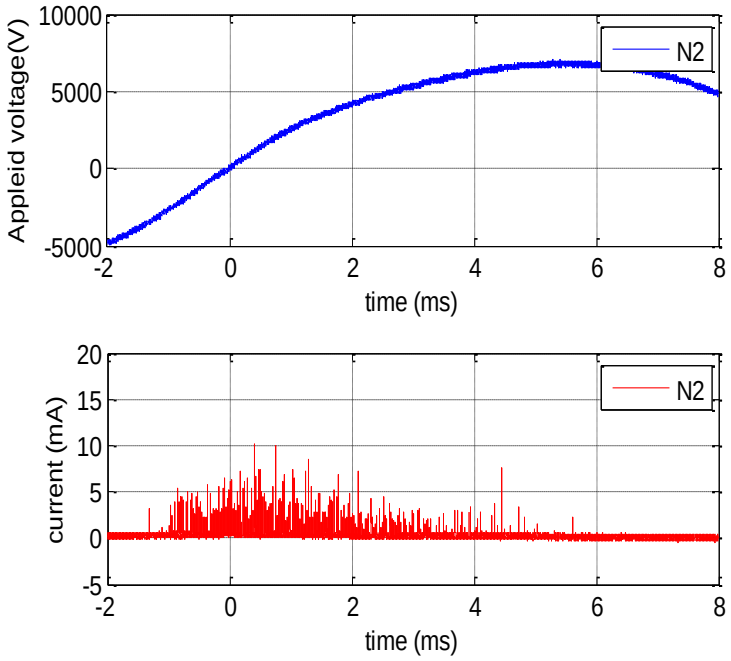

Figure 0-5 Discharge voltage and current waveforms at 210mL/min N_2 and 7 kV peak applied voltage for positive half period (10,000 current impulses measured)

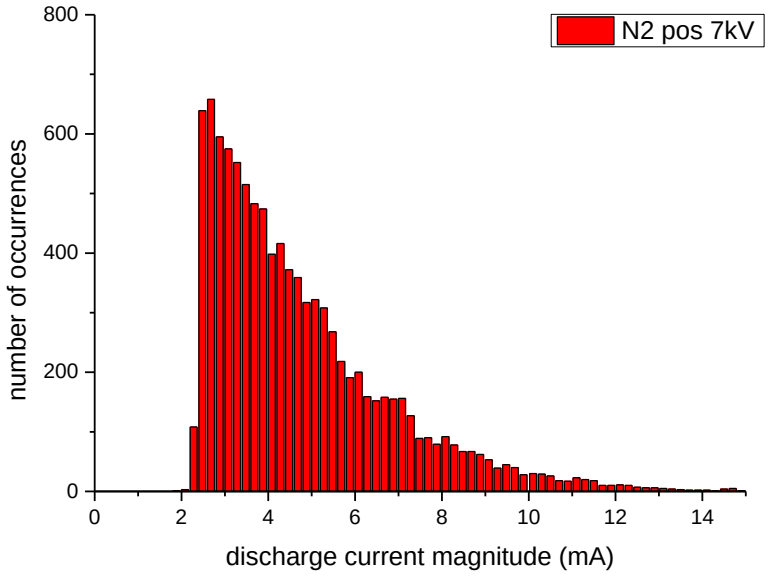

Figure 0-6 Discharge current amplitude distribution at 210mL/min N_2 and 7 kV peak applied voltage for positive half period (10,000 current impulses measured)

(d) For the mixture of N_2 and O_2

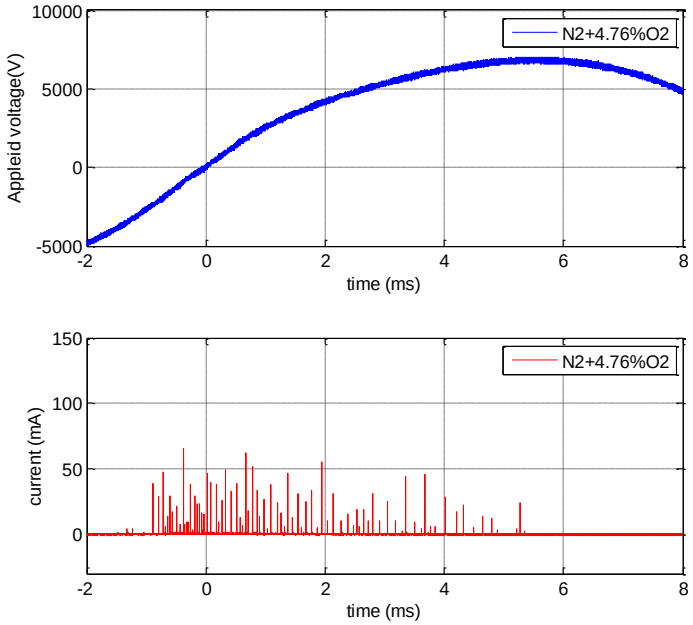

Figure 0-7 Discharge voltage and current waveforms at 210mL/min (4.76% O_2 in N_2) and 7 kV peak applied voltage for positive half period (10,000 current impulses measured)

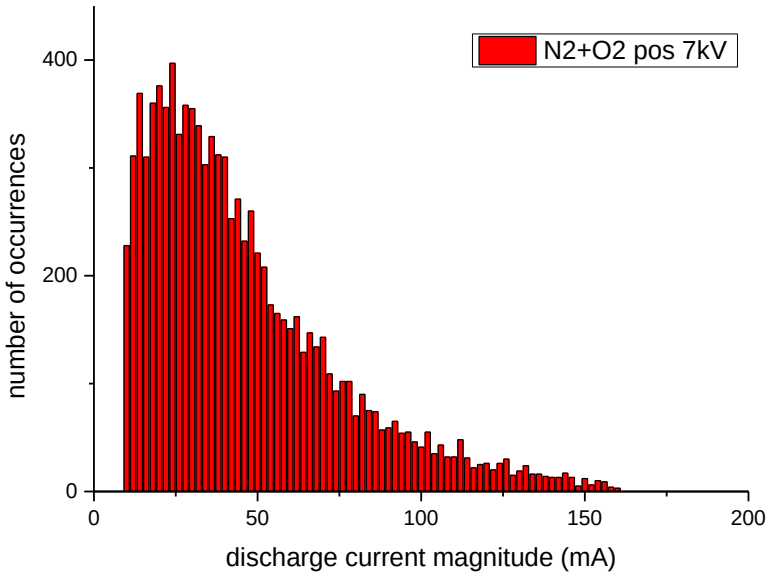

Figure 0-8 Discharge current amplitude distribution at 210mL/min (4.76% O_2 in N_2) and 7 kV peak applied voltage for positive half period (10,000 current impulses measured)

Appendix B - O_3 formation and energy efficiency at different temperatures

When water vapour was added to gas mixture, O_3 formation and energy efficiency are suppressed as shown in Figure 0-9 and Figure 0-10. In general, both temperature and water vapour have a negative effect on NOx removal treatment.

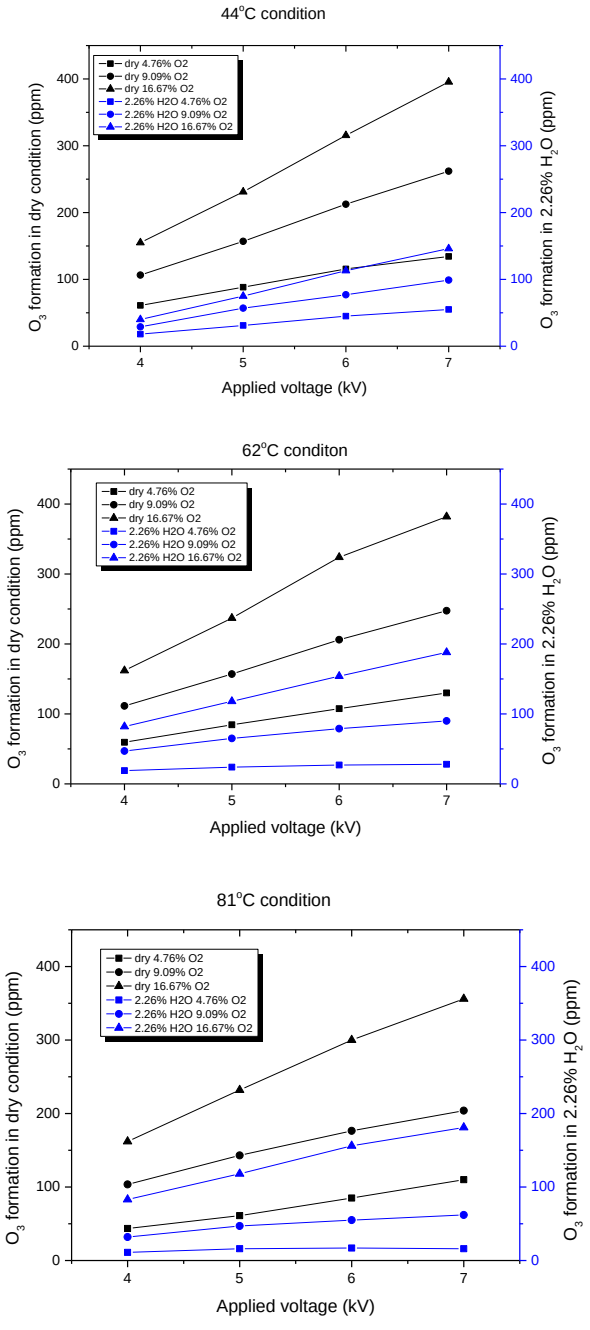

Figure 0-9 O_3 formation at zero and 2.31% H_2O condition in different applied voltage and O_2 concentration at 44°C, 62°C and 81°C gas temperature

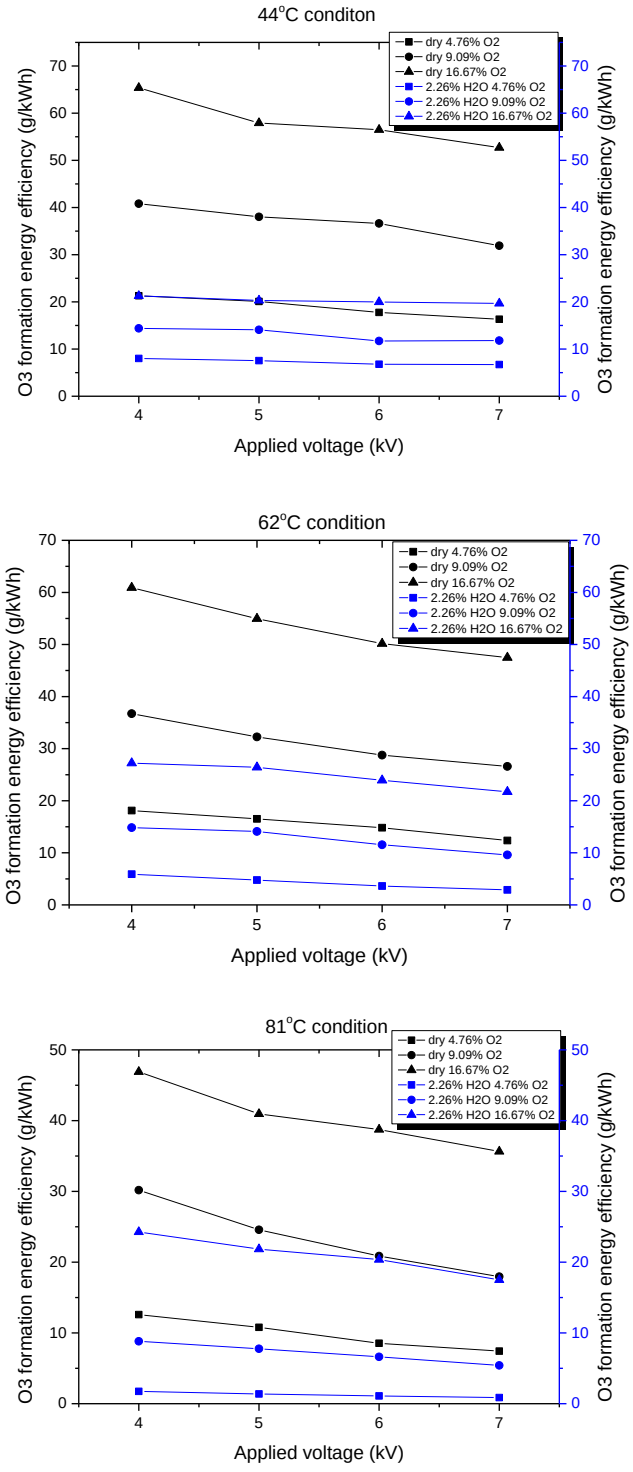

Figure 0-10 O_3 formation energy efficiency at dry and 2.31% H_2O condition in different applied voltage and O_2 concentration at 44°C, 62°C and 81°C gas temperature

Appendix C - Matlab Code: for discharge current and Lissajous figures

A) Positive half period discharge current amplitude comparison under different gas mixtures

```
load 'positive VI curve under diff gas mixture.mat';
time=time.*1000;
%pure nitrogen:
subplot(5,1,1),plot(time,Va_N2);
set(gca,'FontSize',12);
xlabel('time (ms)','fontsize',12);
ylabel('Appleid voltage(V)','fontsize',12);
axis([-2,8,-5000,10000]);
grid on;
legend('N2');
%
subplot(5,1,2),plot(time,I_N2*1000,'r');
set(gca,'FontSize',12);
xlabel('time (ms)','fontsize',12);
ylabel('current (mA)','fontsize',12);
axis([-2,8,-5,20]);
legend('N2');
grid on


subplot(5,1,3),plot(time,I_N2O2*1000,'k');
set(gca,'FontSize',12);
xlabel('time (ms)','fontsize',12);
ylabel('current (mA)','fontsize',12);
axis([-2,8,-30,150]);
legend('N2+4.76%O2');
grid on
%
%
subplot(5,1,4),plot(time,I_N2O2NO*1000,'b');
set(gca,'FontSize',12);
xlabel('time (ms)','fontsize',12);
ylabel('current (mA)','fontsize',12);
axis([-2,8,-30,250]);
legend('N2+4.76%O2+1000ppmNO');
grid on

%
subplot(5,1,5),plot(time,I_N2O2NOH2O*1000,'g');
set(gca,'FontSize',12);
xlabel('time (ms)','fontsize',12);
ylabel('current (mA)','fontsize',12);
axis([-2,8,-5,20]);
legend('N2+4.76%O2+1000ppmNO+2.31%H2O');
grid on
```

B) Negative half period discharge current amplitude comparison under different gas mixtures

```
load 'negative V I curve under diff gas.mat';
time=time.*1000;
%pure nitrogen:
subplot(5,1,1),plot(time,Va_N2);
set(gca,'FontSize',12);
xlabel('time (ms)','fontsize',12);
ylabel('Appleid voltage(V)','fontsize',12);
axis([-2,8,-10000,5000]);
grid on;
%legend('N2+4.76%O2');
%
subplot(5,1,2),plot(time,I_N2*1000,'r');
set(gca,'FontSize',12);
xlabel('time (ms)','fontsize',12);
ylabel('current (mA)','fontsize',12);
axis([-2,8,-20,5]);
legend('N2');
grid on

% %
subplot(5,1,3),plot(time,I_N2O2*1000,'k'); % 1.3 times
set(gca,'FontSize',12);
xlabel('time (ms)','fontsize',12);
ylabel('current (mA)','fontsize',12);
axis([-2,8,-100,30]);
legend('N2+4.76%O2');
grid on

% %
subplot(5,1,4),plot(time,I_N2O2NO*1000,'b');
set(gca,'FontSize',12);
xlabel('time (ms)','fontsize',12);
ylabel('current (mA)','fontsize',12);
axis([-2,8,-300,100]);
legend('N2+4.76%O2+1000ppmNO');
grid on

%
subplot(5,1,5),plot(time,I_N2O2NOH2O*1000,'g');
set(gca,'FontSize',12);
xlabel('time (ms)','fontsize',12);
ylabel('current (mA)','fontsize',12);
axis([-2,8,-20,5]);
legend('N2+4.76%O2+1000ppmNO+2.31%H2O');
grid on
```

C) Lissajous figures comparison under difference gas mixtures

```
load('liss.mat')

plot(Va_N2_7kV,Vcm_N2_7kV.*100,'r');

hold on;

plot(Va_7kV_noH2O_noNO,Vcm_7kV_noH2O_noNO.*100,'k');

plot(simp_Va_7kV_noH2O,simp_Vcm_7kV_noH2O.*100,'b');

plot(simp_Va_7kV_H2O,simp_Vcm_7kV_H2O.*100,'g');




set(gca,'FontSize',16);
xlabel('Voltage (V)','fontsize',16);
ylabel('Charge transfer (nC)','fontsize',16);

axis([-8000,8000,-800,800]);
% set(gca,'xTick',-7000:4000:7000);
% set(gca,'yTick',-8:2:8);

grid on;
```